UNIVERSITY OF MINES AND TECHNOLOGY (UMaT),
TARKWA

FACULTY OF ENGINEERING

DEPARTMENT OF MECHANICAL ENGINEERING

PRODUCTION OF BRAKE PADS FROM INDIGENOUS MATERIALS

BY

EMMANUEL MAWULI SECKLEY

OCTOBER, 2023

UNIVERSITY OF MINES AND TECHNOLOGY (UMaT),
TARKWA

FACULTY OF ENGINEERING

DEPARTMENT OF MECHANICAL ENGINEERING

A PhD THESIS REPORT ENTITLED

PRODUCTION OF BRAKE PADS FROM INDIGENOUS MATERIALS

BY

EMMANUEL MAWULI SECKLEY

SUBMITTED IN FULFILMENT OF THE REQUIREMENT FOR THE AWARD OF THE DEGREE OF DOCTOR OF PHILOSOPHY IN MECHANICAL ENGINEERING

THESIS SUPERVISORS

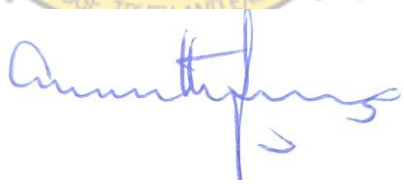

……
PROF ANTHONY SIMONS

……..
PROF AKINTUNDE O. DAHUNSI

TARKWA GHANA

OCTOBER, 2023

DECLARATION

I declare that this thesis is my own work. It is being submitted for the degree of Doctor of Philosophy (PhD) in Mechanical Engineering at the University of Mines and Technology (UMaT), Tarkwa. It has not been submitted for any degree or examination in any other University.

……..

…30th…day of…October…2023

ABSTRACT

This study investigated the potential of producing automobile disc brake pads in Ghana using environmental friendly local materials, namely Periwinkle Shell Powder (PSP), Coconut Shell Ash (CSA), and kaolin (K), as alternatives to asbestos. Asbestos, widely used in the brake lining industry, was banned due to its carcinogenic properties. The properties of these base materials were characterised to determine their suitability as asbestos replacements. To create the brake lining samples, copper powder, zinc powder, aluminium powder, graphite, and epoxy resin binder were combined with the base materials. Two sets of samples were produced: one with PSP and CSA as the base material (PSP/CSA combination) and the other with PSP and kaolin (PSP/K combination). Different particle sizes (106 μm, 150 μm, 212 μm, and 300 μm) of the base materials were used, with 106 μm showing the best results. Brake pads were manufactured with a particle size of 106 μm using a mould designed to match the dimensions of a Toyota Camry saloon car, Model 2000. They were moulded at a pressure of approximately 50 bars, cured for 72 hours, and heat treated at 150 °C for 2 hours. Extensive tests were conducted to analyse the physical, mechanical, morphology, thermal, and tribological features of the brake linings. Commercial brake pads and an asbestos-based brake pad were used as controls for comparison. The results revealed that the bulk densities of the base materials (ranging from 0.833 g/cm^3 to 1.718 g/cm^3) were lower than that of asbestos (2.22 g/cm^3), indicating that the materials would create lighter brake linings. The chemical and mineralogical compositions of the base materials were similar to those of asbestos, all containing SiO_2, CaO, MgO, and Al_2O_3. The base materials exhibited similar thermal behaviour to asbestos, with peak degradation temperatures as follows: 745.88 °C for PS powder, 675.19 °C for CSA, 492.85 °C for kaolin, and approximately 688 °C for asbestos. The developed brake pads displayed favourable properties compared to asbestos-based and branded commercial brake pads. The PSP/CSA pad exhibited compressive strength and hardness values of 115.0 N/mm^2 and 107.0 HBN, respectively, while the PSP/K pad had compressive and hardness values of 138.7 N/mm^2 and 121 HBN, respectively — higher than those of the asbestos-based pad (110.0 N/mm^2 and 101.0 HBN). The coefficient of friction for the developed pads ranged from 0.30 to 0.53, matching the asbestos-based pad. The average wear values of the PSP/CSA and PSP/K pads compared well with commercial and asbestos-based brake pads. Notably, the PS/K brake pad exhibited better wear performance with a value of 2.70 mg/m, compared to 3.80 mg/m for the asbestos-based pad. The developed pads demonstrated a density similar to that

of the asbestos-based pad (1.890 g/cm^3), with density values of 1.910 g/cm^3 for the PSP/CSA pad and 2.160 g/cm^3 for the PSP/K pad. Thermal analysis indicated that the developed pads could withstand high temperatures, decomposing only at temperatures close to 700 °C. Therefore, the periwinkle shell powder, coconut shell ash, and kaolin can effectively serve as filler or reinforcement materials, replacing asbestos in automotive disc brake lining development. Brake pads produced using these materials performed satisfactorily, akin to asbestos-based pads along with other commercial brake pads in the market. It is recommended to exclusively produce the newly developed pads using a hot moulding process and thereafter reexamine their performance characteristics. Additionally, conducting longer-term on-road effectiveness and durability investigations will facilitate a comprehensive assessment of the composite linings.

DEDICATION

Dedicated to my children and Fafa, my adorable wife, who improved my life for having been here.

ACKNOWLEDGEMENTS

I, first, thank the Almighty God for His continuous guidance from the beginning to the end of this research. I am extremely grateful to my supervisors; Professor A. Simons of Mechanical Engineering Department, UMaT and Professor O. A. Dahunsi from the Department of Mechanical Engineering, The Federal University of Technology, Akure (FUTA), Nigeria for their willing cooperation, love, patience and thorough supervision that finally led to the successful completion of this work.

I am also grateful to the management of the university, UMaT for extending to me the staff development package and for granting me leave to travel outside Ghana to continue with this research. May the Almighty bless you all. Long live UMaT!

My appreciation also goes to my Vice-Chancellor Professor R. K. Amankwah for making time out of his heavy schedule to tutor me on the interpretation of SEM micrographs and for his desire to see me finish this work on time. Live long, Prof. I also thank Professor J. R. Danquah of the Minerals Engineering Department, UMaT for assisting me with the drawing of the EDS spectrums for the SEM-EDS analysis of the brake pads, and Dr Shadrack Fosu of the same department for also helping with the interpretation of the TGA-DTA thermographs.

I also say a big thank you to Ing. Alhassan Ogwu and Ing. Amos Olalere both of Federal Institute of Industrial Research Oshodi (FIIRO), Lagos in Nigeria for their numerous contributions towards the accomplishment of this work especially for assisting in carrying out all the experiments on the brake pad samples. My special thanks also go to my good friend, Professor Anthony Ewusi, of the Geological Engineering Department, UMaT who has been my source of encouragement during the course of this work.

I am also grateful to all members of staff of the Department of Mechanical Engineering, UMaT for their assistance in one way or the other throughout the duration of this undertaking.

My sincere appreciation also goes to all the members of my family for their love, prayers, understanding and encouragement. My virtuous wife, Fafali, and my children Esee, Etor, Enam and Elikem for their forbearance and encouragement. I am also grateful to my sister Mary and my brother Victor for their constant support and devotion.

TABLE OF CONTENTS

LIST OF FIGURES

LIST OF TABLES

CHAPTER ONE

INTRODUCTION

1.1 Background of the Study

Indeed, the automobile brake system is an essential component in any vehicle, comprising various parts such as master cylinder, brake pads, wheel cylinders, and a hydraulic control system (Maleque *et al*., 2012). Among these, the brake pad plays a crucial role in enabling gear changes in automatic transmissions and facilitating vehicle deceleration, complete stops, and stationary holding. When brakes are applied, the interaction between the brake pads and the rotating disc converts the vehicle's kinetic energy into heat, leading to its slowdown or stoppage. Brake pads consist of steel base plates with friction materials attached to their surface opposing the brake disc (also known as the rotor) (Anderson, 1992).

For effective braking, brake pads must possess characteristics such as frictional efficiency across a wide temperature spectrum, quieter operation, prolonged lifespan, improved durability and firmness, and minimal porosity. To achieve these features, brake pad materials are designed to be heterogeneous, comprising various elements, each serving a specific purpose in enhancing friction, durability, and noise reduction. Continuous research and development by automotive manufacturers and material scientists aim to improve brake pad materials to enhance their performance, safety, and reliability. and as such offer various types like organic, semi-metallic, and ceramic options, each catering to specific needs and preferences of driver (Toboldt *et al.*, 1989). The materials used in brake pads usually consist of several sub-components, which include fillers, binders, additives, and reinforcing fibres (Chan and Stachowiak, 2004).

Modifying the weight proportion or the composition of elements in the formulation of brake pad materials can lead to changes in their properties (Zaharudin *et al.*, 2012; Mutlu *et al*., 2005; Cho *et al*., 2005 and Jang *et al*., 2004). Researchers have found that there is no straightforward relationship between the friction and wear properties of brake pad materials and their mechanical and material characteristics (Tanaka *et al*., 1973; Todorovic, 1987 and Talib *et al*., 2006).

Therefore, each newly developed formulation needs to undergo several tests to assess its friction and wear characteristics. These tests include on-road braking capabilities

evaluations and techniques for evaluating abrasion resistance. The purpose of these tests is to ensure that the friction material complies with the minimum specifications for its intended purpose (Talib *et al*., 2006). By conducting rigorous testing, manufacturers can verify that the brake pad materials perform effectively and safely in real-world conditions.

The development of brake pads spans a history of more than a century, with various materials being used for braking systems. Early wagon brakes were constructed using wood and leather. In 1897, Herbert Frood is credited with inventing the first brake pad material, which was a bitumen-soaked cotton-based material (Nicholson, 1995). This invention was utilised for both wagon wheels and early automobiles and eventually led to the establishment of the Ferodo Company, which continues to supply frictional materials to this day.

During her pioneering long-distance car trip in 1888, Bertha Benz, the wife of Carl Benz, made a significant contribution to the field by inventing and patenting the first vehicle brake pad (Blau, 2001). Initially, brake pad materials were interwoven, however, in the early 1920s, materials moulded from chrysotile asbestos fibres, an abundant mineral, replaced them. As the years progressed, advancements were made, and in the 1950s, resin-bonded metallic pads were introduced, followed by the development of semi-metallic pads with higher metal additives in the 1960s (Nicholson, 1995).

Despite the introduction of alternative materials, asbestos remained a preferred choice among brake pad manufacturers, and its content in vehicle friction lining materials ranged from 30 % to 70 % (Amaren, 2016). This was due to its noise reduction properties, adequate tensile strength, thermal stability, resistance to electricity, and chemical damage. However, over time, concerns about the health hazards associated with asbestos led to its gradual phasing out in favour of safer alternatives in brake pad production (Lema *et al*., 2008).

The discontinuation of asbestos use as a brake friction material in many regions has spurred significant research and development efforts to find safer alternatives and asbestos-free brake pads. This has led to the emergence of various brake pad and shoe compositions during the last decade, each claiming to perform as well or better than traditional materials. To address the uncertainty surrounding these new materials, Chan and Stachowiak (2004) conducted a review that delves into the advantages and disadvantages of the key constituents used in contemporary solid and wet friction linings for pads and shoes. Their work aims to

provide insights into the suitability of different brake materials for modern brake applications.

In the pursuit of safer alternatives, researchers are exploring the use of industrial and agricultural waste materials as raw materials for brake pads (Leman *et al*., 2008). Utilising suitable waste materials not only offers added value but also helps minimise environmental impacts and waste disposal costs. As a result, various waste materials such as bagasse, palm kernel shell or fibre, coconut shell or fibre, banana peels, periwinkle shell, cow bones and hooves, maize husk, rice husk, cocoa bean shells, and palm oil clinker have been investigated for their potential use as brake pad materials (Aigbodion *et al.*, 2010; Dagwa *et al*., 2012; Dagwa and Ibhadode, 2006; Aku *et al*., 2012; Onyeneke *et al*., 2014; Idris *et al*., 2013; Fono-Tamo and Koya, 2013 and Zamri *et al*., 2011).

Ghana is endowed with a lot of materials, especially rice, cocoa, coconut, and oil palm. Among these resources, rice husks, cocoa bean shells, coconut shells, palm kernel shells, and periwinkle shells, for example, are some of the waste products. Ceramic materials especially kaolin and other clay materials also abound in the country. All these materials are seen to be good replacement of asbestos in brake pad manufacture.

1.2 Statement of the Problem

Ghana has been a low middle-income country since 2010 and on her way of becoming a middle-income country. One way of achieving this is to establish a strong industrial base. A lot of individuals, artisans and established organisations have set the pace by trying to develop better and more economical ways of producing and manufacturing goods and products locally by using local materials and then promoting these goods. Establishments like Kristo Asafo Technological Centre and Ghana Regional Appropriate Technology Industrial Service (GRATIS) have taken giant strides in these areas. Artisans, mechanics and skilled workers at Abossey Okai in Accra, Suame Magazine in Kumasi and Kokompe in Takoradi are also making tremendous contributions in these areas.

One important area much work is being done is in the automotive industry, where various bodies and skilled artisans are trying to produce spare parts for automobiles. One of such is the brake pad, which is one important automobile spare part, but unfortunately nothing is being done in this area in terms of its production. The brake pads come in two forms; the

original brake pad from the vehicle manufacturers with a backing plate attached and after - market replacement pad without the backing plate. Figure 1.1 shows samples of the original brake pads while Figure 1.2 shows samples of the after-market replacement brake pads.

Figure 1.1 Samples of the Original Brake Pads

Figure 1.2 Samples of After-market Replacement Brake Pads

Although Ghana is endowed with a lot of the current trends of materials used in place of asbestos for brake pad production, literature indicates that no thorough, if any, research has been conducted to identify the most suitable of these materials and their use in producing brake pads for the local Ghanaian market. Moreover, as stated by Abutu *et al*. (2018) most of the research done elsewhere in other countries on brake pad materials and production, normally end up on shelves without fabrication and real time testing. A lot of after – market replacement brake pads have flooded the Ghanaian market whose specifications and characteristics are not known, and which pale in comparison with the conventional ones from suppliers like Toyota, Nissan, Mercedes, Honda and the like. Yet these pads continue to be heavily patronised by vehicle owners, simply because they are cheaper in comparison to the conventional ones.

The lifespan of brake pads can significantly differ depending on factors such as the type of vehicle, driving habits, terrain, and frequency of use. While some vehicles may need new brake linings after covering 17,000 to 20,000 miles, others can last much longer, up to 60,000 to 70,000 miles (James and Andrew, 1998). Interestingly, in the Ghanaian market, individuals who purchase replacement brake pads often express dissatisfaction, reporting that the pads wear out quickly, sometimes failing within just a few days or weeks after installation.

The failure of these pads, as reported by drivers and vehicle owners, are in two folds:

(i) Braking action not fully achieved most times.

(ii) Breaking or cracking of brake pads during braking operations.

Probable causes of such failures may be:

(i) The materials utilised in the production of the aforementioned brake pads lack the necessary strength to endure the intense thermal and mechanical stresses that arise during braking operations.

(ii) Brake effectiveness is compromised by a phenomenon known as "brake fade," which occurs when the friction coefficient within the interface of the brake pads and the brake drums is insufficient to achieve consistent or complete braking action. As a result, the braking system struggles to generate enough friction to slow down or stop the vehicle efficiently.

(iii) Poor wear resistance of the brake linings.

Indeed, addressing these issues is essential, and one way to do so is by leveraging locally available materials in the country to develop and manufacture eco-friendly and high-quality brake pads for commercial use. By doing this, Ghana can significantly reduce the cost of importing such products and create a sustainable and viable local industry. The development of asbestos-free brake pads will not only improve safety and environmental concerns but also open opportunities for local businesses to thrive and contribute to the country's economy.

1.3 Objectives of the Research

The main objective of this research is to create brake pads using locally sourced materials. Since brake linings are crucial and delicate components in vehicles, the specific goals of this study are:

(i) To identify and assess locally available materials that have the potential to meet the stringent requirements for brake pads. This involves evaluating their properties to ensure they can withstand the demanding conditions during braking.

(ii) To develop suitable formulations and compositions using the selected indigenous materials to produce the brake pads and to achieve the desired brake pad frictional and wear characteristics.

(iii) To construct a mould and use it to produce brake pads of standard dimensions corresponding to the ones used on a typical Toyota Camry Model 2000 salon car.

(iv) To characterise the produced brake pads, compare them with the conventional asbestos-based brake pads, some after-market replacement pads in the Ghanaian market and brake pads produced from related past research works.

(v) To carry out a real time on-road performance evaluation of the produced brake pads so as to determine their suitability and competitiveness with the conventional ones.

1.4 Research Methodology

In addition to extensive review of related literature on brake pads and current trends of research in brake pad materials development, the following methods were also used in achieving the objectives:

(i) I conducted visits to Suame Magazine in Kumasi, Abossey Okai in Accra, Kokompe in Takoradi, and other regions where brake linings are bonded onto the backplates. This allowed me to gain firsthand knowledge of these activities and become familiar with the diverse after-market replacement brake pads available in the market.

(ii) Characterisation of the pad materials and the produced brake pads were done using a range of physical and mechanical testing equipment, as well as advanced analytical techniques such as X-Ray Fluorescence (XRF), X-Ray Diffraction (XRD), Scanning Electron Microscope with Energy Dispersive Spectroscopy (SEM-EDS), Thermogravimetric Analysis and Differential Thermal Analysis (TGA-DTA), Differential Scanning Calorimetry and Thermogravimetric Analysis (DSC-TGA) techniques.

(iii) The optimum formulation (mixing or combination ratios) of the various materials were done using Design Expert Software (DX), Version 13.

(iv) Design drawings of the mould were obtained using a 3D CAD software, Creo Parametric 7.0.2.0 designed by Parametric Technology Company whiles the fabrication of the mould was done using machine tools at Federal Institute of Industrial Research, Oshodi (FIIRO) in Nigeria.

(v) The on-road performance evaluation was carried out by installing the produced brake pads on the braking system of a Toyota Camry saloon car. Two key parameters (disc temperatures and pad wear rates) were measured during the evaluation.

1.5 Facilities Employed

The facilities used for this research include:

(i) The University of Mines and Technology (UMaT) Library.

(ii) UMaT Mechanical Engineering Workshop.

(iii) Mechanical, Ceramic and Foundry Workshops at Federal Institute of Industrial Research Oshodi (FIIRO) in Lagos, Nigeria, and

(iv) 3D CAD and DX – 13 Software Packages.

1.6 Contribution to Knowledge

The properties of the materials used in the development of the brake pads, as well as the performance characteristics of the produced brake pads, have been thoroughly established and documented. This valuable information is now readily available to serve as a foundation for further research, engineering improvements, and commercial applications. Researchers, manufacturers, and automotive industry stakeholders can rely on this documented data to make informed decisions regarding the production and implementation of these indigenous brake pads in vehicles. Furthermore, the availability of this data and the success of this research open up opportunities for artisans and skilled workers in Ghana for widespread adoption of the locally produced brake pads, contributing to the growth of a sustainable and competitive automotive industry in Ghana.

1.7 Scope of the Study

This study is limited to developing or producing brake pads using locally available materials in Ghana and by utilising the cold moulding technique as the manufacturing process for the brake pads.

1.8 Thesis Organisation

The thesis is structured into 5 chapters. Chapter 1 is the introduction, which briefly introduces the research work, research problem, objectives of the research, the methodology used, facilities employed, contribution of the research to existing knowledge in the field, the scope of the study and the organisation of the report. Chapter 2 reviews related literature involving braking systems, friction lining materials, brake pad production and characterisation and current trends and recent developments in the research on brake pad materials. Chapter 3 contains the resources and methods used, which describes how the solution to the conceived idea was formulated and carried out. Chapter 4 contains the results of the research and compares and analyses the results with those from existing brake pads. Finally, the conclusions, and recommendations for further works are presented in Chapter 5. By organising the thesis into these five chapters, the research work is presented coherently and comprehensively, allowing readers to understand the background, objectives, resources and methods used, results, and implications of the study.

CHAPTER TWO

LITERATURE REVIEW

2.1 Introduction

This chapter focuses on brake pads and braking systems, examining the historical development of brake pad materials and the ongoing research trends in asbestos-free brake material innovation. The chapter also covers the formulation, production, and analysis of brake lining materials.

2.2 Brakes

According to Umamaheswara and Babji (2015), the brake system is of utmost importance in all vehicles as it serves crucial functions, including decelerating the vehicle, bringing it to a complete stop, and maintaining its stationary position after stopping. Khurmi and Gupta (2004) also stated that the primary purpose of most brakes is to generate artificial frictional resistance on a moving component of a machine, thereby slowing down its motion.

Brakes, especially those using brake pads, primarily transform kinetic energy into thermal energy as they perform their functions. However, there are alternative methods of energy conversion as well. Regenerative braking, for instance, transforms a significant portion of the energy into electrical energy, which can be retained for later use. Additionally, some braking systems convert motion energy into potential energy by storing it in pressurised air or oil forms. Moreover, certain methods transfer kinetic energy to a rotating flywheel. Nevertheless, friction brakes remain the commonly employed braking mechanism in automobiles.

2.3 Overview of Brakes and Brake System

Natarajan and Rajmohan (2016) stated that the contemporary vehicle braking system, which has undergone continuous refinement for over a century, has evolved into a highly reliable and efficient mechanism. Typically, this system comprises front disk brakes and either disk or drum brakes at the rear, interconnected by a network of hoses and tubes that extend from the wheels to the master cylinder situated under the vehicle's hood. When the driver presses the brake pedal, the force applied to the master cylinder's plunger causes hydraulic oil,

commonly known as brake fluid, to flow through the hoses and tubes, eventually reaching the brake assemblies at every wheel. Figure 2.1 depicts automotive brake system.

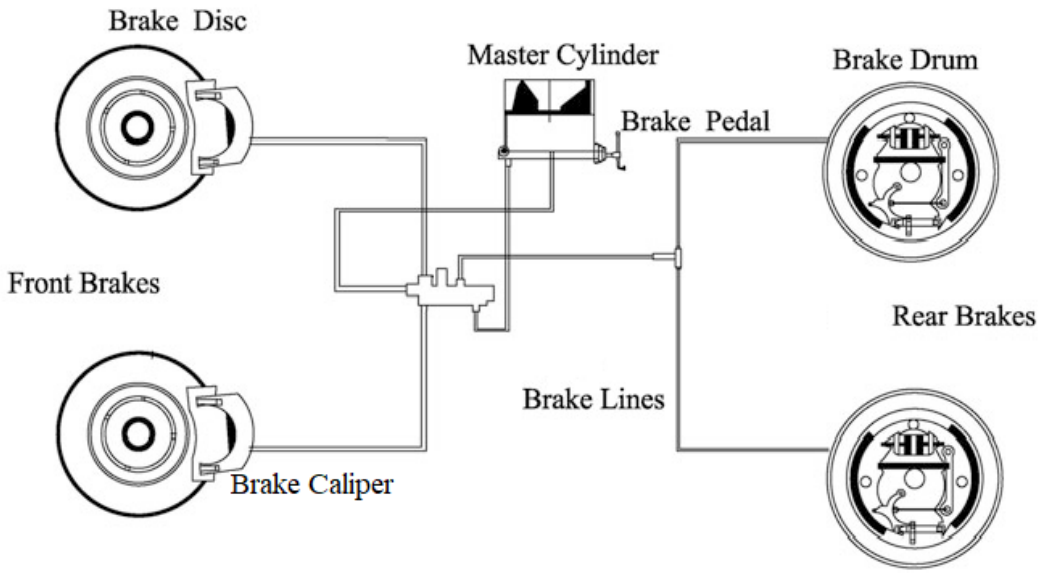

Figure 2.1 Automotive Brake System
(Source: Natarajan and Rajmohan 2016)

2.3.1 Drum Brake

Drum brakes function through the generation of friction, achieved by shoes or pads that exert outward pressure against a rotating cylindrical component known as the brake drum. In this setup, the pads make contact with the inner lining of the drum. The key elements of a drum brake system consist of the brake drum, pads, backing plate, hydraulic cylinder, along with assorted pins and springs (Chandgude and Ganiger, 2016).

When the driver applies the brakes, the piston cup receives pressurised hydraulic fluid from the master cylinder, propelling the pistons in the direction of the shoes and thereby compelling them to engage with the drum. As a result, a rubbing action occurs, leading to a reduction in the rotation of the brake drum, which is directly linked to the wheel. This reduction in rotation leads to a decrease in the vehicle's speed. Figure 2.2 shows a drum brake.

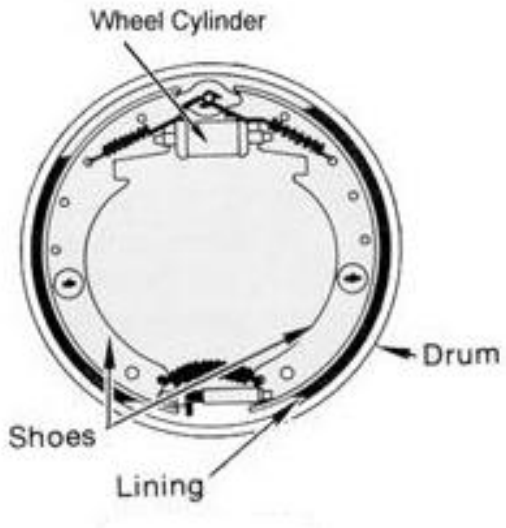

Figure 2.2 Drum Brake

(Source: Chandgude and Ganiger, 2016)

2.3.2 Disc Brake

Gujrathi and Damale (2015) provide a definition of a disc brake as a mechanical device designed to absorb kinetic energy via friction. In this type of brake, the brake pads exert pressure on a rotating disc. Chandgude and Ganiger (2016) reported that a disc braking arrangement consists of three main components: the brake pads, the brake disc, and the brake calliper, as depicted in Figure 2.3. The brake disc, typically made of cast iron or ceramic material, is attached to either the axle or the wheel. The calliper assembly is affixed to the hub carrier, and the brake pads are situated within the calliper assembly.

When the driver presses the brake pedal, high-pressurise hydraulic fluid is applied through the calliper piston, inducing the friction material of the brake pad to contact the surface of the spinning brake disc. As a consequence of this contact, friction is generated, allowing the vehicle to slow down or come to a complete stop.

One advantage of disc brakes is that their friction interface is continually open to air, facilitating effective heat dissipation and minimising brake fade. Moreover, this design facilitates self-cleaning, as dust and water are expelled from the surface, minimising friction differentials and maintaining optimal braking performance.

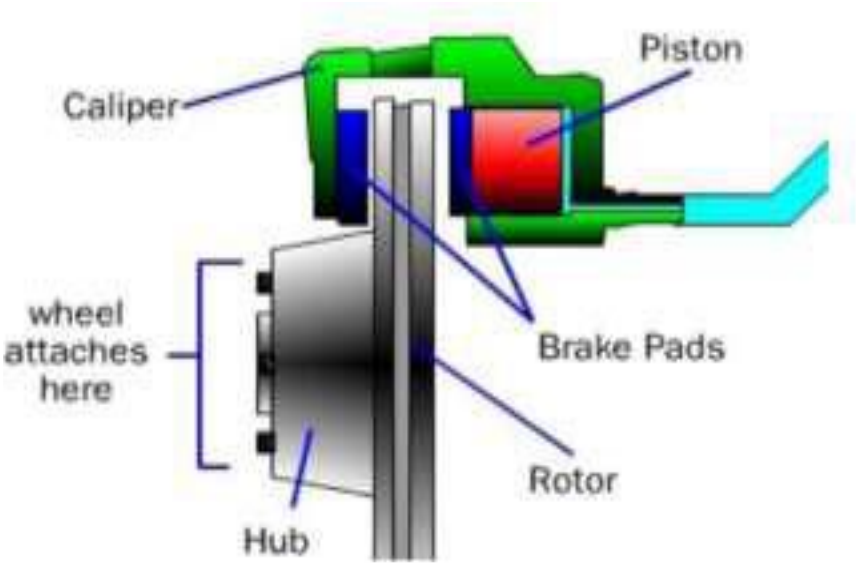

Figure 2.3 Disc Brake

(Source: Chandgude and Ganiger, 2016)

Disc rotor

According to Chandgude and Ganiger (2016), the disc rotor used in disc brake systems is typically composed of gray cast iron and comes in two variations: ventilated, or solid. The aerated disc rotor features a wider design featuring cooling fins integrated through the centre, which aids in effective cooling. Proper cooling is essential to prevent brake fading and help prolong the life of the brake pads.

Certain ventilated disc rotors are equipped with spiral fins, which further enhance airflow and cooling. However, it is important to note that spiral finned rotors exhibit a specific directionality, requiring precise mounting on one side of the vehicle to function optimally. This directional mounting ensures that the fins can maximize their cooling effect and provide consistent braking performance.

Brake calliper

This is a crucial assembly that accommodates both the pistons and the brake pads. It typically incorporates a range of one to four pistons and is securely mounted to either the torque plate, steering knuckle, or wheel carrier. The pistons themselves can be made from various materials like aluminium, plastic, or chrome-plated steel.

Two main types of callipers exist: fixed and floating callipers. A fixed calliper remains stationary in relation to the disc and deploys one or multiple sets of opposing pistons to apply pressure from both sides of the disc. However, it is less forgiving of imperfections on the disc surface. This type of calliper tends to be intricate and costlier compared to a floating calliper. On the other hand, a floating calliper, also recognised as a "sliding calliper," is capable of parallel movement to the disc's axis of rotation. It operates by having a piston on one side of the disc that pushes the inner brake pad into contact with the braking surface. Then, it draws the calliper body along with the outer pad, effectively applying pressure from both sides of the disc. This design provides better tolerance to disc defects and is generally simpler and more cost-effective than fixed callipers (Chandgude and Ganiger, 2016).

2.4 Introduction to Brake Pads

As stated by Anderson (1992), brake pads are composed of steel backing plates that are coated with a layer of friction material. The primary function of brake pads is to transform the motion energy of the vehicle into heat energy through the process of friction. Within the brake calliper, friction surfaces of two brake pads are oriented towards the rotor. When the brakes are applied, the calliper is activated by hydraulic actuation, causing it to clamp and apply pressure to both pads, causing them to press against the rotating discs. This action effectively slows down or brings the vehicle to a stop.

During the braking process, the contact between the brake pad and the rotor generates heat, which can lead to gradual transfer of friction material to the disc surface, giving it a dull grey appearance over time. While it is commonly believed that the friction material makes direct contact with the metal disc, bringing the vehicle to a stop, the pads actually work with microscopic film of their material, stablishing a lubricated semi-fluid interface to facilitate friction. This interface produced the effective braking force, allowing for effective braking performance.

2.5 Components of Brake Pads

Brake pads are composed of three main components: a steel support plate, a wear indicator or sensor, and a frictional lining.

2.5.1 Steel Backing Plate

The component responsible for holding the brake lining in the brake pad assembly is known as the backing plate. Its primary function is to transfer the force exerted by the brake calliper pistons to the brake pad. Typically, low-carbon steels are used in fabricating the backing plates. To ensure the backing plate's flatness and prevent issues like vibrations, noises, and depletion of friction lining, a 400 kg press is utilised during the stamping process.

Achieving complete flatness is crucial, and the backing plate is stamped to meet this requirement. Additionally, the brake pad material is affixed to the forged steel support plate utilising a heat-resistant bonding agent, which is then cured under the application of heat and pressure. The assembly may also incorporate retention features like serrated edges or holes, enhancing the adhesion and anchoring of the friction material to the backing plate.

2.5.2 Wear Sensor or Indicator

As friction materials naturally wear down over time, each set of brake pads is equipped with a wear indicator to notify the driver when replacement is necessary. These wear indicators come in two distinct types: mechanical and electric.

Mechanical wear indicator

Mechanical indicators for brake pad wear typically involve a straightforward approach, often employing a basic steel spring which is riveted to the backing plate of the brake pad. A slit is incorporated on the pad’s face, indicating the permissible wear limit of the pad and also allowing for the escape of gas and the dust from braking. As the friction lining gradually wears down and reaches the point of replacement, the steel spring comes into contact with the rotor, resulting in a high-pitched whistling or screeching noise, alerting the driver that it is time to replace the brake pads.

To reduce brake squeal, some applications may include metal plates, or in certain cases, multiple plates referred to as anti-squeal shims. These shims are positioned toward the piston on the brake pad and serve to minimise the occurrence of brake noise.

Electric wear indicator

The electric type of wear indicator operates differently by triggering an alert indicator on the vehicle's dashboard when the electrical connection of the integrated wire in the brake pad is lost, signalling that it is time to replace the pads. Electric pad sensors come in two variations: the detachable wear lead wire type and the built-in wear lead wire type.

2.5.3 Frictional Lining

The friction material is a crucial component with specific dimensions designed to be fixed onto the shoe or backing plate. It functions as the main wear component in the braking system and is responsible for contacting the rotor, thereby transforming kinetic energy to generate heat during the braking process. As a result, the friction material slowly wears away over time, necessitating replacement.

In terms of high-performance braking, it can be said that the friction material is highly critical among all the brake pad parts. Multiple brake system designs necessitate varying types of friction materials to achieve optimal braking performance. During the development of brake pads, several factors and considerations are taken into account to ensure that the chosen friction material is well-suited for the specific braking requirements of the vehicle.

2.6 Requirements of a Good Brake Friction Lining

According to Talib *et al*. (2007), friction linings play a crucial role in the performance of a braking system, and as such, the optimal brake lining should possess certain characteristics. It should maintain a consistent friction coefficient across wide temperature ranges and diverse operating conditions, including different loads, speeds, braking methods, and both dry and damp environments, to ensure consistent braking performance for a vehicle. In addition, the perfect brake pad material should be capable of functioning effectively at high temperatures without experiencing fading. It should also exhibit oil and water resistance and have a reduced wear rate and avoid rapid wear of the brake disc. Moreover, brake pads are designed to maintain high stability, produce minimal noise, and avoid causing damage to the brake disc while minimising vibrations.

To ensure the best performance from brake pads, it is recommended to replace them every 17,000 to 20,000 miles, depending on factors such as the brake pad material and the driving

surface (James and Andrew, 1998). Vehicle owners have the option to instal new pads using either original equipment pads or aftermarket replacement pads.

2.7 A Brief Look at Types of Brake Pads

Sarvendra and Jain (2013) have identified varied categories of brake pads available, catering to the specific purposes of different vehicles. The main categories of brake pads typically employed in modern vehicles include asbestos pads, metallic pads, semi-metallic pads, eco-friendly materials pads, carbon-carbon pads, and non-asbestos organic or ceramic pads. The various types of pads offer a range of features and characteristics to meet diverse braking requirements.

2.7.1 Metallic Pads

As mentioned by Sarvendra and Jain (2013), metallic brake pads are composed of a metal lattice enhanced by elements like copper, steel, graphite, or other metallic elements. These pads are known for their cost-effectiveness and durability, offering superior strength and excellent heat conduction. However, due to their metal composition, metallic pads are relatively hard, leading to increased wear damage and a higher likelihood of generating squeal noise. Additionally, they are more susceptible to corrosion. Moreover, metallic brake pads may not perform optimally in cold conditions and tend to produce a significant amount of brake dust.

2.7.2 Semi Metallic Brake Pads

As per Sarvendra and Jain (2013), this category of brake pads comprises approximately 30 % to 65 % metal content, constituting a blend of metals and organic materials. These components are often crafted from copper, steel wool, wire, or other metallic substances. While semi-metallic brake pads are highly durable, they have the potential to wear down brake rotors at a faster rate. Like metallic pads, semi-metallic brake pads may not perform optimally during frigid conditions, and they are known for generating noise during braking.

2.7.3 Non-asbestos Organic or Ceramic Pads

According to Sarvendra and Jain (2013), Non-asbestos Organic (NAO) brake pads are made from a blend of ceramics and organic substances like rubber, glass fibres, and sometimes

Kevlar. These pads are generally softer, resulting in reduced noise during braking. However, they have a faster wear rate and tend to produce a significant amount of brake dust. NAO brake pads exhibit high strength, excellent thermal resistance, and wear resistance, while also being lightweight. However, they can become brittle and experience increased wear under high-temperature conditions.

2.7.4 Carbon-Carbon Pads

According to Sarvendra and Jain (2013), these brake pads share similarities with ceramics but offer superior properties. They exhibit excellent friction performance, superior thermal resistance, and exceptional wear resistance. Additionally, carbon-carbon pads are lightweight. However, they may not perform efficiently in cold environments. One drawback of these pads is that they are relatively expensive to produce due to high material and manufacturing costs.

2.7.5 Eco-friendly Materials Pads

According to Chan and Stachowiak (2004), these brake pads belong to a category in which organic fibres like hemp, jute, coconut shell, sisal, banana peels, flax, kenaf, or palm kernel fibres are utilised as reinforcement materials. These pads are characterised by strong mechanical characteristics, consistent friction behaviour, outstanding wear durability, lightweight construction, environmentally friendly, and cost-effectiveness. However, they may face challenges with agglomeration during mixing processes and are susceptible to wear caused by ecological factors.

2.7.6 Asbestos Pads

As per Leman *et al.* (2008), asbestos was used as a filler material in this type of brake pads. At the time, asbestos was considered as an excellent choice for the production of brake linings due to its favourable physical properties, including reduced heat conduction and high temperature resistance, which are crucial characteristics in brake pads. Moreover, asbestos was widely accessible, making it a convenient choice.

During the early 1980s, however, it was found that asbestos was cancer-causing (carcinogenic) and had the potential to cause serious health issues such as Asbestosis and

Mesothelioma. As a result, the use of asbestos in brake pads and other products has been banned or significantly restricted in many countries to protect public health and safety.

2.8 Components of Brake Pad Materials

As stated by Brijendra and Ashish (2015), during the braking process, the heat energy is initially absorbed by the dual contact interfaces of the brake: the brake pad (or drum and shoe in the case of drum brakes) and the brake disc. Afterward, it is subsequently transferred to other components of the brake system, including the callipers, along with the surrounding environment.

Eriksson *et al*. (1999) also emphasised that the brake pads face specific demands, requiring them to maintain strong frictional response with the brake disc. The choice of brake pad materials is, therefore, crucial to ensure effective braking performance.

Blau (2001) categorised brake materials and additives based on their anticipated functions, and they can be grouped as follows:

(i) Abrasive materials

(ii) Friction Additives/Modifiers

(iii) Filler materials

(iv) Reinforcement materials

(v) Binders

According to Blau (2001), the categorisation of brake materials and additives may lead to some uncertainty, as certain materials can fulfil multiple functions and fall into multiple categories simultaneously.

2.8.1 Abrasives

Abrasives in brake materials serve several functions, including keeping the contacting surfaces clean and regulating the accumulation of frictional coatings. They also play a role in enhancing friction, particularly during the initial stages of braking, thereby increasing the "bite" or initial braking force. Common examples of abrasives used in brake materials are

silica, quartz, iron oxides, zirconium silicate, and aluminium oxide. Table 2.1 provides an overview of some specific abrasives and their descriptions.

One of the advantages of abrasives is their ability to eliminate unwanted surface deposits that can occur during braking. However, it is important to note that friction materials with a higher content of abrasives can lead to significant variabilities in the friction coefficient. These variations may result in fluctuations in the braking torque, as highlighted by Jang *et al*. (2004). Therefore, finding the right balance in abrasive content is critical to achieving stable and consistent braking performance.

Table 2.1 Types of Abrasive

Abrasive	Comment/Description
Aluminium Oxide	(i) The water-bound version is often added to brake materials as a polishing agent and to enhance wear resistance. However, its presence may also lead to brake fade. (ii) On the other hand, the anhydrous version is even more abrasive than the water-bound version, offering enhanced friction characteristic. (iii) The fused form is extremely hard and stands out as the harshest abrasive variant among the different variations.
Iron Oxides	(i) Hematite (Fe_2O_3) and magnetite (Fe_3O_4) both serve as mild abrasive. They can remove unwanted surface films and enhance friction properties.
Silica	(i) SiO_2 is a common example of a synthetic abrasive which is used to enhance friction characteristics.

(Source: Chan and Stachowiak, 2004)

2.8.2 Friction Modifiers or Additives

Certain materials used in brake pads serve specific functions such as lubrication, enhancing friction, or participating in chemical reactions to manage surface films. These materials include carbon (graphite), brass, friction dust, antimony trisulphide, and friction powder (possibly containing Fe sponge, especially in partially metallic brake pads). Lead oxide

(PbO) has been utilised as a friction modifier in the past, but it poses toxicity concerns, as noted by Nicholson (1995). Other additives include metal-fluxing compounds and metal oxides.

Jang *et al*. (2004) highlighted that the stability of the friction coefficient is significantly influenced by the amount of lubricants or abrasives used in the brake lining. An optimal balance of these materials is crucial. Increasing the volume of lubricating substances in the lining results in higher friction coefficient uniformity. In contrast, increasing the volume of abrasive materials may result in variability in the friction coefficient, as mentioned earlier. Table 2.2 provides a summary of some lubricants and their respective properties used in brake materials.

Table 2.2 Types of Lubricants

Lubricant	Comment/Description
Graphite	(i) Graphite is highly utilised lubricant. It can be found as organic or man-made variation and can be obtained as flakes or powder. Flaked-graphite is known for its superior lubrication properties, while powdered-graphite excels in fiddling away the braking-induced heat. (ii) When used in brake materials, graphite has the ability to rapidly create a lubricating film on the opposing friction surface facilitating smoother frictional interaction. (iii) While graphite is advantageous as a lubricant, it should not be excessively used in a phenolic resin. This is because the graphite and phenolic resin are weakly bonded, resulting in reduced shear strengths within the brake materials.
Metal Sulphides	(i) These materials including brass, copper, tin, lead sulphides and antimony, possess favourable lubricating attributes compared to graphite. They also exhibit decreased heat conduction, which can be beneficial in certain brake applications.

(Source: Chan and Stachowiak, 2004)

2.8.3 Fillers

As explained by Chan and Stachowiak (2004), fillers play a part in contributing to the integrity of friction materials used in brake pads. The term "filler" encompasses any component that is utilised in substantial amounts in brake pads. For instance, certain manufacturers incorporate substantial amounts of hard and abrasive metal silicates into their brake friction linings, categorising them as "fillers" rather than "abrasives." While not as critical as reinforcing fibres and other components, fillers still play a crucial role in brake friction linings. They have a significant impact on the overall composition of brake pads, and influencing the ultimate characteristics of brake performance, including heat resistance, abrasion resistance, and overall strength.

Fillers can be diverse ranging from ceramics, alloys, metals, organic substances to antioxidants, each contributing specific properties to the brake friction material. A commonly used filler in metal-ceramic composite brakes is graphite, while asbestos was widely used in early-era brake materials. Additional examples of fillers include barium sulphate, which increases density and enhances wear resistance, and calcium carbonate, which is somewhat less stable at elevated temperatures. Cotton reinforcing fibres and mineral wool, containing inorganic components like magnesia, alumina, silica, and calcium, are also employed as fillers in brake pads. These fillers play roles in controlling brake fade, improving braking effectiveness, bringing down manufacturing costs, and enhancing the ease of producing brake pads (Eriksson *et al*., 2002).

2.8.4 Reinforcements

Chan and Stachowiak (2004) emphasize that friction materials rely on these substances to enhance their mechanical resilience. Recent studies have revealed that the responsibility of bearing the braking load lies with minute plateaus that emerge above the adjacent lower regions within the friction materials. These plateaus come into existence due to the presence of reinforcing fibres immersed in a matrix of compressed softer materials. Thus, the significance of these reinforcing fibres cannot be overstated in friction materials. Typically, a combination of diverse reinforcing fibres, each offering complementary characteristics, is used in friction materials. Table 2.3 presents various reinforcement materials along with their respective descriptions.

Table 2.3 Reinforcing Materials

Reinforcing Materials	Comment/Description
Glass Fibres	(i) When glass fibres are bound together with a resinous binder, they demonstrate remarkable physical strength making then an excellent choice intended for reinforcement purposes. (ii) In addition to their strength, they exhibit exceptional thermal resistance, boasting elevated melting points that can reach up to 1430 ^{o}C. (iii) Nevertheless, it is important to note that typical glass fibres have a relatively low heat conduction of 0.04 W/mK. Moreover, their inherent brittleness poses a limitation, rendering them unsuitable as the sole brake lining reinforcement agent.
Aramid	(i) They are manufactured from the condensate of isophthalic or terephthalic acids and m-or p-phenylenediamine. (ii) They have a significantly lower weight compared to other materials and demonstrate exceptional thermal stability. Additionally, they possess an excellent rigidity-to-mass ratio and exhibit superior wear resistance properties. (iii) However, as a result of their relative soft nature, it is improbable that they can single-handedly bear the braking load. As a result, they are typically used in conjunction with other reinforcing fibres.

Table 2.3 Continued

Reinforcing Materials	Comment/Description
Sepiolite	(i) Sepiolite is a hydrated magnesium silicate mineral, characterized by its fibrous chain-structure formation. (ii) This mineral exhibit remarkable thermal resilience, with melting temperature of around 1550 °C. Additionally, it has the ability to take in small amounts of fluids. (iii) However, it is essential to handle sepiolite with caution as it poses a possible health risk. Prolonged exposure to sepiolite has been linked to the progression of lung inflammation and interstitial lung disease (ILD), making it harmful to human health.
Potassium Titanate	(i) These fibres are produced from extensively purified single crystals. (ii) They possess exceptional resilience and can withstand high temperatures, with a melting point of about 1371°C. (iii) These fibres are highly durable and demonstrate excellent resistance to wear. (iv) Despite their advantageous properties, they pose a health risk due to their association with mesothelioma, a serious health condition.
Ceramics	(i) These fibres are composed of metal oxides, such as alumina, and carbides, like silicon carbide. (ii) They exhibit remarkable thermal resistance and melting points that span from 1850 °C to 3000 °C. Additionally, they possess a high strength-to-weight ratio, an added advantage. (iii) Nonetheless, their brittleness is a limitation, and as a result, they cannot be used as standalone materials.

Table 2.3 Continued

Reinforcing Materials	Comment/Description
Metallic	(i) Metallic fibres, also known as metallic chips or granules, are frequently utilised as reinforcement in various applications. Examples of metallic fibres include copper, steel, and brass. (ii) These fibres exhibit exceptionally high conductivity, allowing them to rapidly dissipate heat from the rubbing surface. (iii) However, there is a drawback with certain metallic fibres, like steel, which may rust, particularly if the vehicle functions in a corrosive setting. This rusting can sacrifice their effectiveness as reinforcing agents. (iv) Moreover, when present in significant proportions, metallic fibres, such as steel, can lead to excessive brake disc wear and cause fluctuations in the friction coefficient.

(Source: Chan and Stachowiak, 2004)

2.8.5 Binders

The primary role of a binder in a brake pad is to ensure the structural integrity of the pad under different braking conditions. It functions as a cohesive element, binding together all the constituents of the brake pad, preventing their disintegration during use (Chan and Stachowiak, 2004). The binder needs to possess certain characteristics, including elasticity to transmit the load to the fibres. Depending on the application, the binder must exhibit intermediate strength at high temperatures, as well as appropriate performance at low temperatures. Furthermore, it should showcase outstanding resilience to chemicals, depending on the specific application requirements. Another important aspect is that the binder should have ease of processing during the manufacturing of the final brake pad composite shape and maintain stability in its dimensions to preserve its overall form (Pandey *et al.*, 2001). Given these requirements, selecting appropriate binders for brake pads

becomes a crucial aspect. For reference, Table 2.4 provides a list of commonly used binders along with their respective descriptions.

Table 2.4 Commonly Used Binders

Binder	Comment /Description
Phenolic Resin	(i) This type of polymer is derived from the condensation interaction between phenol and formaldehyde. (ii) It serves as the prevailing binder. However, using it in small amounts can weaken the lining, and using excessive quantities can cause a drop in frictional performance at high temperatures. (iii) Despite its drawbacks, this binder is preferred for its affordability and ease of production. It offers a good balance of mechanical properties, including high compressive strength, moderate thermal and creep resistance, high hardness, and excellent wetting capability with most materials. (iv) Despite its advantages, these resins are susceptible to the influence of heat and moisture. Additionally, they tend to undergo slow in situ polymerization even at ambient temperature, leading to a limited shelf life. Furthermore, they are brittle and have limited impact resistance.
COPNA Resin	(i) COPNA resin stands for 'Condensed Poly-nuclear Aromatic resin.' (ii) This type of resin exhibits a strong bonding affinity with graphite, which is a prevalent lubricant. As a result, COPNA resin offers superior anti-wear properties compared to pure phenolic resin. (iii) One drawback of COPNA resin is that it undergoes decomposition at moderate temperatures, typically between 450 °C and 500 °C.

Table 2.4 Continued

Binder	Comment/Description
Silicone-modified Resin (Phenolic Siloxane Resins)	(i) Phenolic siloxane resins are created through the reaction of silicone rubber or silicone oil with phenolic resins. (ii) To address its inherent brittleness, the resin is enhanced with strengthening agents. (iii) However, the addition of toughers can result in a compromise of the original chemical and thermal durability traits of the phenolic resins, and the enhanced resin may become highly toxic. (iv) Despite the challenges in modifying the resin, Kane and Mowers achieved success in blending phenolic resins with silicone, resulting in phenolic siloxane resins that offer enhanced impact resistance.
Cyanate Ester Resin	(i) Cyanate ester resins are created from polyfunctional cyanate monomers. (ii) These resins exhibit stability at high temperatures and possess chemical inertness. Additionally, they demonstrate damping properties, which means they can absorb and dissipate mechanical energy. (iii) Despite their advantageous properties, cyanate ester resins share a common drawback with phenolic-based resins in that they tend to be brittle.
Epoxy-modified Resin	(i) They typically undergo degradation well over 260 °C. To enhance their operating temperature range, specialised curing agents need to be employed. (ii) By incorporating epoxy into phenolic resins, a synergistic effect is achieved leading to a material with improved heat resistance compared to phenolic or epoxy resin alone. Additionally, the resulting material exhibits a higher friction stability.

Table 2.4 Continued

Binder	Comment /Description
Thermoplastic Polyimide Resin	(i) This material is formed by combining fluoro resin with calcium carbonate. (ii) It demonstrates remarkable resistance to abrasion and does not suffer from thermal fade, which is a common issue experienced with phenolic-based resins. Furthermore, it does not cause excessive wear on the brake disc. (iii) Despite its benefits, this material's thermal conductivity is roughly one-third of that of phenolic resins, resulting in reduced effectiveness in dissipating heat off the contact surface.

(Source: Chan and Stachowiak, 2004)

2.9 Automotive Brake Pad Formulations

To meet the required properties of brakes, brake materials are typically composite materials consisting of multiple elements and compounds. There is a wide array of over 2000 distinct materials and variations used in commercial brake components (Weintraub, 1998). Predicting the friction and wear characteristics of automotive brake pads is challenging due to their complexity, as they are influenced by various factors such as rotating speed, the metallic counter face, the microchemical structure of the pad, contact surface temperature, and pressure (Ingo *et al*., 2004).

Having evolved over the course of a century, the formulation of commercial frictional brake pad materials remains varied and intricate. The makeup and configuration of brake pads significantly impact their frictional behaviour. However, due to the limited understanding of the composition-property relationship, formulating brake pads often relies on trial and error, making it both time-consuming and expensive (Osterl and Urban, 2004). It's worth noting that the precise compositions of commercial friction materials are rarely disclosed in the public domain.

In some cases, authors have provided representative sample compositions of friction materials, some of which are presented here. It's worth noting that some authors reported a variety of compositions rather than single values. This practice is often done to hide the exact formulations of the materials, and as a result, the percentages of constituents may not add up to 100 %. Additionally, some compositions are given in weight percent, while others are given in volume percent. However, according to Nicholson (1995), volume percent is considered the appropriate metric for friction material formulation.

Friction tests on multiple asbestos-free materials were carried out by Tsang *et al*. (1985). The compositions of these materials are provided in Table 2.5, Table 2.6, and Table 2.7.

Table 2.5 First Material Formulation Used by Tsang and Others

Function	Material	Amount (wt. %)
Binder (resin)	Thermoset	13 – 18
Fiber reinforcements	Fiberglass	6 – 24
Inorganic fibre	-	8 – 16
"Friction dust"	-	0 – 20
Elastomer (polymer)	-	0 – 20
Carbon/graphite	Carbon	1 – 4
Inorganics	-	12 – 32
Metals/oxides	-	0 – 19

(Source: Tsang *et al.*, 1985)

Table 2.6 Second Material Formulation Used by Tsang and Others

Function	Material	Amount (wt. %)
Binder (resin)	Thermoset	8 – 14
Fiber reinforcements	Fiberglass	14 – 16
Inorganic fibre	-	10 – 16
"Friction dust"	-	0 – 7
Elastomer (polymer)	-	0 – 7
Antioxidant	Carbon/Graphite	18 – 34
Filler	Barium Sulfite	30
Inorganics	-	7 – 24
Metals/oxides	-	4 – 22
Other	-	0 – 10

(Source: Tsang *et al.*, 1985)

Table 2.7 Third Material Formulation Used by Tsang and Others

Function	Material	Amount (wt. %)
Binder (resin)	Thermoset	10 – 20
Metal fibre	Steel	0 – 70
Metal powder	Iron	20 – 70
"Friction dust"	Proprietary	0 – 18
Elastomer (polymer)	-	0 – 18
Antioxidant	Carbon/Graphite	10 – 30
Filler	Barium Sulfite	0 – 15
Inorganics	Proprietary	0 – 10

(Source: Tsang *et al.*, 1985)

In a study conducted by Howell and Ball in 1995, a comparison was made between the friction and wear characteristics of an aluminium/SiC composite and cast iron when used with three different pad materials. The compositions of the pad materials reported in Table 2.8 were used in this comparison.

Table 2.8 Brake Pad Formulations Used by Howell and Ball

Function	Material	Organic Pad (wt. %)	Semi-met Pad A (wt. %)	Semi-met Pad B (wt. %)
Binder	Phenolic resin	43	25	16
Fibers	Organic fibre	20		
Metal	Cu	0.6	15	15
	Fe		43	3
	Al		3	2
Lubricant	Graphite	15	7	4
Abrasive	Alumina			5
Filler	Rubber	2	5	
	Paper	15		52
Other	Unspecified	4.4	2	3

(Source: Howell and Ball, 1995)

In their study, Gudmand-Hover *et al.* (1999) examined the impact of dry lubricants on disc brake behaviour utilising a dynamometer. The disc brake utilised Volvo standard non-aerated back brake discs with the formulation detailed in Table 2.9. Additionally, Eriksson *et al*. (2000) employed a typical formulation in the brake pad of a Volvo 850 car. The composition of this formulation is presented in Table 2.10.

Table 2.9 Brake Pad Formulation Used by Gudmand-Hover and Others

Function	Material	Amount (wt. %)	Comments
Matrix (Binder)	Resin and Rubber	23 – 26	
Fillers	Barytes, Friction Dust and Vermiculite	25.5 – 41	
	Brass	0 or 5	
Fibers	Aramid	0 or 9	
Friction modifiers	Metal Sulphides	8	Cu, Pb, or Sb sulphides
Abrasives	Zirconia	0 or 5	
	Alumina	0 or 5	

(Source: Gudman-Hover *et al.*, 1999)

Table 2.10 Brake Pad Formulation used for Volvo 850 Car Pad

Function	Material	Amount (wt. %)
Matrix (Binder)	Binder Material	8
	Other	11
Fillers	Clay and Iron Oxide	8
Fibers	Steel, Aramid, Glass	30
Friction modifiers	Brass/Bronze	15
	Graphite	15
	Metal Sulphides	8
Abrasives	Quartz	5

(Source: Eriksson *et al.*, 2000)

Similarly, to analyse how each component affects friction and wear, Kato and Soutome (2001) used the formulation presented in Table 2.11.

Table 2.11 Brake Pad Formulations Used by Kato and Soutome

Function	Material	Amount (wt. %)	Comments
Matrix (Binder)	Phenolic Resin	25.0	
Fillers	Barium Sulphate	0.02	
	Cashew Dust	19.4	
	Calcium Carbonate	0.0	Not in the optimal composition
Fibers	Aramid	3.0	
	Ceramic	15.0	
Metal	Copper Powder	20.0	
Abrasive	Alumina	10.0	
Lubricant	Graphite	7.3	
	Molybdenum Disulphide	0.0	Not in the optimal composition

(Source: Kato and Soutome, 2001)

2.9.1 Recommended Ranges of Brake Pad Materials Formulations

The composition of brake pad materials, whether commercial or experimental, can vary considerably, but certain elements are frequently present in most formulations. Given the diverse functions that brake pad materials serve and their sensitivity to even minor changes in concentration, precise control over the composition is of utmost importance. In light of this, it becomes crucial to have a clear understanding of each constituent's impact on performance to achieve the desired characteristics in brake pads. In this context, Blau (2001) has provided a range of values for some commonly used constituents in brake pad formulations to serve as a guide for brake pad development. These ranges are presented in Table 2.12. As stated by the author, the term "friction dust" in the table may encompass some of the constituents mentioned earlier under other categories, such as fillers or lubricants. Additionally, "friction dust" could also contain additives that are derived from cashew particles.

Table 2.12 Typical Ranges of Some Constituents in Brake Pads Formulation

Constituent	Range (vol.%)	Typical Value (vol. %)
Phenolic resin	10 – 45	20 – 25
Barium sulphate	0 – 40	20 – 25
Cashew particles	3 – 30	15 – 20
Fibers	5 – 30	-
Graphite	0 – 15	5 – 7
Metal sulphides	0 – 8	0 – 5
Abrasive	0 – 10	2 – 3
“Friction dust”	0 – 20	-

(Source: Blau, 2001)

2.10 Current Trends of Research into Asbestos-free Brake Pad Materials

As mentioned in the study by Leman *et al.* (2008) and reiterated earlier, asbestos was widely used in brake pad manufacturing due to its favourable properties and easy availability. However, its association with severe health risks, including carcinogenic effects has prompted a significant effort to find alternative fibres for brake pad production. Some of the research conducted into these alternative fibres has been presented in this section.

Blesdzki and Gassan (1999), Seki (2006), and Garcia *et al*. (2007) have all explored the potential application of rice husk as a filler or reinforcing material in the production of friction pads. Rice husk dust and rice straw dust are particularly attractive owing to their abundant silica content and minimal lignin content, which imparts a ceramic-like behaviour to friction materials (Ibrahim, 2009). In a study conducted by Acharya and Samantrai (2012), they examined the friction and wear behaviour of rice husks when used as a filler material. The findings indicated that as the quantity of rice husk fibres increases, wear rates show a corresponding decrease under all testing conditions. As a conclusion, they found that integrating rice husk fibres into epoxy is highly effective in enhancing the wear resistance of the brake pads. Figure 2.4 illustrates the appearance of rice husks.

Figure 2.4 Rice Husk
(Source: Garcia *et al*., 2007)

In their research, Mathur *et al*. (2004) also developed a friction material by formulating a blend with cashew nutshell liquid as the reinforcing component. They conducted a comprehensive investigation into the material's tribological properties. The formulation comprised modified phenolic resin serving as the binder, with graphite and cashew dust acting as friction modifiers. Additionally, wollastonite, barium sulphate, and talc were utilised as fillers in the formulation. The researchers reported that the obtained results showed favourable performance comparable to asbestos-based pads. Based on their findings, the authors concluded that there is significant potential for the use of cashew nuts hell in brake pad formulations.

In a study conducted by Ibhadode *et al*. (2008), they explored the potential of using palm kernel shells as a friction lining material for brake pads. Through their experiments, they

compared palm kernel shell with other agro waste materials such as hyphaene thebaica kernel shell and deleb palm kernel shell. Ultimately, they found that palm kernel shell exhibited superior performance after a series of tests. The researchers concluded that palm kernel shell demonstrated favourable physical and mechanical properties, and its performance was comparable to that of commercial friction linings containing asbestos. However, despite these promising findings, the researchers also noted a need for improvement. They recommended further refinement of the palm kernel shell lining formulation to achieve a wear rate comparable to that of asbestos-based linings, particularly at higher vehicular speeds. Figure 2.5 shows the palm kernel shells used.

Figure 2.5 Palm Kernel Shell
(Source: Ibhadode *et al.*, 2008)

In their study, Aigbodion *et al*. (2010) explored the use of bagasse, a fibrous residue from sugarcane, to produce brake pads. They formulated the brake pads using a ratio of 30 % phenolic resin (phenol formaldehyde) and 70 % bagasse. The bagasse used in the study (Figure 2.6) was separated into different grades through sieving, ranging from 100 μm to 710 μm. During their investigation, the researchers identified optimal values for various properties of the brake pads. These included a hardness of 92 at 3000 kgf, a density of 1.65 g/cm^3, a compressive strength of 103.5 MPa, flame resistance with 46 % ash charred, and water and oil absorption rates of 5.04 % and 0.44 %, respectively. Additionally, a microstructure analysis was conducted. Aigbodion and colleagues noted a consistent pattern in their study regarding the compressive strengths and hardness values of the brake pad samples. They observed that as the sieve size of the bagasse decreased, both the compressive strength and hardness improved. Based on their findings, the researchers recommended that the most favourable properties for friction pads could be attained by employing a finer sieve

grade of 100 μm bagasse and a composition consisting of 70 % bagasse and 3 0% phenolic resin.

Figure 2.6 Bagasse

(Source: Punyapriya, 2007)

To quantify the search for an alternative and environmentally friendly fibre in production of brake pads, Maleque *et al.* (2012) used coconut fibre in their research. As per the researchers' observations, the microstructure analysis of their brake pads exhibited a homogeneous arrangement of the phenolic resin and coconut fibre throughout the matrix. Based on this analysis, they concluded that formulations containing 5 % and 10 % coconut fibre exhibited superior mechanical properties compared to other formulations. Consequently, they identified natural coconut fibre as a promising candidate material, either as a fibre reinforcement or filler, for the formulation of automotive brake pads. Figure 2.7 shows coconut fibre.

Figure 2.7 Coconut Fibre

(Source: Maleque *et al.*, 2012)

In 2012, Bashar and colleagues developed a novel brake pad material utilising coconut shell powder. This material was combined with various components, including cast iron fillings, silica, a catalyst, an accelerator, and epoxy resin. During the study, they experimented with different weight ratios of epoxy resin and coconut shell powder while keeping the other ingredient weights constant. A series of corrosion and mechanical tests were performed to analyse the impact of these variations on the resulting products. The research findings revealed that as the proportion of coconut shell powder rose, certain properties of the brake pads, such as hardness, impact strength, breaking strength and compressive strength decreased. This indicated that higher percentages of coconut shell powder led to increased brittleness in the brake pad samples.

However, the study identified specific compositions that showed promise: brake pad samples with 50 % matrix and 10 % reinforcement, as well as samples with 60 % matrix and 10 % reinforcement. These compositions were found to be significantly lighter and exhibited better overall properties compared to other combinations. These coconut shell-reinforced brake pad formulations were considered potential alternatives to asbestos, by the authors, due to their lower wear resistance. Figure 2.8 illustrates the coconut shells used in the study.

Figure 2.8 Coconut Shells
(Source: Bashar *et al*., 2012)

Idris *et al*. (2013) developed a novel brake pad using both carbonized and uncarbonized banana peels as a substitute for asbestos. They employed phenolic resin as a binder and varied its weight percentage from 5 % to 30 % with 5 % intervals. The study focused on examining the physical, mechanical, morphology, and wear properties of the brake pads.

The researchers found that as the weight percentage of resin increased, the compressive strength, hardness, and specific gravity of the produced samples also increased. Conversely, the oil soak, water soak, wear rate, and percentage of charred material decreased with higher resin content. Based on their findings, they identified samples containing 25 % uncarbonized banana peels and 30 % carbonized banana peels as having superior properties overall. In conclusion, Idris and others suggested that banana peels can be effectively utilized as a replacement for asbestos in the production of brake pads. Figure 2.9 depicts the banana peels used in their study.

Figure 2.9 Banana Peels
(Source: Idris *et al.*, 2013)

In 2013, Amaren and colleagues developed an asbestos-free brake pad by utilising typical periwinkle shells. The shells were ground and then sieved into various grain sizes, specifically 125 μm, 250 μm, 335 μm, 500 μm, and 710 μm. These sieved periwinkle shell particles were mixed with a 35 % phenolic resin binder. Upon analysing the results, the researchers found that the brake pads formulated with the periwinkle shell particles of 125 μm sieve size performed comparably well to commercial brake pads. Based on this positive outcome, they concluded that periwinkle shell particles are a highly effective substitute for asbestos in the production of brake pads. Figure 2.10 illustrates the type of periwinkle shells used in their study.

Figure 2.10 Periwinkle Shells
(Source: Amaren *et al*. (2013)

In 2014, Ikpambese and colleagues developed a brake pad material utilising eco-friendly palm kernel fibres as the primary natural fibre. They combined the fibre with $CaCO_3$, graphite, and Al_2O_3, while using epoxy resin as the binder. After conducting various tests, the researchers identified a specific composition that yielded superior properties. This composition consisted of 40 % epoxy resin, 10 % palm kernel fibre, 6 % Al_2O_3, 29 % graphite, and 15 % calcium carbonate. The study compared the results of their brake pad material with those of commercial asbestos brake pads. The findings showed that the fibre, when used with epoxy resin as the binder, can effectively serve as a suitable replacement for asbestos in brake pads. Figure 2.11 shows the palm kernel fibres used in their study.

Figure 2.11 Palm Kernel Fiber
(Source: Ikpambese *et al*., 2014)

Darlington *et al.* (2015) conducted a study focused on producing eco-friendly brake pads using locally sourced raw materials in Nsukka. In their study, Darlington and others utilized palm kernel shell and coconut shell powders as the primary materials to create a disc brake friction lining with the shape corresponding to Mitshibushi L-300 disc brake pad. To form the brake pad material, they combined these shell powders with polyester resin, which served as the binder. Additionally, graphite was used as a lubricant, and metal chips and carbides were added as abrasives to enhance the performance of the brake pads. The researchers produced three different brake pad samples by using different mass compositions of palm kernel shell and coconut shell while maintaining the other components constant. All the samples were subjected to the same testing conditions. After conducting the tests, the authors concluded that the sample with a smaller mass of palm kernel shell (14.79 %) and a bigger mass of coconut shell (35.92 %) showed promising potential and could serve as a viable replacement for asbestos as brake pad material. This particular sample demonstrated moderate water absorption, wear rate, and hardness, despite having the least coefficient of friction.

In 2015, Ademoh and Adeyemi did a study in which they utilised maize husks as a base material for brake pads. The properties of their formulated maize-husk based brake pad were found to be comparable to asbestos-based pads. As a result, the researchers concluded that maize husks could effectively serve as a suitable and eco-friendly substitute for asbestos and other agro-biomass materials. Similarly, in 2017, Asotah and Adeleke also developed eco-friendly brake pad utilising corn husks. The husks were milled and sieved into two grain sizes, 100 μm and 200 μm. These different proportions of corn husk and silicon carbide were combined with fixed amounts of steel dust, resin and graphite. The researchers investigated various properties such as compressive strength, density, flame resistance, hardness, wear rate and porosity. The authors reported that the finer 100 μm screen yielded better results, and the overall findings closely aligned with those of asbestos-based pads. Based on these results, it was suggested that corn husks can be effectively used in the production of asbestos-free brake pads. Figure 2.12 shows maize or corn husks.

Figure 2.12 Maize or Corn Husks

(Source: Ademoh and Adeyemi, 2015)

Mayowa *et al*. (2015) developed a novel friction material by incorporating cow bone and palm kernel shell as reinforcing agents. They found that these materials demonstrated potential as suitable substitutes for asbestos in friction materials. However, it is worth noting that they did not explore important tribological characteristics like friction and wear resistance, which significantly influence the overall performance of friction linings. Figure 2.13 depicts the cow bones that were utilised in the study.

Figure 2.13 Cow Bones

(Source: Mayowa *et al*., 2015)

In 2016, Adeyemi and his team formulated an eco-friendly brake pad by utilising cocoa bean shells as the primary material. They combined silica sand, anhydrous iron oxide, graphite, calcium carbonate, and epoxy resin with the cocoa bean shells. To explore different formulations, they created three samples with varying proportions of epoxy resin (ranging from 50 % to 60 %) and cocoa bean powder (ranging from 21 % to 31 %), while maintaining the silica, anhydrous iron oxide, graphite, and calcium carbonate at constant levels of 7 %, 3 %, 5 %, and 4 %, respectively. Their findings indicated that the brake pad sample composed of 60 % epoxy resin and 21 % cocoa bean shell powder exhibited the most satisfactory performance in comparison with other combinations. Moreover, the test results obtained from this sample were comparable to those of commercially available brake pads. Figure 2.14 displays the cocoa bean shells used in their study.

Figure 2.14 Cocoa Bean Shells
(Source: Foodbev Media, 2015)

In 2016, Bala and colleagues also carried out a study exploring the potential of cow hooves as a replacement for asbestos in brake pads. They combined pulverized cow hoof powder with barium sulphate, aluminium oxide, graphite, and epoxy resin to create different samples. After conducting various tests, the authors reported that a sample comprising 15 % pulverized cow hooves and 35 % epoxy resin, as well as another sample with 10 % pulverized cow hooves and 7 % epoxy resin, yielded the most favourable outcomes. Based on these results, they concluded that pulverized cow hoof is a viable and effective reinforcing agent for the production of brake pads. Figure 2.15 illustrates the cow hooves used in their study.

Figure 2.15 Cow Hooves

(Source: Bala *et al*., 2016)

Amaren, (2016) also conducted a study focused on creating eco-friendly brake pads utilising periwinkle shell, fan palm shell, phenolic resin, engine oil (SAE 20/50), and tap water. The research involved five different particle sizes, ranging from 125 μm to 710 μm, for both the periwinkle shells and the fan palm shells. The study aimed to assess the mechanical and tribological characteristics of the formulated brake pads. The findings revealed that the 125 μm particle size was the most optimal formulation for the brake pads, producing the best results. Moreover, the obtained results from these brake pads showed favourable comparisons with those of commercially available brake pads. As a result, the author concluded that utilizing periwinkle shell and fan palm shell particles could effectively be employed in the production of brake pads. Figure 2.16 shows fan palm fruits.

Figure 2.16 Fan Palm Fruits

(Source: Amaren, 2016)

Lawal *et al*. (2017) conducted research on the development of a new eco-friendly brake pad utilising sawdust (agro-waste material) in combination with other components. The sawdust was divided into three grades with sizes of 100 μm, 355 μm, and 710 μm, and it served as the base material. The brake pad was formulated with a composition of 55 % sawdust, 10 % silicon carbide, 5 % graphite, 15 % steel dust, and 15 % epoxy resin. Various properties of the brake pad were examined, including microstructure, density, water absorption, hardness, wear rate, compressive strength, and ash content. The research findings indicated that the brake pad properties improved as the sieve size of the sawdust became finer. The authors noted a strong resemblance between the obtained results and the performance of a commercial brake pad that contained asbestos. This study demonstrated the potential of using sawdust as a viable alternative material for producing ecofriendly brake pads. Figure 2.17 illustrates the sawdust used in their research.

Figure 2.17 Sawdust
(Source: Lawal *et al*., 2017)

Anaidhuno *et al*. (2017) formulated a brake friction lining and developed a brake pad designed to match the specific dimensions and requirements of a Toyota Camry 2000 model. Their formulation included palm kernel shell powder and coconut shell powder as the primary materials, carbon for fibre reinforcement, cashew nutshell, zinc, copper and aluminium as abrasives, and epoxy resin as the binder. Additionally, rubber dust from shoes served as filler materials. In their research, the authors found that the produced brake pads exhibited a friction coefficient ranging from 0.4 to 0.65, bonding strengths of 25 to 27 kg/cm^2, wear rates ranging from 0.025 mm/min to 0.06 mm/min, and scratch hardness

values between 80 and 85. The obtained values were similar to those typically found in traditional brake pads that contain asbestos. Consequently, the authors concluded that their formulation could be effectively used for brake pads installed in a Toyota Camry 2000 model.

Edokpia *et al*. (2014) also worked on developing eco-friendly brake pads, utilising eggshells as the main constituent. They employed Gum Arabic, a plant-based gum, as the binder, with varying binder composition ranging from 3 % to 18 % by weight. The researchers examined several properties of the brake pads, including swelling in water and SAE oil, wear rate, compressive strength, specific gravity, hardness, thermal resistance, and microstructure characteristics. The authors found that the formulations containing 15 % to 18 % Gum Arabic displayed the most satisfactory bonding properties. They concluded that the sample containing 18 % Gum Arabic had properties, including highest temperature degradation, superior to asbestos and other substitute materials employed. Moreover, the research indicated that eggshells hold promise as a viable replacement for asbestos in the production of brake pads. Figure 2.18 depicts eggshells used in their research.

Figure 2.18 Egg Shells
(Source: Edokpia *et al.*, 2014)

Ramanthan *et al*. (2017) investigated the feasibility of utilising powder obtained from lemon peels as filler material for brake pad manufacturing. They produced two samples with compositions of lemon peel particles (10 – 20 %), calcium hydroxide (10 %), graphite (15 %), aluminium oxide (7.5 - 12.5 %), iron oxide (7.5 - 12.5 %), and epoxy resin (40 %). The researchers experimented with different ratios of lemon peel powder, aluminium oxide, and

iron oxide. The authors concluded that one sample composed of 10 % lemon peel powder, 12.5 % iron oxide, 12.5 % aluminium oxide, 15 % graphite, 10 % calcium hydroxide and 40 % epoxy resin exhibited optimum properties suitable for brake pad applications. However, the tests also revealed a high wear rate, which may be a limitation of this particular formulation. Figure 2.19 shows lemon peels.

Figure 2.19 Photograph of Lemon Peels

Elakhame and colleagues also conducted a study in 2017 where they created a brake pad without using asbestos. Instead, they used a powdered periwinkle shell as the main component along with carbon black, steel slag dust and epoxy resin. To test different variations, they used three different sizes of periwinkle shell particles: 100 µm, 200 µm, and 350 µm. The brake pads were then subjected to mechanical and morphological tests. The researchers found that the brake pads with a sieve size of 100 µm exhibited the best overall properties, outperforming the other variations and even showing comparable results to those of the existing pads in the market. Based on their findings, the authors suggested that periwinkle shell can be a highly effective substitute for asbestos in brake pad production.

However, despite the comprehensive survey, it is evident that there has been no investigation into the potential of utilising alternative materials like periwinkle shell combined with coconut shell ash or periwinkle shell combined with kaolin as substitutes for asbestos in brake friction materials. Therefore, there is a crucial need to further explore and develop affordable, eco-friendly brake pad materials to enhance brake performance. In light of this context, this study aims to assess the viability of employing powdered periwinkle shell as a reinforcing agent and coconut shell ash and kaolin as filler materials in brake pads.

2.11 The Production Process of Brake Pads

The production of brake pads involves five steps, which include ingredient mixing, preforming, compression moulding machine curing, post baking, and finishing. Figure 2.20 illustrates a flowchart depicting the production process of brake linings.

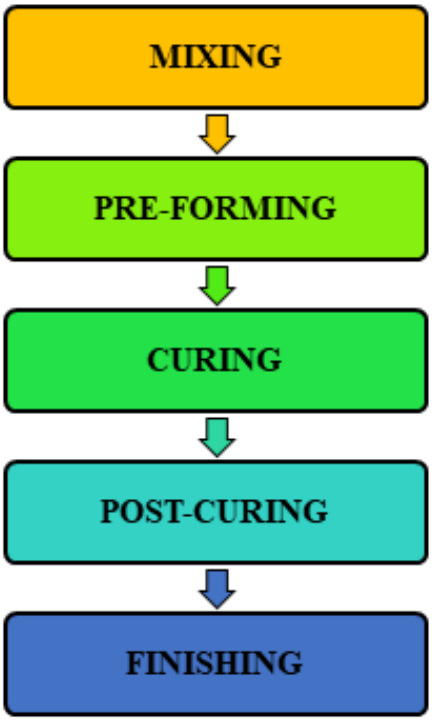

Figure 2.20 Flowchart for Production of Brake Pads
(Source: Author's Construct, 2022)

2.11.1 Mixing of Components

This is the stage where the different friction materials or the constituents are introduced into a mixer for blending. To achieve a consistent and even mixture, a step-by-step blending process is utilised based on previous experience. Initially, fibres, fillers, and abrasives are mixed, followed by the addition of additives and binders. The mixing duration may vary, but typically, total mixing times range from 5 to 15 minutes (Aleksendric and Carlone, 2015). The success of this phase in preparing the friction material relies on the selection of appropriate ploughs and choppers, as mixing at high speeds can result in the shearing and fragmentation of the ingredients (Nicholson, 1995). Consequently, the choice of mixer and mixing time depends on the specific formulation of the friction material, which encompasses the selection of ingredients (Suryarajan *et al*., 2016). After achieving the desired mixture, it

is precisely weighed using a weighing machine according to the specified proportions, and then forwarded for preforming. A commonly utilised mixer is the Lodigee type shear mixer, as depicted in Figure 2.21.

Figure 2.21 Lodigee Type Shear Mixer
(Source: Suryarajan *et al*., 2016)

2.11.2 Pre-forming Process

The crucial stage in the production of friction materials involves moulding and initial curing of the composite under controlled heat and pressure. The brake pads are molded in a molding machine and then pressed using manual or mechanical, hydraulic, pneumatic, or servo electric driven presses. However, hydraulic hot molding presses are the ones mainly designed for the brake lining industry. They allowed pressing to be done at various ranges of pressures depending on their capacity. During the moulding step, a consistent mixture of ingredients is compressed in a preheated mould at temperatures ranging from 150 °C to 200 °C, and at a pressure between 30 MPa and 70 MPa (Aleksendric and Carlone, 2015). Figures 2.22 and 2.23 depict a standard compression moulding machine and a typical hydraulic press, respectively.

Figure 2.22 A Standard Compression Molding Machine
(Source: Suryarajan *et al*., 2016)

Figure 2.23 A Typical Hydraulic Press
(Source: Anon., 2021)

2.11.3 Curing or Sintering Process

The moulded components are cured or sintered at different temperatures for different periods. For organic brake linings, curing temperatures can range between 150 ^{o}C and 200 ^{o}C depending on the materials involved. Sintering temperatures can also range between 600 ^{o}C to 1200 ^{o}C or more depending on the melting temperature of the base material and it is normally carried on metallic brake linings (Suryarajan *et al.*, 2016). During sintering, the atoms constituting the materials diffuse through the interfaces between the particles, resulting in their fusion and the formation of a single solid piece. Sintering is done to evacuate gases and resins trapped in the friction material during mixing. Additionally, sintering decreases porosity and improves various properties, including thermal conductivity, electrical conductivity, and strength.

2.11.4 Post-curing Process

In this step, the brake pads are positioned in an oven and subjected to temperatures ranging from 120 °C to 160 °C for varying durations, based on the curing temperature requirements of the binder in the formulation. This process allows the heat to activate and solidify the binder, and other ingredients, ensuring consistent performance throughout the pad's lifespan. Figure 2.24 displays a typical post-curing furnace used for this purpose.

Figure 2.24 A Typical Post Curing Furnace
(Source: Suryarajan *et al.*, 2016)

2.11.5 Finishing Process

After the curing process, the surfaces of the brake pads undergo grinding using a grinding wheel to obtain the required thickness and remove any resinous surface layer. To ensure quality, visual inspections are conducted to check for characteristics such as gapping between the lining and backing plate, splits, unprocessed material surface and bubbles. Some manufacturers also coat the surface of the pads using a high temperature paint or a powder coating that is baked on (Andrew, 2016).

2.12 Characterisation of Brake Pads

Brake pads are typically assessed based on their mechanical, tribological, thermal, and physical properties (Suryarajan *et al*., 2016). These properties are crucial as they aid in the investigation of the performance, as well as in determining the quality of the brake pads. In this section details of measurement of some physical, thermal, mechanical and tribological properties are given.

2.12.1 Physical Tests

Some of the physical tests conducted on brake pads include specific gravity, swell thickness, water or oil absorption, porosity, and bulk density.

Specific gravity test

The nondestructive test is utilised as quality assurance examination to assess the uniformity of formulation and manufacturing of brake linings. It is used to determine the level at which particles are packed tighter inside the formulation. Normally, the theoretical and actual specific gravity should not differ by more than 2 %. The specific gravity and its range vary for each formulation, making it essential to establish acceptable values or ranges specific to each formulation (Suryarajan *et al*., 2016).

Swell thickness test

When brake pads are exposed to water, they can expand in volume due to attributes of the friction material surfaces. The degree of swelling depends on various factors, including the initial moisture content, the composition of the pore fluid, compacted density and the curing

process applied to the pads. The swelling thickness is ascertained by computing the ratio between the change in thickness and the initial thickness of the specimen before it was immersed (Suryarajan *et al*., 2016).

Water and oil absorption test

This test involves measuring the quantity of water or oil the material can absorb when submerged for a specific duration. It is quantified as the ratio between the weight of the absorbed water or oil and the weight of the dry material. The water and oil absorption capacity of brake pads are influenced by factors such as the type of base materials utilised, the additives incorporated, as well as the temperature and duration of material exposure.

Porosity test

Porosity refers to the proportion of voids or empty spaces, such as trapped air spaces, and pores, within a material. This characteristic holds significant importance in brake systems. According to Ibrahim *et al*. (2015), brake pads require a certain level of porosity to reduce the impact of water and oil on the coefficient of friction. The porosity is determined by calculating the percentage of the test piece's volume occupied by absorbed water or oil. To ensure the brake pad's acceptability, the cavities should constitute less than 5 % of the pad's surface and should not adversely affect its shape (Vivek *et al*., 2020). Excessive porosity can lead to early degradation, while insufficient porosity may result in squealing issues.

Bulk density test

This property of brake linings is an important parameter that indicates the material's capability to serve as structural support, facilitate water and dissolved substance transport, and enable aeration. It represents the mass of the brake pad material per unit volume in its dry state. Density, in this context, refers to the material's apparent compactness (Charles, 2003). Bulk density accounts for both the solid components and the pore spaces within the material. It tends to rise as the material undergoes compaction.

2.12.2 Mechanical Tests

According to Suryarajan *et al*. (2016), mechanical tests normally conducted on brake pads include hardness, tensile, compression, and shear tests.

Hardness test

This test is conducted to measure the material's resistance to plastic deformation or surface scratching, while also offering strong resistance against corrosion and wear. It is a measure of the friction material's longevity. Typically, a "sturdy brake pad" is considered more appropriate for various braking procedures or circumstances. The most common ways of measuring hardness of friction linings are by use of Brinell test or Rockwell testing machine.

Compression test

This test is performed on brake pads to evaluate their ability to withstand the compressive forces exerted during braking. This test helps evaluate how the brake linings behave when exposed to applied compressive forces. Typically, a test specimen of the brake pad, often in the shape of a cuboid or cylinder, is subjected to compressive pressure using platens or specialized features on a universal compressive testing machine.

Tensile strength test

Tensile strength refers to the material's capability to withstand being stretched or pulled without breaking. It is evaluated through a test in engineering and materials science that involves deliberately subjecting a sample to controlled tension until it fails. The material's desirable quality lies in ensuring that the failure occurs at the intended location, and its significance is determined by the localization of the failure. Tensile tests on brake pads are conducted using universal tensile testing machine.

Shear strength test

Brake pad shear strength is defined as the load-to-bond area ratio at failure This type of test is performed to assess the resilience of the bond between the friction material and the steel support plates. The applied shearing force represents the highest force exerted through the outer edge of the brake pad. Following the shear force test, the bonding is examined, which includes any residue left on the backing plate and may comprise adhesive agents, sublayers, frictional elements, or their amalgamation.

2.12.3 Thermal Analysis

Brake pads undergo various thermal tests to assess their performance under different temperature conditions. These tests include measuring thermal conductivity, flame resistance, heat swell, and determining the ash point.

Thermal conductivity test

The role of thermal conductivity is crucial when evaluating the performance of materials in high-temperature applications, and this holds true for friction materials such as brake pads. The heat conduction properties of a friction material are influenced by several factors, including the type and quantity of fillers incorporated, the manufacturing method employed, and the working parameters like temperature. Additionally, the method used to measure thermal conductivity and the size of the sample being tested also play a role in determining the material's heat conduction properties (Suryarajan *et al.*, 2016). This test is carried out by using thermal conductivity analyzers.

Heat swell test

This test is designed to assess the heat swell of the brake pads in a laboratory setting under controlled conditions. Initially, thickness readings are taken at room temperature with a precision of 0.02 mm. The measurements are obtained from at least six points, approximately located between 12 and 20 mm from the pad edge. Subsequently, these values are compared with measurements taken at the same points on the specimen after it has been heated to around 200 °C in an oven (Vivek *et al.*, 2020). The increase in pad thickness is recorded as the swell.

Ash point test

Ash refers to the incombustible residue left behind after subjecting a material or specimen to complete combustion in a controlled high-temperature environment. Determining ash values is useful for assessing the quality and purity of brake lining materials. The ash point is determined by dividing the total weight of the residue (ash) by the weight of the initial sample. This measurement provides valuable insights into the amount of non-combustible material present in the brake lining material, which can impact its performance and overall characteristics.

Flame resistance test

This attribute is a vital criterion for a high-quality brake pad. Flame resistance refers to the characteristic or capacity of the brake pad material to endure burning and withstand extreme heat. It ensures that the brake pad does not catch fire when exposed to intense heat. To determine flame resistance, the sample's weight is measured before and after burning, and the percentage of flame resistance is calculated based on the difference in weights.

2.12.4 Tribological Properties

The measured tribological properties include wear rate and the coefficient of friction of the friction materials.

Friction coefficient test

When assessing a brake pad's performance, the friction coefficient is a crucial factor to consider. It represents the ratio between the force of friction acting between two surfaces and the force pressing those surfaces together. In the context of calculating the coefficient of friction for a car's braking system, data such as the braking moment experienced during braking and hydraulic pressure necessary for engaging the brake pad are taken into account. A higher coefficient of friction indicates a stronger resistance to slipping between the surfaces, making the brake lining more efficient. To determine the coefficient of friction, a Universal Friction Testing Machine can be utilised, which allows precise measurements and evaluation of the brake pad's frictional performance.

Wear rate test

Wear in a brake pad is a combination of abrasion, adhesion, fatigue, transfer, and oxidation of the material, resulting in the formation of free debris particles. The wear process significantly impacts the pad's lifespan and susceptibility to various influencing factors. The extent of pad wear is influenced by the unique wear properties of both the friction material and the rotor, the number of brake stops performed, and the aggressiveness of the braking action. A lower wear rate is indicative of a more efficient and longer-lasting brake pad. To assess the wear rate, standardised tests are conducted, providing valuable data to evaluate and compare the wear performance of different brake pad materials under controlled conditions.

CHAPTER THREE

RESOURCES AND METHODS USED

3.1 Introduction

In this work two different types of asbestos-free brake pads have been developed using Periwinkle Shell Powder (PSP) as reinforcement. The PSP was combined with Coconut Shell Ash (CSA) and kaolin as filler materials. Four different particle sizes of these materials were utilised in the manufacturing of the brake pads. Figure 3.1 is a work chart that summarises the methodology used in this study covering the overall activities undertaken in the chapter.

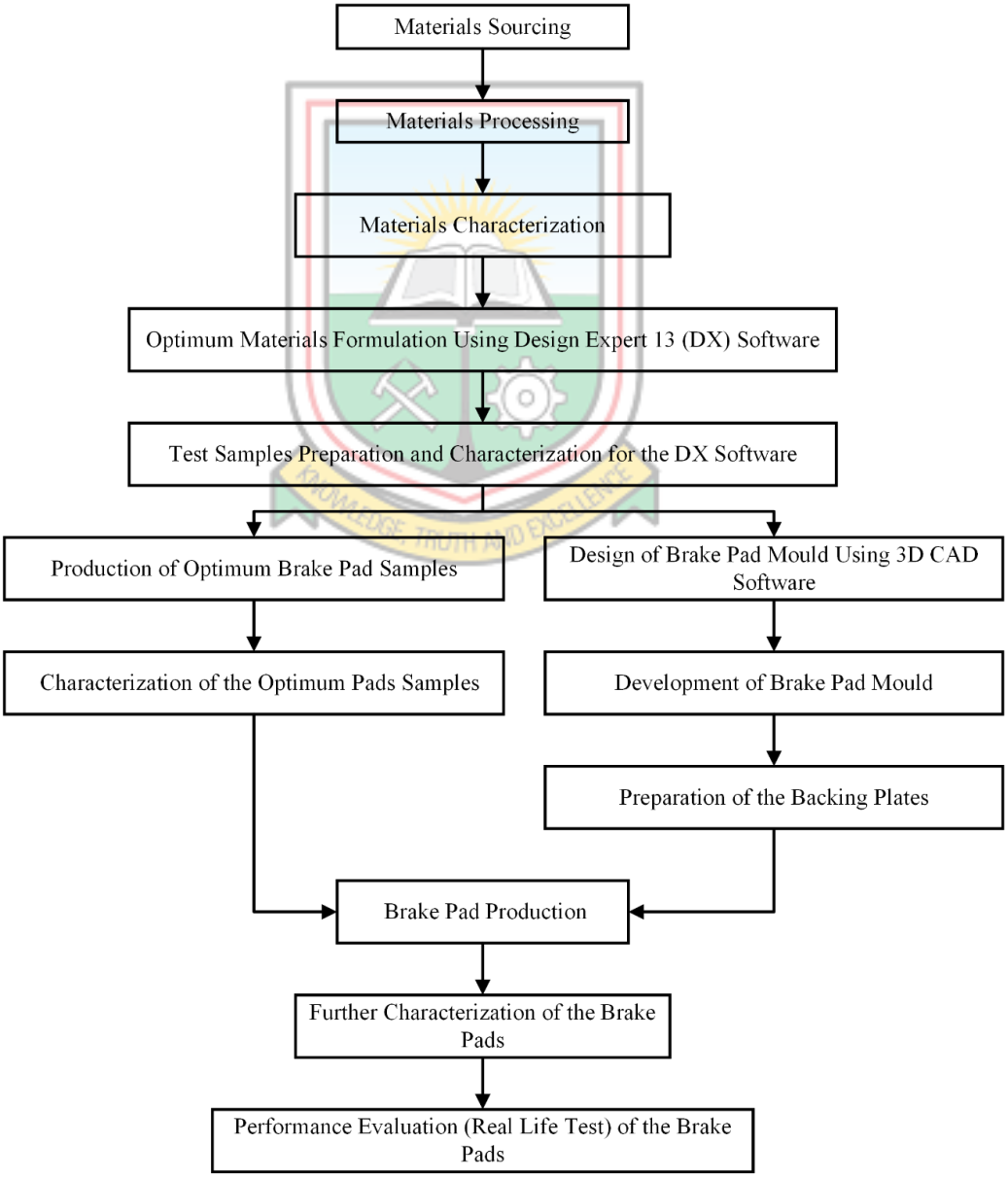

Figure 3.1 Work Chart of the Brake Pad Development and Testing

3.2 Sourcing of the Materials

The raw materials utilised in this work are, periwinkle shell, coconut shell, kaolin, graphite, copper powder, zinc powder, aluminium powder, epoxy resin, and WD – 40 Specialist Silicone spray. The periwinkle shell was collected from Atiavi, a town at the bank of the Keta lagoon in the Volta Region of Ghana. Kaolin was obtained from Abonko a village near Mankessim in the Central Region of Ghana. The coconut shells were obtained from a local distributor and coconut oil producer (who processes coconut from Central and Western regions of Ghana) at Armed Forces Shopping Arena in Oshodi, Lagos, Nigeria. Aluminium, zinc, and copper powders with specific grades were sourced from a chemical and equipment supplier shop outlet located in Mushin, Lagos, Nigeria. The binder (epoxy resin with hardener), graphite and WD – 40 sprays were obtained off shelf in Ilasamaja, Industrial Chemical Market, Lagos.

3.3 The Roles of the Various Materials Used

The functions of the different materials employed in the brake pads development in this study are presented in this section. As stated earlier, brake pad materials can be categorised into more than one group owing to their fulfilment of several functions. As a result, there are certain inevitable overlaps in the classification.

3.3.1 The Reinforcement Used in this Study

Periwinkle Shell (PS) can serve as both a filler and a reinforcement fibre in composites. However, in this work, it is chosen as the primary reinforcement, along with copper powder, to provide mechanical strength to the two formulations. Periwinkle is a small univalve gastropod mollusk. According to Adewuyi and Adegoke (2008), the shells of this mollusk have been utilized by people in the coastal areas of Nigeria for over 30 years as a conglomerate in concrete reinforcement for construction purposes. Similarly, Ekop *et al.* (2013) have noted that many researchers in Nigeria and elsewhere have recently been exploring the use of periwinkle exclusively for construction purposes and for the removal of lead, ion, and copper from industrial wastewater. Numerous pieces of literature support these assertions. For example, Raju *et al*. (2016) investigated the compressive strength of concrete with partial replacement of aggregates using granite powders and cockle shell. Dahunsi (2003) also examined the strength of concrete with PS used as a partial replacement

for granite; and Offing and Akpan (2017) also assessed the physico-chemical properties of PS ash as a cement substitute in concrete. However, not much work has been conducted to explore its application in automotive brake pads, as there is limited literature available on this subject, except for the works by Yawas *et al*. (2013), Amaren (2016), and Elakhame *et al.* (2017) referenced in Section 2.11 of this study. These authors reported that periwinkle shell particles can effectively replace asbestos in brake pad production. Consequently, in this study, periwinkle is utilised to further determine its suitability or otherwise for use in brake pad production.

The type of periwinkle used in this work is *Tympanotonos fuscatus* (radula Linnaeus, 1758**)** also known as the West Africa Mud Creeper, belonging to the family Potamididae. According to Reid *et al.* (2008), it represents the sole surviving species within the Tympanotonos genus. Its distribution spans the coastal regions of Africa, stretching from the southern coast of Angola to the northern coast of Senegal, including Cape Verde. (Appleton *et al*., 2010). It is the most common and dominant species of snail thriving in the brackish waters of West Africa. Within the sub-region, it is commonly found in the lagoons and mudflats of Ghana, Nigeria, and Togo (Hughes, 1992). Periwinkles are typically located at the edges of these lagoons (in shallow waters) rather than the main body (Egonmwan, 2008). The elongated shells of periwinkles display consistently expanding spirals, subtly curved ribs, and delicate grooves adorned with dark brown streaks. They can grow up to 25 – 95 mm in length and weigh between 0.02 g – 9.42 g (Moruf and Lawal-Are, 2015).

According to Ekop *et al*. (2013), the shells of these small gastropods are agricultural waste, which is often stockpiled in open fields, causing environmental issues in many areas where they are found. Therefore, exploring its suitability as an automobile brake pad material will contribute to effectively managing the waste generated daily. In this study, copper powder is also chosen to serve as a secondary reinforcement fibre, enhancing the mechanical strength of the brake pad.

3.3.2 The Fillers Used in this Study

In this study, two distinct fillers, namely coconut shell ash and kaolin, were incorporated as alternative options for the base material and for comparative analysis. These fillers are included to ensure the overall composition of the formulations is preserved.

Coconut shell ash

Coconut is a fibrous one-seeded drupe with the scientific name *Cocos Nucifera*. It belongs to the palm family and exists in various varieties. The West African Tall variety is commonly found in Ghana, primarily concentrated in coastal regions (Quaicoe *et al*., 2009). The 'Tall' variety can grow up to a height of 30 m, with the trunk diameter reaching up to 80 cm and tapering to about 40 cm. According to Caulum (2012), coconuts are distributed along the entire coast of Ghana, although they are less common in the driest parts of the coastal savanna in the east.

Coconut shell refers to a protective covering of the coconut to which the nut or kernel is adhered on the inside and the husk is attached to on the outside (Last, 2001; Rachel, 2010). For immature coconut, the shell is normally soft but for a fully grown and dry coconut, the Coconut shell refers to the protective covering of the coconut to which the nut or kernel is adhered on the inside, and the husk is attached to on the outside (Last, 2001; Rachel, 2010). For immature coconuts, the shell is normally soft, but for a fully grown and dry coconut, the shell becomes very hard and brittle. An undamaged extracted shell is spherical to oblong in shape, brown in colour, and usually has three 'seams' and three 'eyeholes' on the top of the shell, which are softer than the rest of the shell. The kernel is the most important part of the coconut, and for easy transportation, the coconut is normally dehusked, leaving only the shell with the kernel inside. According to Caulum (2012), coconut shells have many uses, including decoration, jewellery, as cups and ladles, as fuel, and for constructional purposes. However, despite these uses, coconut shells are often left as wastes that are stockpiled in open fields in many areas after the nut has been removed from them; some are even dumped into water bodies, causing an imbalance in the ecological system.

The ongoing research into the use of agro-based materials to replace asbestos has identified coconut shell powder as a potential candidate filler or reinforcement. Nevertheless, in this study, Coconut Shell Ash (CSA) has been utilised as a filler material instead of coconut shell powder. CSA is the residue from the combustion of the coconut shell, which appears grey in colour, and is usually odourless and tasteless. The decision to use CSA is based on its current research applications as a filler in the construction and rubber industries. For instance, Tamalkhani *et al*. (2019) investigated the use of CSA as a filler in porous asphalt mixtures, along with discarded Low-density Polyethylene (LDPE) plastic as alternative materials and concluded that the addition of CSA yielded satisfactory results. Similarly,

Bheel *et al*. (2021) reviewed works by various researchers on the use of CSA as a cementitious material in concretes, and they found that the inclusion of CSA improved compressive, split tensile, and flexural properties over time due to its pozzolanic nature. As a result, this study explores the possibility of utilising CSA as an alternative to asbestos in brake pad manufacturing.

Kaolin

Kaolin, also known as white clay or China clay, primarily consists of the mineral kaolinite with the chemical composition $Al_2Si_2O_5(OH)_4$. Its formation can occur through geothermal clay deposits or accumulated and stratified clay deposits (Olalere *et al*., 2019). The mineral's purest form displays a brilliant white hue, yet the clay typically exhibits varying hues determined by the mineral composition of the mining area. For instance, a reddish hue may arise from abundance of iron oxide sediments, whereas green tint is linked to the presence of decomposed plant. Additionally, it can display blue or brown colours due to the presence of other minerals.

This mineral finds extensive use in numerous domestic and industrial applications. The selection of kaolin for industrial purposes depends on various factors, involving precise specifications for the development of specific technologies (Nkoumbou *et al*., 2009). It is widely utilised in industries such as ceramics, medicine, and cosmetics. According to Sheikh *et al*. (2017), kaolin also exhibits the potential for use as a filler material in rubber composites.

Recent scientific research in Ghana concerning kaolin deposits has primarily concentrated on its application as a strengthening agent and raw material for producing firebricks and permeable filters (Yaya *et al*., 2017; Efavi *et al*., 2012). As a result, studies investigating the use of kaolin as reinforcement or filler material in the production of brake linings are scarce. Additionally, Aderiye (2015) proposed that kaolin clay can be utilised as a raw material for friction linings due to its heat-resistant properties; however, there has not been any significant work conducted to confirm his findings. Therefore, this study specifically selects kaolin to assess its potential for incorporation in brake pads.

The production and utilisation of kaolin in Africa, particularly in Ghana, has a long history that spans several centuries due to the widespread availability of the material. Among the

well-known kaolin deposits in Ghana, the ones at the Abandze – Saltpond by-pass in the Central Region, as reported by Efavi *et al.* (2012), and at Kibi in the Eastern Region are noteworthy. Yaya *et al*. (2017) also reported that Ghana has kaolin deposits in Assin-Fosu and Kumasi, found in the Central and Ashanti regions, respectively. Additionally, deposits can be found in the Volta Region, notably in a town called Anfoega.

3.3.3 The Lubricants Used in this Study

The primary lubricant selected for this study is graphite. It is chosen because, as reported by Osterle and Dmitrier (2016), it is the most extensively employed solid lubricant for various applications, including application in friction materials. As a solid lubricant, its function is to promote friction-free movement while preserving the composite's frictional performance. As indicated by Blau (2001), the effect of graphite on the frictional properties of brake pads can vary contingent upon its structural variants, impurities, and prevailing environmental factors.

Graphite is a dark gray to black, soft mineral with a metallic lustre, often occurring in flakes due to the sheet-like arrangement of its atoms (Rehren, 2003). It represents the most stable and crystalline form of carbon, demonstrating ability to withstand thermal shocks and intermediate electrical conduction. Unlike melting, graphite undergoes sublimation at temperatures well above 3000 ^{o}C. Although it occurs naturally in the Earth's crust, it can also be artificially manufactured from petroleum coke using an electric furnace.

According to Su et *al.* (2015), well-defined mixtures of graphite and copper powder can yield a high coefficient of friction for friction pads. Similarly, Melcher and Faullant (2000) reported that combining lubricants such as graphite with certain metallic sulphides and oxides (e.g., copper oxides) produces superior tribological results compared to using a standalone lubricant. Nicholson (1995) also mentioned that copper powder can function as a lubricant to control heat transport in friction materials. Thus, copper powder is utilised as a second lubricant in this study. It possesses softness, malleability, and ductility, along with exceptional ability to conduct heat and electricity. Furthermore, it exhibits a distinctive red-orange colour and has a melting point of about 1085 ^{o}C.

According to the Geological Survey of Africa, graphite is primarily found in Cameroon, Kenya, and Nigeria (Nwobi, 2002). However, in 2012, a significant graphite deposit was

discovered in northern Ghana, specifically in Kambale – a town located in the Upper West Region, approximately 6 km from Wa (the regional capital). The discovery was made by Castle Minerals Limited from Australia. The deposit is estimated to be 14.4 million tonnes at 7.2 % (graphite carbon), with 1.03 million tonnes of graphite inferred resources, thereby offering the potential for its utilisation in Ghana.

3.3.4 The Abrasives Used in this Study

In this study, aluminium, kaolin, and zinc are intended to function as abrasive materials. Their role is to preserve the cleanliness of contacting surfaces and regulate the accumulation of friction films.

Aluminium

Aluminium is a silvery-white metal with a melting point of 660.3 ^{o}C. It is one of the lightest metals in the world, yet also remarkably strong and corrosion resistant. Additionally, it possesses high specific heat and excellent thermal conductivity (Rettig *et al*. 2020). Being the most cost-effective and widely used material in the family of engineering ceramics, it is readily available and reasonably priced. Due to its affinity for binding with other elements, aluminium finds extensive applications across various industries (Rettig *et al*. 2020). In this study, aluminium powder is selected as it quickly forms a thin, hard film of aluminium oxide when exposed to air. Aluminium oxide, also known as alumina, ranks among the most widely used abrasives in brake pads. Kaolin is also expected to act as an abrasive in the PSP/K formulation. Numerous studies, including the one conducted by Sennett (1990), demonstrate that dry kaolin powder possesses abrasive properties that even increase with rising temperatures.

Zinc

It is a bluish-white lustrous metal with a melting point of 420 ^{o}C. It possesses good elasticity and malleability properties and has a high heat capacity, making it an efficient conductor of heat. Zinc was chosen as an abrasive due to its rapid reaction with air, forming a dull grey zinc oxide (ZnO). Zinc oxide has demonstrated excellent abrasive properties, as confirmed by several researchers, including Casamassa *et al*. (2019). According to Nicholson (1995), ZnO also functions as a lubricant, but its use must be controlled to avoid drum polishing.

3.3.5 The Binder Used in this Study

The binder utilised in this study comprises epoxy resin combined with a hardener. Its purpose is to securely hold the components of the brake pads together thereby preventing them from disintegrating. Epoxy resin is widely employed as a binder in commercial brake pads worldwide. It is chosen for its excellent bonding strength with graphite and vice versa. Epoxy resins have the advantage of not emitting chemical residues during curing, resulting in limited curing shrinkage. Additionally, they exhibit superior adhesion to other substrates, excellent environmental resistance, favourable chemical properties, and effective insulating characteristics. Manufacturers generally produce epoxy resins by reacting Epichlorohydrin (ECH) with bisphenol A (BPA), although alternative raw materials may be used to replace the latter, resulting in different resins depending on the ratio of the two. While pure epoxy resin binders degrade at temperatures above 260 ^{o}C (*Tsang et al.,* 1985), modified epoxy resins can withstand temperatures of up to 400 ^{o}C, providing enhanced frictional stability. Consequently, they are widely employed in resin-based brake pads.

3.4 Materials Processing

The periwinkle shell, coconut shell, and kaolin, which are the main materials used, undergo the following processing steps:

3.4.1 Processing of the Periwinkle Shell

Although the periwinkle shells collected were parts of a heap left in the open for more than six months and were fully dried, they were further spread in the sun for two days to reduce their moisture content. Subsequently, they were oven-dried at 110 ^{o}C for 5 hours to ensure proper drying. The dried shells were then control-crushed using a hammer. Secondary and tertiary crushing were performed using a Metso jaw crusher (4×6″ type) and a Denver cone crusher (911MPE-TM-LCC21), respectively, to produce particle sizes between 2 mm and 1 mm. Next, the material was milled. The crushed samples were ground for 60 minutes in a cascading ball mill (BICO type) with approximately 15 kg of steel balls to obtain fine powders. The milled product was screened into four particle sizes: 106 µm, 150 µm, 212 µm, and 300 µm, using a Retsch mechanical stacking-type vibratory sieve shaker AS 200 for 30 minutes, with the sieve having the finest mesh size at the bottom. All these processes were carried out in the Minerals Engineering Laboratory at the University of Mines and

Technology (UMaT), Tarkwa, Ghana. Figure 3.2 shows the type of periwinkle shell used, while Figure 3.3 displays the periwinkle powder obtained after processing.

Figure 3.2 Type of Periwinkle Shell Used

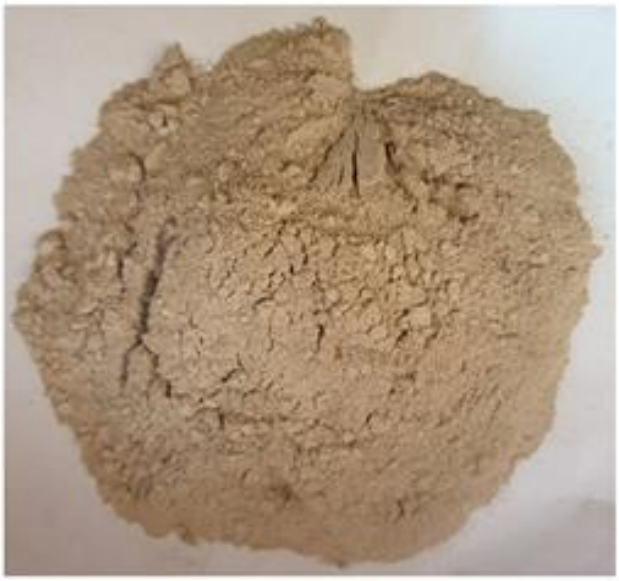

Figure 3.3 Periwinkle Shell Powder

3.4.2 Processing of the Coconut Shell

The coconut shells were carefully sorted to remove any spoilt shells that might have been bagged together with the good ones, and the fibres attached to the shells were completely removed. Subsequently, the shells were loaded into an off-cut cylindrical steel drum and

burnt in an open setting. After the burning process, the red-hot residues were allowed to cool in the drum for a day. The resulting ash and carbon were then collected and separated using a 1.00 mm ASTM sieve. The gray ashes were further collected and sieved into particle sizes of 106 µm, 150 µm, 212 µm, and 300 µm using the vibratory sieve shaker. All these processes were conducted at the Foundry Workshop of the Federal Institute of Industrial Research, Oshodi (FIIRO) in Lagos, Nigeria. Figure 3.4 depicts the type of coconut shells used, while Figure 3.5 displays the coconut shell ash obtained from the process.

Figure 3.4 Type of Coconut Shells Used

Figure 3.5 Coconut Shell Ash

3.4.3 Processing of the Kaolin

The kaolin, as obtained, was sundried for two days, and subsequently dried in an oven at 100 ^{o}C for a period of 5 hours for complete moisture content removal. Subsequently, it was milled for 50 minutes in a tumbling ball mill using approximately 15 kg of steel balls to procure fine granules. After grinding, the powder was screened through 106 µm, 150 µm, 212 µm, and 300 µm sieves for 30 minutes using a vibratory sieve shaker. All these processes were carried out in the Minerals Engineering Laboratory at the University of Mines and Technology (UMaT), Tarkwa. Figure 3.6 depicts the kaolin ore used, while Figure 3.7 displays the kaolin powder obtained from the process.

Figure 3.6 Kaolin Ore

Figure 3.7 Kaolin Powder

3.4.4 Other Materials

The remaining materials, including graphite, copper powder, zinc powder, aluminium powder, and the epoxy resin binder, were sourced from the market and did not undergo any further processing. Figure 3.8 to Figure 3.11 display the graphite, copper powder, zinc powder, and aluminium powders used, respectively.

Figure 3.8 Graphite

Figure 3.9 Copper Powder

Figure 3.10 Zinc Powder

Figure 3.11 Aluminium Powder

3.5 Characterisation of the Indigenous Raw Materials

The primary objective of the characterisation of the primary materials was to establish a comprehensive understanding of the properties of these materials, namely periwinkle shell powder, coconut shell ash, and kaolin, which are utilised in the formulations. The aim was to assess their influence on the performance of the intended friction lining. The raw materials underwent various chemical and morphological tests, including X-Ray Fluorescence (XRF), X-Ray Diffraction (XRD), Differential Scanning Calorimetry and Thermogravimetric Analysis (DSC-TGA), and Scanning Electron Microscopy and Energy Dispersive Spectroscopy (SEM-EDS). Additionally, physical and mechanical tests were

conducted, which involved determining bulk densities, dry compressive strength, and dry shear strength. The microstructure and elemental information acquired for each primary material were gathered and documented for future reference in the analysis phase.

3.5.1 XRF Analysis of the Materials

This non-invasive analytical method determines the chemical makeup of materials like rocks, minerals, sediments, and fluids. XRF analysis of the powders (raw materials) was performed using a Genius-IF EDXRF spectrometer located at the Yaba College of Technology laboratory in Lagos, Nigeria. Approximately 5 g of pulverised sample was placed in a thin film covered cup, filled to a third of the cup's capacity, and securely sealed to prevent leakages or loose particles. The sample was then inserted into the sample turret, and the X-ray Lamp was powered, allowing 2 minutes for stabilization. The RUN tab was used to set the voltage and emission current values to ensure an observed dead time between 35 – 40 kV. The analysis was then executed to obtain the spectrum data. Refer to Figure 3.12 for the Genius IF spectrometer setup.

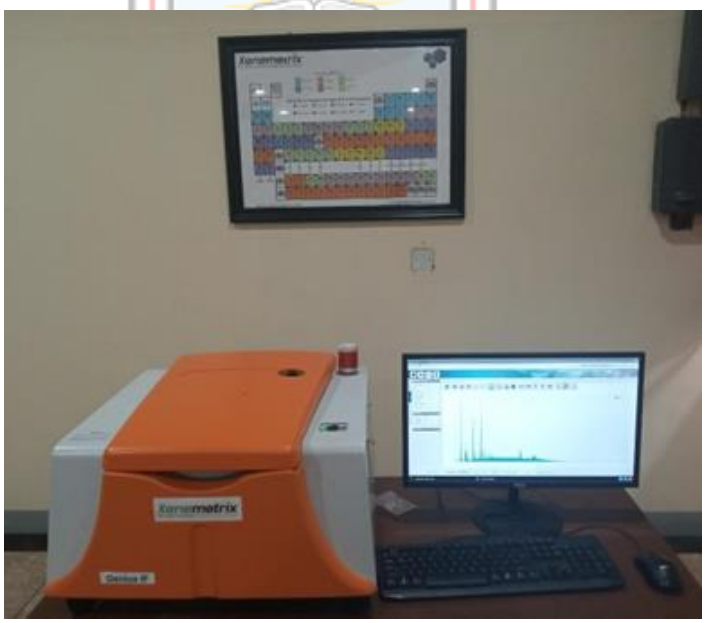

Figure 3.12 Genius IF Spectrometer Set-up

3.5.2 XRD Analysis of the Materials

This test employs a non-invasive analytical method to provide comprehensive information about the lattice arrangement, elemental makeup, and material characteristics. The X-ray diffraction (XRD) pattern, representing the intensity of X-rays scattered at various angles

by a sample, was obtained using the Goniometer MiniFlex 300/600 at the Materials Laboratory of the University of Lagos (UNILAG) in Nigeria.

For analysis, the material was thoroughly powdered, homogenised, and its mean bulk composition was established. The XRD analysis utilised a dual-mode sample holder and theta-theta settings, with a 2θ starting position of 4 degrees and ending at 75 degrees, in increments of 0.026261 at 8.67 seconds per step. The tube current was set to 40 mA, and the tension to 45 VA. A divergent slit equipped with a 5 mm wide mask was employed. During the analysis, continuous measurements were taken for the intensity of diffracted X-rays as both the detector and sample were angularly adjusted. Figure 3.13 illustrates the MiniFlex XR - Diffractometer used in the experiment.

Figure 3.13 MiniFlex XR-Diffractometer Set-up

3.5.3 DSC – TGA Analysis of the Materials

These tests involve techniques used to identify and quantitatively characterise the chemical makeup of materials by monitoring their heat response as they are heated. The Thermogravimetric Analysis (TGA) method determines variations in sample weight with respect to temperature, while the Differential Scanning Calorimetry (DSC) measures the difference in heat transfer rate over temperature or time. A plot of weight or weight percentage against time or temperature is referred to as a thermogram or thermogravimetric curve.

The simultaneous DSC-TGA measurements were performed on powder samples utilising an SDT Q600 V20.9 Build 20 thermogravimetric instrument. A heating rate of 20°C per

minute was applied to the samples, starting from 30°C and reaching a top temperature of 950°C, with a nitrogen flow rate of 100 ml/min. An alumina crucible served as a control during the experiments. The DSC-TGA curves and other data were acquired and analysed using Pyris™ Software on a computer. The tests were conducted at the Department of Materials Science and Engineering, University of Ghana, Legon. Refer to Figure 3.14 for the thermogravimetric analyser used.

Figure 3.14 SDT Q600 V20.9 Build 20 Analyzer Set-up

3.5.4 SEM – EDS Analysis of the Materials

The morphological characteristics of the fundamental raw materials were obtained at the Environmental Laboratory of UMaT. This examination aims to investigate the materials' morphology, encompassing their shape, size, texture, and phase distributions. Energy Dispersive Spectroscopy (EDS) is an investigative method employed for determining the elemental composition or chemical properties of a sample. The micrographs were captured utilising a Carl Zeiss EVO MA 15 Scanning Electron Microscope (SEM). A secondary electron detector enables sample visualization under high vacuum conditions. For energy dispersive X-ray detection, a BRUKER QUATAX EDS system with XFlash Detector 610 M was utilised. To ensure optimal imaging due to the non-conductive nature of the samples, they were sputter coated using a g old/palladium target. SEM images of the specimens were

taken with voltage acceleration level of 4 kV and a working distance ranging between 9.5 mm to 10 mm. EDS spectra of the samples were collected at 20 kV. Figure 3.15 illustrates the equipment utilised in this study.

Figure 3.15 Zeiss EVO MA 15 SEM

3.5.5 Sample Preparation and Mechanical Characterisation

The raw powders were used for the untapped bulk density test, while for the other tests (dry density, dry compressive, and dry shear tests), the specimens were created by blending 150 g of each material (powders) with 5 g of water and sodium silicate (as binders). The mixture was then poured into a sample holder of Ridsdale Standard Laboratory Sand Rammer, conforming to a diameter of 50 mm and a height of 50 mm. Three consecutive ramming blows were delivered onto the mixture. The compacted samples were then removed from the holder and fired in a controlled oven environment at a specified temperature of 115 °C for a duration of 1 hour.

All the test samples with standard dimensions were prepared at the Sand Laboratory in the Foundry Department of (FIIRO) in Lagos, Nigeria. Figure 3.16 shows some of the samples produced from (a) CSA, (b) PS powder, and (c) kaolin powder.

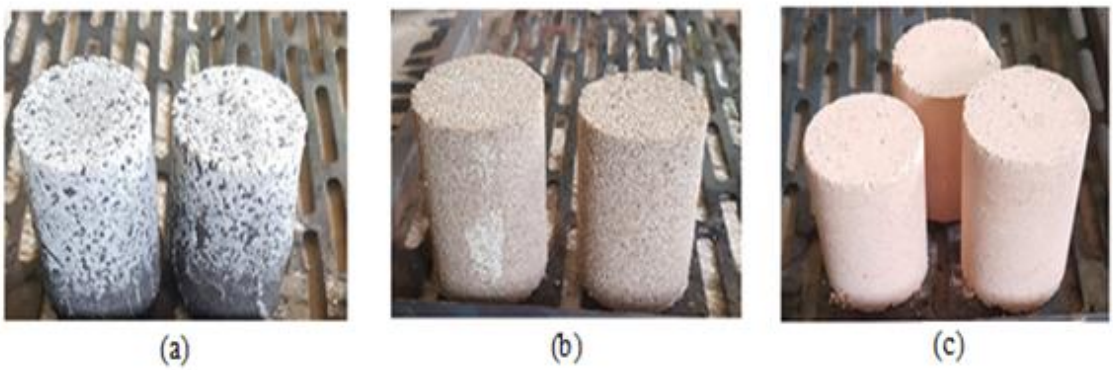

Figure 3.16 Samples Produced from the Three Raw Materials (a) CSA Samples (b) PS Powder Samples (c) Kaolin Powder Samples

Untapped bulk density

Approximately 100 g of each powder material was carefully weighed using a digital Ohaus analytical balance Model PA 224 with a readability of 0.0001 g. The weighed powders were gently poured through a laboratory sieve with a 1.0 mm aperture into a dry 250 mL cylinder, and the corresponding volumes were recorded. The test was conducted in accordance with ASTM-D7481-18 standard guidelines. The untapped densities were then calculated by dividing the weights by the volumes. The entire procedure was replicated three times to ensure accuracy, and the average values of the densities were determined.

Bulk dry density

The bulk dry density was obtained by weighing the samples using a digital balance, and their volumes were calculated based on their dimensions (50 mm diameter × 50 mm height). The densities were then calculated in g/cm^3 by dividing the sample weights by their corresponding volumes.

Dry compressive strength

The samples produced were placed between two compressive heads of a Ridsdale Universal Sand Strength Tester. A consistent load was then applied until fracture occurred, and the compressive strength value at the point of fracture was measured in kN/m^2. Three samples of each material were tested, and the average values were calculated and recorded.

Dry shear strength

The dry shear strength was assessed by placing the samples on the Risdale Strength Tester, between two shear heads, and applying a consistent load until the samples sheared. The corresponding values at that point were recorded in kN/m^2. Three samples of each material were tested, and the average values were calculated and recorded. Figure 3.17 depicts the Risdale Universal Sand Strength Tester.

Figure 3.17 Ridsdale Universal Sand Strength Tester

3.6 Optimal Formulations of the Brake Pad Materials

This section discusses the process of determining the optimal formulations for the brake pad materials through the utilisation of Design Expert Software, DX-13. The term "optimum" here denotes a specific combination of parameters obtained from controlled and sequential test conditions that yields superior performance qualities (Ibhadode and Dagwa 2008).

3.6.1 The Design Expert (DX-13) Software

Design Expert, a software package for statistical analysis developed by Stat-Ease Incorporated, is dedicated to conducting design of experiments (DOE). Numerous researchers, including Abutu *et al*. (2019), Chauhan *et al*. (2010), Harshvardhan *et al*. (2017), Oladosu *et al*. (2016), Radhika (2011), Ibhadode and Dagwa (2008), and Kim *et al*. (2003), have utilised this software for screening, characterising, and optimising various

effects. The software plays a crucial role in decision-making when all design, experimentation, and analysis steps are sequentially followed.

During the design stage, researchers plan the screening of factors and define the expected responses from the design. The experimental or characterisation stage involves step-by-step practical experiments, including sample measurements, preparations, and testing, to achieve the desired results for each response stated in the design. The analysis stage employs ANOVA (Analysis of Variance) technique, wherein the model is adjusted to achieve significant F and P values, helping determine the best factor combinations for optimisation. The optimisation process, whether for maximisation, target setting, or minimisation, can be accomplished numerically or graphically. Figure 3.18 depicts the DOE work environment.

Figure 3.18 The Design Expert DX 13 Work Environment

3.6.2 The Use of the Software for the Optimisation of the Formulations

For optimisation, the Box-Behnken option of the Randomized Design under Response Surface was employed. A range of percentage values, guided by Table 2.12 (Blau, 2001), was assigned to three numeric factors: filler materials, reinforcement material, and binder (as detailed in Table 3.1), while the percentages of lubricants and abrasives were held constant. This approach resulted in a set of 17 runs with diverse possible percentage formulations. Six test specimens were produced for each run using 106 μm particle size of

the reinforcement and filler materials, for both PSP/CSA and PSP/K combinations. Consequently, a total of 156 material samples were prepared.

These samples were characterised for eight different brake pad properties, namely, bulk density, apparent porosity, water and oil absorption, linear shrinkage, volume shrinkage, compressive strength, and hardness. The obtained test results served as the responses in the software's ANOVA tool. The optimum formulations for both the PSP/CSA and PSP/K combinations were then derived from the ANOVA analysis, as shown in Table 3.2 and Table 3.3, respectively. Detailed test results of the samples are presented in Appendix A

Table 3.1 Range of Percentage Values Assigned to the Numeric Factors

Numeric Factor	Name	Unit	Level	
			Minimum	Maximum
A.	Periwinkle Shell Powder (PSP)	%	26.00	45.00
B.	Coconut Shell Ash (CSA)	%	26.00	45.00
C.	Epoxy Resin (ER)	%	15.00	25.00

Table 3.2 Optimum Brake Pad Formulation for PSP/CSA Combination

Materials	Amount (wt. %)
Periwinkle Shell Powder	23.97
Coconut Shell Ash	41.48
Epoxy Resin Binder	23.05
Graphite	5.50
Copper Powder	2.00
Aluminium Powder	2.50
Zinc Powder	1.50

Table 3.3 Optimum Brake Pad Formulation for PSP/K Combination

Materials	Amount (wt. %)
Periwinkle Shell Powder	40.36
Kaolin Powder	34.69
Epoxy Resin Binder	13.45
Graphite	5.50
Copper Powder	2.00
Aluminium Powder	2.50
Zinc Powder	1.50

3.6.3 The Optimisation Procedure using the Box- Behnken Technique

The optimisation procedure for the brake pad formulations is as follows:

To initiate the Design Expert DX 13 software, you will first need to click on the Desktop shortcut, launching version 13.0.1.0. Once launched, you will be presented with several options: 'New Design Tab,' 'Open Design,' 'Import Data,' and 'Design Wizard.'

Choose the 'New Design Tab' to begin the process. On the feature panel situated to the left, navigate to 'Response Surface' and select 'Random Response.' Subsequently, select 'Box-Behnken.'

Specify the number of numeric factors, then select 'Horizontal' and complete the displayed table with all the necessary information. The software will automatically calculate the number of runs required for the experiment. Click 'Next' to proceed.

In the next step, select the number of desired responses and their units (within the range of 1-999). Click 'Finish' to continue.

Now, it's time to prepare samples in accordance with the generated experimental data. Ensure that the instructions closely followed for accuracy.

Supply all the necessary response data as per the experimental results. This data will be vital for the analysis and interpretation of the study.

Navigate to the note, summary, graph column, and evaluation tabs on the navigation panel to view the information. All the responses you have supplied will be enlisted under analysis. Click on the first response to begin.

Proceed to 'Configure' and 'Fit Summary,' then move on to the 'Model and ANOVA.' Ensure that the model is adjusted to make it statistically significant.

Click on the 'Diagnostics' and 'Model Graphs' tabs within the window.

Next, access the 'View' tab in the toolbar and navigate to 'New Graph.' Select your preferred graph display type, such as '3D surface cube,' 'One factor,' 'All factors,' 'Perturbation,' 'Contour,' 'Pred. vs. Actual,' '3D surface,' or 'Cube.'

3.7 Preparation of the Test Samples

All test samples were fabricated using the conventional procedure known as dry formulation (Powder Metallurgy). This process involves compressing powder materials at ambient temperature to neglect the thermal deformation mechanisms, like diffusion creep and distortion. Careful weighing of the various components was done using an Ohaus digital balance, and they were placed into small stainless-steel plates. The fillers, reinforcement, abrasives, and friction modifiers were thoroughly dry mixed inside the plates for ten minutes. Later, the binding agents (epoxy and the hardener mixture) were added in a ratio of 2:1 and mixed with the other components for an additional five minutes to achieve a semi-paste-like homogeneous mixture.

After the mixing process, the semi-paste was compressed and moulded into shape at room temperature using a pressure of about 3 bars, utilising a 100-ton Weber hydraulic press, Model P100EH. A vertical steel die with a closed end (bottom sealed by a pressing tool) and a cavity diameter of 25 mm was employed. WD-40 spray acted as a lubricant for the matrix walls to facilitate the extraction of the compacted samples. All samples were then dried for a week, followed by oven drying at a temperature of 150 °C for 2 hours to ensure complete curing of the entire brake specimens. The oven was subsequently powered down and left to cool to room temperature naturally after a day, Afterward, the samples were removed. Measurements were taken for all samples' dimensions using a Mitutoyo Vernier Calliper 530-105 Standard Model before and after the curing process. Figure 3.19 (a) and

(b) showcase some of the produced test samples for both PSP/CSA and PSP/K formulations, respectively.

Figure 3.19 Produced Samples Showing (a) PSP/CSA (b) PSP/K Samples

3.8 Test Samples Characterisation

All the test samples undergo the following tests: Bulk Density, Water Absorption, Oil Absorption, Apparent Porosity, Linear Shrinkage, Volume Shrinkage, Hardness, and Compressive Strength.

3.8.1 Bulk Density Test

Density is a quantitative measure of the 'heaviness' or mass per unit volume of objects, which remains constant even as the volume changes. To determine the density of the samples, dried weights (DW) were initially measured using the Ohaus analytical balance. Subsequently, the volume of the samples was determined through the water displacement method, following the guidelines of Malaysian Standard MS 474: 2003.

The procedure involved suspending the samples by a thread in a 250 ml measuring cylinder filled with water, and the volume of the water displaced ($V_{displaced}$) was then measured in cubic centimeters (cm^3). The bulk density was calculated using Equation 3.1.

$$\text{Bulk Density} = \frac{DW}{V_{displaced}} \qquad 3.1$$

3.8.2 Water Absorption Test

The water uptake of the specimens was assessed in accordance with ASTM D570 standards. Firstly, the weights of the oven-dried and cooled samples were measured using a digital weighing machine. Subsequently, the samples were immediately immersed in water at ambient temperature for a duration of 24 hours. Afterward, the samples were taken out, cleaned, and new weights were recorded. The water absorption was then determined using Equation 3.2.

$$\text{Water Absorption} = \frac{\text{SW} - \text{DW}}{\text{DW}} \times 100\ \% \qquad 3.2$$

where, SW = Weight of sample after being soaked in water, (g)

DW = Dry weight of the samples, (g)

3.8.3 Oil Absorption Test

The initial weights of the oven-dried and cooled samples were measured in grams using the digital analytical weighing machine. Subsequently, the samples were promptly immersed in SAE 40 Oil under ambient conditions for a duration of 24 hours. After this soaking period, samples were taken out, cleaned, and weighted. The change in weight due to oil absorption is then calculated using Equation 3.3.

$$\text{Swell in Oil} = \frac{\text{SW} - \text{DW}}{\text{DW}} \times 100\ \% \qquad 3.3$$

where, SW = Weight of sample after being soaked in oil, (g)

DW = Dry weight of the samples, (g)

3.8.4 Apparent Porosity Test

Porosity refers to the volume fraction of voids within a material in relation to the total volume. These cavities, known as pores, can be either open or enclosed and vary in dimensions, configuration, and arrangement. The dry samples were initially weighed and subsequently immersed in water at ambient temperature for a duration of 24 hours. After the soaking period, the samples were taken out, cleaned, and their new weights were recorded. To determine the apparent porosity, the soaked samples were suspended by a

thread in a measuring cylinder filled with a known amount of water, and the displaced weights were measured. Equation 3.4 was then used to calculate the apparent porosity:

$$\text{Porosity} = \frac{\text{SW}-\text{DW}}{\text{SW}-\text{SSW}} \times 100\ \% \qquad 3.4$$

where, DW = Weight of the dried samples, (g)

SW = Weight of the samples after being soaked in water, (g)

SSW = Weight of the soaked samples when suspended in water, (g)

3.8.5 Linear Shrinkage Test

With the dimensions of the samples measured earlier both before and after oven drying using the digital Vernier calliper, the linear shrinkage was calculated using Equation 3.5.

$$\text{Linear Shrinkage} = \frac{\text{Initial height}-\text{Final height}}{\text{Initial height}} \times 100\ \% \qquad 3.5$$

3.8.6 Volume Shrinkage Test

Using the dimensions of the samples (diameter, D, and height, h) obtained earlier, the initial volume (V_o) and the final volume (V_f) of the samples were calculated using the formula $V = \pi D^2 h/4$ and recorded. The volume shrinkage was subsequently determined using Equation 3.6.

$$\text{Volume Shrinkage} = \frac{V_0 - V_f}{V_o} \times 100\ \% \qquad 3.6$$

3.8.7 Brinell Hardness Test

The hardness of the samples was determined through the Brinell hardness test. The test was conducted using the WP 300, 20 kN – GUNT Hamburg Universal Material Tester (Figure 3.20) in compliance with ASTM standard E10 – 18 specifications. A hardened steel ball with a diameter of 10 mm was employed to indent the test specimens. The applied load was kept constant at 1000 kgf. Using a magnifying glass and an optical micrometer screw gauge, the indentation diameter was recorded along two orthogonal directions, and the mean of these values was either cross-referenced with the applied force in a Standard Brinell Hardness Conversion Table or utilised in Equation 3.7 to determine the Brinell Hardness Number (BHN).

$$H_B = \frac{2 \times F}{\pi D\left(D - \sqrt{D^2 - d^2}\right)} \quad 3.7$$

where, H_B = Brinell Hardness Value

D = The ball diameter, (mm)

d = The diameter of the indentation, (mm)

F = The applied load, (kgf)

Figure 3.20 GUNT Hamburg Universal Material Tester

3.8.8 Compressive Strength Test

This test was performed using the Testometric testing machine (M500 – 25 kN), Model OL11INR, in accordance with ASTM Standard D3410. The fired samples were positioned between two compressive heads and subjected to continuously increasing compressive forces at a rate of 100 mm/min up to failure. To obtain accurate results, three different samples from each run were tested, and the mean values were recorded. The loads and stresses at which failure occurred, along with their mean values, were displayed on the monitor after the test, using the fully integrated winTest Analysis materials testing software. Figure 3.21 illustrates the type of Testometric machine used in the experiment.

Figure 3.21 Testometric Testing Machine

3.9 Preparation and Further Characterisation of the Actual Brake Pad Samples

Using the optimised formulations presented in Table 3.2 and Table 3.3, a total of 24 brake pad samples, consisting of both PSP/CSA and PSP/K combinations, with varying particle grading (106 μm, 150 μm, 212 μm, and 300 μm) of the base materials were manufactured. The production process adhered to the methodology detailed in Section 3.7. Subsequently, the samples were subjected to a comprehensive analysis of their physical and mechanical properties, following the test procedures outlined in Section 3.8. Moreover, the tribological (wear rate and coefficient of friction), morphological, and heat characteristics of the specimens were determined.

To gauge their performance, the test results were benchmarked against asbestos-based brake pads, certain commercial aftermarket replacement pads, and brake pads developed from prior research endeavours. Based on these comparisons, the most suitable particle sieve sizes among the four options for each of the two formulations, were selected. These selected particle sizes were then employed to produce the final brake pads, tailored to match the dimensions of a Toyota Camry 2000 Model, using the appropriate mould. These brake pads underwent on-road testing to assess their performance under real-world conditions.

3.9.1 Determination of Coefficient of Friction and Wear Rate of the Pads

The samples underwent frictional and wear performance evaluations utilising Anton Paar GmbH TRB 3 ball and disc type Tribometer Version 6.1.19 (Figure 3.22) located at Ahmed Bello University (ABU) in Zaria, Nigeria. These tests were conducted under ambient temperature conditions of 29 °C and 55 % relative humidity. The setup was based on the pin-on-disc test concept, complying with the ASTM G 99 accepted guidelines.

Cylindrical pins, with dimensions of 10 mm diameter and 15 mm height, were weighed using an electronic balance with a single pan, accurate up to of 0.0001 units. The tests were carried out at loads of 3 N and 8 N, and at velocities of 5 m/s and 10 m/s to obtain average values, over a constant sliding distance of 50 m. The test specimens were mounted in the jaw chuck of the machine, and the load arm was lowered until it made contact with the sample's surface. Subsequently, the tribometer was activated, and the frictional behaviour, including the mean coefficient of friction, was automatically recorded and displayed by the tribometer software.

Upon completing the constant sliding path, the specimens were extracted, subjected to acetone cleaning, followed by drying and re-weighing to ascertain the loss of weight resulting from wear. The rate of wear for the brake specimens was then calculated using Equation 3.8.

$$\text{Wear Rate} = \frac{\Delta W}{S} \qquad 3.8$$

where, ΔW = the weight difference of the sample before and after the test in kg; and

S = total sliding distance in m.

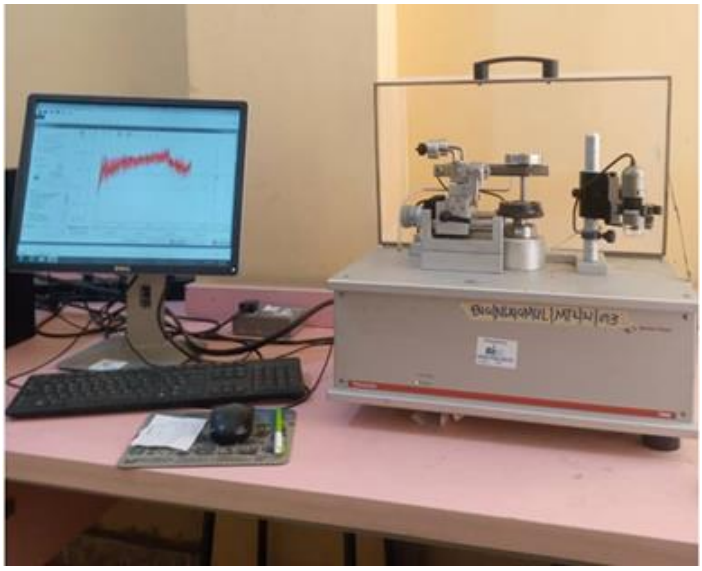

Figure 3.22 Anton Paar TRB 3 Tribometer Ball-On-Disc Type Set-up

3.9.2 SEM – EDS Analysis of the Pad Samples

The morphological characteristics of the brake pad specimens were examined at UNILAG. A Field Emission Gun Scanning Electron Microscope (FEG-SEM), specifically the JEOL JSM 7600 F model furnished with an EDS analyser (as depicted in Figure 3.23), was utilised for this purpose. To prevent charging and enhance imaging, the samples were coated with platinum and securely mounted on the specimen stub. The SEM operated at an accelerating voltage of 15 kV.

Figure 3.23 JEOL JSM 7600 F SEM

3.9.3 TGA – DTA Analysis of the Pad Samples

Thermal analysis was performed on the brake pad samples using a PERKIN ELMER TGA 4000 thermal analyser under a controlled inert atmosphere. The specimens were subjected to a heating rate of 10 °C per minute, starting from 30 °C up to an upper temperature of 950 °C, followed by cooling to ambient temperature. As a reference, an alumina (aluminium oxide) disc was employed. The TGA and DTA plots were generated by a computer with Pyris™ Software at intervals of 4 seconds. The DTA test was carried out at UNILAG in Nigeria. Figure 3.24 illustrates the TGA and DTA Analyzer used for the analysis.

Figure 3.24 TGA and TDA Analyzer Set-up

3.10 Design of Brake Pad Permanent Mould

In this section, the design parameters and the process employed to create the permanent mould for manufacturing the brake pads are examined. The dimensions of the mould are specifically tailored to match the dimensions of a Toyota Camry saloon car from the 2000 Model.

3.10.1 The Design Parameters

The Camry pad shown in Figure 3.25 provides the indicated parameters used for designing the mould.

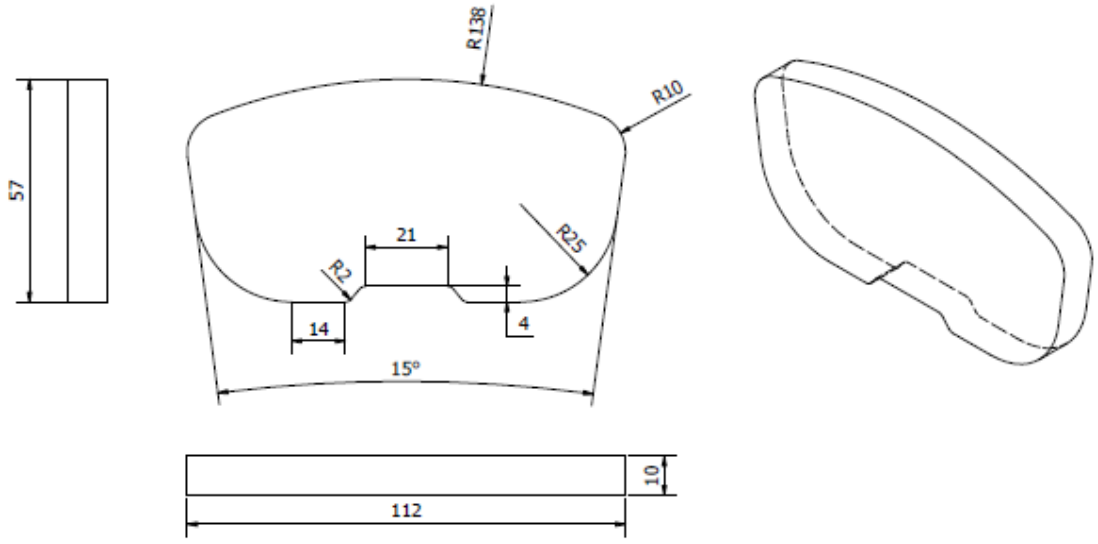

Figure 3.25 Dimensions of Brake Lining of a 2000 Model Camry Saloon Car

3.10.2 The Design Procedure

The 3D design drawing was created using Creo Parametric 7.0.2.0 software, which is developed by Parametric Technology Company. Here is the step-by-step design procedure:

Commence by initiating the software application found on the desktop. Subsequently, establish a dedicated working directory for your project.

Now, within the application, proceed to create a new part. Input a suitable file name, confirm your selection with an 'OK.' Choose the plane you intend to utilize and configure it to your specifications.

Select the line tool from the available toolbar and employ it to create a 2D representation of the plate's dimensions. After completing the sketch, discontinue the use of the selected tool. Shift your attention to the extrude tool.

Specify the extrusion thickness, which will result in a 3D representation of the plate. Sketch and save each part individually as needed.

For assembly, initiate a new assembly project. Utilize the assembly icon to combine the saved parts as you desire. It is essential that the first part you select be defined as the default. Configure the other parts based on your preferences, whether it be automatic, distance-

based, fixed, rigid, coincident, or following other specifications, and save the assembly configuration.

Next, create a new drawing. Opt for the A4 drawing format, which will prompt the system to automatically generate the orthographic views. Make use of the annotation icon to add precise dimensions to the drawing.

To conclude your project, navigate to the 'File' menu and choose the "Save as" option. Select 'Export PDF' to transform your design into PDF format, facilitating easy sharing and access.

3.11 Brake Pad Permanent Mould Development

The fabrication of the brake pad mould was carried out in the machines tool laboratory/machine shop of FIIRO in Lagos, Nigeria. Mild steel plates measuring 500 by 156 by 10 mm and 500 by 150 by 6 mm, along with 14 by 50 mm diameter solid rods procured from Owode Onirin in Lagos, Nigeria, were used in the mould fabrication process. The selection of materials for the permanent mould production was primarily based on the temperature of the feeding materials and the type of envisaged final product. Key material properties taken into consideration included good thermal conductivity, efficient fluid absorption (for slurry materials), excellent machinability, and ability to withstand stresses.

The construction of the mould involved utilising the following steps and tools:

A 6 mm thick plate was marked using a scriber, steel rule, and a power arc saw, resulting in dimensions of 305 by 156 mm. Similarly, a 10 mm thick plate was cut into the dimensions of 290 by 148 mm.

The 305 by 156 by 6 mm plate was marked at its center to accommodate the backing plate of a standard product. This marked point was chain-drilled using a ¾ capacity tabletop drilling press machine known as the EFICO machine tool.

Following the drilling operation, the cut portion of the plate was smoothed using a die grinder (PDG 4003) with a 400 W motor, ø6 mm, operating at 220 – 240 V, 50/60 Hz, and at speeds ranging from 1500 to 2600 rev/min.

Similarly, the 290 by 148 by 10 mm plate was marked at its center to house the brake pad compounded materials. The mark out point was also chain drilled and then smoothed using the die grinder.

Both plates, the 305 by 156 by 6 mm and the 290 by 148 by 10 mm, were drilled at equidistant points from their edges to accommodate 14 mm rods for added rigidity.

Two pieces, each measuring 102 mm in length and 14 mm in diameter, were cut from the mother materials and subsequently welded to the backing plate mould.

The press was produced from the 10 mm thick off-cut material by chain drilling and smoothing. Finally, a surface finishing operation was conducted, and the mould components were assembled.

3.12 Brake Pad Backing Plate Preparation

The structural integrity of brake pads primarily relies on a metal support plate. In an intricate procedure, 10 - 20 different formulations of materials or powdered ingredients, known as friction materials, are compressed onto the backing plate. This section of the brake pad, with its final shape and dimensions, is commonly known as the brake lining (Kemmer, 2002). To enhance the bonding strength and damping behaviour of the friction lining, a distinct composition under layer is inserted between the support plate and the friction material, prior to pressing.

On the opposite side of the support plate, there is often a thin shim known as an insulator, which is attached to reduce emitted noise. For this study, used Toyota Camry 2000 model backing plates were selected from three different locations around FIIRO in Lagos, Nigeria: NITEL, Ilupeju, and Toyota auto shop mechanics village. The worn-out composite materials on the backing plate were carefully chipped out using a handheld ball pen hammer, and subsequently, the plates were thoroughly cleaned with abrasive paper.

3.13 The Actual Brake Pad Production

The steel backing plate was coated with a binder to ensure a secure adhesion of the lining material to its surface. It was then placed into the backing plate holder. The homogeneous paste-like mixture was transferred into the mould and subjected to multiple pressings with

an axial loading of approximately 50 bars using a 100-ton P100EH Weber – hydraulic press. Once fully pressed, the product was removed from the mould and allowed to air dry for 72 hours.

Next, a heat groove was carefully cut into the lining material to a depth of around 3 mm using a grinding machine. The pad was subsequently heated in an oven at a temperature of 150 °C for two hours. After cooling, a grinding machine was utilised to level the surface of the pads, achieving a desired thickness of 10 mm and providing a fine surface finish.

3.14 Performance Evaluation (Real Life Test)

The live test of the newly developed brake pads involved using a Toyota Camry saloon car of the 2000 model. Both the commercially available Camry brake pad (obtained from dealers) and the developed brake pads were weighed together, including their backing plates. Subsequently, they were installed on the front discs of the car – a pair of the commercial pad on the left disc and a pair of the developed pads on the right disc of the vehicle.

The car was then started and driven until reaching speeds ranging from 20 km/hr to 100 km/hr in 20 km/hr increments. During the test, the vehicle was brought to rest after reaching each speed using normal braking, and the temperatures of the discs were measured and recorded using a Digital Multitester UNI-T UT 533, which has a temperature range of -40 ºC to 537 ºC. The measurements were taken twice for accuracy, and averages were obtained.

Subsequently, the brake pads were left installed on the car for a month, allowing them to be used in real conditions. Afterward, they were removed from the callipers, and their weights were measured again to determine the amount of wear they experienced during the testing period.

3.15 Characterisation of Some After-Market Sales Commercial Brake Pads

For comparison purposes, the mechanical, tribological, and thermal properties of two after-market sales commercial brake pads were obtained. The mechanical characteristics of the brake pads were assessed at both FIIRO and UMaT, following the test procedures stated in Section 3.8 of this report. The thermal behaviour of the pads was assessed at the University of Ghana, Legon, using the test procedure outlined in Section 3.5.3 of this report.

To determine friction coefficient and rate of wear of the pads, Envaserv Research Consult Tribology Laboratory in Accra was utilised, employing a Universal Friction and Wear Testing Machine UW-1000. The test equipment, apparatus, and sample preparation were carried out following the procedures outlined in ASTM D3702-94 (2009).

Initially, a testing load of 89.2 N and a rotation speed of 180 rpm were selected for the tests. Subsequent tests were conducted on the sample pads at 300 N and 600 rpm, as well as at 480 N and 180 rpm. Figure 3.26 displays the setup of the Universal Friction and Wear Testing Machine.

Figure 3.26 Setup of the Universal Friction and Wear Testing Machine

CHAPTER FOUR

RESULTS AND DISCUSSION

4.1 Introduction

This chapter begins with the characterisation of the fundamental raw materials: coconut shell ash, periwinkle shell powder, and kaolin. Subsequently, the mould's depiction and its operational mode is presented. The outcomes of the material formulation, carried out using the Design Expert DX 13 software, along with the examination of the impact of particle dimensions on the various brake properties measured, are discussed.

Furthermore, a comparison is made between the experimental findings of the developed brake pads and those previously developed by other researchers, as well as with selected commercial brake pads and an asbestos-based brake pad. Lastly, the chapter concludes with a discussion of the results obtained from the live test of the brake pads on a vehicle.

4.2 Characterisation of the Basic Raw Materials

In this section, the three raw materials are characterised in terms of their mechanical, chemical, morphological and thermal properties.

4.2.1 Physical Characterisation of the Raw Materials

Table 4.1 shows the bulk densities, dry compressive and dry shear values of the CSA, PSP and the kaolin powder.

Table 4.1 Some Mechanical Properties of the Raw Materials

Material	Untapped Bulk Density (g/cm^3)	Dry Bulk Density (g/cm^3)	Dry Compressive Strength (kN/m^2)	Dry Shear Strength (kN/m^2)
PSP	1.316	1.718	350	155
CSA	0.833	1.273	120	90
Kaolin	1.250	1.457	250	160

The PSP exhibits the highest untapped bulk density at 1.316 g/cm^3, followed by kaolin at 1.250 g/cm^3 and CSA at 0.833 g/cm^3. Additionally, the PSP exhibits the greatest dry bulk density at 1.718 g/cm^3, while kaolin follows at 1.457 g/cm^3 and CSA at 1.273 g/cm^3.

Regarding compressive strength, the same trend is observed, with PSP having the highest value of 350 kN/m^2 and CSA the lowest at 120 kN/m^2. However, the shear strength shows a different pattern, with kaolin exhibiting the highest shear strength of 160 kN/m^2 and CSA the lowest value of 90 kN/m^2.

Notably, asbestos has a dry bulk density of 2.22 g/cm^3 according to Chand *et al*. (2004), while Kusiorowski *et al*. (2012) reported the bulk density of asbestos fibres to range between 2.4 g/cm^3 and 2.6 g/cm^3. Comparatively, this indicates that CSA, PSP, and kaolin are all lighter than asbestos, making them more suitable as filler or reinforcement materials in brake linings. Consequently, the use of these three materials would result in lighter brake lining.

4.2.2 Chemical Characterisation of the Raw Materials

In Figure 4.1, 4.2, and 4.3, the XRD patterns of the PSP, the CSA, and the kaolin powder are presented, respectively. Additionally, the results of the XRD quantitative analysis for each powder are shown in Table 4.2 – 4.4.

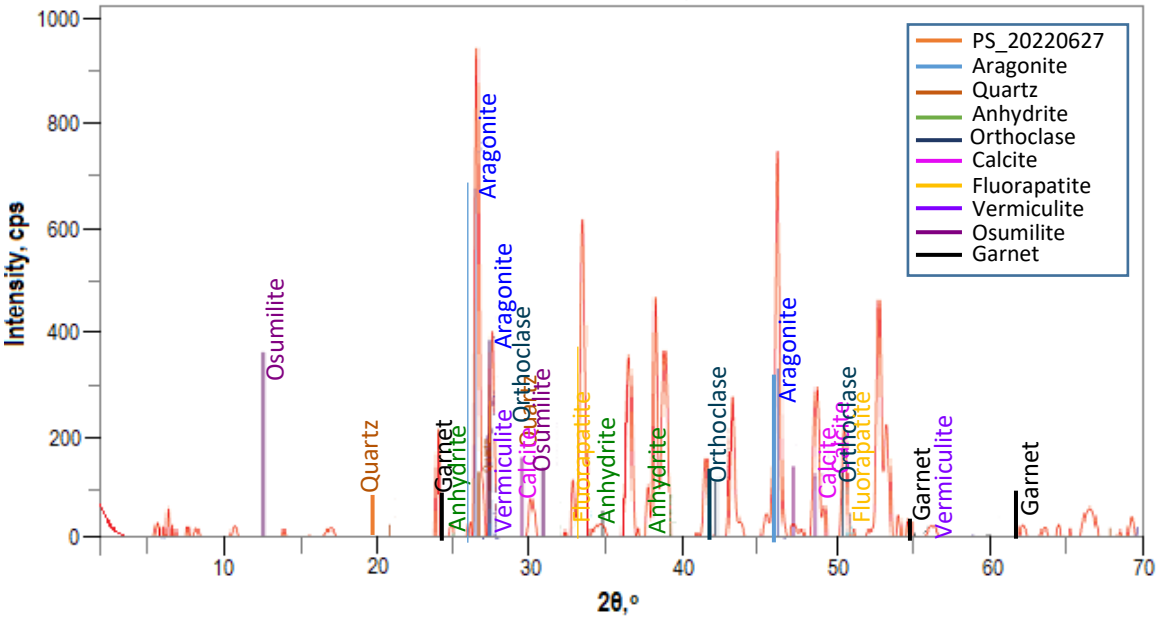

Figure 4.1 XRD Spectrum of PS Particles

Table 4.2 Quantitative Analysis Results of XRD of PS Particles

DB Card Number	Space Group	Figure of Merit	Phase Name	Formular
01-085-6705	62 : Pnma	0.851	Aragonite	$CaCO_3$
00-001-0649	154 : P3221	1.417	Quartz	SiO_2
01-085-6126	63 : Bmmb	1.668	Anhydrite	Ca (SO_4)
00-005-0518	12 : C2/m	1.215	Vermiculite	Na - K - Al - O - Si.$12H_2O$
00-002-0475	12 : C12/m1	1.376	Orthoclase	$Al_2O_3.K_2O.6SiO_2$
00-002-0629	167 : R – 3c:H	1.360	Calcite	$CaCO_3$
00-002-0845	176 : P63/m	1.605	Fluorapatite	(Ca F) Ca_4 $(PO_4)_3$
00-010-0413	192 : P6/mcc	1.751	Osumilite	K - Na - Ca - Mg - Fe - Al - S …
00-002-0981	230 : 1a – 3d	3.100	Garnet	3(Ca, Fe, Mg) O. (Al, Fe ….

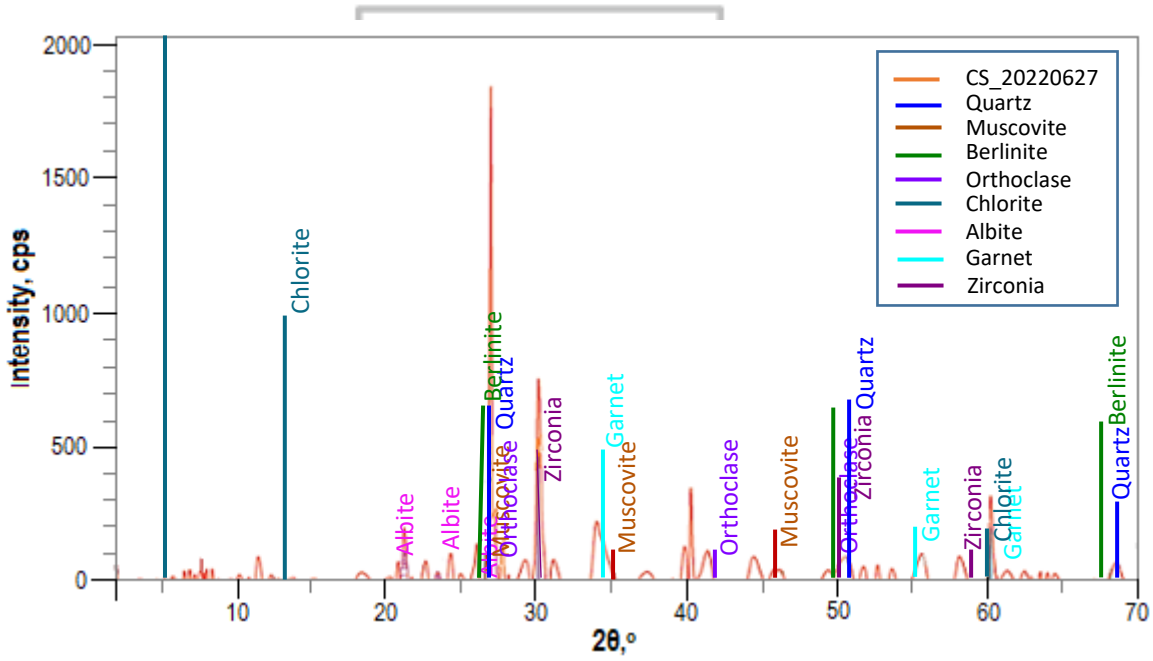

Figure 4.2 XRD Spectrum of CSA Particles

Table 4.3 Quantitative Analysis Results of XRD of CSA Particles

DB Card Number	Space Group	Figure of Merit	Phase Name	Formular
00-002-0471	154 : P3221	2.106	Quartz	SiO_2
00-002-0467	15 : C12/c1	1.825	Muscovite	$KAl_2(Si3Al)$ O10 (OH, F)2
00-003-0447	147 : P - 3	1.810	Berlinite	$AlPO_4$
00-002-0475	12 : C12/m1	3.104	Orthoclase	$Al_2O_3.K_2O.6SiO_2$
00-002-0028	15 : C12/c1	1.725	Chlorite	(Mg, Fe)5 (Al, Si)5 O10 (….
00-003-0451	2 : P – 1	2.877	Albite	$NaAlSi_3O_8$
00-002-0981	230 : 1a – 3d	1.995	Garnet	3(Ca, Fe, Mg) O. (Al, Fe ….
04-016-1792	137 : P42/nmc:2	1.617	Zirconia	ZrO_2

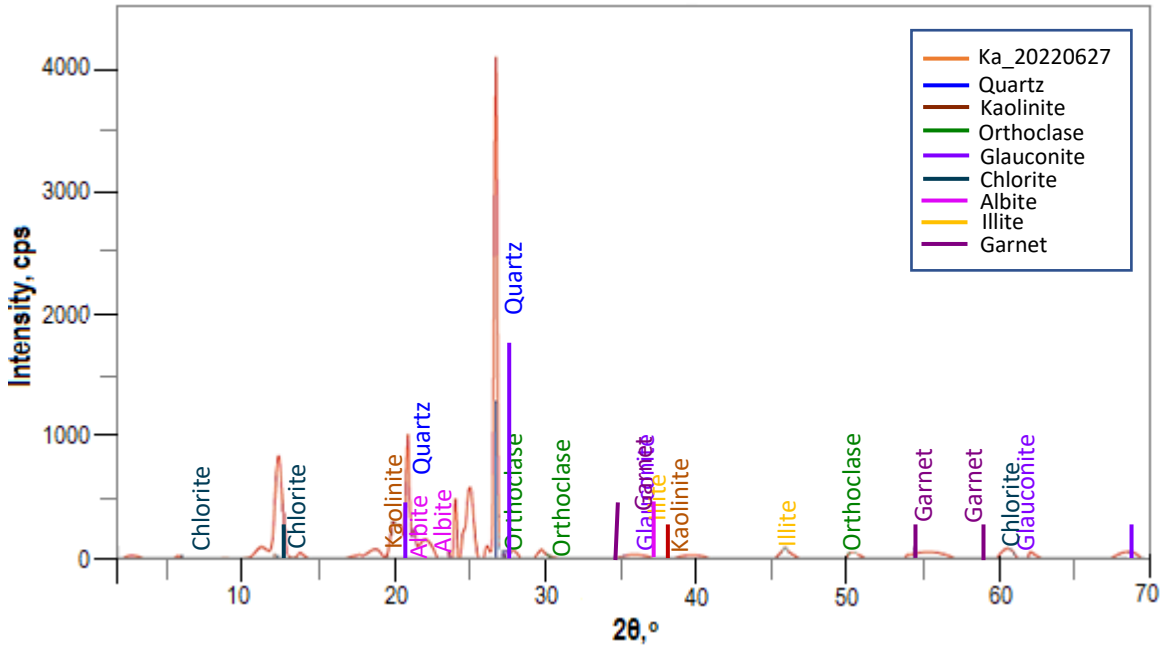

Figure 4.3 XRD Spectrum of Kaolin Particles

Table 4.4 Quantitative Analysis Results of XRD of Kaolin Particles

DB Card Number	Space Group	Figure of Merit	Phase Name	Formular
00-001-0649	154 : P3221	1.725	Quartz	SiO_2
00-003-0052	2 : P – 1	3.154	Kaolinite	$Al_2O_3.2SiO_2.2H_2O$
00-002-0475	12 : C12/m1	3.269	Orthoclase	$Al_2O_3.K_2O.6SiO_2$
00-002-1010	10 : P12/m1	3.001	Glauconite	(K, CaO.5, Na) O84(AlO.47…….
00-002-0028	15 : C12/c1	3.237	Chlorite	$(Mg, Fe)_5$ (Al, Si)$_5$ O_{10} (...
00-003-0451	2 : P – 1	3.305	Albite	$NaAlSi_3O_8$
00-015-0603	12 : C2/m	3.186	Illite	$K(AlFe)_2AlSi_3O_{10}(OH…$
00-002-0981	230 : 1a – 3d	2.850	Garnet	3(Ca, Fe, Mg) O. (Al, Fe…

In Figure 4.1, several major diffraction peaks of the PS particles are observed at (2θ) positions of 26.50º, 33.42º, 38.83º, 46.16º, and 48.67º. The corresponding inter-planar distances are measured at 3.361 Å, 2.679 Å, 2.317 Å, 1.965 Å, and 1.869 Å, respectively. The XRD spectrum identifies the main mineral components at these peaks along with their respective figures of merit, and these are presented in Table 4.2.

Likewise, in Figure 4.2, the major diffraction peaks of the CSA particles can be seen at (2θ) positions of 21.18º, 27.00º, 30.24º, 50.58º, and 60.34º, with inter-planar distances at 4.191 Å, 3.300 Å, 2.953 Å, 1.803 Å, and 1.533 Å, respectively. The prominent minerals found within the spectrum are also listed in Table 4.3, along with their figures of merit.

Similarly, Figure 4.3 displays the diffraction peaks of the kaolin particles at (2θ) positions of 12.68º, 20.34º, 24.32º, 27.82º, and 46.00º, with inter-planar distances at 6.976 Å, 4.363 Å, 3.657 Å, 3.204 Å, and 1.971 Å, respectively. The major minerals identified in the spectrum are detailed in Table 4.4.

The XRD analysis of the three materials reveals clear, narrow, and sharp major diffraction peaks, indicating their predominantly crystalline nature, similar to chrysotile asbestos, as observed by Kusiorowski *et al*. (2012). Dellisanti *et al*. (2002) have reported that the mineralogy of chrysotile asbestos mainly comprises chrysotile, silica, calcite anhydrite, and quartz, as indicated by the presence of SiO_2, CaO, MgO, and Al_2O_3. Tables 4.2 to 4.4 illustrate that, apart from chrysotile, the three materials exhibit the presence of the same or similar minerals as observed in chrysotile asbestos.

Table 4.5 presents the XRF analysis results of the CSA, PSP, and kaolin powder. Additionally, the table includes the XRF analysis of asbestos obtained from Dellisanti *et al*. (2002).

Table 4.5 Chemical Composition of the Three Basic Raw Materials from XRF

Specification Compounds	Concentration (% weight)			
	Coconut Shell Ash (CSA)	**Periwinkle Shell Powder (PSP)**	**Kaolin Powder**	**Asbestos**
SiO_2	38.2321	31.8601	56.645	34.69
Al_2O_3	23.2776	11.4178	23.189	1.23
P_2O_5	1.0699	0.3191	-	0.04
SO_3	3.2382	0.3042	0.426	0.94
K_2O	2.4976	0.2682	1.612	0.00
CaO	4.2641	43.1553	0.591	4.16
MgO	0.800	1.7115	–	32.89
TiO_2	0.0575	–	1.733	0.08
MnO	0.0523	0.0333	0.195	0.13
Fe_2O_3	12.4071	6.3855	13.775	9.46
Cr_2O_3	–	–	0.059	–
cl	–	–	0.774	–

The XRF investigation of the samples confirms the XRD results, showing that all three materials (CSA, PS, and kaolin powders) contain calcium, potassium, silica, aluminum, and iron, which aligns with the elements identified in their XRD analyses. Similarly, asbestos also contains these elements, but their proportions differ among the four filler agents, as detailed in Table 4.5. The XRF data confirms that the major compounds present in the three materials are CaO, K_2O, SiO_2, Al_2O_3, and Fe_2O_3. These compounds are known to be among the hardest substances, according to Aku *et al*. (2012). The presence of these hard oxides in the materials will influence the properties of the final brake pads.

It's worth noting that the XRF analysis did not detect any radioactive materials such as Xenon (Xe), Praseodymium (Pr), and Europium (Eu) in the three materials. This suggests that CSA, PS, and kaolin powders can be suitable ingredients for filling or reinforcing to replace asbestos in brake lining production.

4.2.3 Morphological Characterisation of the Raw Materials

The SEM micrographs and EDS spot analysis reveal the characteristics of the three materials: PSP, CSA, and kaolin powder, as depicted in Figures 4.4 - 4.6, respectively.

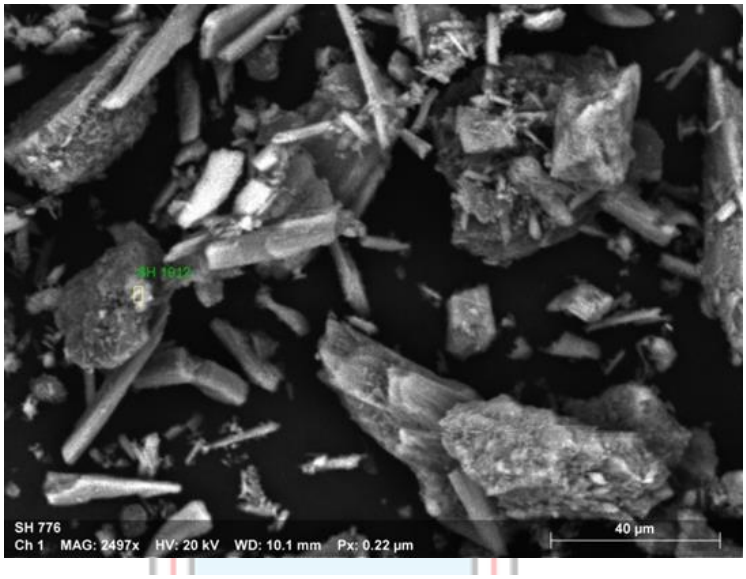

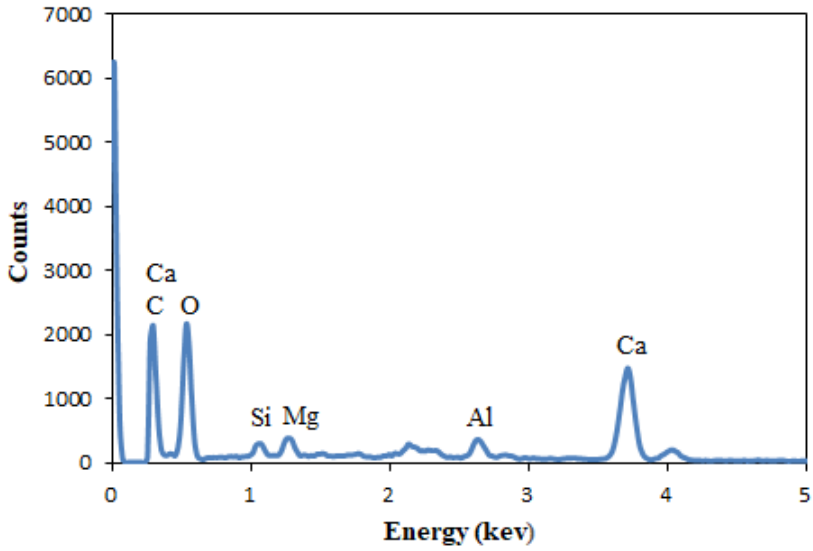

Element	At. No.	Netto	Mass [%]	Mass Norm. [%]	Atom [%]	abs. error [%] (1 sigma)	rel. error [%] (1 sigma)
Carbon	6	5327	13.22	34.54	44.07	2.07	15.67
Oxygen	8	7177	20.23	52.84	50.61	3.00	14.85
Silicon	14	442	0.31	0.81	0.54	0.05	17.67
Magnesium	12	704	0.35	0.92	0.58	0.05	14.79
Aluminium	13	696	0.24	0.63	0.27	0.04	16.02
Calcium	20	8592	3.93	10.26	3.92	0.15	3.82
		Sum	**38.28**	**100.00**	**100.00**		

Figure 4.4 SEM Micrograph and EDS Analysis of PS Powder

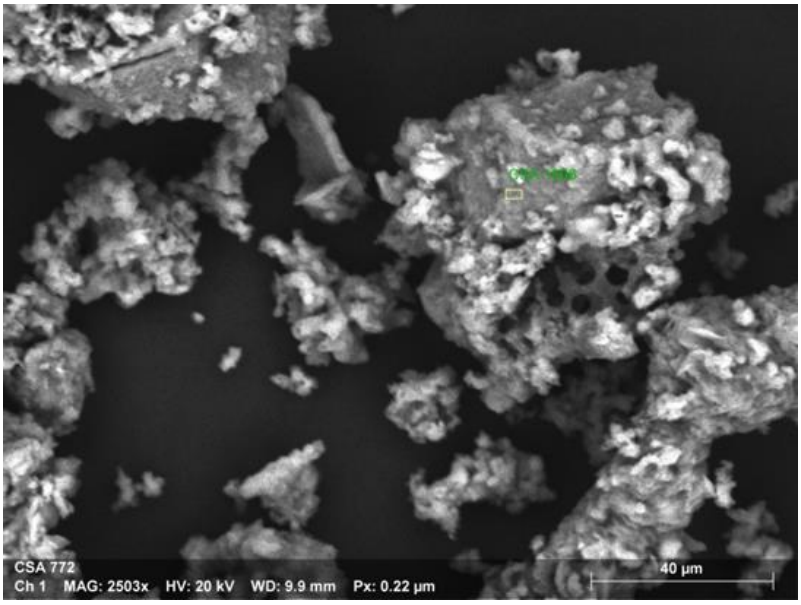

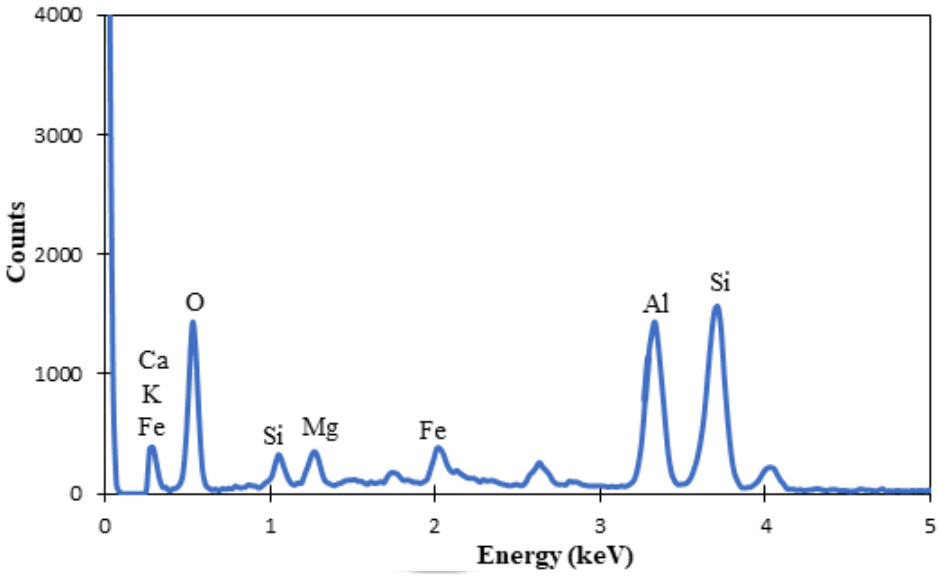

Element	At. No.	Netto	Mass [%]	Mass Norm. [%]	Atom [%]	abs. error [%] (1 sigma)	rel. error [%] (1 sigma)
Oxygen	8	9602	5.34	17.76	8.46	0.19	3.62
Silicon	14	4654	17.06	56.72	67.69	2.73	16.01
Aluminium	13	817	2.75	9.16	14.56	0.69	24.90
Potassium	19	734	0.33	1.10	0.68	0.05	13.63
Magnesium	12	648	0.48	1.59	1.25	0.06	13.10
Calcium	20	580	0.61	2.02	1.68	0.08	13.15
Iron	26	7957	3.50	11.65	5.69	0.14	4.03
		Sum	**30.07**	**100.00**	**100.00**		

Figure 4.5 SEM Micrograph and EDS Analysis of CSA

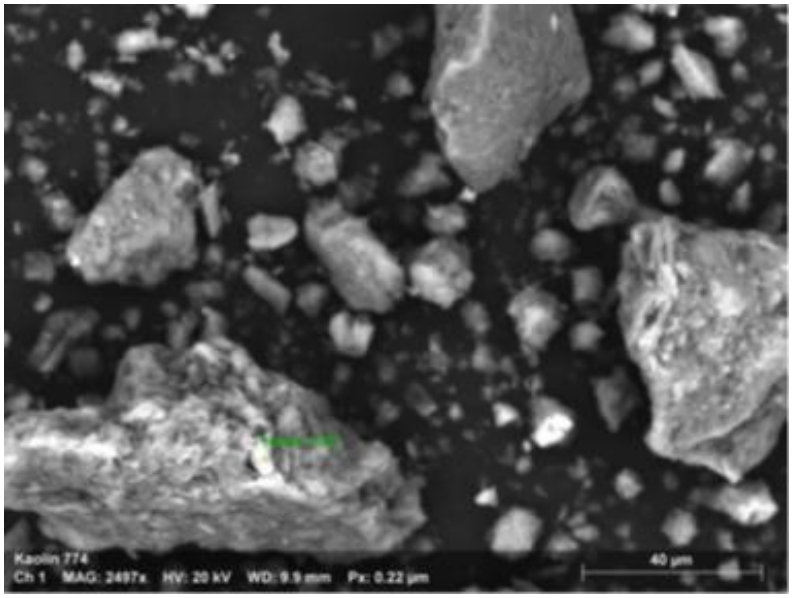

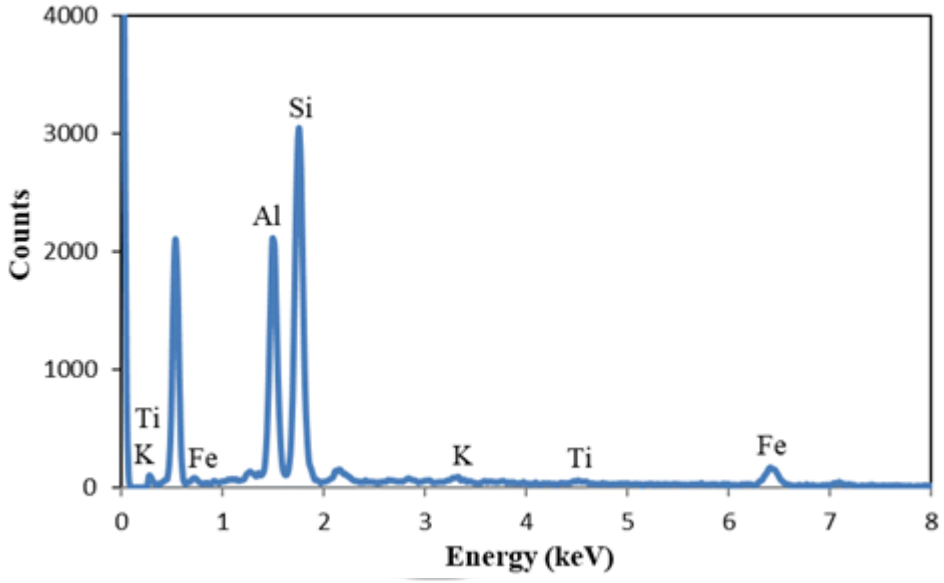

Element	At. No.	Netto	Mass [%]	Mass Norm. [%]	Atom [%]	abs. error [%] (1 sigma)	rel. error [%] (1 sigma)
Aluminium	13	8365	7.19	28.64	31.95	0.39	5.39
Silicon	14	13990	13.68	54.53	58.43	0.63	4.61
Potassium	19	231	0.49	1.95	1.50	0.06	13.00
Titanium	22	123	0.26	1.03	0.65	0.05	19.68
Iron	26	1220	3.47	13.85	7.46	0.17	4.86
		Sum	**25.09**	**100.00**	**100.00**		

Figure 4.6 SEM Micrograph and EDS Analysis of Kaolin Powder

The micrographs of the three materials demonstrate variations in particle sizes and shapes. In all three materials, the particles appear solid and non-uniform in size. This observation aligns with findings from Kusiorowski *et al*. (2012), who also observed a similar morphology in

chrysotile asbestos, except for asbestos having thin intertwined fibres, which are also solid and non-uniform in size.

The EDS elemental analysis reveals that PSP contains Si, Ca, Al, and Mg in addition to carbon and oxygen. For CSA, EDS elemental mapping indicates the presence of Si, Al, Fe, Ca, Mg, and K, along with oxygen. In the case of the kaolin powder, its morphology indicates significant amounts of Si, Al, K, Fe, and Ti within its structure. These results are consistent with the data acquired from XRD and XRF examination of these three substances.

Overall, the XRD, XRF, and SEM-EDS analyses collectively suggest that the chemical composition of CSA, PSP, and kaolin powder closely resembles that of asbestos.

4.2.4 Thermal Characterisation of the Raw Materials

The thermal analysis of the PS particles, CSA particles, and kaolin particles was conducted using DSC-TGA, and the results are illustrated in Figures 4.7- 4.9, respectively.

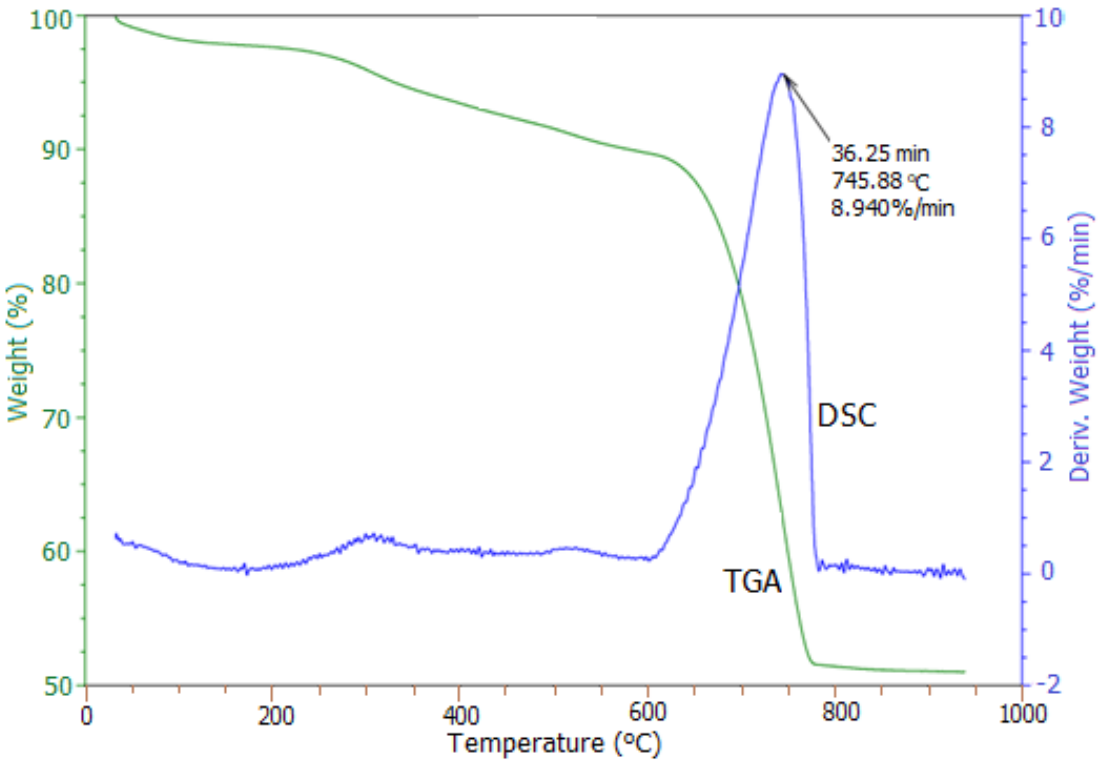

Figure 4.7 DSC and TGA Curves of Periwinkle Shell Powder

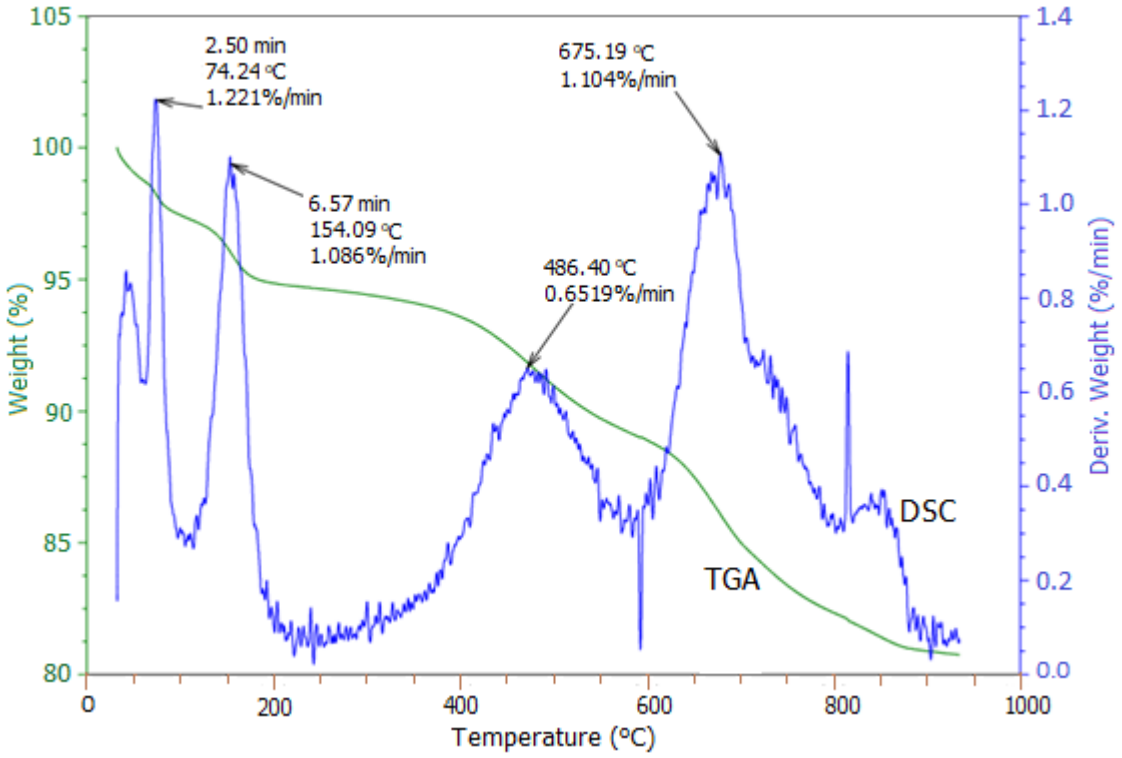

Figure 4.8 DSC and TGA Curves of Coconut Shell Ash

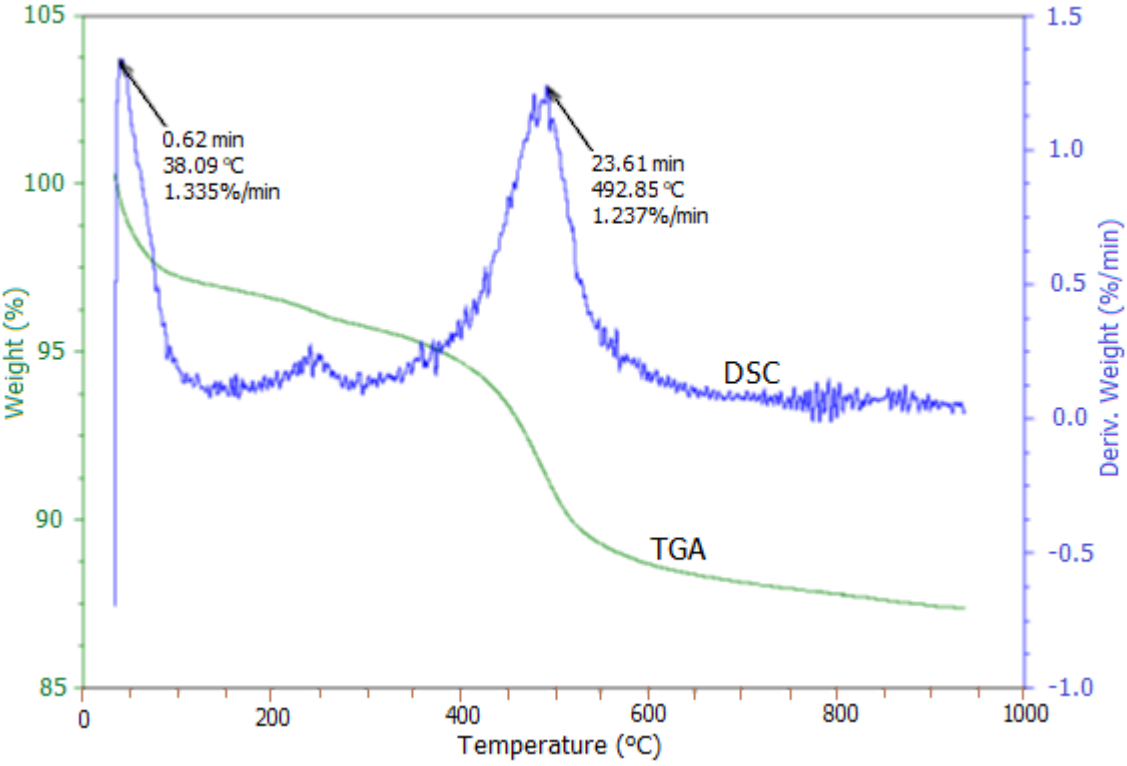

Figure 4.9 DSC and TGA Curves of Kaolin Powder

In Figure 4.7, the DSC analysis of PSP reveals the highest degradation occurring at 745.88 °C, resulting in a weight loss of 36.92 %. The TGA reveals three distinct weight loss stages: from 32 °C to about 94 °C due to the removal of absorbed water and light volatiles, from 94 °C to 400 °C due to further removal of light volatiles, and from 400 °C to about 885 °C due to pyrolysis.

Figure 4.8 illustrates the thermal analysis of CSA, exhibiting four weight loss stages in the DSC curve: peaks at 74.24 °C, 154.09 °C, 486.40 °C, and a maximum decomposition peak at 675.1 9°C. The first two stages of weight loss, between 32 °C and 260 °C, are attributed to the extraction of mechanically held water, while the third stage, from 260 °C to about 580 °C, may be due to volatilization of matter. Subsequent combustion or decomposition of the carbon phase then occurs between 580 °C and 910 °C. The cumulative weight reduction at the maximum decomposition temperature is observed to be 13.80 %.

In Figure 4.9, the DSC analysis of the kaolin powder shows the highest degradation at a peak temperature of 492.85 °C with a percentage weight loss of 8.75 %. The TGA curve exhibits two regions of weight loss: from 3 2°C to about 215 °C due to the removal of absorbed water from the powder surface pores, and weight loss from 215 °C to 700 °C due to kaolin dehydroxylation with metakaolin formation.

The results of the thermal analysis of PSP, CSA, and the kaolin powder are compared with the thermal behaviour of chrysotile asbestos from Dellisanti *et al*. (2002) in Figure 4.10. The TG curve of the asbestos indicates three stages of weight loss: up to 250 °C, representing the removal of absorbed water, from 250 °C to 500 °C, relating to the combustion of organic matter, and removal of structural OH of the chrysotile fibre from over 450 °C up to 70 0°C. The maximum degradation of the chrysotile occurs at around 700 °C with a weight loss of 11.90 %.

This finding is supported by Kusiorowski *et al*. (2012), who reported that different chrysotile asbestos, at temperatures of 600 °C to 810 °C, lose their chemically bonded water, causing complete breakdown of their mineral structures, with peak temperatures between 700 °C to 730 °C.

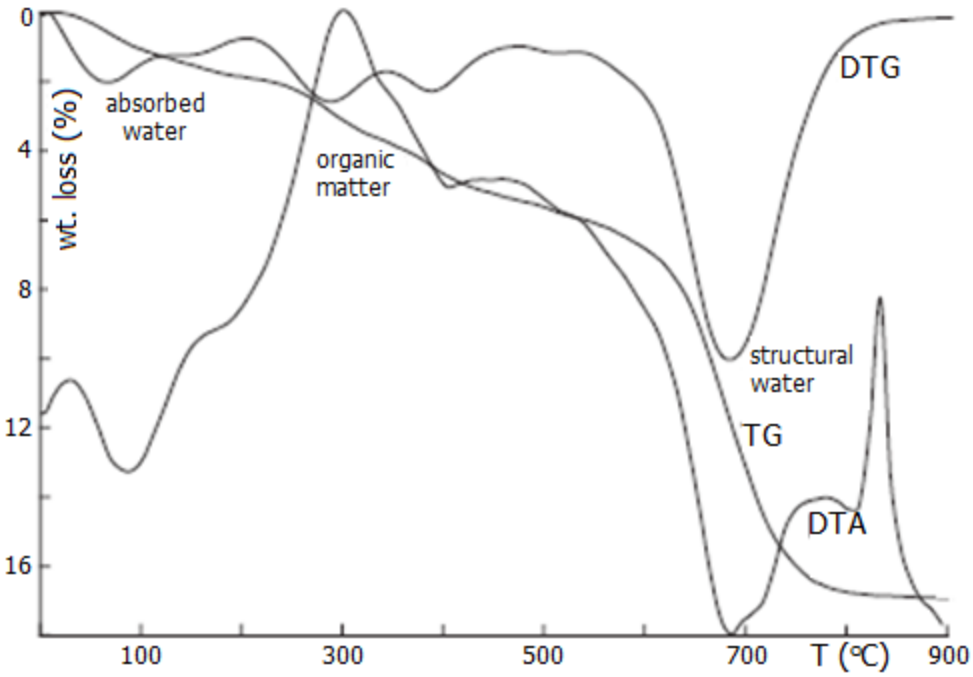

Figure 4.10 Thermal Behaviour of Chrysotile Asbestos Fibre

(Source: Dellisanti *et al*., 2002)

In comparison, the thermal degradation temperatures of PSP, CSA, and kaolin powder are nearly identical to those of asbestos. Kaolin experiences degradation at a slightly lower temperature (492.85 °C) compared to asbestos (685 °C), while PSP degrades at a slightly higher temperature (745.88 °C) than that of asbestos. Additionally, the weight losses at the degradation temperatures of the three materials are similar to those of asbestos. At an equivalent degradation temperature to asbestos, PSP will experience a weight loss of only about 16 %. Consequently, all three materials offer a level of thermal stability comparable to that of asbestos.

The analysis of CSA, PSP, and kaolin powder encompassing physical, chemical, morphological, and thermal aspects reveals that these three materials exhibit comparable performance traits to asbestos. As a result, they hold the potential to serve as suitable alternatives for asbestos in automotive disc brake pads.

4.3 Optimisation of Brake Pad Materials Formulation

This section presents the results of the brake pad formulation optimisation. Tables 4.6 and 4.7 show the design layout and response data for the PSP/CSA and PSP/K formulation optimisations, respectively.

Table 4.6 Design Layout and Response Data for PSP/CSA Formulation Optimisation

Std	Run	Factor A: Periwinkle Shell (%)	Factor B: Coconut Shell Ash (%)	Factor C: Epoxy Resin (%)	Response 1 Compressive Strength (N/mm^2)	Response 2 Linear Shrinkage (%)	Response 3 Volume Shrinkage (%)	Response 4 Bulk Density (g/cm^3)	Response 5 Apparent Porosity (%)	Response 6 Swell in Water (%)	Response 7 Swell in Oil (%)	Response 8 Hardness (HBN)
1	5	26	35.5	15	0.507	0.08	6.41	1.67	43.75	31.58	40	22.26
2	14	35.5	35.5	20	0.453	2.01	8.73	1.8	40	26.32	27.78	47.5
3	10	35.5	45	15	0.6103	8.56	6.38	1.83	37.5	31.82	47.62	31.8
4	15	35.5	35.5	20	0.453	2.01	8.73	1.8	40	26.32	27.78	31.8
5	3	26	45	20	0.3317	4.38	10.3	1.9	40	30	38.89	47.5
6	12	35.5	45	25	0.2433	2.39	10.26	2.12	43.75	31.58	47.37	47.5
7	4	45	45	20	0.7023	2.79	11.99	1.43	33.33	26.32	35	138
8	16	35.5	35.5	20	0.453	2.01	8.73	1.8	40	26.32	27.78	76.3
9	6	45	35.5	15	1.032	0.69	7.57	2.63	33.33	28.57	22.73	76.3
10	2	45	26	20	0.7817	5.46	18.07	1.58	33.33	25	36.84	138
11	8	45	35.5	25	0.7927	3.92	17.15	1.7	38.46	27.78	25	138
12	11	35.5	26	25	0.5963	2.82	11.87	2.12	38.46	22.22	27.78	76.3
13	9	35.5	26	15	1.1007	5.78	15.53	1.75	30.77	26.32	19.05	76.3
14	1	26	26	20	0.61	6.92	20.81	1.45	50	25	11.11	76.3
15	17	35.5	35.5	20	0.453	2.01	8.73	1.8	40	26.32	27.78	76.3
16	13	35.5	35.5	20	0.453	2.01	8.73	1.8	40	26.32	27.78	76.3
17	7	26	35.5	25	0.524	4.69	15.47	1.8	42.86	37.5	35.29	76.3

Table 4.7 Design Layout and Response Data for PSP/K Formulation Optimisation

Std	Run	Factor A: Periwinkle Shell (%)	Factor B: Kaolin (%)	Factor C: Epoxy Resin (%)	Response 1 Compressive Strength (N/mm^2)	Response 2 Linear Shrinkage (%)	Response 3 Volume Shrinkage (%)	Response 4 Bulk Density (g/cm^3)	Response 5 Apparent Porosity (%)	Response 6 Swell in Water (%)	Response 7 Swell in Oil (%)	Response 8 Hardness (HBN)
1	5	26	35.5	15	9.6985	0.5622	0.4003	0.575	31.25	21.74	47.37	76.3
2	11	35.5	26	25	7.926	0.7187	0.7187	0.575	31.25	21.74	8.333	101
3	6	45	35.5	15	16.953	3.0952	3.4122	6	25	16.67	27.2727	89.7
4	7	26	35.5	25	3.87	1.1416	2.3518	0.3485	27.78	21.74	12.5	138
5	8	45	35.5	25	16.216	0.8229	1.6328	0.8571	23.53	16.67	12.5	200
6	9	35.5	26	15	9.753	0.7708	0.0386	1.7857	22.22	16	0	138
7	4	45	45	20	0.989	6.1602	4.1544	2	25	15	8.6957	200
8	15	35.5	35.5	20	9.309	3.4003	1.2828	1.75	30.77	19.05	22.7273	76.3
9	3	26	45	20	9.042	0.326	1.3168	1.9167	21.43	13.04	8.3333	314.93
10	2	45	26	20	5.33	2.6411	2.6411	5.75	23.08	13.04	8.3333	138
11	12	35.5	45	25	16.028	1.0896	2.0831	1.9167	21.43	13.04	16.6667	121
12	10	35.5	45	15	12.795	1.9404	0.5458	11.5	21.43	13.04	8.6957	101
13	16	35.5	35.5	20	10.999	0.6897	1.5889	1.8333	28.57	18.18	13.6364	185
14	17	35.5	35.5	20	10.999	0.6897	1.5889	1.8333	28.57	18.18	13.6364	185
15	1	26	26	20	10.999	0.6897	1.5889	1.8333	28.57	18.18	13.6364	185
16	14	35.5	35.5	20	10.999	0.6897	1.5889	1.8333	28.57	18.18	13.6364	185
17	13	35.5	35.5	20	10.999	0.6897	1.5889	1.8333	28.57	18.18	13.6364	185

Tables 4.8 to 4.13 present the ANOVA tables for bulk density, compressive strength, and volume shrinkage in both formulations (PSP/CSA and PSP/K). Meanwhile, Figures 4.11 to 4.16 illustrate the corresponding 3D surface plots for each formulation. The ANOVA was performed to identify the significant impacts of the materials on the formulations, with a level of confidence of 95 % ($\alpha = 0.05$). The last columns of the ANOVA tables indicate the impact (p) of individual variables on the responses, signifying the magnitude of their effect on the findings. A model term with a value of p below 0.0500 is regarded as significant in the analysis.

Table 4.8 ANOVA of the Bulk Density for the PSP and CSA Formulation

Source	Sum of Squares	df	Mean Square	F-value	P-value
Model	1.00	8	0.1252	4.32	0.0269
A-PERI	0.0338	1	0.0338	1.17	0.3117
B-COCO	0.1089	1	0.1089	3.76	0.0886
C-EPOXY	0.0180	1	0.0180	0.62	0.4528
AB	0.0900	1	0.0900	3.10	0.1161
AC	0.2809	1	0.2809	9.69	0.0144
A^2	0.0538	1	0.0538	1.86	0.2101
C^2	0.2684	1	0.2684	9.26	0.0160
A^2C	0.2664	1	0.2664	9.19	0.0163
Residual	0.2319	8	0.0290		
Lack of Fit	0.2319	4	0.0580		
R^2	0.8120				
Adjusted R^2	0.6240				
Adequate Precision	8.4326				

Table 4.9 ANOVA of the Compressive Strength of the PSP and CSA Formulation

Source	Sum of Squares	df	Mean Square	F-value	P-value
Model	0.7283	6	0.1214	10.94	0.0007
A-Peri	0.2231	1	0.2231	20.11	0.0012
B-Coco	0.1803	1	0.1803	16.26	0.0024
C-Epoxy	0.1495	1	0.1495	13.48	0.0043
AC	0.0164	1	0.0164	1.48	0.2516
A^2	0.0577	1	0.0577	5.20	0.0458
C^2	0.0926	1	0.0926	8.35	0.0161
Residual	0.1109	10	0.0111		
Lack of Fit	0.1109	6	0.0185		
R^2	0.8678				
Adjusted R^2	0.7885				
Adequate Precision	12.3257				

Table 4.10 ANOVA of the Volume Shrinkage of the PSP and CSA Formulation

Source	Sum of Squares	df	Mean Square	F-value	P-value
Model	247.57	6	41.26	7.44	0.0031
A-Peri	0.4005	1	0.4005	0.0722	0.7936
B-Coco	93.50	1	93.50	16.85	0.0021
C-Epoxy	44.46	1	44.46	8.01	0.0178
BC	14.21	1	14.21	2.56	0.1406
A^2	53.67	1	53.67	9.67	0.0111
B^2	36.13	1	36.13	6.51	0.0288
Residual	55.48	10	5.55		
Lack of Fit	55.48	6	9.25		
R^2	0.8169				
Adjusted R^2	0.7071				
Adequate Precision	9.8377				

Table 4.11 ANOVA of the Bulk Density of the PSP and K Formulation

Source	Sum of Squares	df	Mean Square	F-value	P-value
Model	122.15	11	11.10	117.40	<0.0001
A-Periwinkle	12.33	1	12.33	130.41	<0.0001
B-Kaolin	30.56	1	30.56	323.10	<0.0001
C-Epoxy	29.13	1	29.13	307.97	<0.0001
AB	3.67	1	3.67	38.84	0.0016
AC	6.04	1	6.04	63.89	0.0005
BC	17.53	1	17.53	185.29	<0.0001
A^2	0.9318	1	0.9318	9.85	0.0257
B^2	9.84	1	9.84	104.05	0.0002
C^2	1.51	1	1.51	15.97	0.0104
A^2B	27.09	1	27.09	286.47	<0.0001
A^2C	3.68	1	3.68	38.89	0.0016
Residual	0.4729	5	0.0946		
Lack of Fit	0.4674	1	0.4674		
Pure Error	0.0056	4	0.0014		
R^2	0.9961				
Adjusted R^2	0.9877				
Adequate Precision	42.2819				

Table 4.12 ANOVA of the Compressive Strength of the PSP and K Formulation

Source	Sum of Squares	df	Mean Square	F-value	P-value
Model	279.77	12	23.31	40.82	0.0013
A-Periwinkle	96.04	1	96.04	168.14	0.0002
B-Kaolin	31.05	1	31.05	54.35	0.0018
C-Epoxy	0.4942	1	0.4942	0.8652	0.4049
AB	1.42	1	1.42	2.49	0.1899
AC	6.48	1	6.48	11.35	0.0281
BC	6.40	1	6.40	11.21	0.0286
A^2	16.94	1	16.94	29.66	0.0055
B^2	17.95	1	17.95	31.43	0.0050
C^2	38.64	1	38.64	67.65	0.0012
A^2B	38.03	1	38.03	66.57	0.0012
A^2C	7.94	1	7.94	13.91	0.0203
AB^2	138.80	1	138.80	242.99	< 0.0001
Pure Error	2.28	4	0.5712		
Cor Total	282.06	16			
R^2	0.9919				
Adjusted R^2	0.9676				
Adequate Precision	24.1542				

Table 4.13 ANOVA of the Volume Shrinkage of the PSP and K Formulation

Source	Sum of Squares	df	Mean Square	F-value	P-value
Model	16.57	9	1.84	13.34	0.0013
A-Periwinkle	4.78	1	4.78	34.61	0.0006
B-Kaolin	1.21	1	1.21	8.77	0.0210
C-Epoxy	0.7137	1	0.7137	5.17	0.0572
AB	0.7969	1	0.7969	5.77	0.0473
AC	3.48	1	3.48	25.21	0.0015
BC	0.1837	1	0.1837	1.33	0.2865
A^2	4.21	1	4.21	30.51	0.0009
B^2	0.0443	1	0.0443	0.3208	0.5888
C^2	1.41	1	1.41	10.21	0.0152
Residual	0.9663	7	0.1380		
Lack of Fit	0.8913	3	0.2971		
Pure Error	0.0750	4	0.0187		
R^2	0.9449				
Adjusted R^2	0.8741				
Adequate Precision	14.3479				

The examination of the outcomes presented in Tables 4.8 to 4.13 reveals the significant model terms that influence various properties of the PSP/CSA and PSP/K formulations. For the PSP/CSA formulation, it is evident from Table 4.8 that the interaction effect of PSP with epoxy resin (AC), as well as the effects of C^2 and A^2C, significantly influence the bulk density. Similarly, Table 4.9 indicates that the effects of PSP (A), CSA (B), and epoxy resin (C), along with A^2 and C^2, have a significant impact on the compressive strength. Moreover, Table 4.10 shows that CSA (B), epoxy resin (C), A^2, and B^2 are the significant terms affecting volumetric shrinkage.

In the case of the PSP/K formulation, Table 4.11 demonstrates that all the terms have a significant influence on the bulk density. Furthermore, Table 4.12 reveals that PSP (A), kaolin (B), the interaction of PSP with epoxy resin (AC), the interaction of kaolin with epoxy resin (BC), and the effects of A^2, B^2, C^2, A^2B, A^2C, and AB^2 significantly affect the compressive strength. Lastly, Table 4.13 highlights that PSP (A), kaolin (B), the interaction of PSP and kaolin (AB), the interaction of PSP and epoxy (AC), and the effects of A^2 and C^2 are the model terms that influence the volume shrinkage of the PSP/K formulation.

To better visualise the impact of influential factors on the responses, Figures 4.11 to 4.13 present estimated 3D response surface plots for bulk density, compressive strength, and volume shrinkage of the PSP/CSA formulation, respectively. Similarly, Figures 4.14 to 4.16 show estimated 3D surface plots for the same responses for the PSP/K formulation. These plots illustrate how variations in two most significant factors affect the response while keeping the other factor constant.

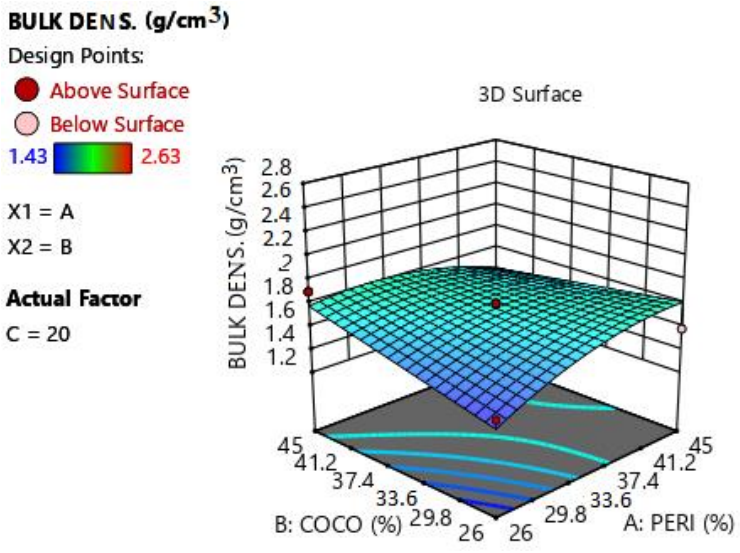

Figure 4.11 Surface Plot of Bulk Density against CSA and PSP

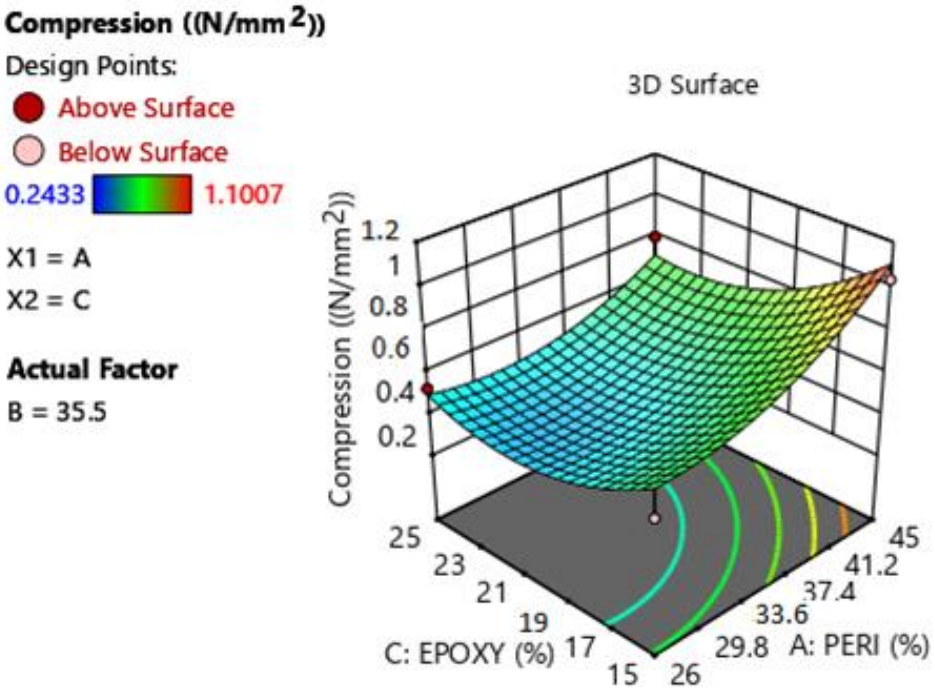

Figure 4.12 Surface Plot of Compressive Strength against Epoxy and PSP

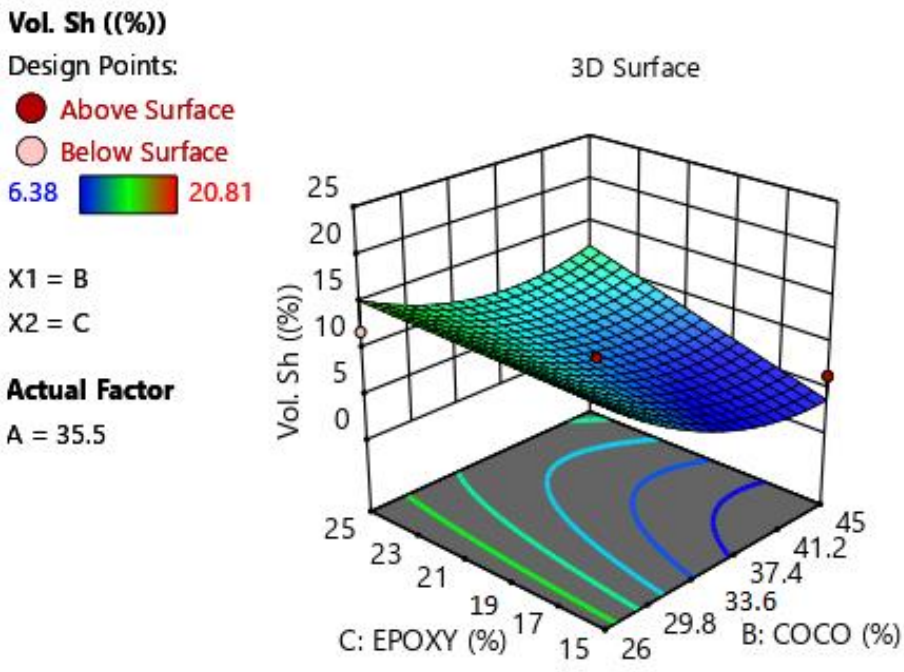

Figure 4.13 Surface Plot of Volume Shrinkage against Epoxy and CSA

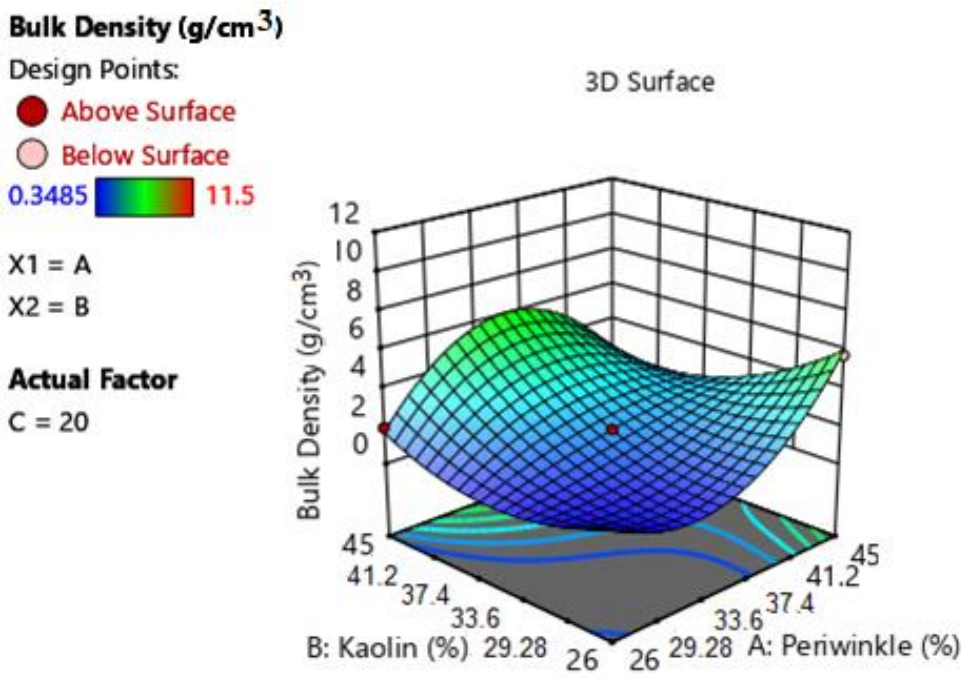

Figure 4.14 Surface Plot of Bulk Density against Kaolin and PSP

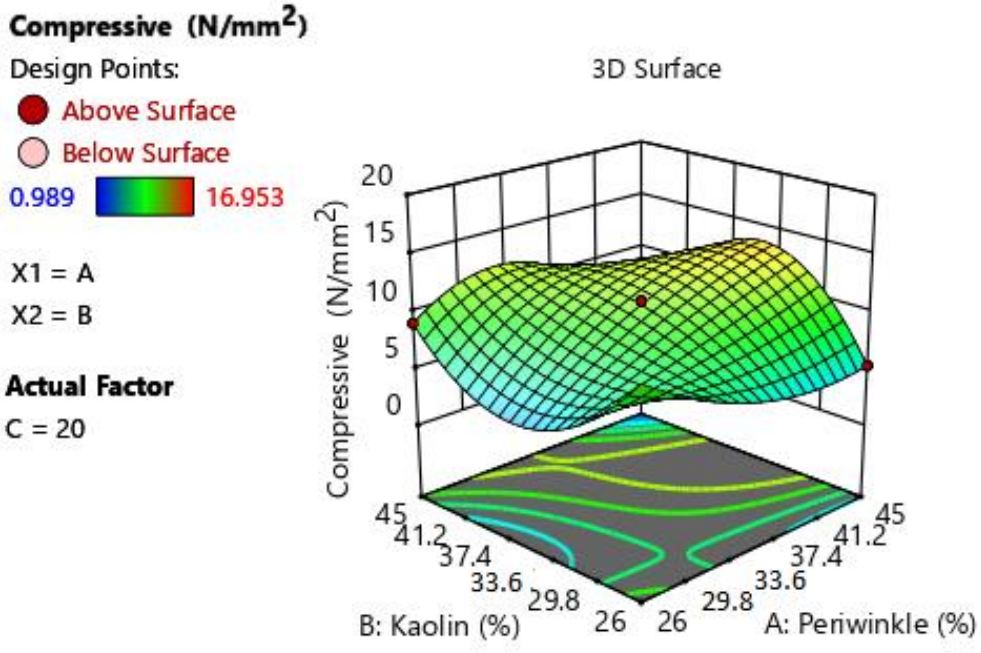

Figure 4.15 Surface Plot of Compressive Strength against Kaolin and PSP

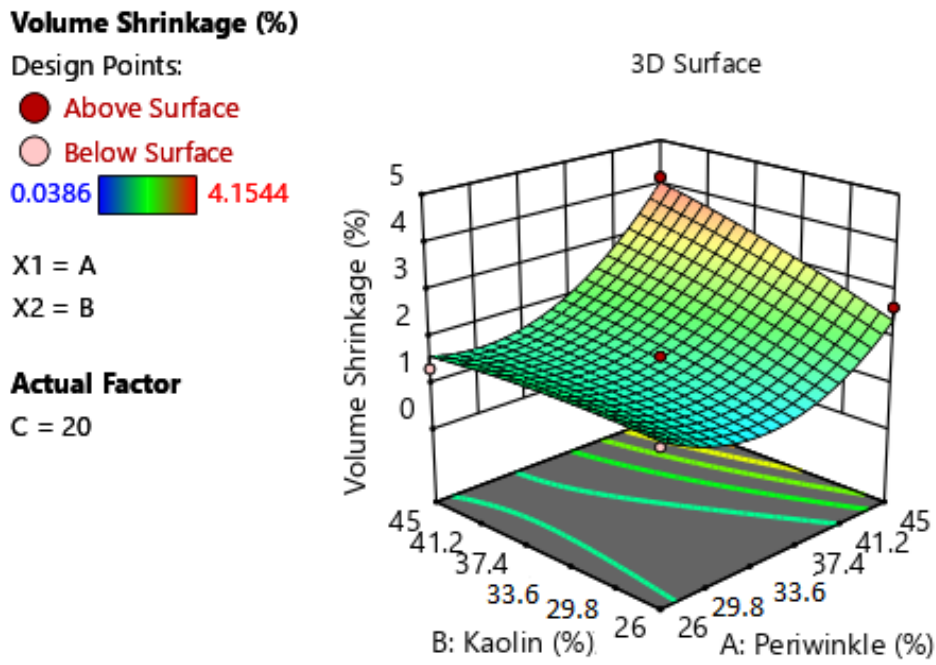

Figure 4.16 Surface Plot of Volume Shrinkage against Kaolin and PSP

Figure 4.17 illustrates the optimised solutions for the primary materials in the PSP/CSA combination, and Figure 4.18 shows the optimised solutions for the PSP/K combination. Additionally, the ANOVA analysis summaries for both formulations can be found in Appendix B.

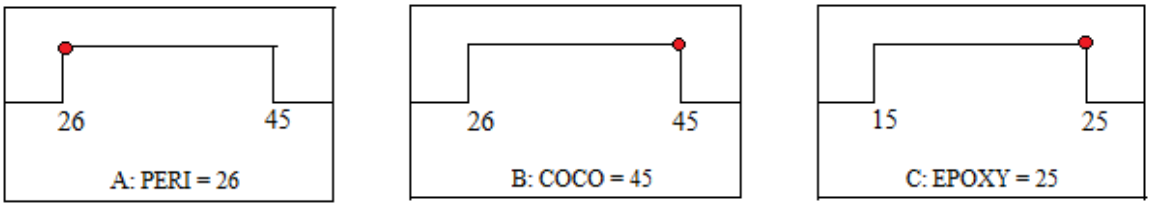

Figure 4.17 Optimum Mixing Ratio of the Major Materials for PSP/CSA Pad

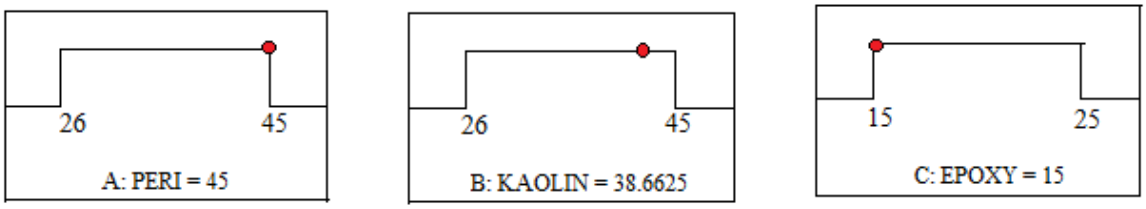

Figure 4.18 Optimum Mixing Ratio of the Major Materials for PSP/K Pad

According to the information in Figure 4.17, the ideal percentage mixing ratio of PSP, CSA, and epoxy resin binder for achieving optimum properties in the PSP/CSA brake pad is as

follows: PSP: 26 %, CSA: 45 %, and epoxy resin binder: 25 %. Similarly, based on Figure 4.18, the optimal mixing ratio of PSP, kaolin, and epoxy resin binder for the PSP/K brake pad is PSP: 45 %, kaolin: 38.6625 %, and epoxy resin binder: 15 %.

4.4 Mould Description and Mode of Operation

The brake pad mould was created and manufactured at FIIRO in Lagos, Nigeria. It consists of a base plate measuring 305 mm by 156 mm by 6 mm, accommodating the backing plate, and supported by two rods of 14 mm diameter and 102 mm height, placed at equal distances of 27 mm from each end of the base plate. At the centre of the 290 mm by 150 mm by 10 mm thick top plate, holes were chain-drilled to match the required dimensions for the brake pad materials. To form the brake pad, the top plate is lowered onto the base plate, and the composite materials are filled into the mould cavity. Using a hydraulic press and the press plate handle, the composite is compacted within the mould cavity under axial pressure. Once compacted, the brake pad is ejected from the mould with the aid of the press plate and subsequently processed. Figure 4.19 illustrates the mould assembly, while Figure 4.20 demonstrates the mould's usage.

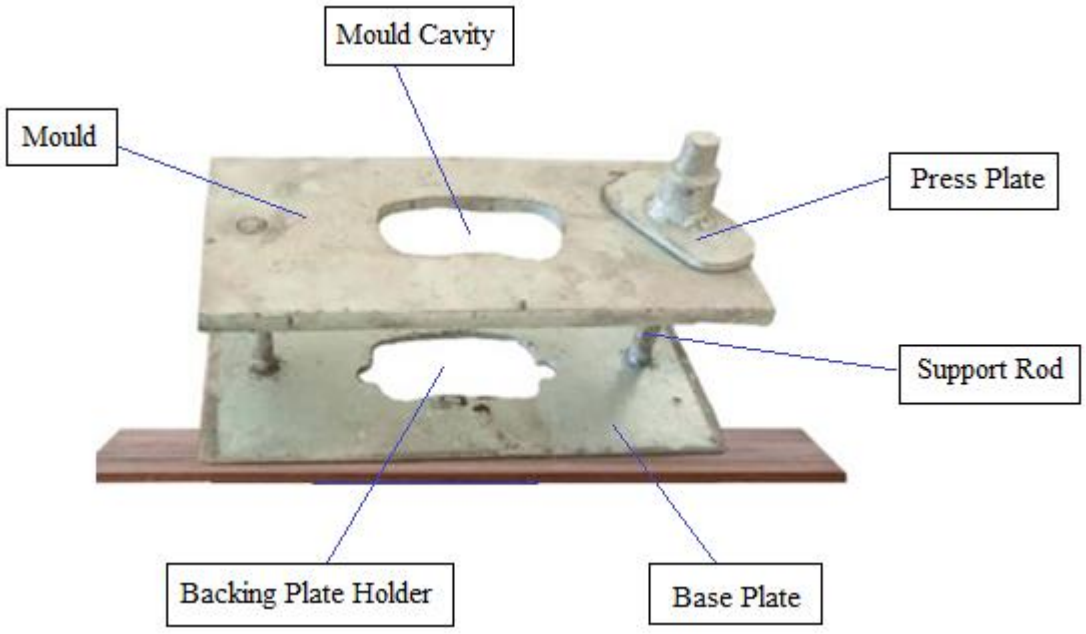

Figure 4.19 The Mould Assembly

Figure 4.20 The Mould in Use

4.5 Physical and Mechanical Characterisation of the Actual Brake Linings

This section focuses on the characterisation and comparison of the real brake pads/linings, consisting of samples with particle sizes of 106 µm, 150 µm, 212 µm, and 300 µm. The comparison is based on various properties such as density, water and oil absorption, apparent porosity, compressive strength, hardness, friction coefficient, and wear values. The outcomes of these measurements can be found in Appendix C.

4.5.1 Effect of Particle Size on the Density of the Samples

Figure 4.21 illustrates how the bulk density of the developed PSP/CSA and PSP/K brake linings varies with different particle sizes.

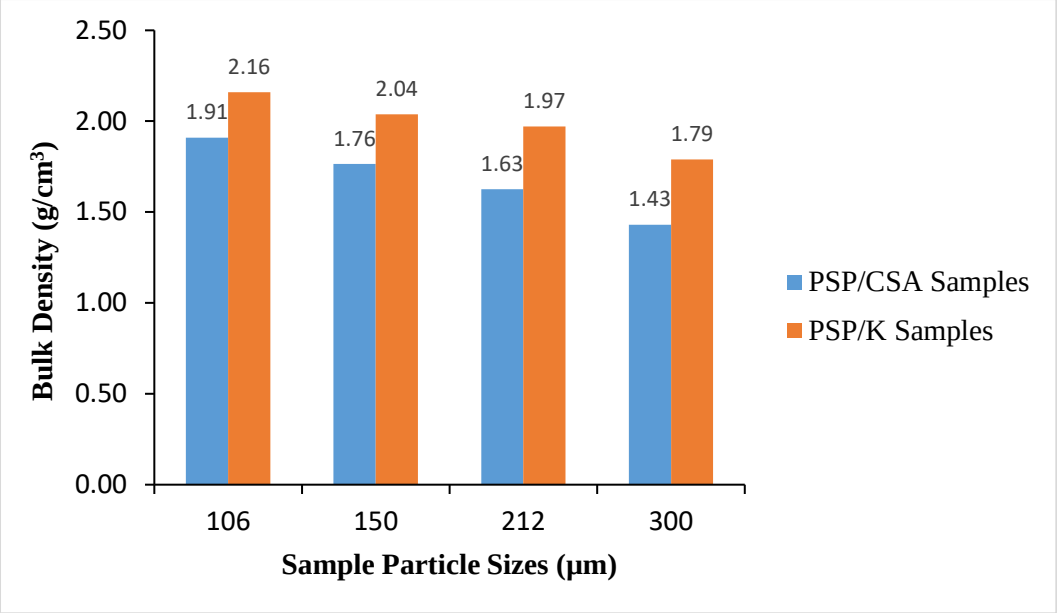

Figure 4.21 Comparative Analysis of Bulk Density of the Developed Pads

From the figure, it is evident that the bulk densities of the specimens decrease as the sieve sizes increase from 106 µm to 300 µm. The higher bulk densities observed in the smaller grit sizes of both formulations indicate that these smaller particle sizes are tightly packed and homogeneous throughout the compositions. This trend may also be attributed to better bonding between the smaller grains and the binder used.

Furthermore, the decreasing density trend from 106 µm particle sizes to 300 µm particle sizes implies an increase in porosity within this range. Additionally, the density values of the PSP/CSA samples are lower than those of the corresponding PSP/K samples, likely due to the different properties of CSA and kaolin. Specifically, CSA is lighter than kaolin.

These findings are consistent with the results of Lawal *et. al*. (2017) and align well with the recommended density values of brake pads on the market, falling within the range of 1.010 g/cm³ to 2.060 g/cm³ as stated by Abutu *et al*. (2018).

4.5.2 Effect of Particle Size on Water and SAE 40 Oil Absorption

Figure 4.22 and Figure 4.23 display the comparative analysis of water and oil absorption results for the developed samples of the brake pads.

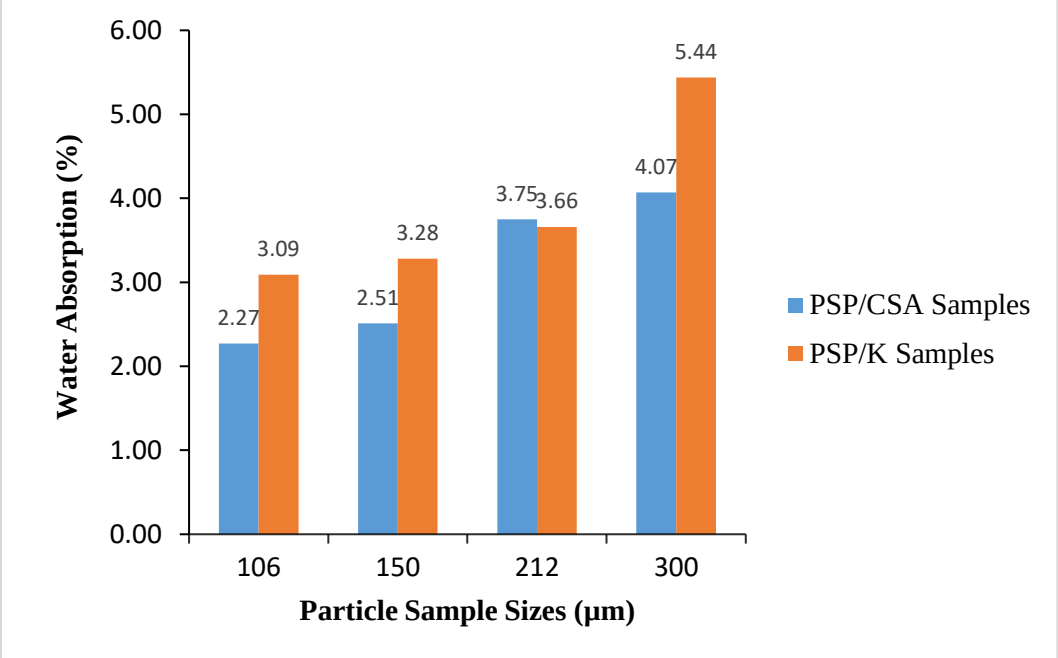

Figure 4.22 Comparative Analysis of Water Absorption of the Developed Pads

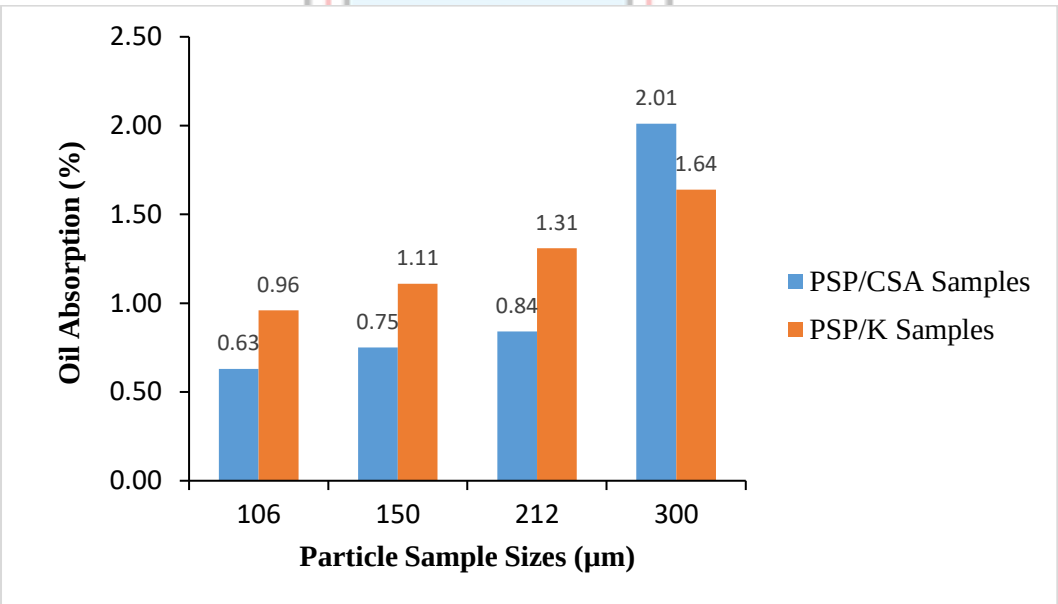

Figure 4.23 Comparative Analysis of Oil Absorption of the Developed Pads

The findings indicate that oil and water uptake values increase with an increase in grain sizes, as the 106 µm samples exhibit lower absorption rates compared to the 150 µm, 212 µm, and 300 µm samples. This phenomenon can be ascribed to enhanced bonding between the finer particles and the binder. In other words, larger sieve sizes lead to higher water and oil absorption due to the presence of more pores resulting from greater interfacial distances between the grains.

Furthermore, the PSP/CSA samples demonstrate superior water and oil absorption compared to the PSP/K samples. Additionally, both formulations display higher water absorption in 24 hours than oil absorption. This behaviour may be attributed to water's higher surface tension and lower viscosity compared to SAE 50 oil, making free hydroxyl groups of the samples more readily bond with water at molecular levels.

These trends in water and oil absorption align with previous research findings noted by others, including Amaren *et al.* (2013).

4.5.3 Effect of Particle Size on Apparent Porosity

Figure 4.24 displays the graph of porosity for both the PSP/CSA and PSP/K combinations, based on sample sizes. The results reveal that the apparent porosity of the samples increases with larger particle sizes, as shown in the figure. This trend can be attributed to the reduction in pore sizes between the grains as the particle sizes decrease from 300 µm to 106 µm.

Interestingly, a significant drop in porosity is observed between the 212 µm and 300 µm graded sieve particles in the PSP/CSA formulation. This may be a result of fundamental interactions and carbon cross-linking between the particles, which seal up the pores within the 300 µm graded sieve particles. Furthermore, the PSP/K samples exhibit lower porosity values compared to the PSP/CSA samples, which can be attributed to the different properties of the two fillers used in the formulations.

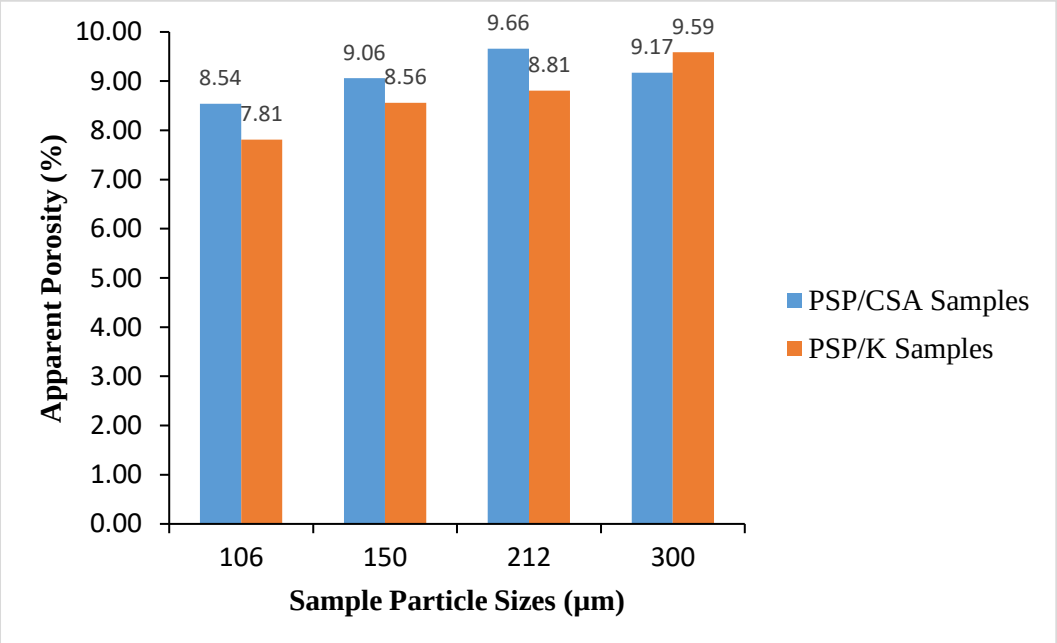

Figure 4.24 Comparative Analysis of Porosity of the Developed Pads

4.5.4 Effect of Particle Size on Compressive Strength

Figure 4.25 presents the graph of resistance to compression values against particle sizes for both PSP/CSA and PSP/K combinations. It can be observed from Figure 4.25 that the compressive strengths of the samples increase as the particle sizes decrease. This trend aligns with the findings of previous researchers, including Ademoh and Adeyemi (2015) and Idris *et al*. (2013), who studied brake linings. The PSP/K samples show higher compressive strength values, which may be attributed to the differences in properties of the two fillers used in the formulations.

The increase in compressive strength values with decreasing grain sizes can be attributed to the resin binder more effectively hardening the smaller aggregates, leading to a larger exposed surface of the samples. On the other hand, according to Mohanty and Cough (2007), the decline in compressive strength as the particle sizes increase is due to interference created as the result of the binding agent physically interacting and immobilizing, because of the mechanical constraints present. This, in turn, reduces the robustness of the samples with larger particle dimensions.

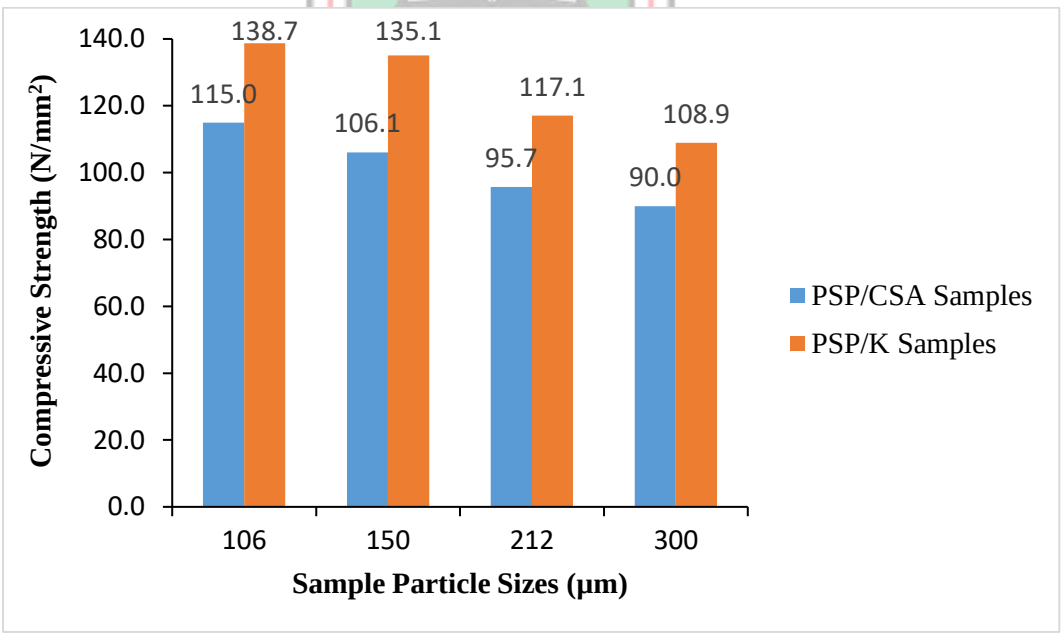

Figure 4.25 Comparative Analysis of Compressive Strength of the Developed Pads

4.5.5 Effect of Particle Size on Hardness

Figure 4.26 displays the hardness values of the samples from both formulations. The data in the figure demonstrate a variation in hardness with changes in particle sizes. Specifically,

the hardness decreases as the particle sizes increase. The 106 µm samples exhibit the highest hardness values, reaching 107.0 HBN for the PSP/CSA combination and 121.0 HBN for the PSP/K combination. On the other hand, the 300 µm samples have the lowest hardness values, measuring 84.9 HBN for the PSP/CSA combination and 92.3 HBN for the PSP/K combination.

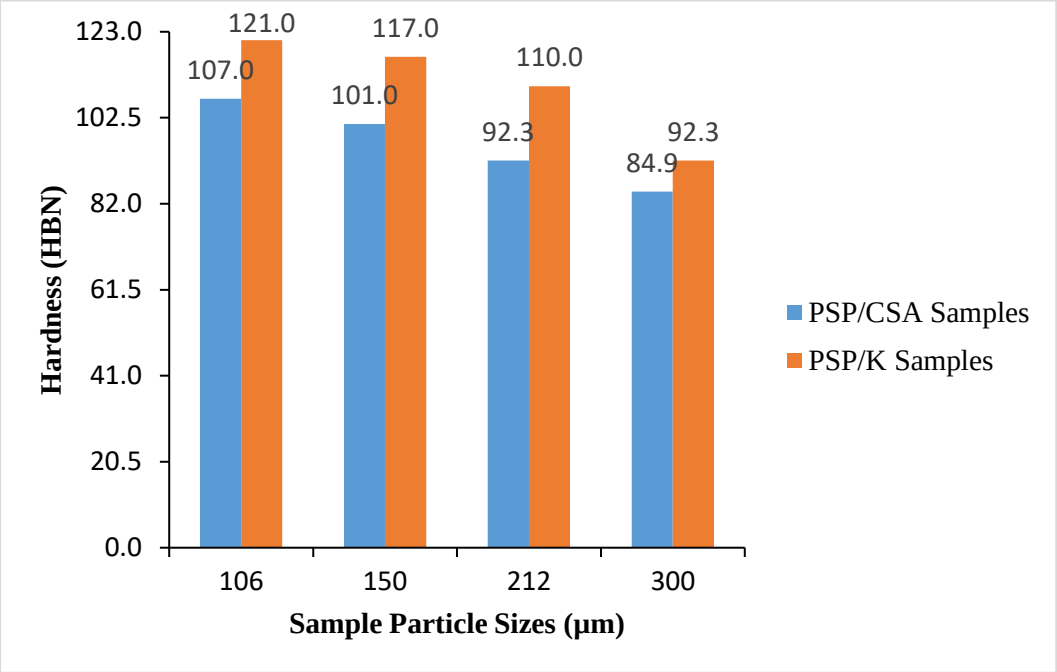

Figure 4.26 Comparative Analysis of Hardness Values of the Developed Pads

The higher hardness values observed in samples with smaller particle sizes may be attributed to an increased bonding ability between the smaller aggregates and the resin binder. Additionally, the more homogeneous distribution of the binder and filler materials (CSA and kaolin) could contribute to an expanded surface area, resulting in higher hardness values. Ademoh and Adeyemi (2015) and Idris *et al*. (2013) have also suggested this trend and phenomenon in their research. The relationship between hardness values and particle size is further supported by Yawas *et al*. (2016) and Elakhame *et al*. (2017), who noticed a similar trend in their studies on periwinkle shell powder.

Moreover, the PSP/K samples exhibit an improvement in hardness values compared to their PSP/CSA counterparts. This improvement may be due to the presence of more Si and Fe in the kaolin, which, according to the XRF data, also contains some amount of Cr. These elements, known for their strength and hardness, likely contribute to the enhanced hardness in the PSP/K samples.

4.5.6 Effect of Particle Size on Coefficient of Friction

Figure 4.27 illustrates the relationship between particle size and the friction coefficient for the two formulations. Generally, reduced friction coefficient values were observed with an increase in the grain sizes of both formulations. This trend is supported by other researchers, including Amaren *et al*. (2013) and Asotah and Adeleke (2017).

The marginally higher friction coefficient of the samples with lower grit sizes can be attributed to the homogeneous distribution of the finer and smaller particles within the binder. This leads to increased bonding, surface area, and hardness, resulting in a greater number of atomic particles in close proximity for interaction.

Additionally, the results indicate that the average friction coefficient values of the PSP/K samples are slightly higher than those of the PSP/CSA pad samples. This could be due to the kaolin powder showing a more homogeneous distribution and better bonding capability with the epoxy binder compared to the coconut shell ash.

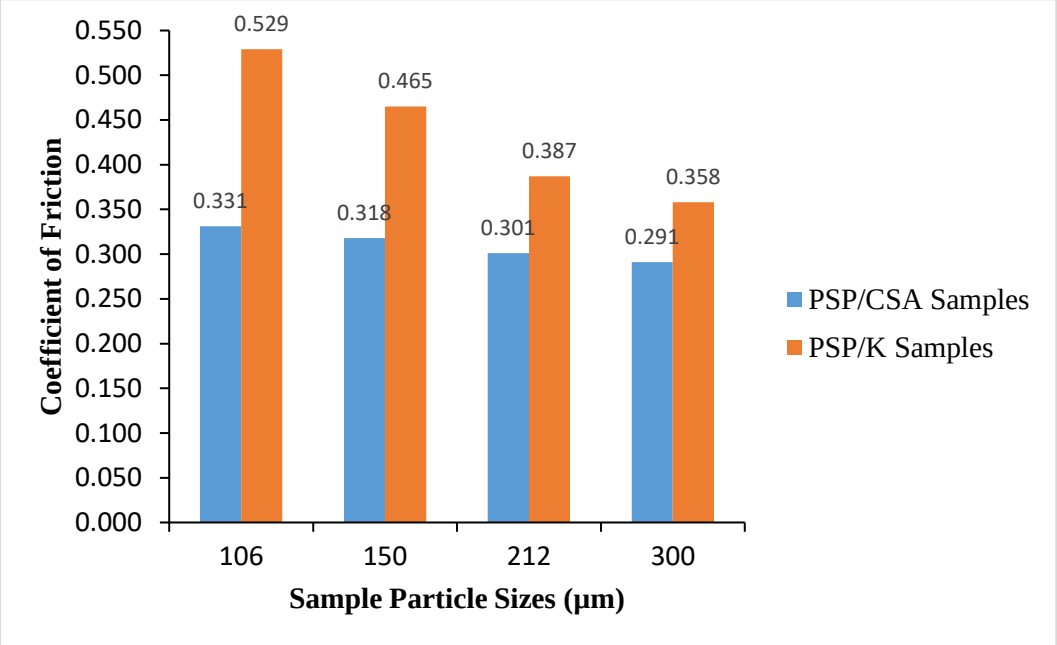

Figure 4.27 Comparative Analysis of Friction Values of the Developed Pads

4.5.7 Effect of Particle Size on Wear Rate

Figures 4.28 depict the correlation between wear values and particle sizes for the two material combinations. The figures demonstrate that the wear rate rises as particle sizes increase for each sample. This trend aligns with the findings reported by Amaren (2016)

and Amaren *et al*. (2013), who noted a similar relationship between wear rate and particle sizes. According to Amaren (2016), the influence of grain size on the rate of wear is linked to a greater tendency for fracturing in larger particles and decreased sliding distance at finer particle sizes. Additionally, Kawai *et al*. (1998) observed a reciprocal linear relationship between hardness and rate of wear, indicating that composites with higher surface hardness experience lower wear rates due to improved interfacial bonding between finer particle sizes and the resin binder.

Furthermore, Figure 4.28 reveals an enhancement in wear resistance for the PSP/K samples compared to the PSP/CSA samples. As mentioned earlier, this improvement is attributed to the higher mean hardness values and crush resistance values of the PSP/K samples (see Figures 4.25 and 4.26).

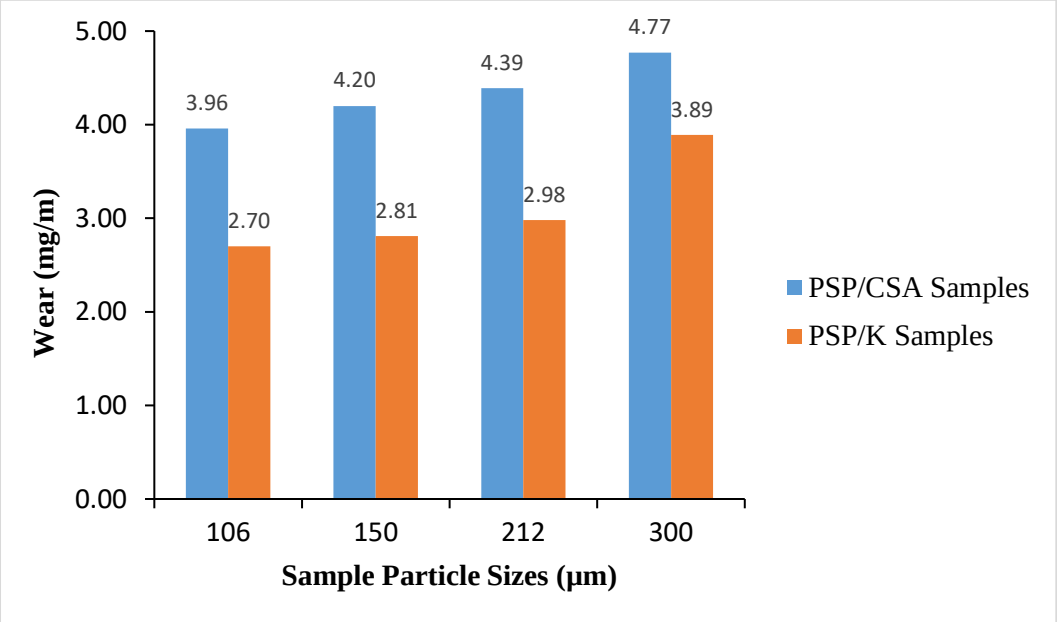

Figure 4.28 Comparative Analysis of Wear Values of the Developed Pads

4.6 Morphological Analysis of the Brake Pad Samples

In this section, the morphology of different samples is compared. Figures 4.29 to 4.32 present the morphological characteristics of the PSP/CSA developed brake lining at 106 µm, 150 µm, 212 µm, and 300 µm sieve sizes, respectively. On the other hand, Figures 4.33 to 4.36 display the morphological characteristics of the PSP/K counterparts.

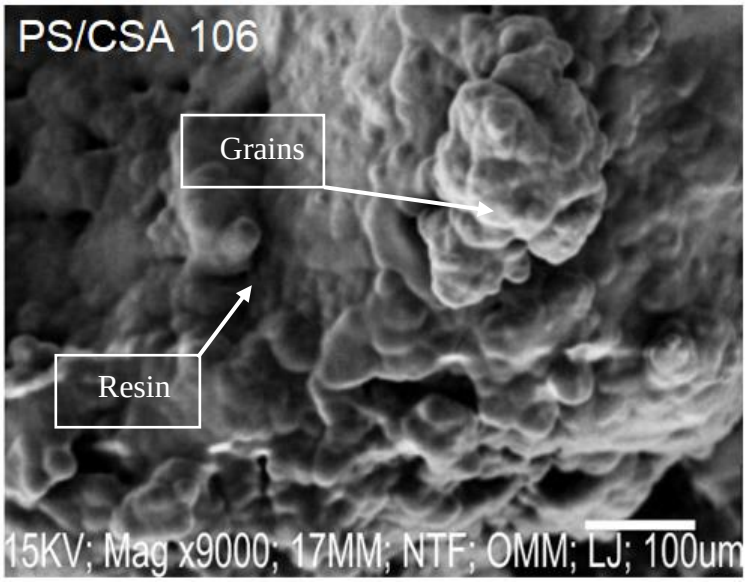

Figure 4.29 Microstructure of PSP/CSA Pad with 106 µm Particle Size

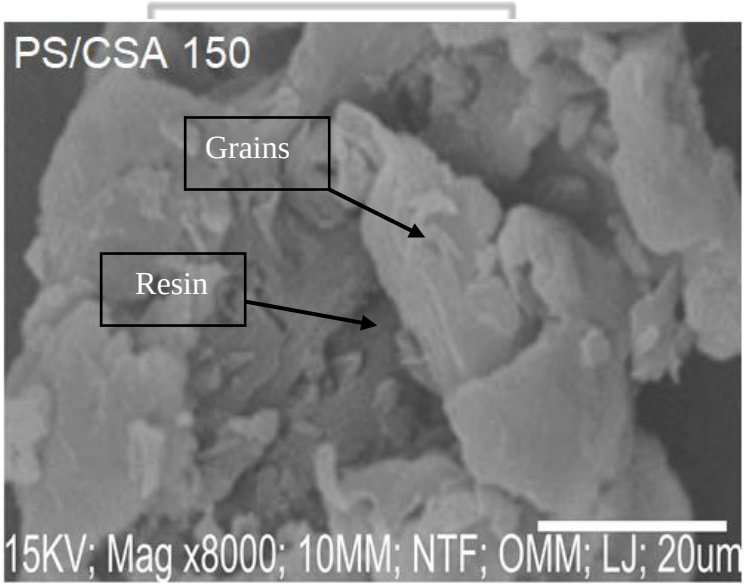

Figure 4.30 Microstructure of PSP/CSA Brake Pad with 150 µm Particle Size

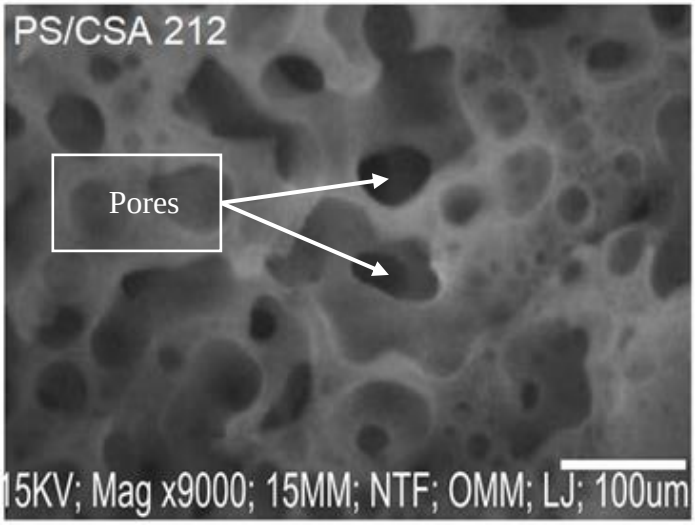

Figure 4.31 Microstructure of PSP/CSA Brake Pad with 212 µm Particle Size

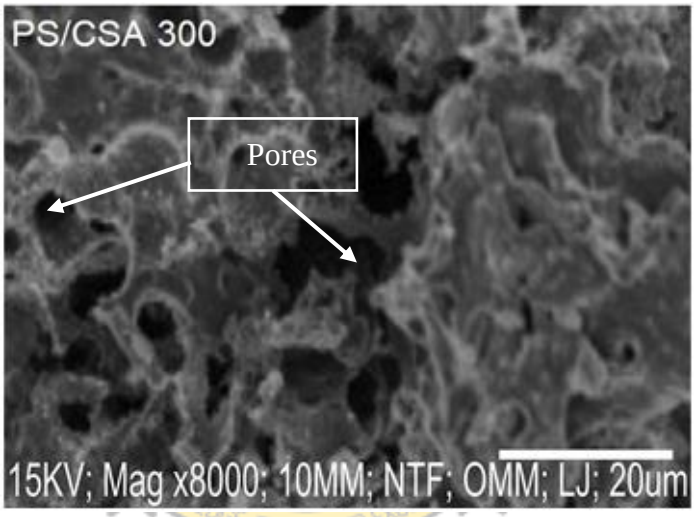

Figure 4.32 Microstructure of PSP/CSA Brake Pad with 300 µm Particle Size

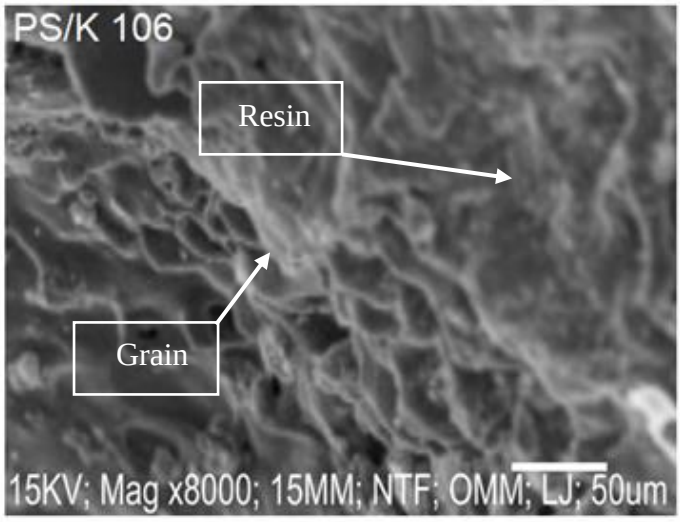

Figure 4.33 Microstructure of PSP/K Brake Pad with 106 µm Particle Size

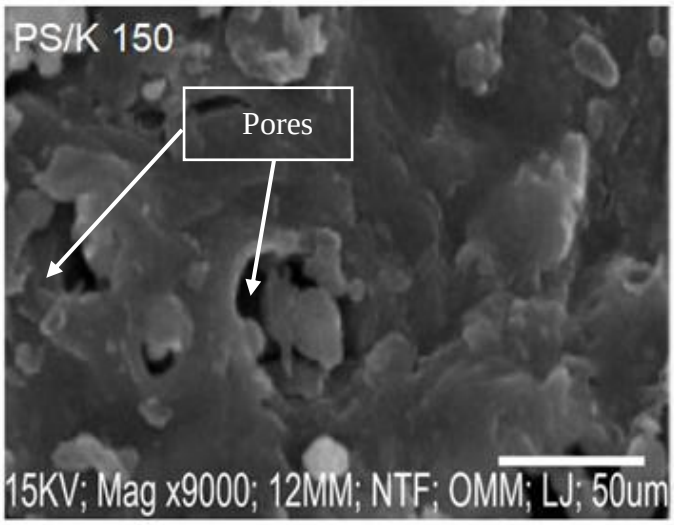

Figure 4.34 Microstructure of PSP/K Brake Pad with 150 µm Particle Size

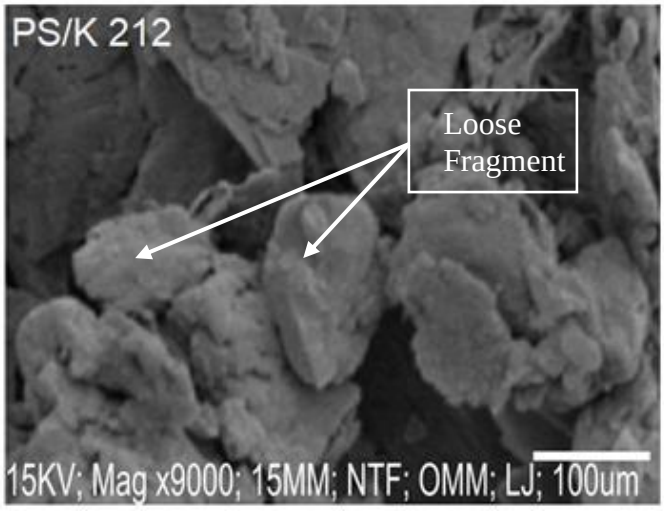

Figure 4.35 Microstructure of PSP/K Brake Pad with 212 µm Particle Size

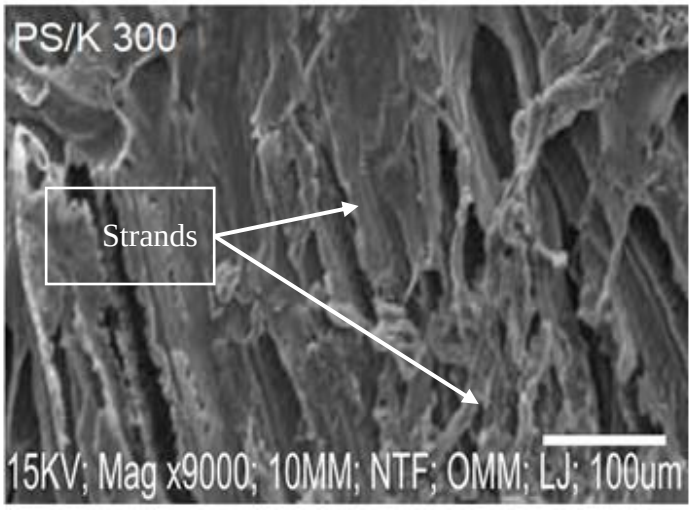

Figure 4.36 Microstructure of PSP/K Brake Pad with 300 µm Particle Size

Based on the micrographs, it was observed that there is generally a more even distribution of the resin binder (darker spots) and the other particles in the mixture (whiter phases), although some pores are visible. As the particle sizes increase, the pores become clearer and larger in the mixture, resulting in a spongy texture on the surface (when comparing Figures 4.29 and 4.30 with Figures 4.31 and 4.32; Figure 4.33 and 4.34 with Figure 4.35 and 4.36).

This indicates that there is better bonding between the resin and the smaller particle sizes, leading to a closer inter-packing interface compared to the larger particle sizes. In other words, the interfacial bonding in 106 µm particle size pads for both formulations is superior to that of the 300 µm particle size pads.

In contrast, the PSP/K mixture appears more compact than the corresponding PSP/CSA mixture at a particle size of 106 µm, but with a few pores. This may be due to improved adhesion between the resin and the kaolin particles. However, the 212 µm and 300 µm particle samples of the PSP/K mixtures appear rougher with more loose fragments on their surfaces compared to their PSP/CSA counterparts. Specifically, the 300 µm PSP/K sample has a strand-like texture when compared to the 300 µm PSP/CSA sample.

4.7 Thermal Analysis of the Brake Pad Samples

In this section, the thermal stability of the different particle size samples is examined for both formulations.

Figure 4.37 to 4.40 display the TGA and DTA curves of the PSP/CSA formulated samples at sieve sizes of 106 µm, 150 µm, 212 µm, and 300 µm, respectively.

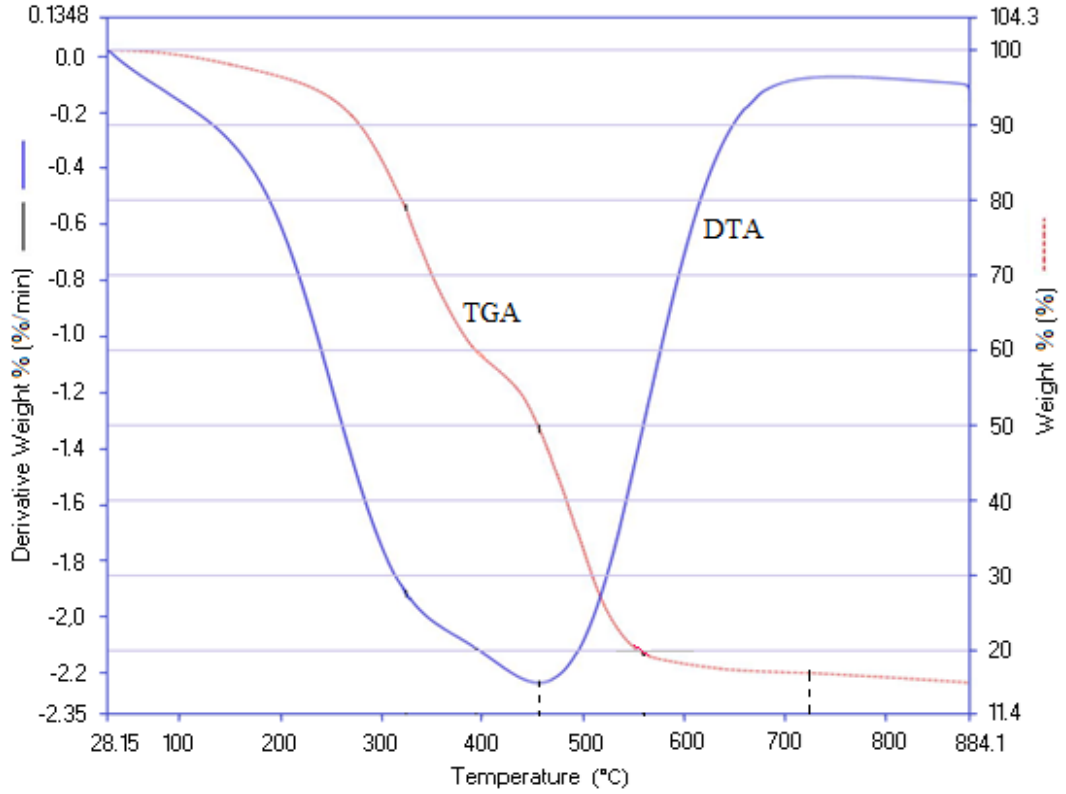

Figure 4.37 TGA and DTA Curves of 106 µm PSP/CSA Sample

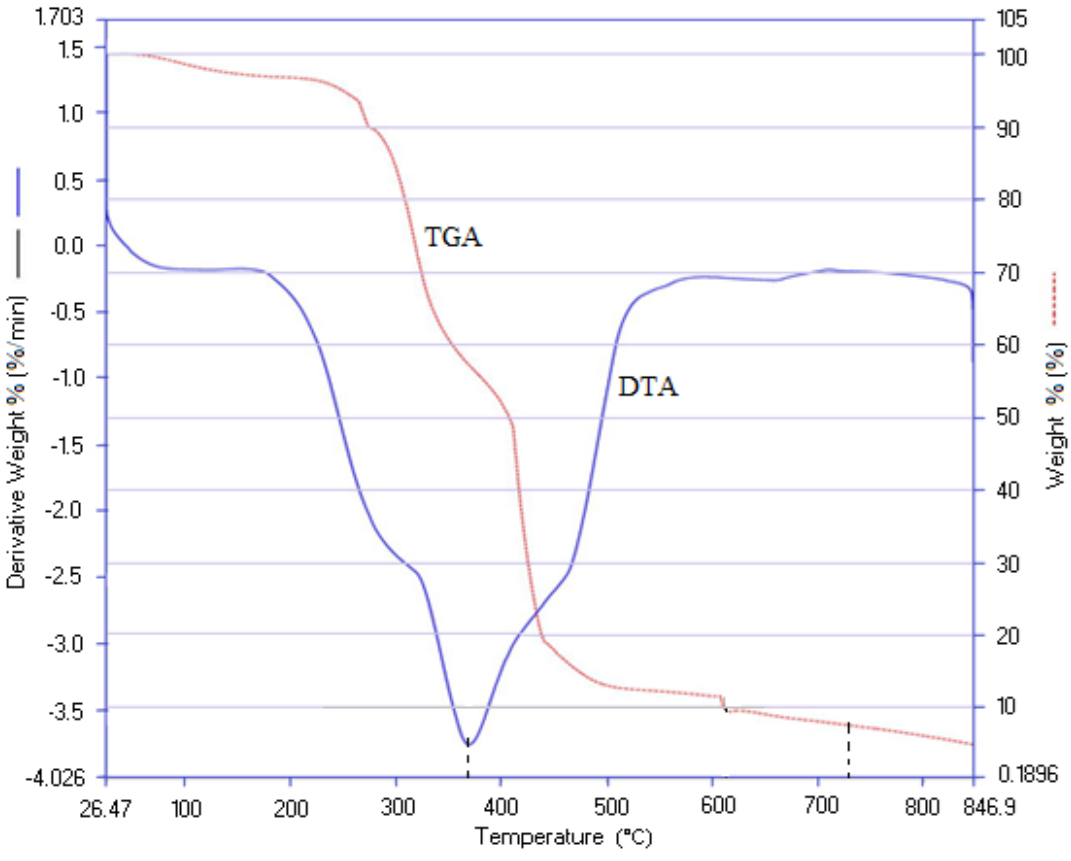

Figure 4.38 TGA and DTA Curves of 150 µm PSP/CSA Sample

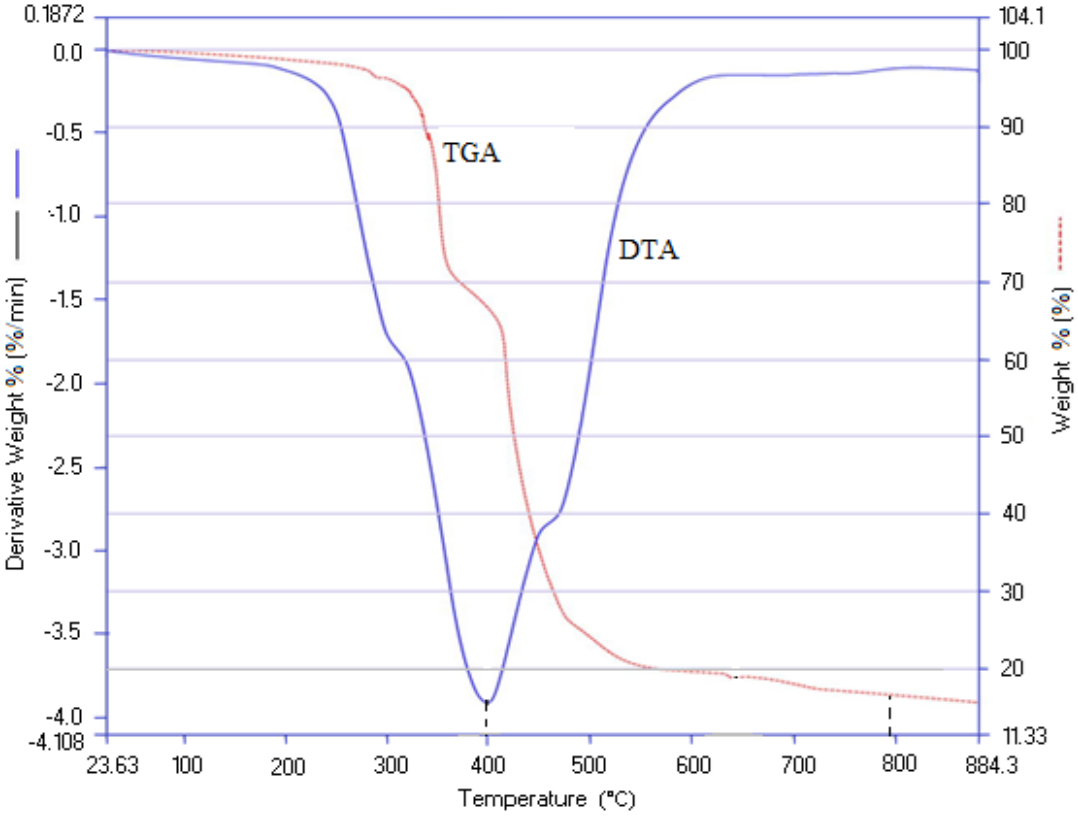

Figure 4.39 TGA and DTA Curves of 212 µm PSP/CSA Sample

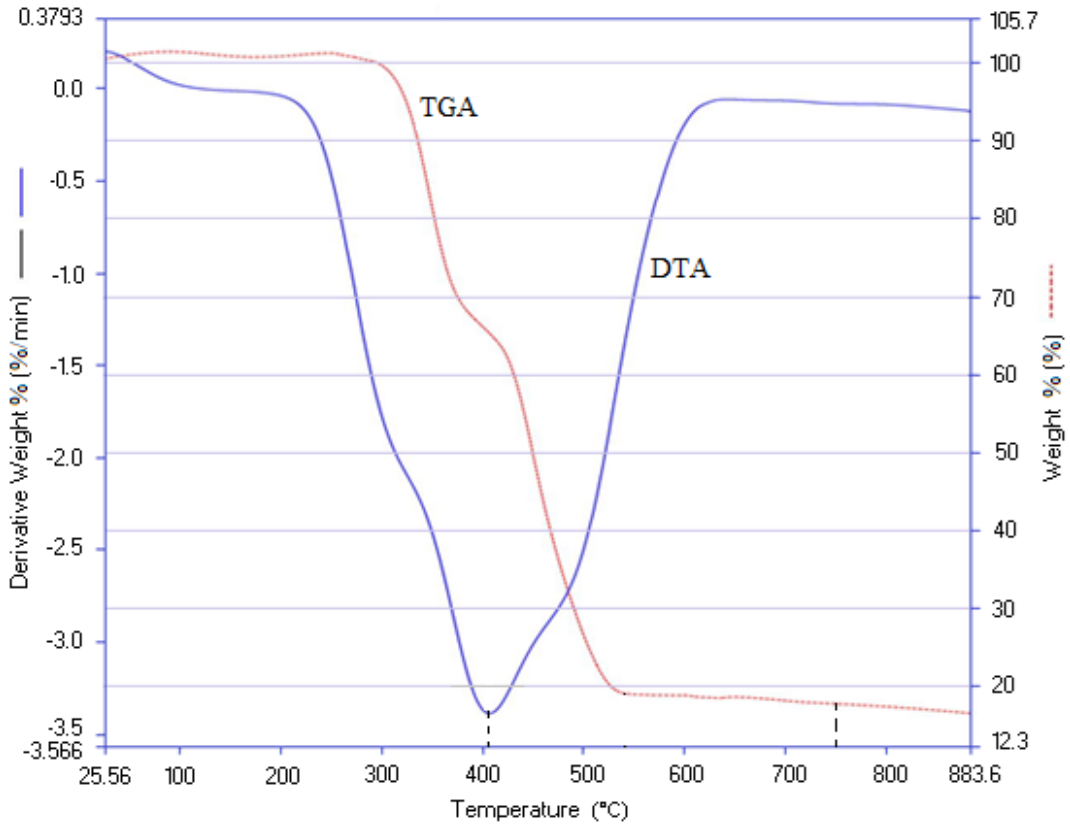

Figure 4.40 TGA and DTA Curves of 300 µm PSP/CSA Sample

Figure 4.37 shows the TGA of the 106 µm sample particles, displaying an overall weight loss of almost 83 % between 30 °C and about 720 °C. The DTA graph indicates the maximum degradation of the sample occurs at a peak temperature of 459 °C.

Similarly, the thermal characterisation of the 150 µm PSP/CSA sample (Figure 4.38) reveals a total weight loss of about 93 %, occurring between 30 °C and about 725 °C. The maximum decomposition of the sample occurs at a temperature of about 370 °C.

Moving on to the 212 µm PSP/CSA sample particles (Figure 4.39), the thermograph indicates that the maximum degradation of the particles occurs at a temperature of 400 °C, with an overall weight loss of about 83 % occurring between 30 °C and 795 °C.

Figure 4.40 presents the DTA curve for the 300 µm PSP/CSA sample, revealing a maximum degradation temperature of almost 410 °C, with an overall weight loss of 82.5 % observed between 300 °C and about 750 °C.

The thermal characterisation of the PSP/K formulated samples at sieve sizes of 106 µm, 150 µm, 212 µm, and 300 µm is illustrated in Figure 4.41 to 4.44, respectively.

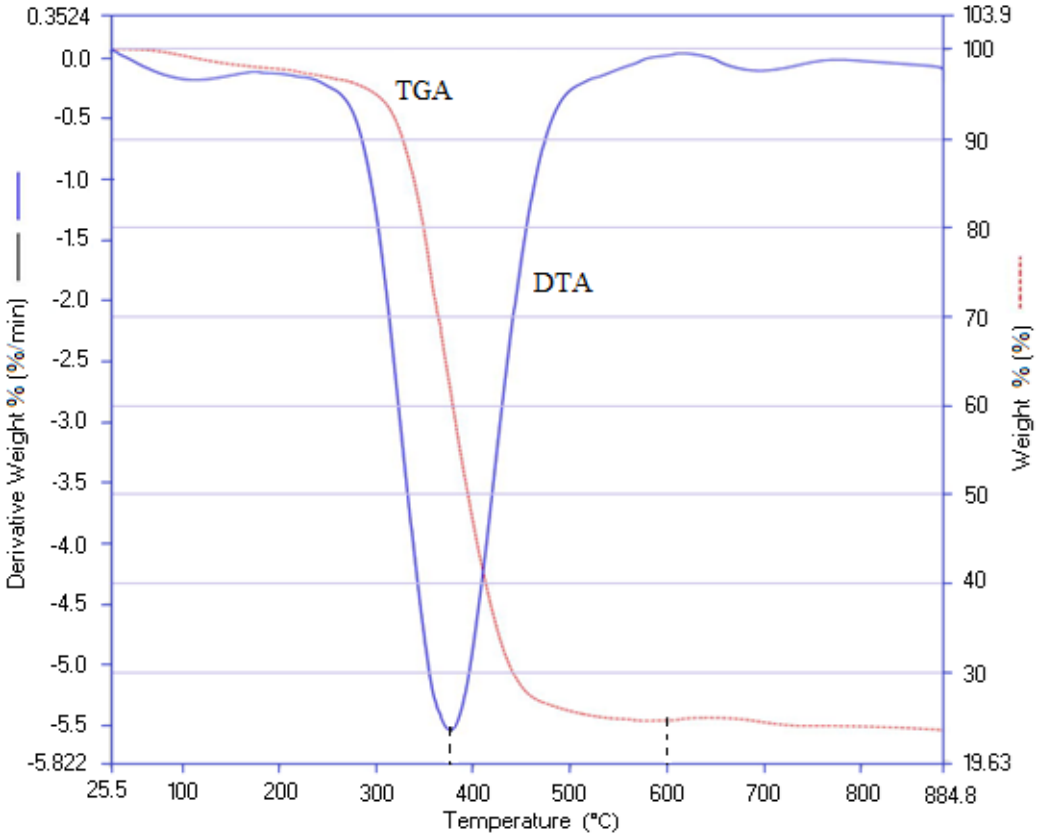

Figure 4.41 TGA and DTA Curves of 106 µm PSP/K Sample

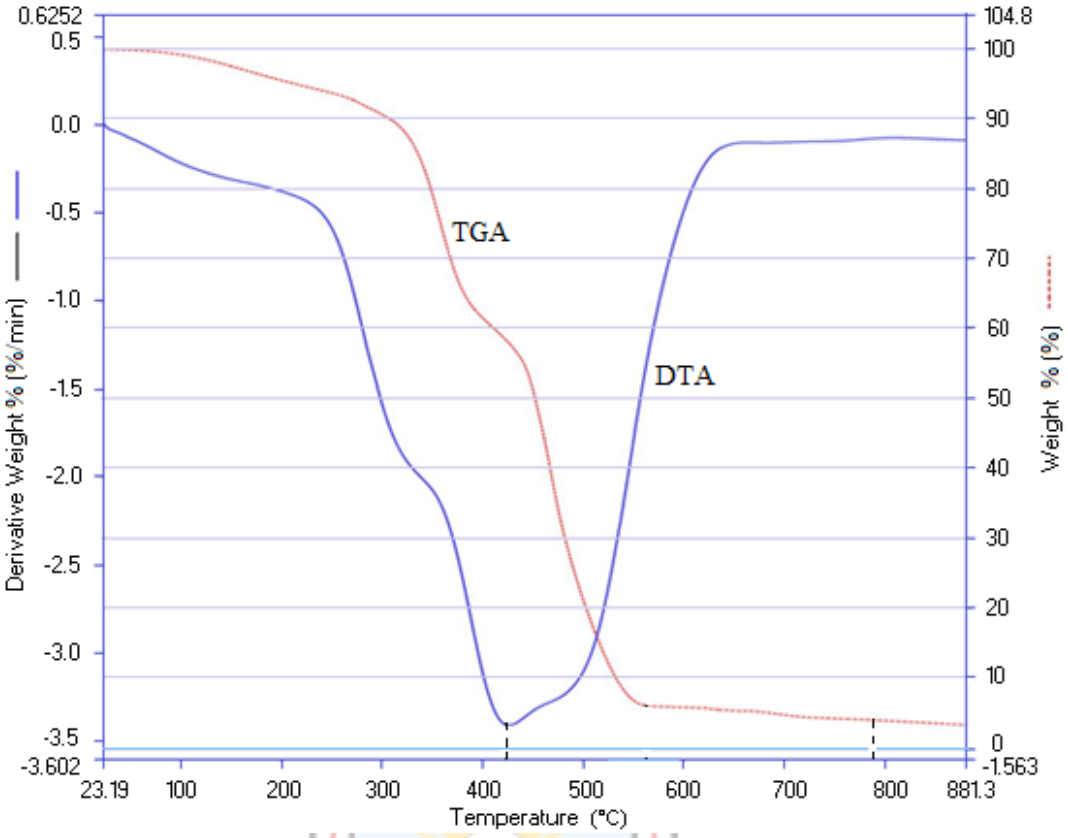

Figure 4.42 TGA and DTA Curves of 150 µm PSP/K Sample

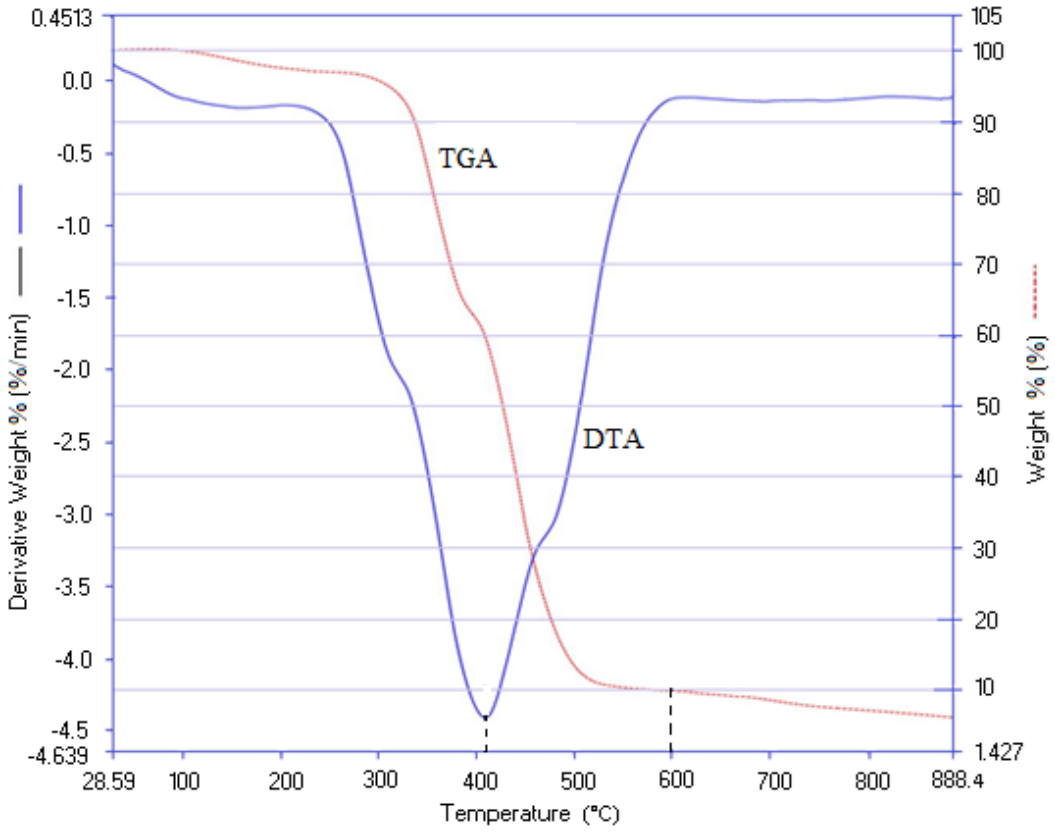

Figure 4.43 TGA and DTA Curves of 212 µm PSP/K Sample

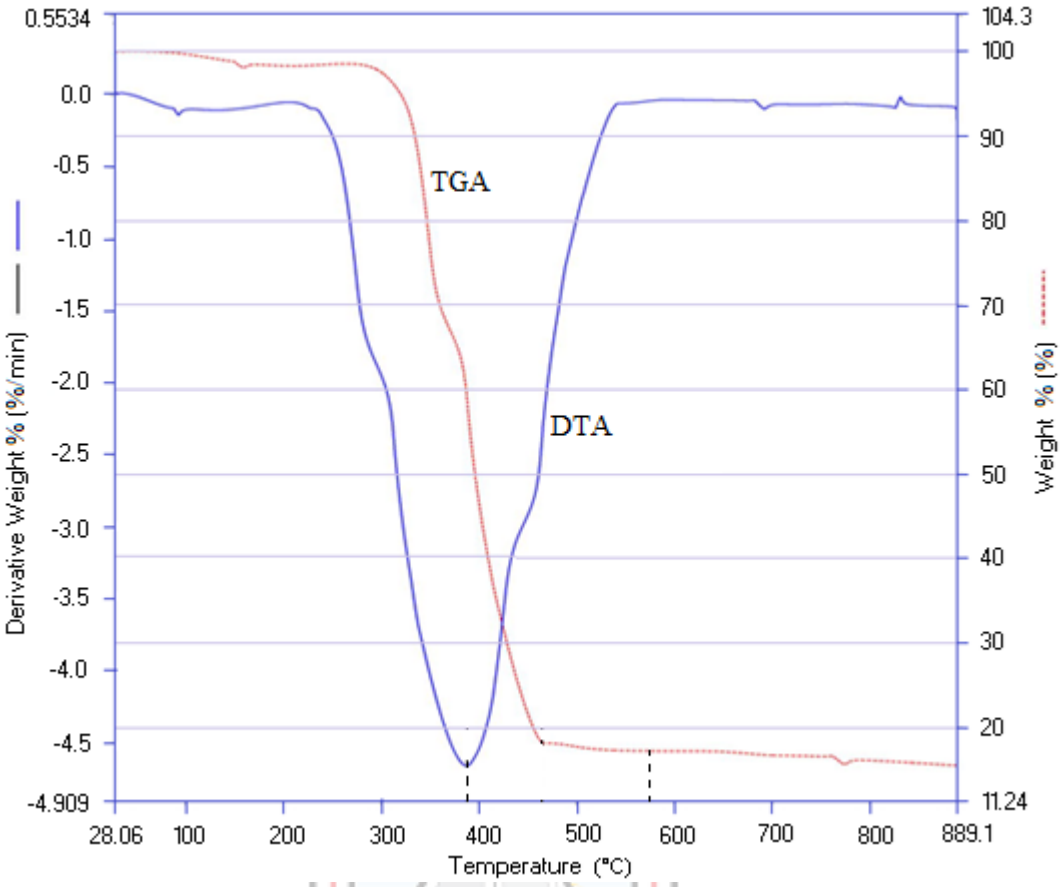

Figure 4.44 TGA and DTA Curves of 300 µm PSP/K Sample

In Figure 4.41, the thermal analysis of the 106 µm PSP/K sample shows a peak temperature of 377 ^{o}C, while the TGA curve reveals an overall weight loss of about 75 % between 30 ^{o}C and 600 ^{o}C.

Figure 4.42 displays the maximum decomposition temperature of the 150 µm PSP/K sample as 428 ^{o}C. An overall weight loss of about 96.3 % was observed between 30 ^{o}C and 790 ^{o}C.

For the 212 µm PSP/K sample, the DTA curve (Figure 4.43) indicates a maximum decomposition temperature of 409 ^{o}C, with an overall weight loss of 90 % occurring within a temperature range of 30 ^{o}C to 600 ^{o}C.

Similarly, the 300 µm PSP/K sample (Figure 4.44) shows a decomposition temperature of 390 ^{o}C, with an overall weight loss of 83 % seen within 30 ^{o}C and 580 ^{o}C.

Both formulations exhibit a similar pattern of thermal behaviour, showing only one stage of endothermic degradation/burning, as observed from the DTA curves. This is expected since the materials are the same, with only varying particle sizes.

As per Amaren (2016), the suggested upper temperature operating range for regular street vehicles falls within 300 ºC to 500 ºC. The comparison of percentage weight loss for different sieve sizes of the PSP/CSA and PSP/K samples at temperatures of 300 ºC, 400 ºC, and 500 ºC within the recommended range is presented in Tables 4.14 and Table 4.15, respectively.

Table 4.14 Weight Loss of PSP/CSA Samples within the Recommended Temperature Range

Particle Size (µm)	Weight Loss (%)		
	300 ºC	400 ºC	500 ºC
106	14.8	40.7	66.2
150	15.0	47.0	87.2
212	3.5	33.5	75.8
300	0.0	33.8	73.5

Table 4.15 Weight Loss of PSP/K Samples within Recommended Temperature Range

Particle Size (µm)	Weight Loss (%)		
	300 ºC	400 ºC	500 ºC
106	5.3	53.3	74.3
150	8.9	38.4	78.4
212	2.7	53.2	81.9
300	3.9	37.9	86.3

According to Table 4.14, the percentage weight loss of the PSP/CSA formulations for the 106 µm, 150 µm, 212 µm, and 300 µm particle sizes within the recommended temperature range are 51.4 %, 72.2 %, 72.3 %, and 73.5 %, respectively. Similarly, Table 4.15 shows that the percentage weight loss of the PSP/K formulation for the 106 µm, 150 µm, 212 µm, and 300 µm particle sizes are 69.0 %, 69.5 %, 79.2 %, and 82.4 %, respectively.

The results indicate that the lower particle brake pad samples experienced lower overall weight loss than the higher particle samples. Specifically, the 106 µm particle sizes of both the PSP/CSA and PSP/K samples are more thermally stable than the other sample grit sizes, with the PSP/CSA pad demonstrating better thermal stability due to the differences in properties of the CSA and the kaolin.

4.8 The Developed Brake Pads

The diverse characteristics and outcomes of the thermal analysis for all brake pad samples indicate that the ideal particle size for both formulations (PSP/CSA and PSP/K combinations) is 106 µm. Figure 4.45 displays the final brake pads produced from these formulations using this specific material grit size.

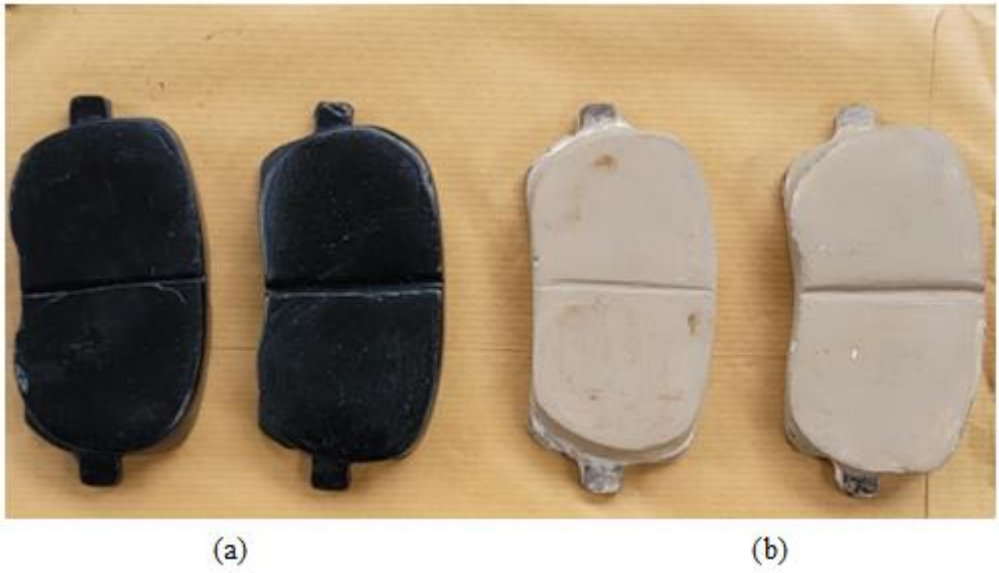

Figure 4.45 Photographs of the Developed Brake Pads Showing (a) PSP/CSA (b) PSP/K Brake Pads

4.9 Comparison of the Newly Developed Brake Pads and Other Brake Pads

In this section, the contrast between the outcomes of the 106 µm graded brake pads developed in this study and those from prior research, certain commercial brake pads, and an asbestos-based brake pad, are examined.

4.9.1 Comparison of the Developed Brake Pads and Pads from Related Past Works

The brake pads analysed from previous studies include those made from Palm Kernel Shell (PKS) by Ibhadode and Dagwa (2008), bagasse by Aigbodion *et al*. (2010), eggshell by Edokpia *et al*. (2014), periwinkle and fan palm by Amaren (2016), and maize husk by Ademoh and Adeyemi (2015). These brake pads are compared with the newly developed brake pads as presented in Table 4.16.

Table 4.16 Properties of the Developed Brake Pads and Brake Pads Produced from Related Past Works

Properties	Brake Pads from Related Past Works						Developed Brake Pads	
	PKS Based 125 µm	Bagasse Based 100 µm	Egg Shell Based 125 µm	Periwinkle Based 125 µm	Fan Palm Based 125 µm	Maize Husk Based 300 µm	PSP/CSA Based 106 µm	PSP/K Based 106 µm
Bulk Density (g/cm^3)	1.650	1.430	1.650	1.120	0.990	0.853	1.910	2.160
Water Absorption (%)	5.03	3.48	3.21	0.39	4.00	0.91	2.27	3.09
Oil Absorption (%)	0.44	1.11	1.15	0.37	4.56	0.58	0.63	0.96
Apparent Porosity (%)	22.45	-	-	-	-	-	8.54	7.81
Compressive Strength (N/mm^2)	103.5	105.6	103.0	147.0	92.9	10.3+	115.0	138.7
Hardness (HBN)	92.0	100.5	99.1	116.7	95.7	127.8	107.0	121.0
Coefficient of Friction	0.44	0.42	0.30	0.35 – 0.41	0.20 – 0.31	0.37 – 0.40	0.33	0.53
Average Wear (mg/m)	4.40	4.20	4.00	-	-	2.146	3.96	2.70

Table 4.16 reveals that the newly developed brake pads are slightly heavier compared to the brake pads produced in previous studies. The PSP/CSA and PSP/K pads are 48.89 % and 68.49 % denser, respectively, than the mean density of 1.282 g/cm^3 for the brake pads from related past works. Among the compared brake pads, the maize husk-based brake pad is the lightest, with a density of 0.853 g/cm^3.

Regarding water absorption, the new brake pads generally exhibit lower rates than most other brake pads, except for the periwinkle-based and maize husk-based pads. Notably, the periwinkle-based brake pad demonstrates the best water absorption value of 0.39 %. On the other hand, the produced brake pads have oil absorption values lower than those of bagasse-based, eggshell-based, and fan palm-based formulated brake pads, but higher than those of PKS-based, periwinkle-based, and maize husk-based brake pads. Specifically, the periwinkle-based pad stands out with the lowest oil absorption value of 0.37 %, while the fan palm-based pad records the highest value of 4.56 %.

The porosities of the formulated brake pads are lower than that of the PKS-based brake pad. Blau (2001) indicates that a porosity of 5 – 10 % is typically present in commercial brake pads, and the porosities of the newly developed brake pads fall within this range, measuring at 8.54 % for the PSP/CSA pad and 7.81 % for the PSP/K pad.

In terms of compressive strength, the new brake pads exhibit higher values than all other brake pads, except for the periwinkle-based pad, which is about 27.8 % and 6 % stronger in compression than the PSP/CSA and PSP/K brake pads, respectively.

The PSP/K brake pad displays a hardness value (121.0 HBN) greater than all other developed pads, except the maize-husk-based brake pad. Meanwhile, the PSP/CSA pad performs better than all other brake pads, except the maize-husk and periwinkle-based brake pads.

Regarding the friction coefficient, the PSP/CSA pad shows lower values compared to the other developed brake pads, except for the fan palm and eggshell-based pads. However, the PSP/K pad exhibits a higher friction coefficient value than all other brake pads, recording a value of 0.53. The developed PSP/CSA and PSP/K brake pads exhibit lower wear rate properties of 3.96 mg/m and 2.70 mg/m, respectively, with only the maize husk-based pad showing a better value of 2.146 mg/m.

The analysis shows that the PSP/CSA and PSP/K brake pads compare well and, in most cases, exhibit more favourable properties than brake pads produced in related past works.

4.9.2 Comparison of the Developed, Commercial and an Asbestos-Based Pads

The newly developed brake pads are contrasted with an asbestos-based brake pad, which serves as a control in this study. Additionally, two after-market sales replacement commercial brake pads, referred to as COM 1 and COM 2, are included in the comparison. The characteristics of the asbestos-based brake pad were obtained from literature sources, while the properties of the commercial brake pads were determined as previously mentioned in Chapter 3. Table 4.17 presents a summary of the characteristics of the developed pads, the commercial pads, and the asbestos-based pad.

Table 4.17 Properties of the Developed and Commercial and an Asbestos-Based Pad

Properties	PSP/CSA Pad	PSP/K Pad	COM 1 Pad	COM 2 Pad	Asbestos Based Pad
Bulk Density (g/cm^3)	1.910	2.160	2.116	2.264	1.890
Water Absorption (%)	2.27	3.09	1.66	1.47	0.90
Oil Absorption (%)	0.63	0.96	1.86	1.57	0.30
Apparent Porosity (%)	8.54	7.81	6.89	6.69	-
Compressive Strength (N/mm^2)	115.0	138.7	66.8	60.1	110.0
Hardness (BHN)	107.0	121.0	101.0	97.7	101.0
Coefficient of Friction	0.32	0.53	0.30	0.31	0.30 – 0.40
Average Wear (mg/m)	3.96	2.70	4.13	5.37	3.80

The densities of the newly developed brake pads are nearly identical to those of the COM 1 and COM 2 brake pads. The density of the PSP/CSA pad aligns well with the asbestos-based pad compared to the other pads. The differences in densities between the PSP/CSA and the PSP/K brake pads and the asbestos-based pad are only 1.06 % and 14.29 %, respectively.

The developed brake pads exhibit higher water absorption values compared to the commercial and asbestos-based brake pads. The water absorption rates of the PSP/CSA and PSP/K pads, 2.27 % and 3.09 %, respectively, significantly differ from the asbestos-based pad.

Although the newly developed pads do not match the oil absorption performance of the asbestos-based brake pad, they outperform the two commercial brake pads in this aspect. However, their apparent porosities are higher compared to the commercial brake pads. Nonetheless, all three pads fall within the recommended porosity range of 5 % to 10 % as given by Blau (2001).

The results indicate that the developed brake pads exhibit higher compressive strength and hardness values than the commercial pads and even the asbestos-based pad. The compressive strengths of the PSP/CSA and PSP/K brake pads are 4.35 % and 20.69 % higher, respectively, than the values for the asbestos-based brake pad. Moreover, the hardness values of the new pads are 5.61 % and 16.53 % higher, respectively, than that of the asbestos-based pad.

The friction coefficient value of the PSP/CSA brake pad is comparable to and almost the same as those of the two commercial brake pads, falling within the friction range of the asbestos-based brake pad, between 0.30 and 0.40. The PSP/K brake pad, however, exhibits a higher friction coefficient than all the other brake pads. Both the PSP/CSA and PSP/K samples fall within the range of friction coefficients for brake materials, as stated by Blau (2001), which spans from 0.3 to 0.6.

The average wear value of the PSP/CSA pad is similar to that of the commercial and asbestos-based brake pads, slightly outperforming the commercial ones, and only 4.21 % higher than the wear value of 3.80 mg/m for the asbestos-based pad. On the other hand, the PSP/K brake pad exhibits better wear properties than all the other pads, with a value about 28.9 % lower than that of the asbestos-based pad. The wear rate results acquired for both formulations fall within the accepted industry standards for automotive brake pad manufacturing, as stated by Bhagwan *et al*. (2000).

4.9.3 Comparison of the Thermal Stability of the Developed and the Commercial Pads

Figure 4.46 displays the DSC and TGA curves of the PSP/CSA brake pads, while Figure 4.47 shows the corresponding curves for the PSP/K brake pads. Additionally, Figure 4.48 and Figure 4.49 depict the DSC and TGA curves of the COM 1 and COM 2 brake pads, respectively.

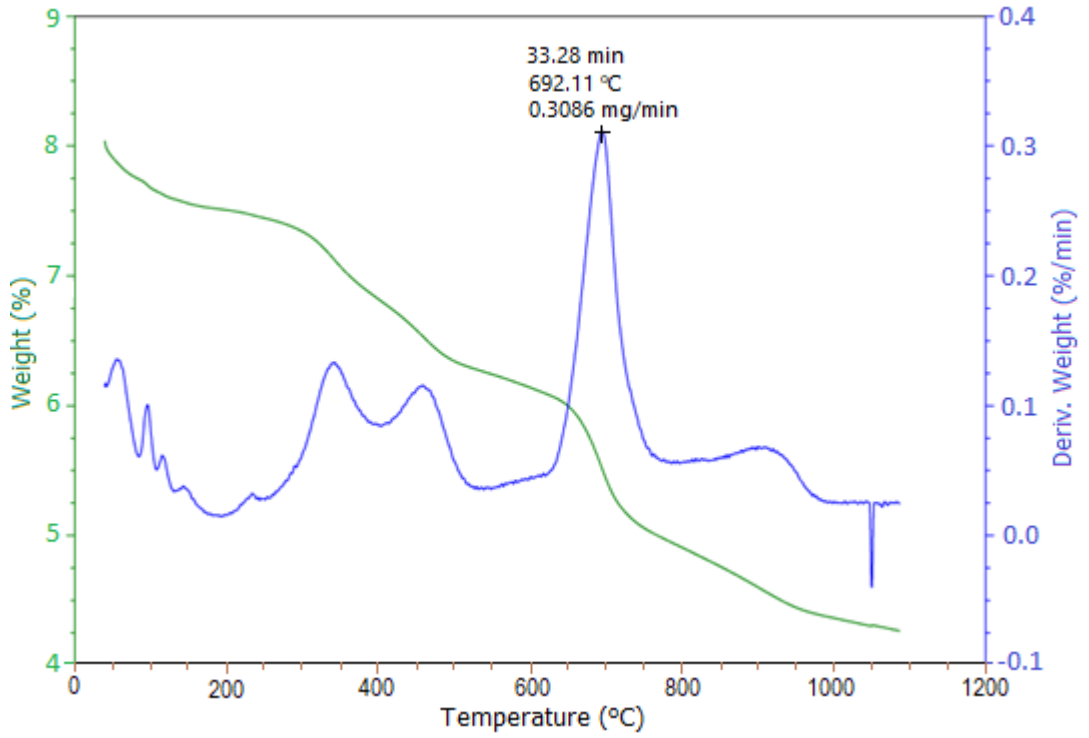

Figure 4.46 DSC and TGA Curves of the Developed PSP/CSA Brake Pad

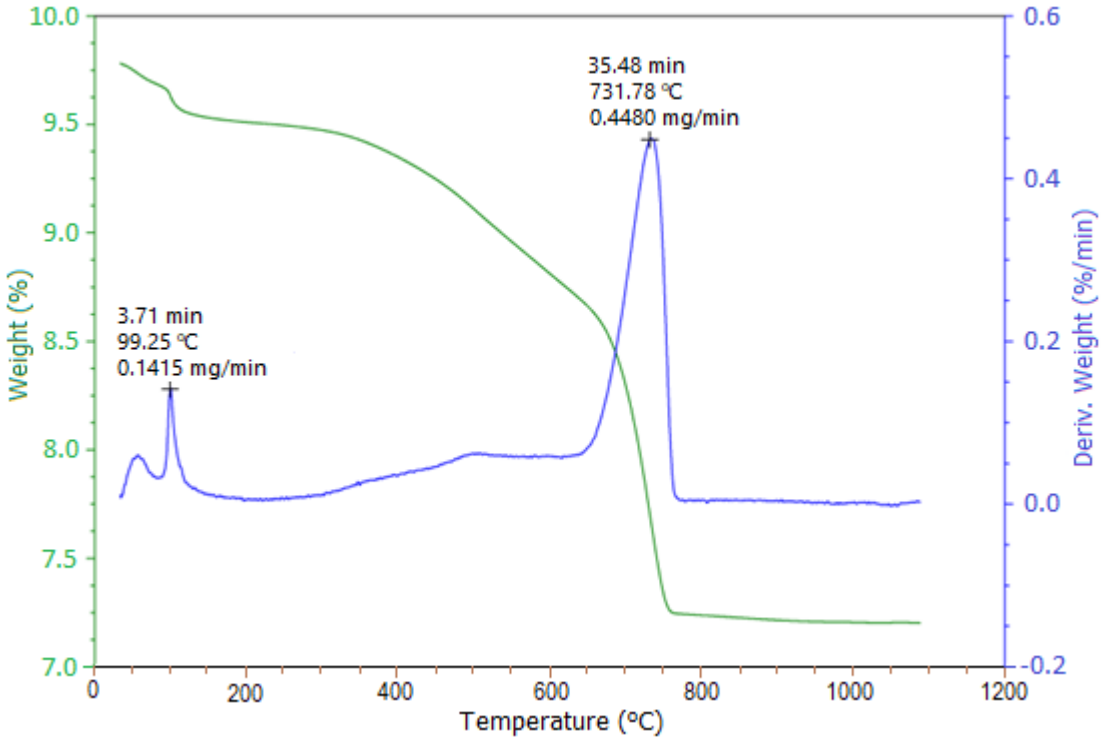

Figure 4.47 DSC and TGA Curves of the Developed PSP/K Brake Pad

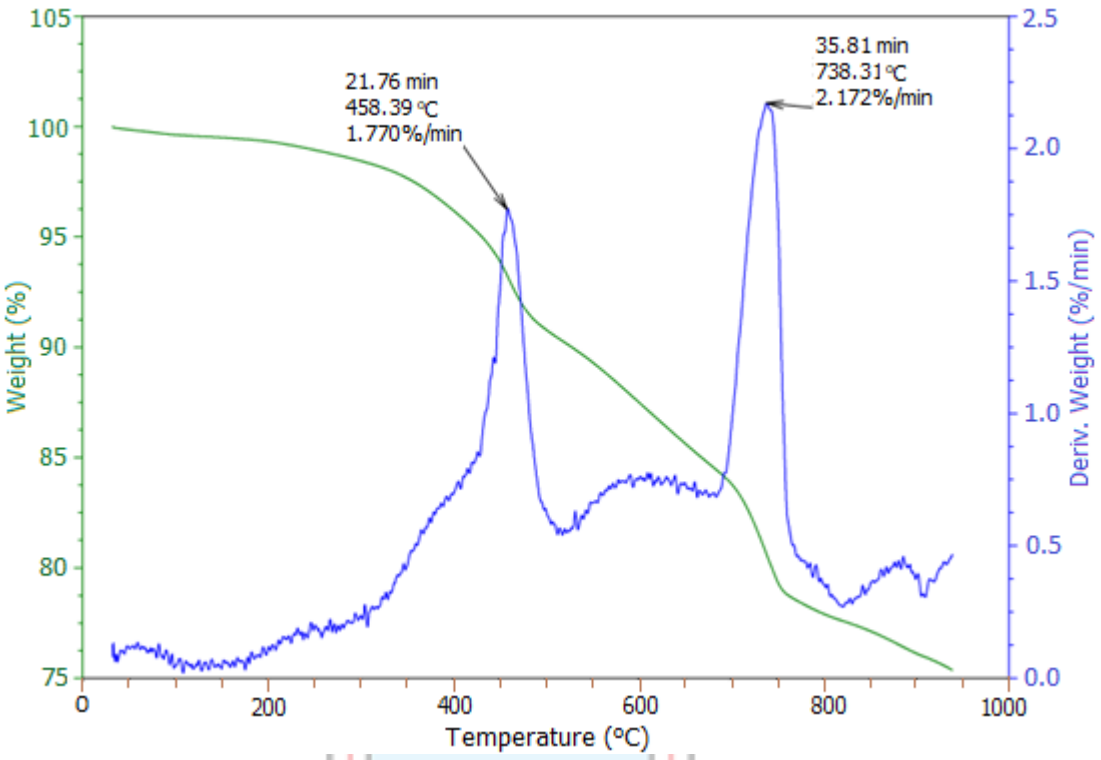

Figure 4.48 DSC and TGA Curves of the Commercial Brake Pad (COM 1)

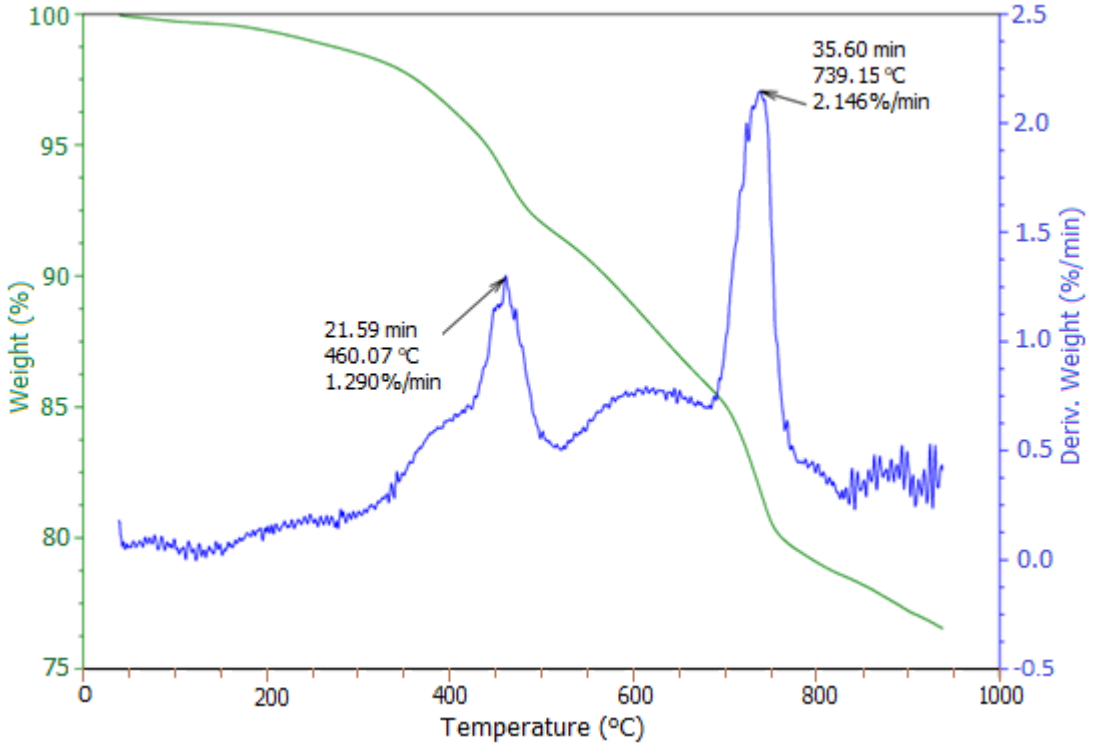

Figure 4.49 DSC and TGA Curves of the Commercial Brake Pad (COM 2)

From Figure 4.46, the PSP/CSA brake pad experienced a maximum degradation temperature of 692.11 °C, resulting in a mass loss of 30.87 %. The overall weight loss at

an equivalent temperature of about 940 °C was recorded as 44.34 %. Similarly, in Figure 4.47, the PSP/K brake pad exhibited a maximum decomposition temperature of 731.78 °C, with a percentage weight loss of 21.22. The overall weight loss of the sample at an equivalent temperature of about 940 °C was 26.31 %.

In Figure 4.48, the COM 1 pad showed two peaks of temperatures: one at 458.39 °C, potentially attributed to water of hydration removal or the evaporation of coating materials on its surface, resulting in a weight loss of 6.75 %. The other peak occurred at 738.31 °C, representing the actual degradation temperature with a weight loss of 19.37 %. The overall weight loss at a temperature of about 940 °C was 24.63 %. Similarly, in Figure 4.49, the COM 2 brake pad also exhibited two temperature peaks: one at 460.07 °C with a weight loss of about 6.11 %, and the other at 739.15 °C with a weight loss of 18.24 %. An overall weight loss of about 23.45 % was observed at a temperature of 940 °C.

Table 4.18 presents the mass reduction of the four brake pads within the recommended temperature range of 300 °C to 500 °C.

Table 4.18 Weight Loss for the Developed and the Commercial Pads within the Recommended Temperature Range

Brake Pads	Weight Loss (%)		
	300 °C	400 °C	500 °C
PSP/CSA	8.65	15.13	21.08
PSP/K	3.15	4.42	6.87
COM 1	1.56	3.79	9.20
COM 2	1.50	3.56	8.00

Table 4.18 provides the weight loss percentages of the PSP/CSA, PSP/K, COM 1, and COM 2 brake pads within the recommended temperature range, which are 12.43 %, 3.72 %, 7.64 %, and 6.50 %, respectively. The results indicate that the PSP/K brake pad exhibits better thermal performance within the recommended range compared to the two commercial brake pads. Additionally, the closeness of the degradation temperatures of 692.11 °C and 731.78 °C for PSP/CSA and PSP/K pads, respectively, to 738.31 °C and 739.15 °C for COM 1 and COM 2 brake pads demonstrates that the newly developed brake pads possess similar thermal stability as the commercial brake pads.

4.10 Vehicle On-Road Tests

The newly developed brake pads and one of the commercial brake pads (COM 1) with a backing plate were simultaneously installed on a Camry saloon car. During operation, the temperatures of the discs were measured, and the amount of wear on the pads was determined after the vehicle had been in use for a month.

4.10.1 Disc Temperature Measurements

The temperatures observed on the discs for different speeds with the PSP/CSA brake pad, the PSP/K pad, and the commercial brake pad are displayed in Figure 4.50.

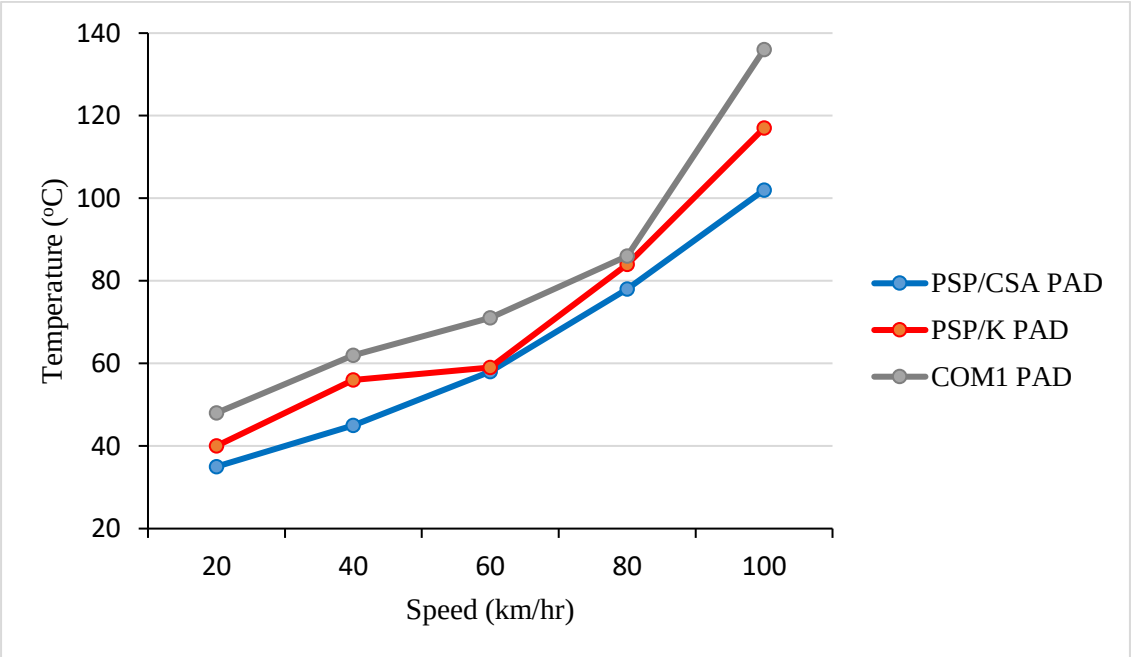

Figure 4.50 Disc Temperatures for the Developed and COM Pad at Various Speeds

The results from Figure 4.50 demonstrate a gradual increase in temperatures as the speed increases, which is as expected since higher speeds result in more increased conversion of kinetic energy into thermal energy when the brakes are applied. Elevated disc or pad temperatures can lead to brake fade or boiling of the brake fluid, resulting in a reduction in braking efficiency. Furthermore, the data reveals that the two newly developed brake pads exhibit slightly better disc temperatures compared to the commercial brake pad. Additionally, the disc temperatures recorded for the PSP/CSA pads are better than those of the PSP/K pad.

4.10.2 Wear Measurements

Table 4.19 presents the wear measurements obtained for the newly formulated brake pads and the commercial brake pad after being installed on the car and utilised for one month in the demanding traffic conditions of Accra.

Table 4.19 Wear Measurements for the Developed and COM 1 Brake Pads

Brake Pads	Initial Weight (g)	Final Weight (g)	Amount of Wear (mg)
PSP/CSA	344.560	341.669	2.891
PSP/K	356.850	355.017	1.833
COM 1	438.625	435.448	3.177

According to the data in Table 4.19, the wear measurements for the PSP/CSA, PSP/K, and COM 1 brake pads are 2.891 mg, 1.833 mg, and 3.177 mg, respectively. The findings indicate that the newly formulated brake pads demonstrate superior wear resistance compared to the commercial brake pad, with the PSP/K pad showing the lowest wear value among the three pads.

CHAPTER FIVE

CONCLUSIONS AND RECOMMENDATIONS

5.1 Conclusions

This research has determined that periwinkle shell powder, coconut shell ash, and kaolin possess properties that are similar to those of chrysotile asbestos, which is the common type of asbestos utilised in brake lining composites. Additionally, the study has demonstrated that the two distinct sets of brake pads (PSP/CSA and PSP/K formulation), produced from periwinkle shell powder, coconut shell ash, and kaolin, with an optimal particle size of 106 μm, exhibit comparable characteristics to brake pads from previous research, asbestos-based brake pads, and aftermarket replacement commercial brake pads. In conclusion, the following observations can be drawn:

(i) The findings reveal that the chemical and mineralogical compositions of the base materials closely resemble asbestos, as they all contain SiO_2, CaO, MgO, and Al_2O_3. Moreover, these materials exhibit comparable thermal stability to asbestos, with PSP degrading at 745.88 °C, CSA at 675.19 °C, kaolin at 492.85 °C, and asbestos at approximately 685 °C.

(ii) The outcomes of this investigation demonstrate that the statistical tool, Design Expert DX 13, plays a crucial role in aiding decision-making regarding material characterisations and optimisation. The software was utilised to determine the optimal mixed ratios, which were then employed in developing the PSP/CSA and PSP/K brake pads.

(iii) A custom-made mould was created and employed to manufacture brake pads specifically designed to match the brake pad dimensions of a Toyota Camry Model 2000 saloon car.

(iv) The size of the material grit significantly influences the characteristics, behaviour, and durability of the end products. For instance, properties like wear rate, apparent porosity, oil and water absorption tend to increase with larger grit sizes, whereas compressive strength, hardness, bulk density, and coefficient of friction increase as the particle size decreases.

(v) The newly formulated PSP/CSA pad exhibits compressive strength and hardness values of 115.0 N/mm^2 and 107.0 HBN, respectively, while the PSP/K pad demonstrates compressive strength and hardness values of 138.7 N/mm^2 and 121 HBN, respectively. These measured results surpass those of the asbestos-based pad, which has compressive strength and hardness values of 110.0 N/mm^2 and 101.0 HBN, respectively.

(vi) The friction coefficient values of the newly developed pads align with those of the asbestos-based pad and fall within the recommended coefficient of friction range of 0.3 - 0.6 for brake pads.

(vii) The average wear value of the PSP/CSA pad shows favourable comparison with both the commercial and asbestos-based brake pads, performing slightly better than the commercial ones and only 4.21 % higher than the wear rate value of 3.80 mg/m of the asbestos-based pad. On the other hand, the PSP/K brake pad displayed superior wear properties compared to all the other pads, with a value approximately 28.9 % lower than that of the asbestos-based brake pad.

(viii) The newly developed brake pads exhibit slightly higher density compared to the asbestos-based pad. However, the deviations in the densities of the PSP/CSA and PSP/K brake pads from the asbestos-based pad are only 1.06 % and 14.29 %, respectively. Similarly, the water and oil absorption values of the developed pads (2.27 % and 0.63 % for the PSP/CSA pad, respectively; 3.09 % and 0.96 % for the PSP/K pad, respectively) do not show favourable comparison with those of the asbestos-based pad (0.9 % and 0.3 %, respectively).

(ix) The findings from the mass losses and the proximity of the degradation temperatures (692.11 °C and 731.78 °C for the PSP/CSA and PSP/K pads, respectively) to 738.31 °C and 739.15 °C for the COM 1 and COM 2 brake pads, respectively, indicate that the manufactured brake pads possess thermal stability comparable to that of the commercial brake pads.

(x) The outcomes of the on-road tests for the developed pads, including the disc temperatures and wear amounts, showed favourable comparison with those obtained from the commercial brake pad.

(xi) In contrast, the PSP/K brake pad exhibits superior brake properties compared to the PSP/CSA pad.

Therefore, the study demonstrates that periwinkle shell powder, coconut shell ash, and kaolin can serve as suitable filler or reinforcement materials to substitute asbestos in the development of automotive disc brake linings.

5.2 Recommendations

The subsequent suggestions have been put forward:

(i) Considering that modern commercial brake pads are now manufactured using hot moulding under high pressures to enhance their properties, it is recommended to exclusively produce the newly developed pads using the hot moulding process and thereafter reexamine their performance characteristics.

(ii) As validating friction materials requires extensive on-road testing as the ultimate measure, it is advised to conduct further, longer-term investigations into the on-road effectiveness and durability of the developed brake pads. This will facilitate a comprehensive assessment of the composite linings.

REFERENCES

Abutu, J., Lawal, S. A., Ndaliman, M. B., Lafia-Araga, R. A., Adedipe, O. and Choudhury, I. A. (2018), "Effects of process parameters on the properties of brake pad developed from seashell as reinforcement material using grey relational analysis". *Engineering Science and Technology, an International Journal*, Vol. 21, Issue 4, pp. 787 – 797. https://doi.org/10.1016/j.jestch.2018.05.014

Abutu, J., Lawal, S. A., Ndaliman, M. B., Lafa-Araga, R. A., Adedipe, O. and Choudhury, I. A. (2019), "Production and characterization of brake pad developed from coconut shell reinforcement material using central composite design", *SN Applied Sciences, A Springer Nature Journal*, Vol. 1, Issue 82, https://doi.org/10.1007/s42452-018-0084.

Acharya, S. K. and Samantrai, S. P. (2012), "The Friction and Wear Behaviour of Modified Rice Husk Filled Epoxy Composite", *International Journal of Scientific and Engineering Research*, Vol. 3, Issue 6, pp. 180 – 184.

Ademoh, A. N. and Adeyemi, I. O. (2015), "Development and evaluation of maize husks (asbestos–free) based brake pad", *Industrial Engineering Letters –IEL*, Vol.5, Issue 2, pp. 67 – 80.

Aderiye J. (2015), "Kaolin Mineral Material for Automobile Ceramic Brake Pad Manufacturing Industry", *International Journal of Technology Enhancements and Emerging Engineering Research*, Vol. 2, Issue 3, pp. 84 – 88.

Adewuyi, A. P. and Adegoke, T. (2008), "Exploratory study of periwinkle shells as coarse aggregates in concrete works", *ARPN Journal of Engineering and Applied Sciences*, Vol. 3, Issue 6, pp. 1 – 5.

Adeyemi, I. O., Ademoh, N. A. and Okwu, M. O. (2016), "Development and assessment of composite brake pad using pulverized cocoa beans shells filler", *International Journal of Materials Science and Applications*, Vol. 5, Issue 2, pp. 66 – 78. https://doi: 10.11648/j.ijmsa.20160502.16

Aigbodion, V. S., Agunsoye, J. O., Hassan, S. B., Asuke, F. and Akadike, U. (2010), "Development of asbestos–free brake pad using bagasse". *Tribology in Industry*, Vol. 32, Issue 1, pp. 12 – 18.

Aku, S. Y., Yawas, D. S., Madakson, P. B. and Amaren, S. G. (2012), "Characterization of periwinkle shell as asbestos free brake pad material". *Pacific Journal of Science and Technology*, Vol. 13, Issue 2, pp. 57 - 62.

Aleksendric, D. and Carlone, P. (2015), *Soft Computing in the Design and Manufacturing of Composite Materials: Applications in brake friction and thermoset matrix composites*, WP – Woodhead Publishing, Cambridge, CB22 3HJ, UK, pp. 15 – 35. ISBN 978-1-78242-180-1 (online).

Amaren, S. G., Yawas, D. S. and Aku, S. Y. (2013), "Effect of periwinkle shell particle size on the wear behaviour of asbestos free brake pad", *Elsevier, Results in Physics*, Vol. 3, pp. 109 – 114. https://doi.org/10.1016/j.rinp.2013.06.004.

Amaren S. G. (2016), "Development of Automobile Disc Brake Pads using Eco-Friendly Periwinkle Shell and Fan Palm Shell Materials", *PhD Thesis*, ABU, Zaria, Nigeria, https://eduprojecttopics.com/product/development-of-automobile-disc-brake-pads-using-eco-friendly-periwinkle-shell-and-fan-palm-shell-materials/

Anaidhuno, U. P., Ologe, S., Maduike, F. and Mgbemena, C. E. (2017), "The Development of Vehicle Brake Pad Using Local Materials – (Palm Kernel, Coconut and Cashew Shells as Base Materials)", *IOSR Journal of Engineering (IOSRJEN*, Vol. 07, Issue 06, pp. 61 – 67.

Anderson, A. E. (1992), *Friction and Wear of Automotive Brakes, in ASM Handbook, Friction, Lubrication and Wear Technology*, Vol. 18, ASM International Materials Park, Ohio, pp. 569 – 577.

Andrew, M. (2016), "Step by Step: How a Brake Pad is Made – Time Review Magazine", https://www.tirereview.com/163702/#. Accessed on 12/12/20 at 7.23 pm.

Anon. (2021) “Hydraulic Press Machine -150 Ton Hydraulic Press Machine Dual Pump Manufacturer from Rajkot”, https://www.sagarengineer.in/hydraulic.press-machine.html. Accessed 15/03/21 at 10;15 pm.

Appleton, C. Jorgensen, A., Kristensen, T. K. and Stensgaard, A. S. (2010), “Tympanotonos Fuscatus IUCN Red List of Threatened Species”, 2010. Vol. 1.

Asotah, W. and Adeleke, A. (2017), “Development of Asbestos Free Brake Pad using Corn Husks”. *Leonardo Electronic Journal of Practices and Technologies,* Issue, 31, pp. 129 – 144.

Assa, R. R., Konan Konan, J. L., Prades, A., Nemlin, J. and Koffi, E. (2010),” Physicochemical characteristics of kernel during fruit maturation of four coconut cultivars (cocos nucifera L.). *African Journal Biotechnology*, Vol, 9, No. 14, pp. 2136 – 2144.

Bhagwan, D. G., Steven, H. C., Patricia, A. M., Peter, J. G., Chris, L. and Graham, A.P. (2000), “Brake Wear Particulate Matter Emissions”, *Journal of Environmental Science and Technology*, Vol. 34, Issue, 21, pp. 4463 – 4469. https://doi.org/10.1021/es001108h.

Bala, K. C., Okoli, M. and Abolarin, M. S. (2016), “Development of automobile brake pad using pulverized cow hooves, *Leonardo Journal of Sciences*, Vol. 15, Issue 28, pp. 95 – 108.

Bashar, D. A., Peter, B. M. and Joseph, M. (2012), “Material Selection and Production of a Coldworked Composite Brake Pad” *World Journal of Engineering and Pure and Applied Science (WJEPAS),* Vol. 2, Issue 3, pp. 92 – 97.

Bheel, N., Mangi, S. A. and Meghwar, S. L (2021), “Coconut Shell as a Cementitious Material in Concrete: A Review”, *Jurnal Kejuruteraan*, https:// doi.org/10.17576/jkukm-2020-33(1)-03. Vol. 33, Issue 1, pp. 27 – 38.

Blau, J. P. (2001), “Compositions, Functions and Testing of Friction Brake Materials and their Additives”, *A report by Oak Ridge National Laboratory for U.S. Dept. of Energy*, http://www.Ornl.- gov/- webworks/cppr/y2001/rpt/112956.pdf, pp. 78 – 80.

Blesdzki, A. K. and Gassan, J. (1999), "Composite Reinforced with Cellulose Based Fibres" *Progress in Polymer Sciences*, Vol. 24, Issue 2, p. 221 – 224.

Brijendra, G. and Ashish, J. M. (2015), "Review of Automotive Brake Friction Materials", *International Journal of Advance Engineering and Research Development*, Vol. 2, Issue 2.

Casamassa, E., Fioravanti, A., Mazzocchi, M., Carotta, M. C. and Faga, M. G. (2019), "Abrasive properties of ZnO: Influence of different nanoforms". *Tribology International*, Vol. 142, 105984. https://doi.org/10.1016/j.triboint.2019.105984

Caulum, B. R. (2012), "Coconut palm on the Coastline of Western and Central Regions of Ghana", *Published Master's Thesis*, University of Northern Arizona, Arizona, WA, 88 pp.

Chan D. and Stachowiak G. W. (2004), "Review of automotive brake friction materials", *Proceedings of the Institution of Mechanical Engineers*, Vol. 218, Part D, Issue 9: J. Automobile Engineering (IMechE), pp. 953 – 966. https://doi.org/10.1243/0954407041856773.

Chand, N., Hashmi, S. A. R., Lomash, S. and Naik, A. (2004), "Development of asbestos free brake pad", *IE (I) Journal - MC*, Vol. 85, pp. 13 – 16.

Chandgude, S. B. and Ganiger, S. G. (2016) "Review on Development of Composite Materials on Disc Brake Pad", *Journal of Emerging Technologies and Innovative Research*, Vol. 3, Issue 5, pp. 63 – 65.

Charles, E. O. (2003), *What is density*, Virtual Chembook, Elmhurst College, 2003, https://chemistry.elmhurst.edu/vchembook/120densityfs

Chauhan, S. R., Anoop, K., Singh, I. and Prashant, K. (2010) "Effect of fly ash content on friction and dry sliding wear behaviour of glass fiber reinforced polymer composites – A Taguchi approach", *Journal of Minerals and Materials Characterization and Engineering*, Vol. 9, No.4, pp. 365 – 387.

Cho, M. H., Kim, D., Kim, S. J. And Jang, H. (2005), "Effect of Ingredients on Tribological Characteristics of a Brake Lining: An Experimental Case Study", *Wear*, Vol. 258, No. (11 – 12), pp. 1682 – 1687. https://doi.org/10.1016/j.wear.2004.11.021.

Dagwa, I. M. and Ibhadode, A. O. A. (2006), "Determination of Optimum Manufacturing Conditions for Asbestos – free Brake Pad using Taguchi Method", *Nigerian Journal of Engineering Research and Development*, Vol. 5, Issue 4, pp. 1 – 8.

Dagwa, I., Builders, P. and Achebo, J. (2012), "Characterization of palm kernel shell powder for use in polymer matrix composites", *International Journal of Mechanical & Mechatronics Engineering*, Vol. 12, Issue, 4, pp. 88 – 93.

Dahunsi, B. I. O. (2003), "Properties of Periwinkle-Granite Concrete", *Journal of Civil Engineering JKUAT*, Vol. 8, Issue 1, pp. 27 – 35. https://doi:104314/jce v8i1.18993.

Darlington, E., Chukwumaobi, O. and Patrick, O. (2015), "Production of Eco-Friendly Brake Pad Using Raw Materials Sourced Locally in Nsukka" *Journal of Energy Technologies and Policy* ISSN 2224-3232 (Paper) ISSN 2225-0573 (Online), Vol. 5, No. 11.

Dellisanti, F., Minguzzi, V. and Morandi, N. (2002), "Experimental results from thermal treatment of asbestos containing materials", *GeoActa*, Vol. 1, No. 61, pp. 61 – 70.

Edokpia, R. O., Aigbodion, V. S., Obiorah, O. B., and Atuanya, C. U. (2014), "Evaluation of the Properties of Ecofriendly Brake Pad Using Egg Shell Particles–Gum Arabic", *Science Direct R, Elsevier B.V*. DOI: 10.1016/j.rinp.2014.06.003.

Efavi, J. K., Damoah, L., Bensah, D. Y., Dodoo-Arhin, D. And Tetteh, D. (2012), "Development of porous ceramic bodies from kaolin deposits for industrial applications". *Journal of Applied Clay Science*, Vol. 65 – 66, pp. 31 – 36, https://doi.org/10.1016/j.clay.2012.04.010.

Egonmwan, R. I. (2008), "The Ecology and Habits of Tympanotonus Fuscatus var. radula (L) (Prosobranchias Potamididae)", *Journal of Biological Sciences*, Vol. 8, Issue 1, pp. 186 – 190.

Ekop, I. E., Adenuga, O. A. and Umoh, A. A. (2013), "Strength characteristics of granite-pachimalania aurita shell concrete", *Nigerian Journal of Agriculture, Food and Environment*, Vol. 9, Issue 2, pp. 9 – 14.

Elakhame, Z. U., Olotu, O. O., Abiodun, Y. O., Akubueze, E. U., Akinsanya, O. O., Kaflo, P. O. and Oladele, O. E. (2017), "Production of Asbestos Free Brake Pad Using Periwinkle Shell as Filler Material", *International Journal of Scientific& Engineering Research*, Vol. 8, Issue 6.

Eriksson M., Bergman F. and Jacobson S. (1999), **"**Surface Characterization of Brake Pads after Running under Silent and Squealing Conditions", *Wear*, Vol. 232, pp. 163 – 167.

Eriksson, M. and Jacobson, S. (2000), "Tribological surfaces of organic brake pads", *Tribol. Intern.*, Vol. 33, pp. 817 – 827.

Eriksson, M., Bergman, F. and Jacobson, S. (2002), "On the nature of tribological contact in automotive brakes", *Wear*, Vo l. 252, pp. 26 – 36.

Fono-Tamo, R. S. and Koya, O. A. (2013), "Evaluation of Mechanical Characteristics of a Friction Lining from Agricultural waste", *International Journal of Advancements in Research and Technology*, Vol. 2, Issue 11.

Foodbev Media (2015), "Ferrero Develops Packaging from Waste Hazelnuts and Cocoa Beans. Retrieved from, http:/www.foodbev.com/news/Ferrero-develops-packaging-from-waste-hazelnuts-and-cocoa-beans-/

Ganguly, A. and George, R. (2008), "Asbestos free friction composition for brake linings", *Bulletin of Materials Science* © Indian Academy of Sciences. Vol. 31, No. 1, pp. 19 – 22.

Garcia, D., Lopez, J., Balart, R., Ruseckaite, R. A. and Stefan, P. M. (2007), "Composites Based on Sintering Rice Husk- waste and Tire Rubber Mixtures", *Material Design*, Vol. 28, pp. 2234 – 2238.

Gudmand-Hoyer, L., Bach, A., Neilsen, G. T.and Morgan, P. (1999), "Tribological properties of automotive disc brakes with solid lubricants", *Wear*, Vol. 232, pp. 168 – 175.

Gujrathi, T.V. and Damale, A.V. (2015), "A Review on Friction Materials of Automobile Disc Brake Pad", *International Journal of Engineering, Education and Technology (ARDIJEET)*, Vol. 3, Issue 2.

Harshvardhan, Z., Ghetiya, N. D. and Dipali, P. (2017) "Development of Friction Pad and Study of Its Wear Characteristics", *International Journal of Mechanical and Production Engineering*, Vol. 5, Issue 2, pp. 5 – 8.

Howell, G. J. and Ball, A. (1995), "Dry sliding wear of particulate-reinforced aluminum alloys against automobile friction materials", *Wear*, Vol. 1813, pp. 379 – 390.

Hughes, R. H. (1992), *A Directory of African Wetlands*, IUCN, ISBN 978 – 2 – 88032 – 949 – 5, 443 pp.

Ibhadode, A. O. A. and Dagwa, I. M. (2008), "Development of Asbestos-Free Friction Lining Material from Palm Kernel Shell", *Nigerian Journal of Engineering Research and Development*, Vol. 5, Issue 4, pp. 1 – 8.

Ibrahim, M. (2009), "Investigation of the Tribological Properties of Brake Pads by using Rice Straw and Rice Husk Dust", *Journal of Applied Sciences*, Vol. 9, Issue 2, pp. 377 – 381.

Idris, U. D., Aigbodion, V. S., Abubakar, I. J. and Nwoye, C. I. (2013), "Eco-friendly Asbestos Free Brake-pad: Using Banana Peels", *J. King Saud Univ.-Eng. Sci.*, Vol. 27, Issue, 2, pp. 185 – 192.
http://dx.doi.org/10.1016/j.jksues.2013.06.006.

Ikpambese, K. K., Gundu, D. T. and Tuleun, L. T. (2014), "Evaluation of Palm Kernel Fibres (PKFs) for Production of Asbestos-free Automotive Brake Pads", *Journal of King Saud University – Engineering Sciences*, Vol. 28, Issue 1, pp. 110 – 118.

Ingo, G. M., Uffizi, M, D., Falso, G., Bultrini, G. and Padeletti, G. (2004), "Thermal and microchemical investigation of automotive brake pad wear residues". *Thermochimica Acta*, Vol. 418, Issue, 1 – 2, pp. 61 – 68.
https://doi: 10.1016/j.tca.2003.11.042.

James, P. W. and Andrew, V. L. (1998), "Brake Friction Materials", *A Market Survey*, (Standard Research Inst.). Conducted for the California NSA Technology Utilization Office. National Aeronautics and Space Administration, Washington DC.

Jang, H., Ko, K., Kim, S. J., Basch, R. and Fash, J. W. (2004), "Effect of Metal Fibres on the Friction Performance of Automotive Brake Friction Materials", *Wear*, Vol. 256, pp. 406 – 414.

Kato, T. and Soutome, H. (2001) "Friction Material Design for Brake Pads Using Database", *Tribology Transactions*, Vol. 44, pp. 137 – 141.

Kawai, K., Iwani, Y. and Ebisu, S. (1998), "Effect of resin monomer composition on toothbrush wear resistance", *J. Oral Rehabil*, Vol. 25, pp. 264 – 268.

Kemmer, H. A. (2002), *Investigation of the Friction Behaviour of Automotive Brakes through Experiments and Tribological Modelling*, Universität Paderborn / Robert. ISBN 3000112308, 9783000112300, 277 pp.

Khurmi R. S. and Gupta J. K. (2008), *A Textbook of Machine Design. First Multicolour Edition*, Eurasia Publishing House (PVT) Ltd., Ram Nagar, New Delhi – 110055, 917 pp.

Kim, S. J., Kim, K. S. and Jang, H. (2003), "Optimization of Manufacturing Parameters for Brake Lining Using Taguchi Method", *Journal of Material Processing Technology*., Vol. 136, Issues, 1 – 3, pp. 202 – 208. https://doi.org/10.1016/S0924-0136(03)00159-6

Kusiorowski, R., Zaremba, T., Piotrowski, J. and Adamek, J. (2012), "Thermal decomposition of different types of asbestos", *Journal of Thermal Analysis and Calorimetry*, Vol. 109, pp. 693 – 704.

Last, F. T. (2001), *Tree Crop Ecosystems (Ecosystems of the World)*, Amsterdam Elservier Science. ISBN-13: 978-0444882660.

Lawal, S. S., Bala, K. C., and Alegbede, A. T. (2017), "Development and production of brake pad from sawdust composite". *Leonardo Journal of Sciences*, Issue 30, pp. 47 - 56.

Leman, Z., Sapuan, S. M., Saifol, A. M., Maleque, M. A. and Ahmad, M. M. (2008), "Moisture Absorption Behaviour of Sugar Palm Fibre Reinforced Epoxy Composites", *Short Communication, International Journal of Materials and Design*, Vol. 29, Issue 8, pp. 95 – 100.

Maleque, M. A., Atiqah, A. Talib, R. J. and Zahurin, H. (2012), "New Natural Fibre Reinforced Aluminium Composite for Automotive Brake Pad", *International Journal of Mechanical and Materials Engineering*, Vol. 7, Issue 2, pp. 166 – 170.

Mathur, R. B., Thiyagarajan, P. and Dhami, T. L. (2004), "Controlling the Hardness and Tribological Behaviour of Non-asbestos Brake Lining Material for Automobiles", *Wear*, Vol .5, pp. 6 – 11.

Mayowa, A., Abubakre, O. K., Lawal, S. A. and Abdulkabir, R. (2015), "Experimental investigation of palm kernel shell and cow bone reinforced polymer composites for brake pad production", *International Journal of Chemistry and Material Research*, Vol. 3, Issue 2, pp. 27 - 40.

Melcher, B. and Faullant, P. A. (2000), "Comprehensive Study of Chemical and Physical Properties of Metal Sulfides", *SAE Technical Paper* 20000-01-2757, SAE Warrendale, PA, USA, pp. 39 – 49.

Mohanty, S. and Chugh, Y. P. (2007), "Development of Fly Ash-Based Automobile Brake Lining", *Tribology International*, Vol. 40, Issue 7, pp. 1217 – 1224, https://doi.org/10.1016/j.Triboint.2007.01.005.

Moruf, R. O. and Lawal-Are, A. O. (2015), "Growth Pattern, Whorl and Girth Relationship of the Periwinkle, Tympanotonus fuscatus var radula (Linnaeus, 1758) from a Tropical Estuarine Lagoon, Lagos Nigeria", *International Journal of Fisheries and Aquatic Studies*, Vol. 3, Issue 1, pp. 111 – 115.

Mutlu, I., Eldogan, O. and Findik, F. (2005), "Production of ceramic additive automotive brake lining and investigation of its braking characteristics", *Industrial Lubrication and Tribology*, Vol. 57, No. 2, pp. 84 – 92.
https://doi.org/10.1108/00368790510583401

Natarajan, M. P., Rajmohan, B. and Devarajulu, S. (2012), "Effect of ingredients on mechanical and tribological characteristics of different brake liner materials", *International Journal of Mechanical Engineering and Robotics Research*, Vol. 1, No. 2, pp. 135 – 157.

Natarajan, M. P. and Rajmohan, B. (2016), "Performance of non-asbestos organic brake liners for light motor vehicles", *Materials Testing*, Vol. 58, Issue, 3, pp. 252 – 259, https://doi.org/10.3139/120.110849

Nicholson, G. (1995), *Facts about Friction*: *A friction material manual, almost all you need to know about friction,* P&W Price Enterprises, Inc., Croydon, PA, 244 pp. Retrieved from https://www.google.com.ng/search?q=facts+about+friction.

Nkoumbou, C., Njoya, A., Njoya, D., Grosbois, C., Njopwouo, D., Yvon, J. and Martin, F. (2009), "Kaolin from Mayouom (Western Cameroon): Industrial suitability evaluation", *Journal of Applied. Clay Science*, Vol. 43, pp. 118 – 124.

Nwobi, B. E., Ahmed A. S. and Aderemi, B. O. (2002), "Beneficiation and characterization of Bauchi graphite", *Journal of Nigerian Society of Chemical Engineers*, Vol. 20, No. 2, pp. 19 – 22.

Offiong, U. and Akpan, G. E. (2017), "Assessment of Physico-chemical Properties of Periwinkle Shell Ash as Partial Replacement for Cement in Concrete", *International Journal of Scientific Engineering and Science*. Vol. 1, Issue 7, pp. 33 – 36.

Oladosu, K. O., Kareem, B., Akinnuli, B. O. and Alade, A. O. (2016) "Optimization of ash yield from the combustion of palm kernel shell and selected additives (Al2O3, CaO and MgO) using D-optimal design", *Leonardo Electronic Journal of Practices and Technologies*, Issue 28, pp. 9 – 18.

Olalere, A. A., Yaru, S. S. and Dahunsi. O. A. (2019), "Evaluation of the chemical and thermo-physical properties of locally aggregated kaolin-based refractory materials", *Journal of Mechanical Engineering and Sciences* © Universiti Malaysia, Pahang, Malaysia. Vol. 13, Issue 1, pp. 4743 – 4755. https://doi.org/10.15282/jmes.13.1.2019.27.0397

Onyeneke, R. N., Anele, J. U. and Ugwuegbu, C. C. (2014), "Production of motor vehicle brake pad using local materials (periwinkle and coconut shell)", *International Journal of Engineering and Science*, Vol. 3, Issue 9, pp. 17 – 24.

Osterle, W. and Urban, I. (2004), "Friction layers and friction films on PMC brake pads", *Wear*, Vol. 257, pp. 215 – 226.

Osterle, W. and Dmitriev, A. I. (2016), "The Role of Solid Lubricants for Brake Friction Materials", *Journal of Lubricants*, Vol. 4, Issue 1, 5. https://doi.org/10.3390/lubricants4010005

Pandey, P. K., Tripathi, V. K., Pandey, M. K. and Mandloi, V. K. (2011), "A Critical Analysis of NAO (non-asbestos organic) Materials of Composite Used for Friction Liners of Trucks", *International Journal of Engineering Science and Technology (IJEST)*, Vol. 3, Issue 2, pp. 1422–1431.

Punyapriya, M. (2007), "Effect of Environment on Mechanical Properties of Bagasse Fibre Reinforced Polymer Composite", *M.Tech Thesis*, National Institute of Technology, Rourkela.

Quaicoe, R. N., Sylvester, K. D., Rene, P., Luc, B., Joseph, O. N., Nkansah-Poku, J., Arther, R., Dare, D., Yankey, E. N., Fabian, P. and Dollet, M. (2009), "Resistance Screening trial on coconut varieties to Cape Saint Paul Wilt Disease in Ghana", *Agronomies Environment*, Vol. 16, pp. 132 – 136.

Radhika, N., Subramanian, R. and Venkat, P. S. (2011) "Tribological Behaviour of Aluminium/Alumina/Graphite Hybrid Metal Matrix Composite Using Taguchi's Techniques", *Journal of Minerals and Materials Characterization and Engineering*, Vol. 10, No.5, pp. 427 – 443.

Raju, P. M., Siva, S. and Dharmala, H. (2016), "Compressive Strength of Concrete with Partial Repalcement of Aggregates with Granite Powder and Cockle Shell", *Malaysian Journal of Civil Engineering*, Vol. 28, Issue 2, pp. 183 – 204.

Ramanathan, K., Saravanakumar, P., Ramkumar, S., Pravin, K. P. and Surender, S. R. (2017), "Development of Asbestos–Free Brake Pads using Lemon Peel Powder",

International Journal of Innovative Research in Science, Engineering and Technology, Vol. 6, Issue 3, pp. 4449 – 4455.

Rehren T. (2003), *Crucibles as Reaction Vessels in Ancient Metallurgy, Mining and Metal Production through the Ages*, British Museum Press, London, pp. 207 – 215.

Reid, D. G., Dyal, P., Lozouet, P., Glaubrecht, M. and Williams, S. T. (2008), "Mudwhelks and Mangroves: The Evolutionary History of an Ecological Association (Gastropoda Potamididae)", *Molecular Phylogenetics and Evolution*, Vol. 47, Issue 2, pp. 680 – 699.

Sarvendra, K. M. and Jain, A. K. (2013), "A Review of Experimental Study of Brake Pad Materials", *International Journal of Emerging Trends in Engineering and Development*, Vol. 6, Issue 3, R. S. Publication, rspublicationhouse@gmail.com.

Seki, Y. (2006), "Rice and its Waste", *Science and Technical*, The Science Technology Resources Council, Turkey.

Sennett, P. (1990), "Changes in the physical properties of kaolin on exposure to elevated temperatures", *Proceedings of the 9th International Clay Conference*, Strasbourg, 1989, V. C. FARMER and Y. TARDY (Eds), Sci. Geol., Mem. Vol. 89, pp. 71 – 79.

Sheikh, S. H., Yin, X., Ansarifar, A. and Yendall, K, (2017), "The potential of kaolin as a reinforcing filler for rubber composites with new sulfur cure systems", *Journal of Reinforced Plastics and Composites*, Vol. 36, Issue, 16, pp. 1132 – 1145. https://doi.org/10.1177/0731 684417712070

Su, L., Gao, F., Han, X., Fu, R., and Zhang, E. (2015), "Tribological Behavior of Copper-Graphite Powder Third Body on Copper-Based Friction Materials", *Tribology Letters*, Vol. 60, No. 2, pp. 1 – 12. https://doi.org/10.1007/s11249-015-0605-3

Suryarajan, B., Sai, B. M. A., Velmurugan, C., Vinoth, B. and Selvaraj, B. (2016), "Tribo Performance of a NA Disc Brake Pad Developed Using Two Types of Organic Friction Modifier", *Proceedings of the International Conference on Materials, Design and Manufacturing Process (ICMDM '16)*, Chennai, India, 4763 pp.

Talib, R. J., Muchtar, A. and Azhari, C. H. (2007), "The Performance of Semi-Metallic Friction Materials for Passenger Cars", *Jurnal Teknologi*, Vol. 46, Issue 1, pp. 53 – 72. https:// doi:10.11113/jt. v46.282

Tamalkhani, S., Firmansyah, R. and Rifki, H. (2019), "Characteristics of coconut shell ash as filler and LDPE plastic waste as substitution materials of porous asphalt mixtures", *International Journal of Recent Technology and Engineering (IJRTE)*, Vol. 8, Issue 3S3, pp. 340 – 344. https://doi:10.35940/ijrte.C1003.11835319

Tanaka, K., Ueda, S. and Noguchi, N. (1973), "Fundamental Studies on the Brake Friction of Resin Based Friction Materials", *Wear*, Vol. 23, Issue, 3, pp. 349 – 365. https://doi.org/10.1016/0043-1648(73)90022-7

Toboldt W. K., Johnson L., and Olive S. (1989), *Automotive Encyclopedia*, Goodheart-Willcox Company: South Holland, IL., 1989.

Todorovic, J. Cedomir, V. D. and Arsenic, Z. (1987), "Modelling of the Tribological Properties of Friction Materials Used in Motor Vehicle Brakes", *Conference Institution*, of Mechanical Engineers at London, UK, Vol. 226/87, pp. 911 – 916. hppts://doi: 10.13140/RG.2.1.1366.9840.

Tsang, P. H., Coyle, J. P., Liu, T. and Vanderpoorte, J. G. (1985), *Method of manufacturing a friction articles – Allied Corporation*, US Pat. 4537823 (United States Patent and Trademark Office).

Umamaheswara, R. and Babji, G. (2015) "A Review Paper on Alternate Materials for Asbestos Brake Pads and its Characterization", *International Research Journal of Engineering and Technology (IRJET)*, Vol. 02, Issue, 02, pp. 556 – 562.

Vivek, S., Jayakumari, L. S., Stephen, B. S., Suresh, G., Javeed, A. and Arulmurugan, S. (2020), "Tribological and Mechanical Properties of a Biobased Reinforcement in Friction Composite Materials", *Materia (Rio J.)*, Vol. 25, No. 3.

Weinstraub, M. (1998), Brake additives consultant. Private communication.

Yawas, D. S., Aku, S. Y. and Amaren, S. G. (2016), "Morphology and properties of periwinkle shell asbestos–free brake pad", *Journal of King Saud University-Engineering Sciences*, Vol. 28, Issue 1, pp. 103 - 109. https://doi.org/10.1016/j.jksues.2013.11.002

Yaya, A., Tiburu, E. K., Vickers, M. E., Efavi, J. K., Onwon-Agyeman, B. and Knowles, K. M. (2017, "Characterization and identification of local kaolin clay from Ghana: A potential material for electroporcelain insulator fabrication", *Elsevier, Journal of Applied Clay Science*. Vol. 150, pp. 125 – 130. https://dx.doi.org/10.1016/j.clay.2017.09.015

Zaharuddin, A. M., Talib, R. J., Berhan, M. N., Budin, S. and Aziurah, M. S. (2012), "Taguchi Method for Optimizing the Manufacturing Parameters of Friction Materials", *International Journal of Mechanical and Materials Engineering (IJMME)*, Vol. 7, No. 1, pp. 83 – 88.

Zamri, Y. B., Shamsul, J. B. and Amin, M. M. (2011), "Potential of palm oil clinker as reinforcement in aluminium matrix composites for tribological applications", *International Journal of Mechanical and Materials Engineering*, Vol. 6, No. 1, pp. 10 – 17.

APPENDICES

APPENDIX A

TEST RESULTS OF BASE MATERIALS AND PRODUCED SAMPLES

Table A1 Dry Bulk Density of the Base Materials

Materials	Mass (g)	Volume (cm^3)	Dry Bulk Density (g/cm^3)
PS Powder	168.701	98.1748	1.718
CSA	125.008	98.1748	1.273
Kaolin	143.015	98.1748	1.457

Table A2 Dry Compressive Strength of the Base Materials

Materials	Compressive Strength (kN/m^2)			
	Value I	Value II	Value III	Mean Value
PS Powder	348	350	350	350
CSA	120	115	125	120
Kaolin	250	250	250	250

Table A3 Dry Shear Strength of the Base Materials

Materials	Shear Strength (kN/m^2)			
	Value I	Value II	Value III	Mean Value
PS Powder	157	157	152	155
CSA	92	89	90	90
Kaolin	160	160	160	160

Table A4 Test Samples Heights for the PSP/CSA Formulation

Samples Initial Heights (Before Oven Drying (mm))						Run	Samples Final Height (After Oven Drying (mm))					
1	2	3	4	5	6		1	2	3	4	5	6
43.65	39.05	34.43	27.73	30.47	36.62	5	41.16	37.19	32.86	25.81	28.39	34.25
35.08	31.58	33.10	35.88	33.38	33.63	3	32.82	29.62	30.80	33.92	31.76	32.07
35.10	32.81	33.62	34.03	34.48	36.46	1	35.38	33.10	33.65	32.54	34.18	34.79
34.94	34.64	34.33	35.88	34.50	32.60	6	33.88	34.58	34.11	34.88	33.79	31.64
34.30	35.05	35.74	36.31	35.02	34.63	2	33.88	35.58	36.26	36.34	34.62	34.24
34.18	36.44	37.23	33.02	33.33	34.35	9	33.80	35.55	36.39	33.25	32.51	33.84
32.46	31.75	35.00	34.69	35.76	34.88	11	30.46	30.29	33.42	33.06	35.22	33.52
34.89	36.35	36.88	34.97	31.95	33.72	7	33.15	35.02	34.86	33.60	30.75	31.46
34.35	34.22	36.77	34.43	35.88	32.52	10	32.64	33.41	36.05	32.44	35.24	31.46
35.06	34.12	33.96	34.33	34.30	34.79	4	33.59	37.00	35.31	37.27	35.36	35.85
35.77	35.75	34.32	32.67	34.52	32.28	12	33.04	33.61	32.89	31.75	33.49	31.81
34.03	33.72	34.90	35.93	34.08	34.46	8	33.95	35.72	35.49	35.07	34.55	34.32
30.22	31.86	33.55	31.86	33.29	34.15	13	28.85	31.57	33.61	31.22	32.79	32.48

Table A5 Test Sample Heights for the PSP/K Formulation

Samples Initial Height (Before Oven Drying (mm))						Run	Samples Final Height (After Oven Drying (mm))					
1	2	3	4	5	6		1	2	3	4	5	6
30.24	29.94	30.47	26.92	31.62	31.99	5	30.07	31.17	29.82	26.99	31.05	31.66
30.61	30.83	33.03	32.31	31.12	31.01	3	30.39	30.38	33.48	32.19	30.95	30.40
30.37	29.97	30.02	28.43	29.91	29.96	1	29.43	29.43	29.27	28.34	29.94	29.08
30.66	30.50	30.28	30.86	30.01	28.95	6	30.31	30.63	29.63	30.39	30.20	28.58
30.38	31.08	30.20	30.41	31.26	31.55	2	30.13	30.77	29.99	30.43	30.92	30.94
29.84	30.06	28.39	27.81	30.20	27.91	9	29.61	29.60	27.72	27.57	30.48	27.92
26.46	27.36	31.07	30.60	26.11	29.56	11	28.09	29.98	31.16	31.97	27.81	31.29
25.88	27.23	29.24	28.61	27.31	30.65	7	26.76	28.99	30.94	30.38	28.91	31.60
27.61	29.37	27.96	28.99	27.65	27.36	10	27.70	29.46	28.06	29.00	27.83	27.78
27.64	26.67	29.45	30.34	29.65	29.92	4	28.37	28.29	31.16	32.05	31.13	30.85
28.45	28.49	28.22	28.90	27.37	27.37	12	28.76	28.64	29.04	28.77	27.72	27.72
28.86	29.74	28.52	27.49	27.91	27.54	8	29.42	29.94	28.51	28.04	28.65	27.75
23.20	28.68	28.06	28.23	28.33	29.15	13	23.04	28.65	27.58	28.02	28.24	28.97

Table A6 Test Samples Diameters for the PSP/CSA Formulation

Samples Initial Diameter (Before Oven Drying (mm))						Run	Samples Final Diameter (After Oven Drying (mm))					
1	2	3	4	5	6		1	2	3	4	5	6
24.81	24.78	24.00	24.77	24.94	24.51	5	24.71	24.46	24.82	23.77	24.25	24.33
24.76	24.98	24.77	24.72	24.71	24.42	3	24.64	24.59	24.68	23.99	24.68	24.12
24.65	24.68	24.92	24.92	24.85	24.80	1	24.49	24.23	23.79	24.96	24.36	25.63
24.65	24.70	24.62	24.98	24.78	24.72	6	24.38	24.28	24.57	24.52	24.71	24.56
24.66	24.84	24.58	24.78	24.46	24.32	2	24.44	24.34	24.05	24.70	24.40	25.10
24.66	25.00	24.74	24.94	24.71	24.88	9	24.63	24.50	24.39	24.69	24.66	24.45
24.45	24.50	24.56	24.89	24.96	24.77	11	24.10	24.65	24.61	24.27	24.42	24.70
24.51	24.60	24.82	24.88	25.00	24.79	7	24.14	24.44	23.98	23.80	24.86	24.68
24.58	24.61	24.56	24.83	24.92	24.47	10	24.58	24.57	25.84	24.40	24.59	25.04
24.65	24.48	24.41	24.93	24.52	24.65	4	24.53	24.27	24.33	24.90	24.47	24.55
24.70	24.59	24.59	24.97	24.99	25.00	12	24.72	24.49	25.82	24.54	24.74	24.93
24.67	24.61	24.27	24.67	24.84	24.51	8	24.25	24.31	24.14	24.56	24.49	24.28
24.46	24.88	24.88	24.73	24.88	24.39	13	24.23	24.31	24.78	24.67	24.58	23.87

Table A7 Test Samples Diameters for the PSP/K Formulation

Samples Initial Diameter (Before Oven Drying (mm))						Run	Samples Final Diameter (After Oven Drying (mm))					
1	2	3	4	5	6		1	2	3	4	5	6
24.59	24.48	25.00	24.38	24.74	24.63	5	24.61	24.46	24.42	24.19	24.10	24.40
24.54	24.81	24.74	24.55	24.45	24.56	3	24.54	24.59	24.36	24.51	24.93	24.45
24.43	24.38	24.93	24.34	24.55	24.71	1	24.39	24.23	24.51	24.24	24.21	24.37
24.43	24.40	24.44	24.35	24.48	24.58	6	24.28	24.28	24.43	24.81	24.56	24.81
24.44	24.54	24.63	24.57	25.16	24.85	2	24.34	24.34	24.61	24.63	24.45	24.47
24.44	24.80	24.33	24.66	24.39	24.37	9	24.53	24.50	24.51	24.63	24.51	24.90
24.23	24.20	24.55	24.44	24.66	24.36	11	24.00	24.65	23.87	24.17	24.27	24.43
24.29	24.30	24.11	24.49	24.86	24.73	7	24.04	24.44	24.40	24.30	24.51	24.41
24.36	24.31	24.26	24.51	24.62	24.58	10	24.48	24.57	24.46	24.37	24.44	24.48
24.43	24.18	24.17	24.10	24.22	24.24	4	24.43	24.27	24.40	24.40	24.32	24.20
24.48	24.29	24.58	24.77	24.28	24.28	12	24.60	24.69	24.52	24.63	24.59	24.59
24.45	24.31	24.27	24.37	24.24	24.54	8	24.15	24.31	24.31	24.24	24.34	24.42
24.24	24.58	24.47	24.22	24.38	24.33	13	24.13	24.31	24.20	24.15	24.25	24.32

Table A8 Test Results of Bulk Density and Porosity of the PSP/CSA Samples

S/N	Run	Dried Weight (g)	Soaked Weight (g)	Suspended Weight (g)	Volume of Water Displaced (cm^3)	Bulk Density (g/cm^3)	Apparent Porosity (%)
1	5	20	27	11	12	1.67	43.75
2	3	19	25	10	10	1.90	40.00
3	1	16	20	12	11	1.45	50.00
4	6	21	26	11	8	2.63	33.33
5	2	19	24	9	12	1.58	33.33
6	9	21	25	12	12	1.75	30.77
7	11	18	23	10	8.5	2.12	38.46
8	7	18	24	10	10	1.80	42.86
9	10	22	28	12	12	1.83	37.50
10	4	20	25	10	14	1.43	33.33
11	12	18	25	9	8.5	2.12	43.75
12	8	17	22	9	10	1.70	38.46
13	13	18	24	9	10	1.80	40.00

Table A9 Test Results of Bulk Density and Porosity of the PSP/K Samples

S/N	Run	Dried Weight (g)	Soaked Weight (g)	Suspended Weight (g)	Volume of Water Displaced (cm^3)	Bulk Density (g/cm^3)	Apparent Porosity (%)
1	5	23	28	12	40	0.5750	31.25
2	3	23	26	12	12	1.9167	21.43
3	1	22	26	12	12	1.8333	28.57
4	6	24	28	12	4	6.0000	25
5	2	23	26	13	4	5.7500	23.08
6	9	25	29	11	14	1.7857	22.22
7	11	23	28	12	40	0.5750	31.25
8	7	23	28	10	66	0.3485	27.78
9	10	23	26	12	2	11.5000	21.43
10	4	20	23	11	10	2.0000	25
11	12	23	26	12	12	1.9167	21.43
12	8	24	28	11	28	0.8571	23.53
13	13	22	26	12	12	1.8333	28.57

Table A10 Test Results of Water Absorption of the PSP/CSA Samples

S/N	Run	Dried Weight (g)	Soaked Weight (g)	Mass of Water Absorbed (g)	Water Absorption (%)
1	5	19	25	6	31.58
2	3	20	26	6	30.00
3	1	20	25	5	25.00
4	6	21	27	6	28.57
5	2	20	25	5	25.00
6	9	19	24	5	26.32
7	11	18	22	4	22.22
8	7	16	22	6	37.50
9	10	22	29	7	31.82
10	4	19	24	5	26.32
11	12	19	25	6	31.58
12	8	18	23	5	27.78
13	13	19	24	5	26.32

Table A11 Test Results of Water Absorption of the PSP/K Samples

S/N	Run	Dried Weight (g)	Soaked Weight (g)	Mass of Water Absorbed (g)	Water Absorption (%)
1	5	23	28	5	21.74
2	3	23	26	3	13.04
3	1	22	26	4	18.18
4	6	24	28	4	16.67
5	2	23	26	3	13.04
6	9	25	29	4	16.00
7	11	23	28	5	21.74
8	7	23	28	5	21.74
9	10	23	26	3	13.04
10	4	20	23	3	15.00
11	12	23	26	3	13.04
12	8	24	28	4	16.67
13	13	22	26	4	18.18

Table A12 Test Results of Oil Absorption of the PSP/CSA Samples

S/N	Run	Dried Weight (g)	Soaked Weight (g)	Weight Difference (g)	Swell in Oil (%)
1	5	20	28	8	40.00
2	3	18	25	7	38.89
3	1	18	20	2	11.11
4	6	22	27	5	22.73
5	2	19	26	7	36.84
6	9	21	25	4	19.05
7	11	18	23	5	27.78
8	7	17	23	6	35.29
9	10	21	31	10	47.62
10	4	20	27	7	35.00
11	12	19	28	9	47.37
12	8	20	25	5	25.00
13	13	18	23	5	27.78

Table A13 Test Results of Oil Absorption of the PSP/K Samples

S/N	Run	Dried Weight (g)	Soaked Weight (g)	Weight Difference (g)	Swell in Oil (%)
1	5	19	28	9	47.37
2	3	24	26	2	8.333
3	1	22	25	3	13.6364
4	6	22	28	6	27.2727
5	2	24	26	2	8.3333
6	9	24	24	-	0
7	11	24	22	2	8.3333
8	7	24	27	3	12.5
9	10	23	25	2	8.6957
10	4	23	25	2	8.6957
11	12	24	28	4	16.6667
12	8	24	27	3	12.5
13	13	22	25	3	13.6364

Table A14 Test Results of Hardness Values of the PSP/CSA Samples

S/N	Run	Average Diameter of Indentation (mm)	Brinnel Hardness Value (BHN)
1	5	7.00	22.26
2	3	5.00	47.50
3	1	6.00	76.30
4	6	6.00	76.30
5	2	5.00	138.00
6	9	5.00	76.30
7	11	3.00	76.30
8	7	4.00	76.30
9	10	4.00	31.80
10	4	3.00	138.00
11	12	3.00	47,50
12	8	4.00	138.00
13	13	4.00	76.30

Table A15 Test Results of Hardness Values of the PSP/K Samples

S/N	Runs	Average Diameter of Indentation (mm)	Brinnel Hardness Value (BHN)
1	5	4.00	76.30
2	3	3.50	314.93
3	1	3.70	185.00
4	6	3.00	89.70
5	2	2.50	138.00
6	9	3.00	138.00
7	11	2.50	101.00
8	7	4.00	138.00
9	10	2.00	101.00
10	4	3.00	200.00
11	12	3.20	121.00
12	8	3.50	200.00
13	13	2.60	185.00

Table A16 Test Results of Compressive Strength Values of the PSP/CSA Samples

S/N	Run	Samples			Mean Value (N/mm^2)
		Line 3	Line 5	Line 6	
1	5	0.7400	0.5060	0.2750	0.5070
2	3	0.3430	0.4270	0.2250	0.3317
3	1	0.6100	0.6100	0.6100	0.6100
4	6	0.9870	1.3350	0.7740	1.0320
5	2	1.0800	1.0330	0.2320	0.7817
6	9	1.5600	1.0520	0.6900	1.1007
7	11	0.8690	0.6130	0.3070	0.5963
8	7	1.0790	0.3410	0.1520	0.5240
9	10	0.8690	0.5810	0.3810	0.6103
10	4	0.9400	0.7970	0.3700	0.7023
11	12	0.1310	0.3560	0.2430	0.2433
12	8	1.4360	0.5680	0.3740	0.7927
13	13	0.5800	0.5430	0.2360	0.4530

Table A17 Test Results of Compressive Strength Values of the PSP/K Samples

S/N	Runs	Samples		Mean Value (N/mm^2)
		Line 4	Line 5	
1	5	10.8570	8.5400	9.6985
2	3	11.4410	6.6430	9.0420
3	1	11.1380	10.8600	10.9990
4	6	18.4880	15.4170	16.9530
5	2	1.0200	9.6400	5.3300
6	9	14.9730	4.5330	9.7530
7	11	2.5230	13.3290	7.9260
8	7	2.8490	4.8920	3.8700
9	10	13.8540	11.7350	12.7950
10	4	0.8810	1.0970	0.9890
11	12	13.1480	18.9080	16.0280
12	8	13.4890	18.9444	16.2160
13	13	11.1380	10.8600	10.9990

APPENDIX B

RESULTS OF THE BRAKE PADS FORMULATION OPTIMISATION

Table B1 ANOVA of Water Absorption of the PSP/CSA Formulation

Source	Sum of Squares	df	Mean Square	F-value	p-value
Model	168.31	7	24.04	5.74	0.0093
A-Peri	33.66	1	33.66	8.04	0.0195
B-Coco	56.07	1	56.07	13.40	0.0052
C-Epoxy	0.0780	1	0.0780	0.0186	0.8944
AC	11.26	1	11.26	2.69	0.1355
A^2	13.89	1	13.89	3.32	0.1019
B^2	10.20	1	10.20	2.44	0.1530
C^2	43.69	1	43.69	10.44	0.0103
Residual	37.67	9	4.19		
Lack of Fit	37.67	5	7.53		
R^2	0.8171				
Adjusted R^2	0.6748				
Adequate Precision	9.4787				

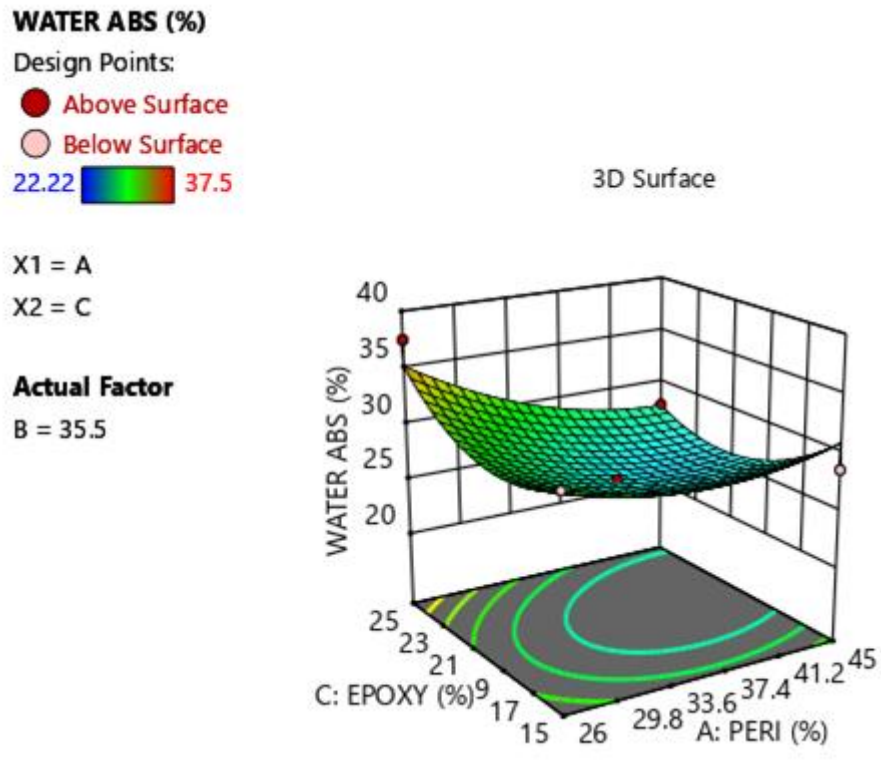

Figure B1 Surface Plot of Water Absorption against Epoxy and PSP

Table B2 ANOVA of Oil Absorption of the PSP/CSA Formulation

Source	Sum of Squares	df	Mean Square	F-value	p-value
Model	1042.56	6	173.76	4.15	0.0235
A-Peri	4.09	1	4.09	0.0978	0.7609
B-Coco	686.35	1	686.35	16.41	0.0023
C-Epoxy	4.56	1	4.56	0.1090	0.7481
AB	219.34	1	219.34	5.24	0.0450
B^2	55.85	1	55.85	1.34	0.2748
C^2	65.27	1	65.27	1.56	0.2401
Residual	418.30	10	41.83		
Lack of Fit	418.30	6	69.72		
R^2	0.7137				
Adjusted R^2	0.5419				
Adequate Precision	8.0321				

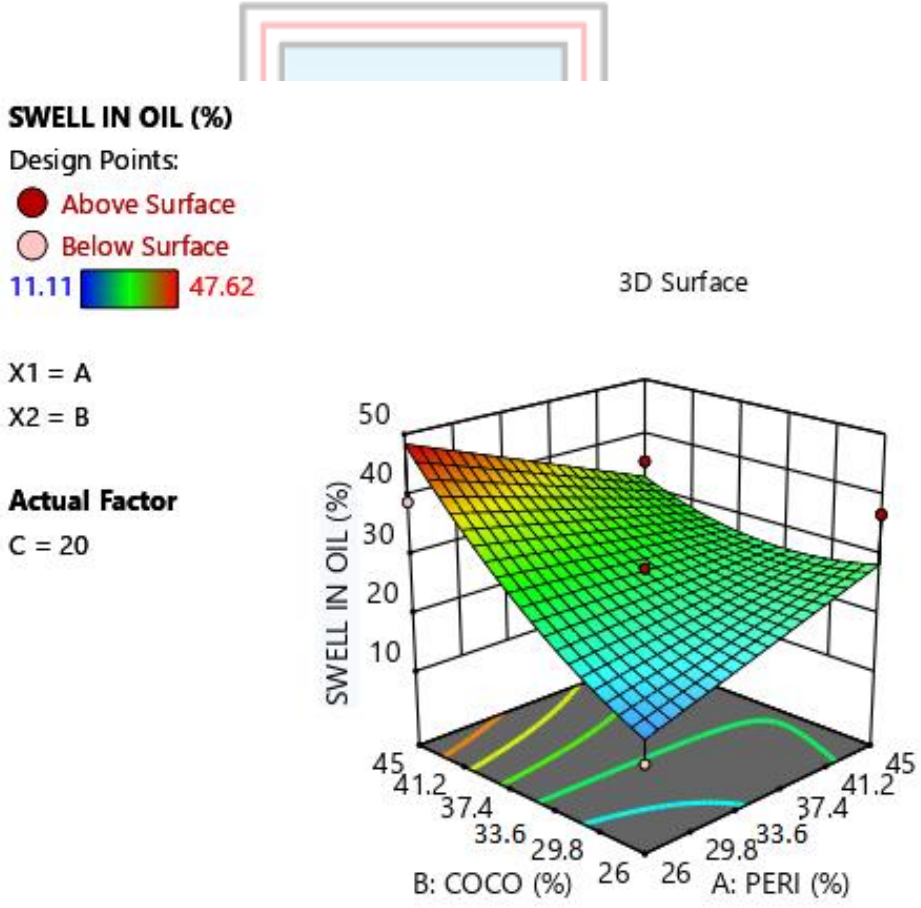

Figure B2 Surface Plot of Oil Absorption against CSA and PSP

Table B3 ANOVA of Apparent Porosity of the PSP/CSA Formulation

Source	Sum of Squares	df	Mean Square	F-value	P-value
Model	257.91	5	51.58	5.93	0.0068
A-Peri	182.02	1	182.02	20.91	0.0008
B-Coco	0.5101	1	0.5101	0.0586	0.8132
C-Epoxy	41.31	1	41.31	4.75	0.0520
AB	25.00	1	25.00	2.87	0.1182
AC	9.06	1	9.06	1.04	0.3295
Residual	95.75	11	8.70		
Lack of Fit	95.75	7	13.68		
R^2	0.7293				
Adjusted R^2	0.6062				
Adequate Precision	8.8802				

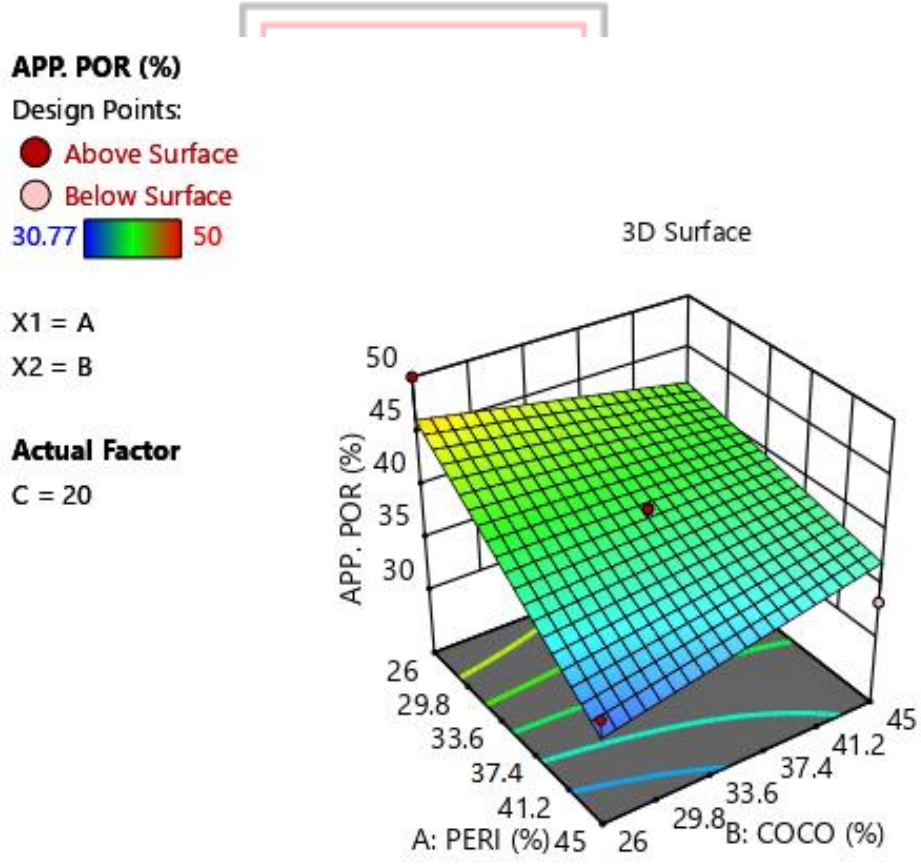

Figure B3 Surface Plot of Apparent Porosity against PSP and CSA

Table B4 ANOVA of Hardness of the PSP/CSA Formulation

Source	Sum of Squares	df	Mean Square	F-value	P-value
Model	16990.70	6	2831.78	7.69	0.0027
A-Peri	8973.98	1	8973.98	24.36	0.0006
B-Coco	1303.05	1	1303.05	3.54	0.0894
C-Epoxy	2159.56	1	2159.56	5.86	0.0360
A^2	3608.53	1	3608.53	9.80	0.0107
B^2	343.71	1	343.71	0.9331	0.3568
C^2	679.12	1	679.12	1.84	0.2044
Residual	3683.46	10	368.35		
Lack of Fit	1948.35	6	324.72		
R^2	0.8218				
Adjusted R^2	0.7149				
Adequate Precision	9.5743				

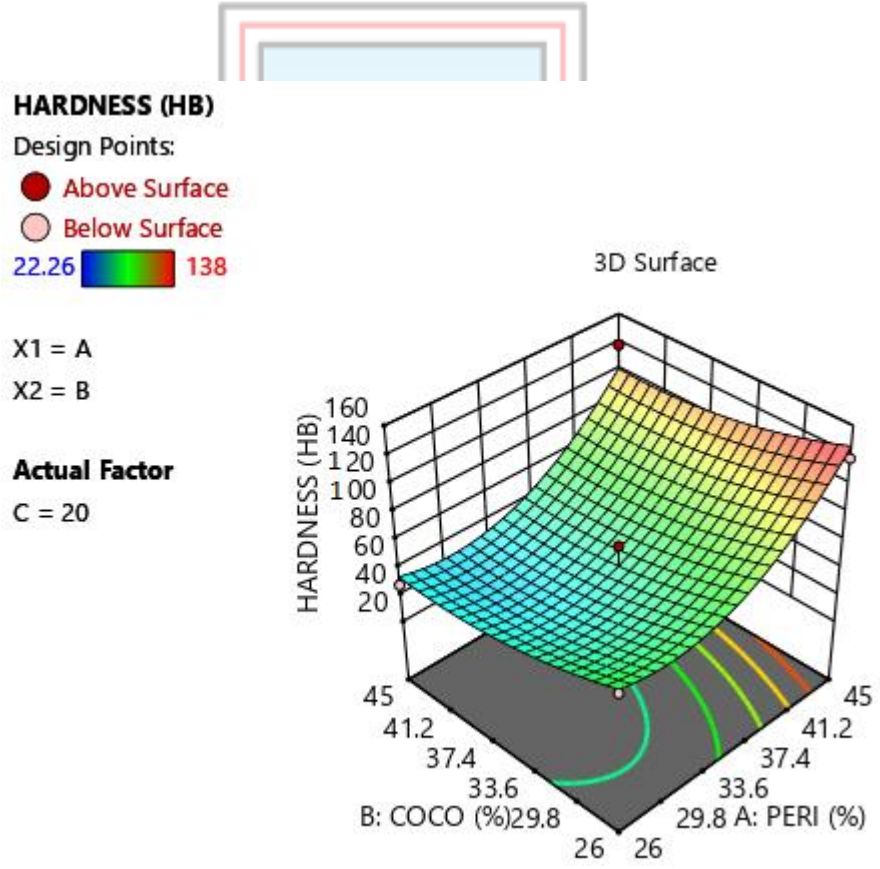

Figure B4 Surface Plot of Hardness against CSA and PSP

Table B5 ANOVA of Water Absorption of the PSP/K Formulation

Source	Sum of Squares	df	Mean Square	F-value	P-value
Model	708.80	4	177.20	2.11	0.1430
A-Periwinkle	78.36	1	78.36	0.9310	0.3536
B-Kaolin	18.27	1	18.27	0.2170	0.6497
C-Epoxy	138.93	1	138.93	1.65	0.2231
B^2	473.23	1	473.23	5.62	0.0353
Residual	1010.04	12	84.17	7.14	
Lack of Fit	943.93	8	117.99		
Pure Error	66.12	4	16.53		
COR Total	1718.84	16			
R^2	0.4124				
Adjusted R^2	0.2165				
Adequate Precision	4.7324				

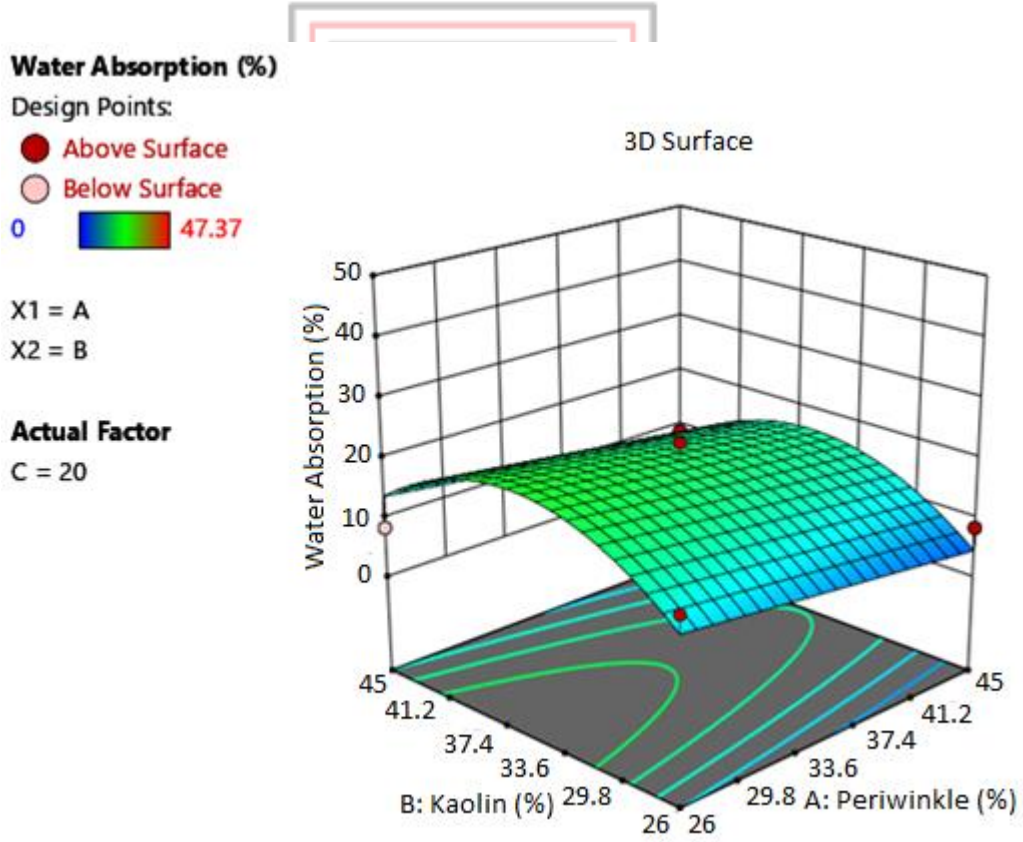

Figure B5 Surface Plot of Water Absorption against Kaolin and PSP

Table B6 ANOVA of Oil Absorption of the PSP/K Formulation

Source	Sum of Squares	df	Mean Square	F-value	p-value
Model	122.12	7	17.45	6.55	0.0059
A-Periwinkle	22.18	1	22.18	8.32	0.0180
B-Kaolin	27.53	1	27.53	10.33	0.0106
C-Epoxy	4.12	1	4.12	1.55	0.2451
AB	12.60	1	12.60	4.73	0.0576
AC	1.421E-14	1	1.421E-14	5.334E-15	1.0000
BC	8.24	1	8.24	3.09	0.1126
B^2	47.45	1	47.45	17.81	0.0022
Residual	23.98	9	2.66		
Lack of Fit	23.37	5	4.67		
R^2	0.8359				
Adjusted R^2	0.7082				
Adequate Precision	7.4148				

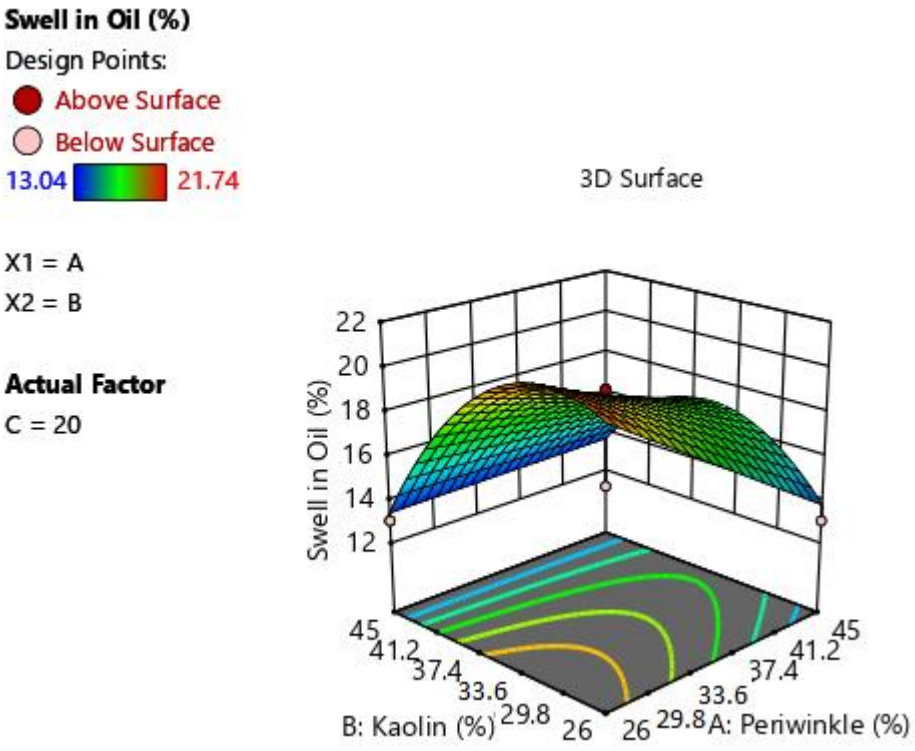

Figure B6 Surface Plot of Oil Absorption against Kaolin and PSP

Table B7 ANOVA of Apparent Porosity of the PSP/K Formulation

Source	Sum of Squares	df	Mean Square	F-value	p-value
Model	161.08	7	23.01	4.59	0.0190
A-Periwinkle	19.28	1	19.28	3.85	0.0814
B-Kaolin	31.32	1	31.32	6.25	0.0338
C-Epoxy	2.09	1	2.09	0.4175	0.5343
AB	20.52	1	20.52	4.10	0.0736
BC	20.39	1	20.39	4.07	0.0744
B^2	57.58	1	57.58	11.50	0.0080
C^2	7.39	1	7.39	1.48	0.2554
Residual	45.08	9	5.01		
Lack of Fit	41.21	5	8.24		
R^2	0.7813				
Adjusted R^2	0.6113				
Adequate Precision	7.0633				

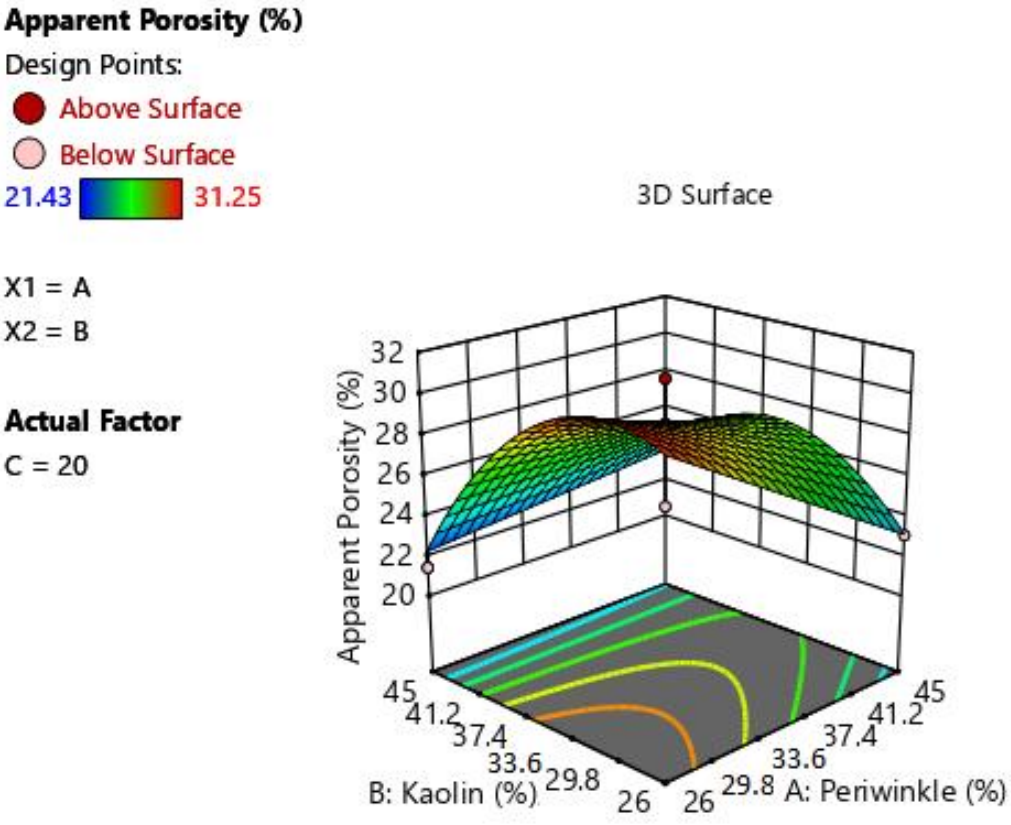

Figure B7 Surface Plot of Apparent Porosity against Kaolin and PSP

Table B8 ANOVA of Hardness of the PSP/K Formulation

Source	Sum of Squares	df	Mean Square	F-value	P-value
Model	26231.55	5	5246.31	1.78	0.1972
A-Periwinkle	935.93	1	935.93	0.3179	0.5842
B-Kaolin	3825.06	1	3825.06	1.30	0.2786
C-Epoxy	3003.13	1	3003.13	1.02	0.3342
B^2	1562.25	1	1562.25	0.5306	0.4816
C^2	17427.96	1	17427.96	5.92	0.0332
Residual	32387.90	11	2944.35		
Lack of Fit	22935.35	7	3276.48		
Pure Error	9452.55	4	2363.14		
COR Total	58619.45	16			
R^2	0.4475				
Adjusted R^2	0.1963				
Adequate Precision	4,5401				

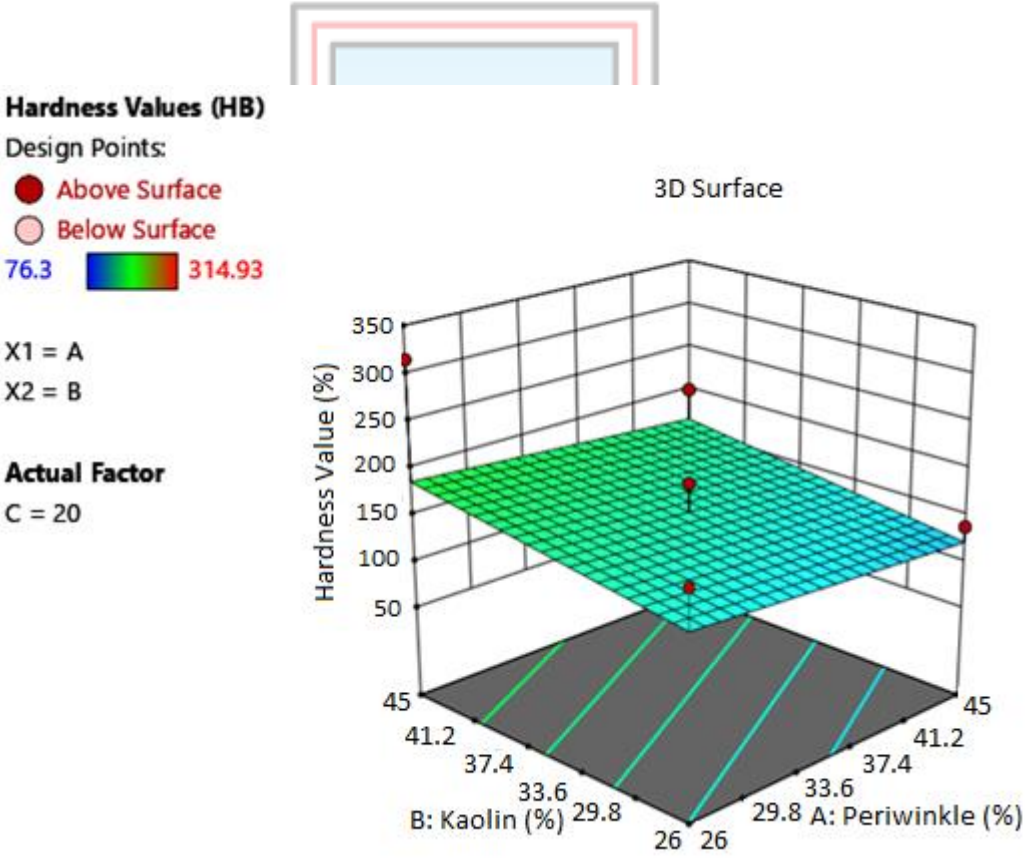

Figure B8 Surface Plot of Hardness against Kaolin and PSP

Table B9 Summary of the ANOVA of the Responses

Responses	Values	
	PSP/CSA Formulation	**PSP/K Formulation**
Compressive Strength (N/mm^2)	0.344452 ± 0.11	14.6479 ± 0.8
Linear Shrinkage (%)	4.76998 ± 1.99	2.76551 ± 1.2
Volume Shrinkage (%)	15.5339 ± 2.36	3.55206 ± 0.4
Water Absorption (%)	36.2762 ± 2.05	20.0214± 9.2
Bulk Density (g/cm^3)	2.09355 ± 0.17	6.00147 ± 0.3
Apparent Porosity (%)	42.4394 ± 2.95	25.7066 ± 2.2
Swell in Oil (%)	53.0608 ± 6.47	16.4291 ±1.6
Hardness Value (HBN)	57.4249 ± 19.19	131.18 ± 62.5

APPENDIX C

TEST RESULTS OF THE DEVELOPED BRAKE PADS

Table C1 Results of the Bulk Density of the Developed Brake Pads

PSP/CSA Brake Pad			
Particle Size (µm)	**Dried Weight (g)**	**Volume of Water Displaced (cm^3)**	**Bulk Density (g/cm^3)**
106	23.875	12.5	1.910
150	15.872	9.0	1.764
212	26.011	16.0	1.626
300	25.736	18.0	1.430
PSP/K Brake Pad			
106	25.920	12.0	2.160
150	27.502	13.5	2.037
212	25.621	13.0	1.971
300	25.061	14.0	1.790

Table C2 Results of Water Absorption and Porosity of the Developed Brake Pads

PSP/CSA Brake Pad						
Particle Size (µm)	**Dried Weight (g)**	**Soaked Weight (g)**	**Weight Difference (g)**	**Suspended Soaked Weight (g)**	**Porosity (%)**	**Water Absorption (%)**
106	22.472	22.983	0.511	17	8.54	2.27
150	22.040	22.592	0.552	16.5	9.06	2.51
212	28.956	30.127	1.171	18	9.66	4.05
300	23.451	24.405	0.954	14	9.17	4.07
PSP/K Brake Pad						
106	25.186	25.964	0.778	16	7.81	3.09
150	26.180	27.039	0.859	17	8.56	3.28
212	27.769	28.785	1.016	17	8.62	3.66
300	26.160	27.450	1.290	14	9.59	5.44

Table C3 Results of Swell in Oil (SAE 40) of the Developed Brake Pads

PSP/CSA Brake Pad				
Particle Size (µm)	**Dried Weight (g)**	**Soaked Weight (g)**	**Weight Difference (g)**	**Oil Absorption (%)**
106	23.456	23.604	0.148	0.63
150	26.392	26.564	0.172	0.65
212	24.862	25.039	0.804	0.71
300	28.976	29.558	0.582	2.01
PSP/K Brake Pad				
106	28.141	28.411	0.270	0.96
150	29.006	29.293	0.287	0.99
212	24.849	25.175	0.326	1.31
300	24.735	25.141	0.406	1.64

Table C4 Results of the Hardness Values of the Developed Brake Pads

PSP/CSA Brake Pad		
Particle Size (µm)	**Diameter of Indentation (mm)**	**Brinell Hardness at 1000 kgf**
106	3.40	107.0
150	3.50	101.0
212	3.65	92.3
300	3.80	84.9
PSP/K Brake Pad		
106	3.20	121.0
150	3.25	117.0
212	3.35	110.0
300	3.65	92.3

Table C5 Results of the Compressive Strength of the Developed Brake Pads

PSP/CSA Brake Pad			
Particle Size (µm)	**Compressive Strength (kN/m^2)**		
	Value I	**Value II**	**Mean Value**
106	112.261	117.739	115.0
150	99.002	113.198	106.1
212	95.502	95.898	95.7
300	90.289	89.711	90.0
PSP/K Brake Pad			
106	133.905	143.495	138.7
150	140.775	135.825	138.3
212	100.100	134.021	117.1
300	105.351	112.485	108.9

Table C6 Results of Friction and Wear Rate of the Developed Brake Pads

PSP/CSA Brake Pad		
Particle Size (µm)	**Mean Coefficient of Friction**	**Wear Rate (mg/m)**
106	0.331	3.96
150	0.318	4.20
212	0.301	4.39
300	0.291	4.77
PSP/K Brake Pad		
106	0.529	2.70
150	0.465	2.81
212	0.387	2.98
300	0.358	3.89

Table C7 Results of Water Absorption of the COM 1 and COM 2 Pads

COM 1 Brake Pad				
Samples	**Dry Mass (g)**	**Soaked Mass (g)**	**Mass Difference (g)**	**Water Absorption (%)**
S1	30.554	30.881	0.327	1.070
S2	26.312	26.902	0.590	2.242
COM 2 Brake Pad				
S1	12.627	12.825	0.198	1.568
S2	10.446	10.590	0.144	1.379

Table C8 Results of Oil Absorption of COM 1 and COM 2 Pads

COM 1 Brake Pad				
Samples	**Dry Mass (g)**	**Soaked Mass (g)**	**Mass Difference (g)**	**Oil Absorption (%)**
S1	24.578	25.266	0.688	2.799
S2	23.994	24.217	0.223	0.929
COM 2 Brake Pad				
S1	16.474	16.688	0.214	1.299
S2	19.244	19.598	0.354	1.840

Table C9 Results of Bulk Density and Porosity of COM 1 and COM 2 Pads

COM 1 Brake Pad						
Samples	**Dried Weight (g)**	**Soaked Weight (g)**	**Suspended Weight (g)**	**Volume of Water Displaced (cm^3)**	**Bulk Density (g/cm^3)**	**Apparent Porosity (%)**
S1	12.040	12.441	6.577	5.93	2.030	7.340
S2	10.260	10.598	5.012	4.6 6	2.202	6.440
COM 2 Brake Pad						
S1	21.040	22.150	6.785	10.11	2.081	7.224
S2	19.170	19.800	9.566	7.83	2.447	6.156

Table C10 Results of Compressive Strength and Hardnes of COM1 and COM 2 Pads

Brake Pads	Compressive Strength (N/mm^2)			Hardness Value (HBN)		
	Sample 1	Sample 2	Mean	Sample 1	Sample 2	Mean
COM 1	67.910	65.690	66.80	101.00	101.00	101.00
COM 2	59.345	60.855	60.10	97.70	97.70	97.70

Table C11 Results of the Disc Temperature Measurements of the Developed and COM 1 Pads

Speed (km/hr)	PSP/CSA Brake Pad	PSP/K Brake Pad	COM 1 Brake Pad
20	35	40	48
40	45	56	62
60	58	59	71
80	78	84	86
100	102	117	136

APPENDIX D

THE DESIGN DRAWINGS OF THE PERMANENT MOULD

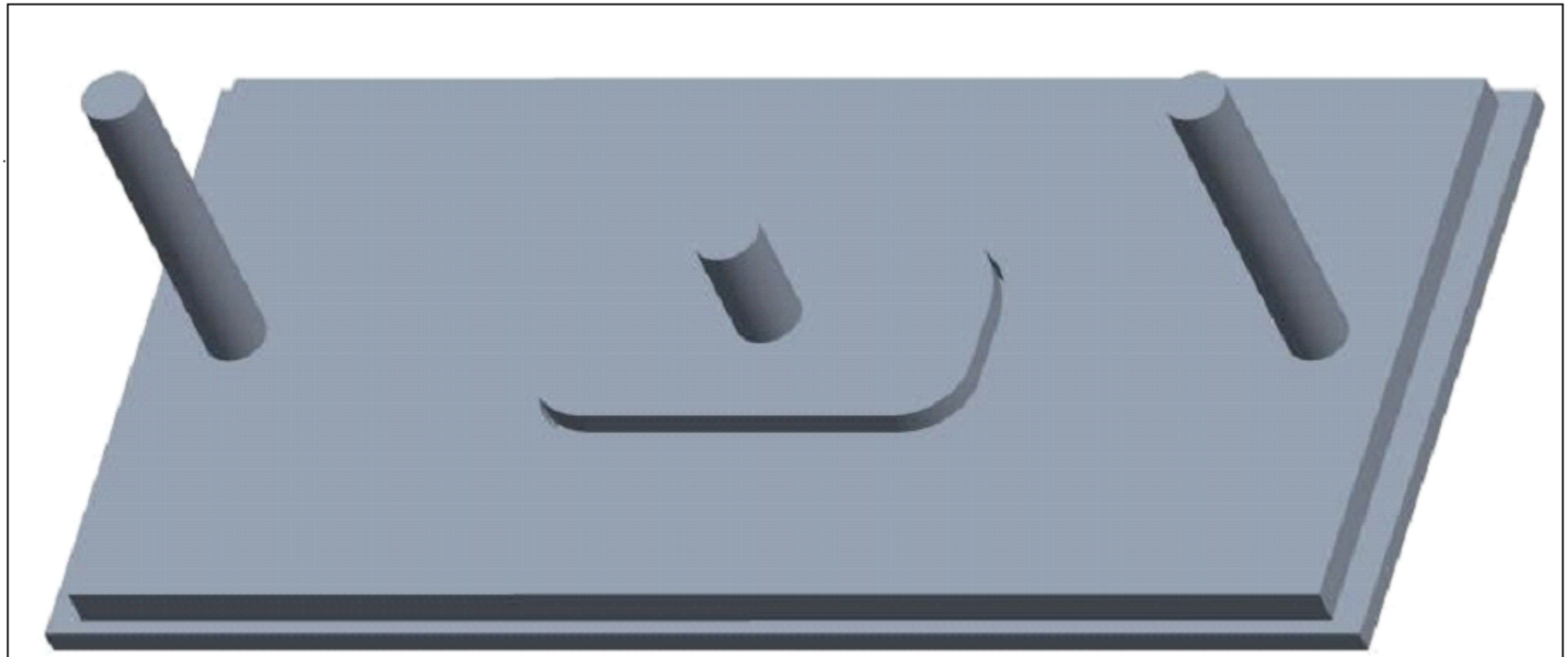

Title: ASSEMBLY VIEW	Checked by: Prof. A. SIMONS Prof. O.A. DAHUNSI			Institution: UNIVERSITY OF MINES and TECHNOLOGY (UMaT)	
Name: EMMANUEL MAWULI SECKLEY Index no.: PG52100215		Scale: 1:1	Units: mm	Date: 10/08/2021	Department: MECHANICAL ENGINEERING

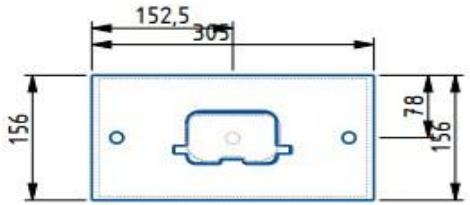

Plan View

Isometric View

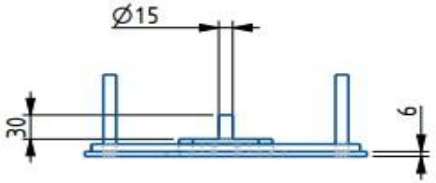

Front View

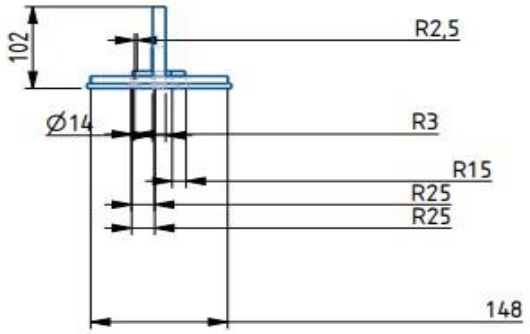

Side View

Title: ORTHO . VIEW	Checked by: Prof. A. SIMONS Prof. O.A. DAHUNSI	Institution: UNIVERSITY OF MINES and TECHNOLOGY (UMaT)

Name: EMMANUEL MAWULI SECKLEY Index no.: PG52100215	Scale: 1:1	Units: mm	Date: 10/08/2021	Department: MECHANICAL ENGINEERING

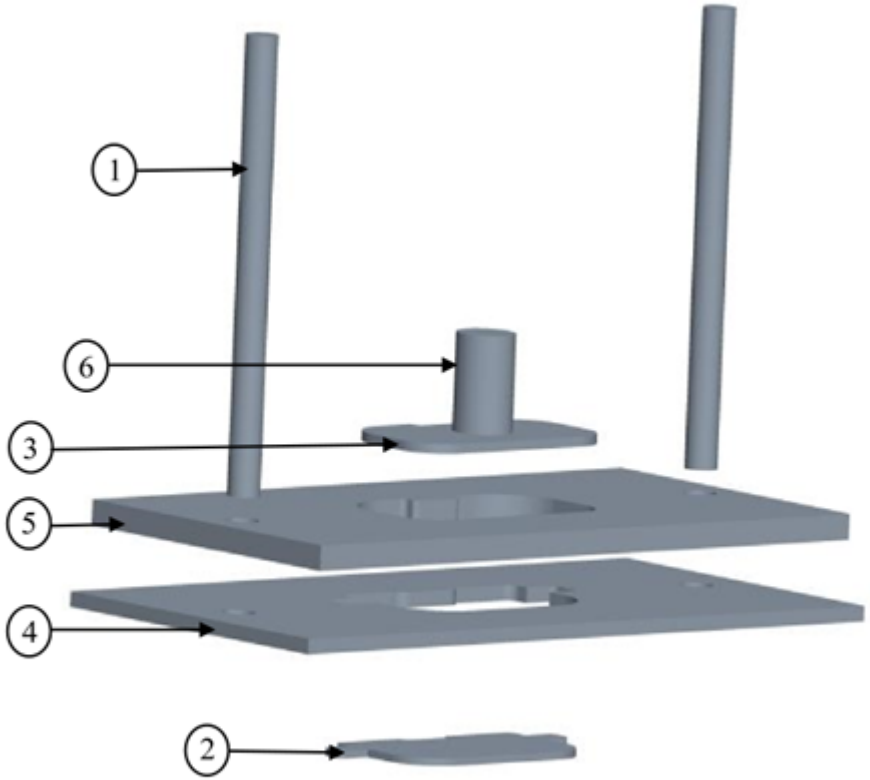

S/N	PART	QTY	MATERIAL
1	Solid Rod	2	Mild Steel
2	Backing Plate	1	Mild Steel
3	Press Plate	1	Mild Steel
4	Mould Support	1	Mild Steel
5	Mould	1	Mild Steel
6	Press Plate Handle	1	Mild Steel

Title: EXPLODED VIEW	Checked by: Prof. A. SIMONS Prof. O.A. DAHUNSI	Institution: UNIVERSITY OF MINES and TECHNOLOGY (UMaT)			
Name: EMMANUEL MAWULI SECKLEY Index no.: PG52100215	Scale: 1:1	Units: mm	Date: 10/08/2021	Department: MECHANICAL ENGINEERING	

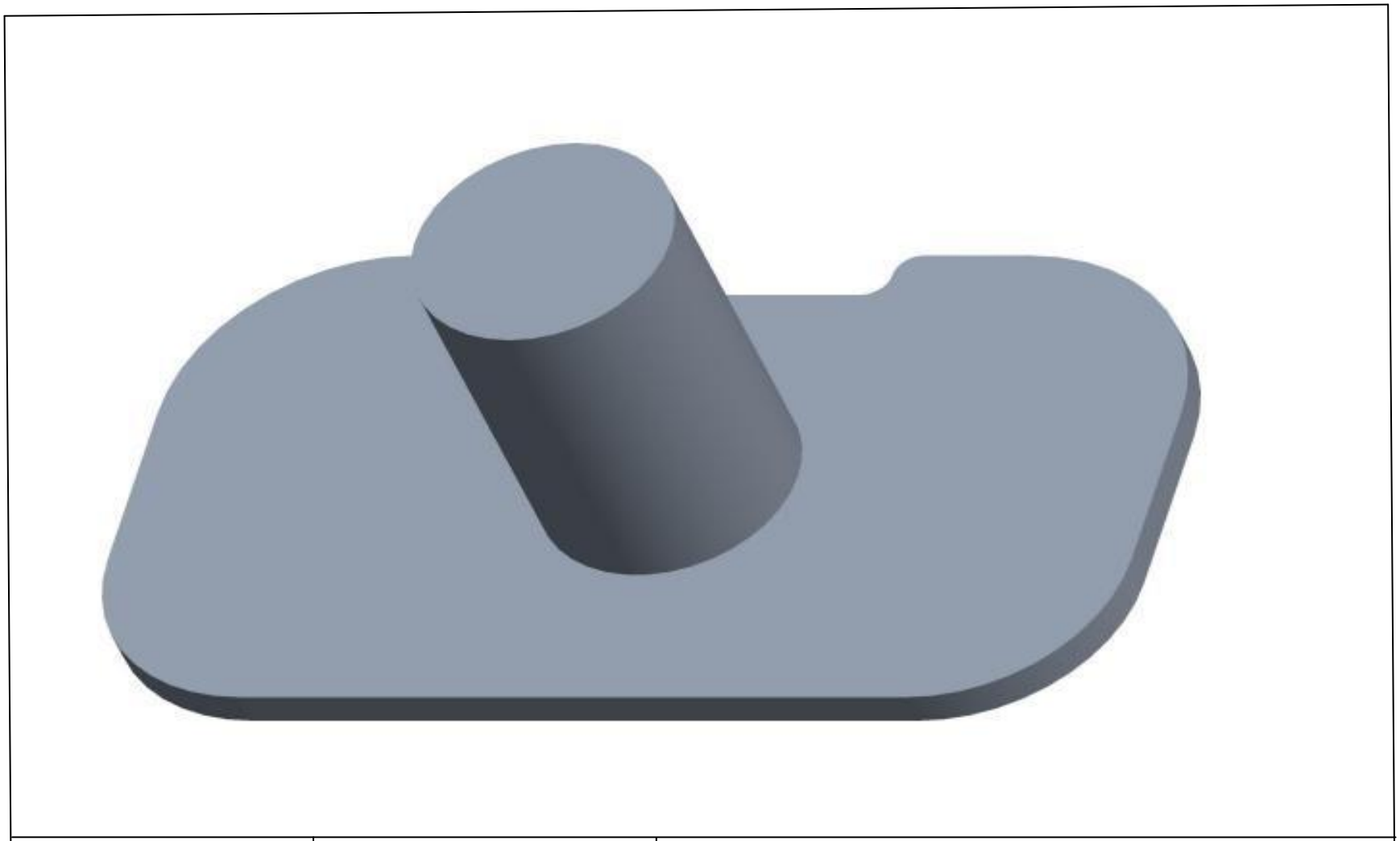

Title: PRESS PLATE	Checked by: Prof. A. SIMONS Prof. O.A. DAHUNSI		Institution: UNIVERSITY OF MINES and TECHNOLOGY (UMaT)		
Name: EMMANUEL MAWULI SECKLEY Index no.: PG52100215	Scale: 1:1	Units: mm	Date: 10/08/2021	Department: MECHANICAL ENGINEERING	

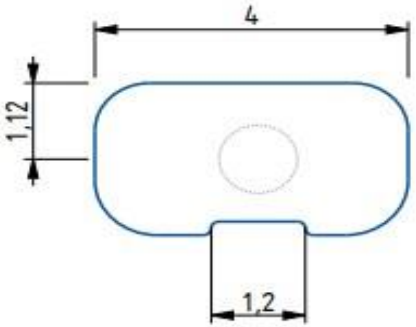

Plan View

Isometric View

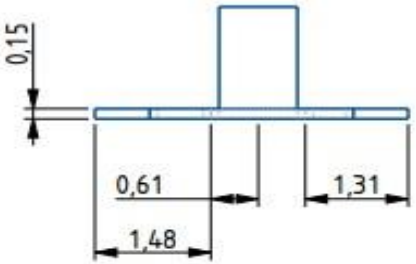

Front View

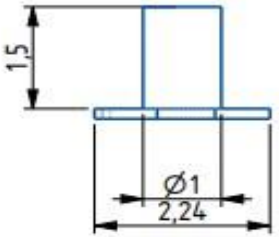

Side View

Title: ORTHO. VIEW	Checked by: Prof. A. SIMONS Prof. O.A. DAHUNSI		Institution: UNIVERSITY OF MINES and TECHNOLOGY (UMaT)	
Name: EMMANUEL MAWULI SECKLEY Index no.: PG52100215	Scale: 1:1	Units: mm	Date: 10/08/2021	Department: MECHANICAL ENGINEERING

Title: BACKING PLATE	Checked by: Prof. A. SIMONS Prof. O.A. DAHUNSI	Institution: UNIVERSITY OF MINES and TECHNOLOGY (UMaT)			
Name: EMMANUEL MAWULI SECKLEY Index no.: PG52100215	Scale: 1:1	Units: mm	Date: 10/08/2021	Department: MECHANICAL ENGINEERING	

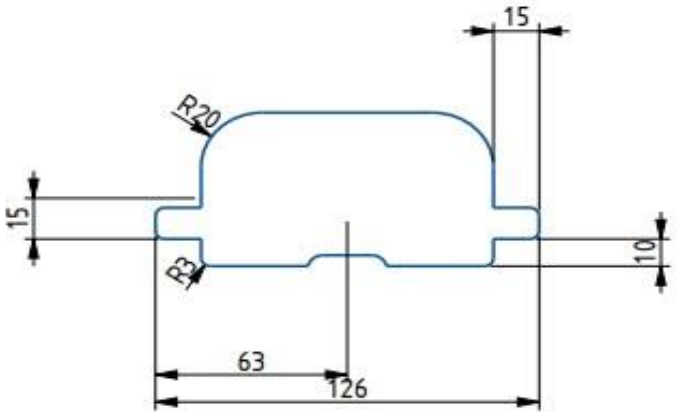

Plan View

Isometric View

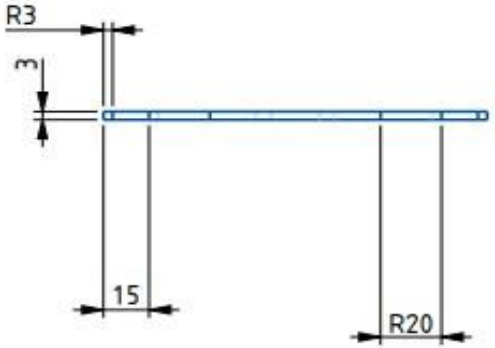

Front View

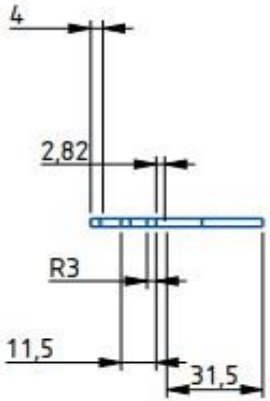

Side View

Title: ORTHO. VIEW	Checked by: Prof. A. SIMONS Prof. O.A. DAHUNSI		Institution: UNIVERSITY OF MINES and TECHNOLOGY (UMaT)	
Name: EMMANUEL MAWULI SECKLEY Index no.: PG52100215	Scale: 1:1	Units: mm	Date: 10/08/2021	Department: MECHANICAL ENGINEERING

Title: MOULD CAVITY	Checked by: Prof. A. SIMONS Prof. O.A. DAHUNSI		Institution: UNIVERSITY OF MINES and TECHNOLOGY (UMaT)	
Name: EMMANUEL MAWULI SECKLEY Index no.: PG52100215	Scale: 1:1	Units: mm	Date: 10/08/2021	Department: MECHANICAL ENGINEERING

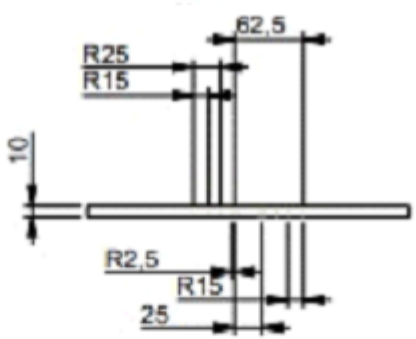

Plan View

Isometric View

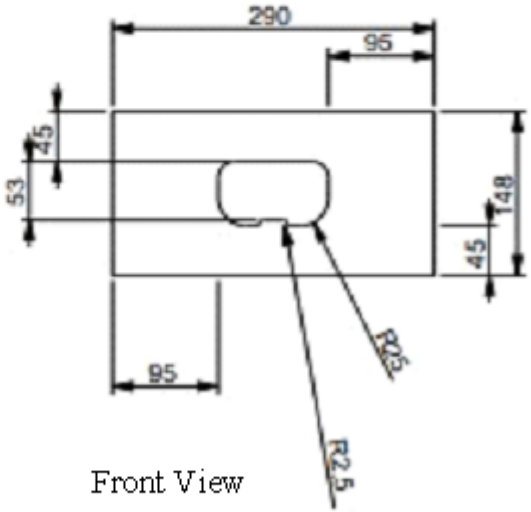

Front View

Side View

Title: ORTHO. VIEW	Checked by: Prof. A. SIMONS Prof. O.A. DAHUNSI	Institution: UNIVERSITY OF MINES and TECHNOLOGY (UMaT)		
Name: EMMANUEL MAWULI SECKLEY Index no.: PG52100215	Scale: 1:1	Units: mm	Date: 10/08/2021	Department: MECHANICAL ENGINEERING

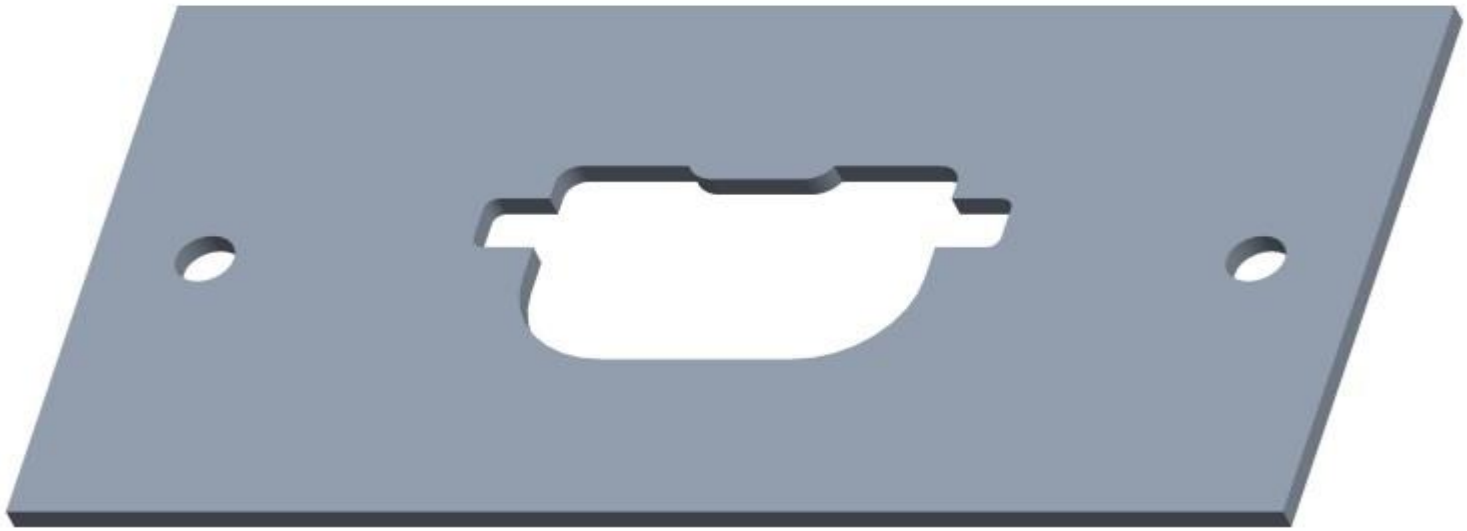

Title: MOULD SUPPORT	Checked by: Prof. A. SIMONS Prof. O.A. DAHUNSI		Institution: UNIVERSITY OF MINES and TECHNOLOGY (UMaT)		
Name: EMMANUEL MAWULI SECKLEY Index no.: PG52100215	Scale: 1:1	Units: mm	Date: 10/08/2021	Department: MECHANICAL ENGINEERING	

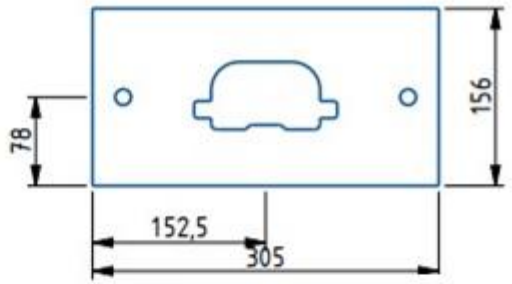

Plan View

Isometric View

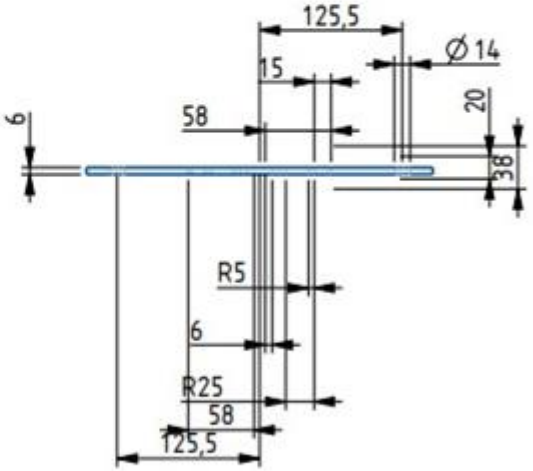

Front View

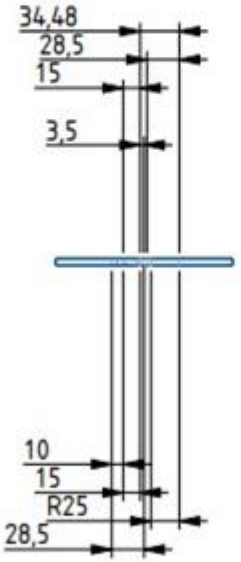

Side View

Title: ORTHO. VIEW	Checked by: Prof. A. SIMONS Prof. O.A. DAHUNSI	Institution: UNIVERSITY OF MINES and TECHNOLOGY (UMaT)

Name: EMMANUEL MAWULI SECKLEY Index no.: PG52100215	Scale: 1:1	Units: mm	Date: 10/08/2021	Department: MECHANICAL ENGINEERING

APPENDIX E

PAPERS RESULTING FROM THE RESEARCH

European Journal of Applied Sciences – Vol. 10, No. 6
Publication Date: December 25, 2022
DOI:10.14738/aivp.106.13534.
Mawuli, S. E., Anthony, S., & Akintunde, D. O. (2022). Development of Asbestos-free Disc Brake Pad Using Periwinkle Shell Powder and Coconut Shell Ash as Base Materials. European Journal of Applied Sciences, 10(6). 473-491.

Development of Asbestos-free Disc Brake Pad Using Periwinkle Shell Powder and Coconut Shell Ash as Base Materials

Seckley Emmanuel Mawuli
Department of Mechanical Engineering
University of Mines and Technology, Tarkwa, Ghana

Simons Anthony
Department of Mechanical Engineering
University of Mines and Technology, Tarkwa, Ghana

Dahunsi Olurotimi Akintunde
Department of Mechanical Engineering
Federal University of Technology, Akure, Nigeria

ABSTRACT

Brake pads are integral part of an automobile braking system that contribute to the full control of the vehicle. The composite materials for their production must therefore possess adequate chemical, mechanical, physical, and thermal properties. The development of asbestos-free disc brake pad using Periwinkle Shell (PS) powder and Coconut Shell Ash (CSA) as reinforcement and frictional filler material respectively is presented. This was done with a view of establishing suitability of PS powder and CSA as replacements for asbestos which has been found to be carcinogenic and capable of causing Asbestosis and Mesothelioma [1]. Other ingredients used are graphite as lubricant, epoxy resin as binder, copper, zinc, and aluminum powders as abrasives and also to impact mechanical strength. The optimum percentage formulation of these materials for the pad was arrived at by using the ANOVA tool of the Box-Behnken technique of Design Expert Software, DX-13. The CSA and PS powders were sieved into grades of 106 µm, 150 µm, 212 µm and 300 µm and then combined with other constituents to produce the brake pad. The pads were characterized in terms of their physical, mechanical and tribological properties. It was observed that increase in particle size distributions leads to decrease in densification and carbon crosslinking of the produced composite brake pads. Therefore, the 106 µm particle size sample has better properties than others. Comparison analysis shows that the performance parameters of the 106 µm size brake pad compares well, and in some cases better, with typical after-market replacement pads, an asbestos-based brake pad and brake pads developed from past research works.

Keywords: Brake pad, asbestos, periwinkle shell powder, coconut shell ash, Design Expert (DX-13), physical, mechanical and tribological properties.

INTRODUCTION

The braking system is an indispensable component of an automobile, and is composed of many parts including brake pads, master cylinder, wheel cylinders, and a hydraulic control system

European Journal of Applied Sciences – Vol. 10, No. 6
Publication Date: December 25, 2022
DOI:10.14738/aivp.106.13535.
Mawuli, S. E., Anthony, S., & Akintunde, D. O. (2022). A Conceptual Review of Automobile Disc Brake Friction Materials. European Journal of Applied Sciences, 10(6). 492-505.

A Conceptual Review of Automobile Disc Brake Friction Materials

Seckley Emmanuel Mawuli
Department of Mechanical Engineering
University of Mines and Technology, Tarkwa, Ghana

Simons Anthony
Department of Mechanical Engineering
University of Mines and Technology, Tarkwa, Ghana

Dahunsi Olurotimi Akintunde
Department of Mechanical Engineering
Federal University of Technology, Akure, Nigeria

ABSTRACT

Providing an alternative filler material for brake pads is crucial because the use of asbestos as filler material in brake pads has some health risks. It is known that asbestos can cause Asbestosis and Mesothelioma. This has, therefore, ignited widespread research into development and finding of eco-friendly brake friction organic materials. In this paper, some works done by various researchers in a bid to finding suitable environmentally friendly and best performed compositions for brake friction materials have been presented. The use of natural fibres such as maize husks, coconut shell, palm kernel shell, cocoa beans shell, bagasse, periwinkle shell, sawdust and banana peels as reinforcement to replace asbestos in the production of brake friction materials with high mechanical properties, stable friction, high wear resistance, lightweight, low environmental impact and low cost have been presented. This extensive survey, however, shows that there is no research on the suitability of other materials such as other types of periwinkle shells, coconut shell ash and kaolin to replace asbestos as major ingredients in a brake friction material. There is, therefore, the need to continue to research into and develop low-cost non asbestos organic brake pad materials for better brake performance.

Keywords: Brake pads, asbestos, filler, organic materials.

INTRODUCTION

According to [1], a brake plays a vital role in any automotive so as to slow down the vehicle or to stop the vehicle completely. During the application of brake, friction between brake pads and rotating disc causes the vehicle to stop or slow down by converting kinetic energy of the vehicle into heat energy. Therefore, a brake pad material should maintain a sufficiently high friction coefficient with the brake disc, not decompose or break down in such a way that the friction coefficient with the brake disc is compromised at high temperatures. [2] reported that brake pads are important components of braking system for all categories of vehicles equipped with brake discs; and according to them, brake pads are steel backing plates with friction materials bounded unto the surface facing the brake disc and are placed in the wheel assembly to

Index

Emmanuel Seckley-- Thesis

by Emmanuel Seckley

Submission date: 25-Oct-2023 05:45PM (UTC+0000)
Submission ID: 2143603369
File name: Mr._Seckley_Work_2.docx (14.71M)
Word count: 35476
Character count: 185699

Emmanuel Seckley-- Thesis

ORIGINALITY REPORT

8%	7%	4%	3%
SIMILARITY INDEX	INTERNET SOURCES	PUBLICATIONS	STUDENT PAPERS

PRIMARY SOURCES

1	dspace.unimap.edu.my Internet Source	1%
2	acta.fih.upt.ro Internet Source	1%
3	www.researchgate.net Internet Source	<1%
4	autodocbox.com Internet Source	<1%
5	hdl.handle.net Internet Source	<1%
6	www.ijemr.net Internet Source	<1%
7	erl.ucc.edu.gh:8080 Internet Source	<1%
8	worldwidescience.org Internet Source	<1%
9	www.ornl.gov Internet Source	<1%